Improvement of impulse voltage distribution of transformer windings

By

Weichuan Zhao

to obtain the degree of Master of Science
at the Delft University of Technology,
to be defended publicly on Friday August 28, 2020 at 2:00 PM

Student number:	4852125	
Project Duration:	December 2019—August 2020	
Responsible supervisor:	Prof. Ir. Peter Vaessen	TU Delft
Daily supervisor:	Dr. Ir. Mohamad Ghaffarian Niasar	TU Delft
Thesis Committee:	Prof. Ir. Peter Vaessen	TU Delft
	Dr. Ir. Mohamad Ghaffarian Niasar	TU Delft
	Dr. Ir. Milos Cvetkovic	TU Delft
Company supervisor:	Luc Dorpmanns	Royal Smit Transformers

TU Delft Delft University of Technology

Contents

1 Abstract

Non-linear voltage response distribution along the hv transformer winding in reaction to a standard lightning overvoltage (1.2/50 μs) could result in severe electric stress specially to the area of the winding close to the high voltage terminals in which the flashovers or breakdown may occur. The main purpose of this thesis project is to find out the best interleaving or inter-shielding method that could improve the voltage response distribution and the optimized number of inter-shield wires for each disc pair that could balance the voltage response performance and the cost of material and labour.

Within this master thesis report, the general analytical formulas for the total series capacitance C_s of the disc pair model with different types of inter-shield wires together with the turn-interleaved disc pair model are derived based on energy summation method. Those formulas are basically verified through the comparison with the results obtained from Comsol Multiphysics and the outcome differences are within the error tolerance. Furthermore, after introducing a certain number of inter-shield wires to the disc pair model, the influence on the total series capacitance C_s and mutual inductance L_s is thoroughly discussed. Also, the assumption that the voltage would distribute uniformly along the disc pair at the frequency of 1MHz is proved to be correct with the aid of the Matlab simulation. Moreover, the question about how could the material of the transformer core (solid iron core and ferrite core) influence the voltage response distribution has also been explained. Last but no least, after comparing the figures for the voltage response distribution among different disc winding configurations and different type of inter-shield wires, the one that could deliver the best performance is selected.

The main conclusion of this work is that the floating electrostatic shield wire would behave as the best type of inter-shield wire. Within one disc pair model, more inter-shield wires would bring more linear voltage response distribution. Whereas, if the balance of the material cost and response performance is required, the third disc winding configuration would become the best option. In addition, the readers could also acquire a lot of knowledge about how to properly simulate a disc winding model in Comsol.

	Configuration one	Configuration two	Configuration three	Configuration four
The number for disc 1	5	5	4	0
The number for disc 2	4	4	3	0
The number for disc 3	3	3	3	0
The number for disc 4	2	3	2	0
The number for disc 5	1	2	2	0
The number for disc 6	0	2	2	0
The number for disc 7	0	1	1	0
The number for disc 8	0	1	1	0

Keywords— voltage response distribution, inter-shielding methods, turn-interleaving methods, improvement factor, decrease factor, disc series capacitance, mutual inductance, lightning overvoltages, eddy currents, fringing effect, skin effect

2 Acknowledgement

This master's thesis project is in collaboration with the Royal Smit Transformers. It could not be achieved without the guidance and support of many people from the Delft University of Technology and Royal Smit Transformers. I would like to take this opportunity to express my sincere gratitude to all of them.

I would like to express my sincere gratitude towards my daily supervisor **Dr. Ir. Mohamad Ghaffarian Niasar** for his constant academic support and counsel. Every time when I encounter some tough problems in Comsol or Matlab simulation, he would always firstly encourage me and then guide me to identify the reasons for those errors. Due to his support, I gradually explore the proper method to simulate a hv disc winding model in Comsol Multiphysics. I am also very grateful to **Prof. Ir. Peter Vaessen** to his guidance and encouragement throughout the master's project. His constructive feedback is critical in accomplishing the master thesis project.

I am deeply indebted to **Luc Dorpmanns** for sharing his insights on the hv disc winding design as well as the important documents corresponding to the thesis topic. I am much obliged to **Dr. Ir. Jianning Dong** for his academic support in understanding how the material of the transformer core influences the mutual inductance between two discs.

Weichuan Zhao
Delft, August, 2020

3 Introduction

3.1 Motivation

In case of a standard lightning impulse (1.2/50 μs) striking an overhead line, the resulted transient overvoltages would propagate along the line, entering the transformer through the bushing and eventually reach the hv disc winding. The overvoltage leads to high electric stress between the transformer discs adjacent to high voltage terminals. The high electric stress would probably result in some flashovers that occur in the corresponding insulation, which would accelerate the breakdown of the transformer. While during the normal operation, the winding would behave inductively and the voltage response distribution along the transformer winding could be regarded as uniform. During a surge overvoltage wave, due to the high $\frac{dV}{dt}$ of the front fraction, current would predominately flows through the turn-turn C_{tt} and turn-ground capacitances C_g, which would lead to the non-uniform voltage distribution along the winding. In other words, the non-uniform voltage distribution is caused because the intensity of the capacitive currents flowing through the C_s close to the top is much larger than those flowing through the C_s nearby the end.

3.2 The goal of this thesis topic

The goal of this thesis topic is to find out the optimized number of inter-shield wires for each disc pair from hv disc winding to provide the uniform voltage response distribution. In other words, the goal is how to properly coordinate the disc pairs with different number of inter-shield wires to improve the voltage distribution of the hv transformer windings.

3.3 The research questions

In order to force the voltage responses distribute linearly, the best and easiest approach is to increase the series capacitance C_s between adjacent discs through adding electrostatic shield wires, wound-in shield wires or interleaving the transformer turns.

1) The first research question is that after the application of certain inter-shielding or interleaving method, how much could the total series capacitance of the disc pair C_s be improved. For the sake of concise, a new parameter named improvement factor λ is defined to reflect the degree for the improvement of C_s. This research question could be tackled after using the analytical formulas derived in chapter 5 or via Comsol modelling explained in chapter 9.

2) The second research question is about how the mutual inductance between two discs L_s would be influenced after introducing certain number of inter-shield wires to the disc pair model. Similarly, a new parameter named decrease factor η is defined to reflect the degree for the influence of L_s. This question could only be solved via the application of Comsol Multiphysics because all of the transformer turns from the corresponding disc should be grouped during L_s calculation and it is simple to fulfill this function in Comsol Multiphysics.

3) The third research question is the verification of the assumption that the voltage would distribute linearly along the disc pair at the frequency range of around 1MHz provided in [1]. This assumption is really important because the voltage drop per transformer turn ΔV_{turn} or inter-shield wire ΔV_{shield} could be directly acquired based on that. This assumption could be verified with the aid of the analytical calculation methods from the reference [2].

4) The forth research question is to find out why the material of the transformer core (solid iron core or ferrite F core) could have an influence on the mutual inductance between the discs L_s. This question could be solve through calculating the induced current density in the transformer core in Comsol Multiphysics. This topic has been explained in detail in chapter 18.

5) The fifth research question is to find out the best inter-shielding method that could deliver the best voltage response distribution. Generally, this question could be solved through three steps. Firstly, an electric network that could represent the hv disc winding ought to be built in Simulink (Matlab) and then all of the electric parameters including resistance matrix, inductance matrix and series capacitances should be acquired through Comsol modelling. Finally, the voltage response distribution figures for different inter-shielding cases should be compared.

3.4 Literature review and the approach used

In [3] and [4], various electrostatic shielding and turn-interleaving arrangements have been demonstrated. According to the critical assumptions in [1], the voltage responses would distribute linearly along the disc pair and the total electrical energy would only located inside the disc pair model. Therefore, the voltage drop per transformer turn is considered to be equal.

In [5] and [6], the analytical formulas of the total series capacitance C_s with one electrostatic inter-shield pair and two inter-shield pairs together with the continuous case have been provided to the readers. However, there are no derivation processes for those formulas. Fortunately, in [1], R.M.Del Vecchio and his colleagues used the energy summation method to specifically derive the general analytical formula for C_s with m wound-in shield wires, which provided us some ideas for derivation of C_s for the disc pair model with m electrostatic shield wires and turn-interleaved disc pair. In [7], M. G Niasar and myself have provided a general analytical formula together with the derivation processes for the calculation of C_s suitable for any number of inserted electrostatic shield wires and this reference paper will be published in 2020 IEEE International Conference on High Voltage Engineering and Application.

In order to use the numerical method to calculate the total series capacitance C_s of the disc pair model, the critical assumption described in [1] should be verified first. Based on that assumption, the voltage values corresponding to relevant transformer turns should be applied to the disc pair model constructed in Comsol. Through the surface integration, the total electric energy of the disc pair model E_{tot} could be obtained. If the total voltage drop of the disc pair model is δV, the series capacitance of the disc pair model could be derived as: $C_{s1} = \frac{2*E_{total}}{\delta V^2}$. Besides, it is worth mentioning that the ground should be totally removed during the surface integration calculation. Therefore, the influence of the ground capacitance C_g could be eliminated. Based on this method, we could eventually get the improvement factor λ for different cases with different number of inserted shield wires. Moreover, all of the total series capacitances C_s are actually independent from the input and output voltage V_1 and V_2.

Based on the results in chapter 8, the series capacitance C_s of the turn-interleaved disc pair model has the highest value. In other words, the turn-interleaved case could bring us the best voltage response performance. Whereas, the turn-interleaved method is really complex for real manufacturing. Nowadays, in the large power transformer company such as Royal Smit Transformers, they would use the disc-interleaved method instead. With respect to the inter-shielding method, if the number of inter-shield pairs in the disc pair is increased, the value of the total series capacitance C_s would also increase but it would be more costly due to extra material and time of manufacturing. Therefore, the best disc pair coordination has to be found out to balance the cost as well as the performance of the voltage response distribution. In [8], the inventors George E. Sauer and his colleagues had provided several inter-shielding methods to us, which are very useful for the transformer designers. In reality, in order to reduce the cost, only 8 or 10 disc pairs nearby the high voltage connections should be inter-shielded or interleaved. A typical improved voltage distribution figure is shown as below.

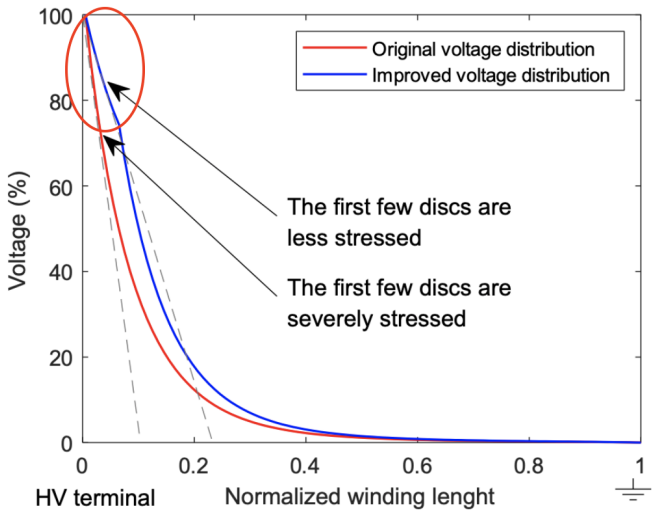

Figure 1. Voltage response distribution for the hv disc winding

Actually, all of the C_s values are obtained based on that critical assumption that the voltage would distribute linearly along the disc pair at the frequency range of 1MHz. Thus, it is very important to validate the correctness of the assumption. There are basically two methods for the assumption verification. The first approach is to build a Simulink model of the equivalent circuit for the disc pair model and then put all of the electric parameters obtained from Comsol inside the model. The Simulink model is made based on the ladder network model from [9] and [10]. After extracting the data from Simulink to Matlab, we could collect all of the crest values from the voltage responses and then plot them in one figure. This method is suitable for the disc pair model when the last turn is grounded or ungrounded.

The second approach is to use the analytical calculation method introduced by C.Kroon from [2]. Based on that reference paper, we are able to program the Matlab codes for the voltage response of the k^{th} transformer turn in the

case of different voltage sources such as sinusoidal and standard impulse voltage source with respect to earth in time domain. After having the voltage responses of transformer turns, the peak values could be obtained and then plot in one figure and observe whether the graph is a linear line or non-linear line. The derivation processes have been explained in chapter 13, 14 and 15 and the Matlab codes are shown in the appendix. Moreover, it is worth mentioning that this method only suitable for the case when the last turn is grounded.

Normally, the material of the transformer core could also play an important role in the voltage response distribution because the conductivity and the relative permeability would vary a lot for different types of material. According to [11], the authors mentioned at higher frequency level such as 1MHz, the solid iron transformer core would behave as an air core due to the severe skin effect and the flux linkages cannot penetrate the solid iron core at that phenomenon. However, this outcome is not that accurate. The reason would be explained in detail in chapter 18.

After introducing certain number of inter-shield pairs to the disc pair model, the magnitude of mutual inductance L_s would decrease compared with the reference mutual inductance, which has been shown in chapter 19. As the number of inter-shield wires rises, the decrease factor η gradually reduces and the magnitude of the mutual inductance also decreases. In [12] and [13], professor K.A.Wirgau and Martinez-Velasco had provided some knowledge about how to use the analytical method to calculate the mutual inductance of the transformer turns that has different cross-sections. After constructing those models for transformer turns in Comsol, the results calculated from numerical method could also be obtained. In [14], the comparison between the results for mutual inductance obtained from analytical methods and numerical methods has been clearly explained and the difference of those results could be regarded as negligible. Therefore, the mutual inductance calculated through numerical method is proved to be correct.

3.5 The main outline of the thesis report

1) Chapter 5 and chapter 6 mainly focus on the analytical formula derivation and verification processes of the total series capacitance C_s for the disc pair model with different types of inter-shield wires and turn-interleaved cases based on the energy summation method as well as micro-element method.

2) Chapter 9 and chapter 10 concentrate on the calculation of the improvement factor λ for total series capacitance C_s of the disc pair model with different type of inter-shield wires and chapter 19 covers the calculation of the decrease factor η for the total mutual inductance L_s between two discs after introducing a certain number of inter-shield wires to the disc pair model.

3) Chapter 11 focuses on proving the most critical assumption that the voltage would distribute linearly along the disc pair model at the frequency range of 1MHz through the Matlab codes which are programmed based on the calculation methods from [2] with the aid of Kirchhoff's law and the application of the Laplacian transformation.

4) Chapter 17 concentrates on the reshape of the geometry for the hv disc winding model in order to acquire the accurate the accurate resistance matrix and the inductance matrix and reduce the total time for simulation.

5) Chapter 20 and chapter 21 cover the selection of the best type of inter-shield wires and the best disc winding configuration together with the voltage response distribution comparison between the cases with ferrite F and solid iron transformer core. Furthermore, within this part, the method about how to properly simulate a disc winding model with different type of inter-shield wires in Comsol Multiphysics is also concluded.

3.6 The steps used to obtain the voltage responses of the hv disc winding

1) The electric network which could represent for the hv disc winding including a certain number of transformer discs is built in Simulink (Matlab).

2) The hv disc winding model in certain configuration is properly simulated in Comsol Multiphysics. The purpose of this step is to calculate the resistance matrix, inductance matrix and the influential capacitances between adjacent discs.

3) All of the electric parameters acquired from the second step is put into the electric network built in Simulink and the computation time T_{period} is selected and the results are extracted.

4 The derivation of the factor α and voltage distribution

In Greenwood book, chapter 11 [15], the author only takes the capacitance matrix into account and overlooks the influence of inductance and resistance matrix. As the lightning impulse propagates along the layer winding model which has the length of l, the total series capacitance of the layer winding is defined as C_s and the total ground capacitance of the layer winding is defined as C_g. Figure 2 illustrates the layer transformer model in reaction to the lightning impulse.

However, when we only focus on a small fraction Δx of the layer transformer winding, the ground capacitance among that fraction would become $C_g(\Delta x) = \frac{C_g}{l} * \Delta x$ and the series capacitance among that fraction would become $C_s(\Delta x) = \frac{C_s * l}{\Delta x}$. Moreover, E represents the voltage on the HV terminals and α is defined as $\sqrt{\frac{C_g}{C_s}}$. Furthermore, the equations below are derived based on figure 3.

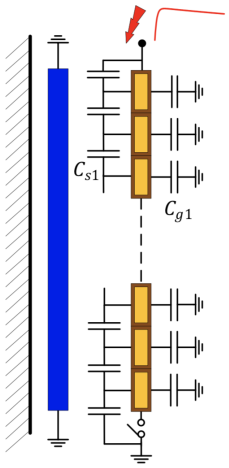

Figure 2. Layer winding model

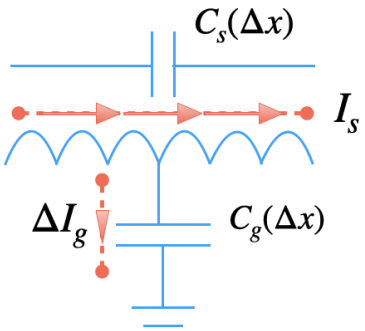

Figure 3. Electric network for part of layer winding

$$\Delta I_g = \frac{E}{X_{Cg}(\Delta x)} = E * \omega * \frac{C_g}{l} * \Delta x = \frac{dI_s}{dx} * \Delta x$$
$$I_s = \frac{\Delta U}{X_{Cs}(\Delta x)} = \omega * C_s(\Delta x) * \Delta U = \omega * \frac{C_s * l}{\Delta x} * \frac{dE}{dx} * \Delta x$$
$$\frac{dI_s}{dx} = \omega * \frac{C_s * l}{\Delta x} * \frac{d^2E}{dx^2} * \Delta x = E * \omega * \frac{C_g}{l}$$
$$\frac{d^2E}{dx^2} = E * \frac{1}{l^2} * \frac{C_g}{C_s} = E * (\frac{\alpha}{l})^2$$

After solving the ordinary differential equation $\frac{d^2E}{dx^2} = E * (\frac{\alpha}{l})^2$, we could obtain the final result as below.

$$E = A_1 * e^{\frac{x}{l} * \alpha} + A_2 * e^{-\frac{x}{l} * \alpha}$$

If the neutral of the layer winding is grounded, the boundary conditions are shown as follows: at x=0, E=0 and at x=l, E=U. The voltage distribution formula along the winding would be derived as the equation below. Besides, the initial voltage distribution lines for different values of α under this condition are shown in figure (iv).

$$E = U * \frac{sinh(\alpha * \frac{x}{l})}{sinh(\alpha)}$$

If the neutral of the layer winding is floating, the boundary conditions are shown as follows: at x=0, $I_s = 0$ and at x=l, E=U. The voltage distribution formula along the winding could be derived as the equation below. Besides, the initial voltage distribution lines for different values of α under this condition are shown in figure(iv).

$$E = U * \frac{cosh(\alpha * \frac{x}{l})}{cosh(\alpha)}$$

With respect to the case with grounded neutral, the lightning impulse has really steep rise time ($1.2\mu s$), which would

bring a huge number of high frequency components. Therefore, during the initial stage of the lightning impulse, only the capacitances could play an important role in the voltage distribution. However, the lightning impulse has fairly flat decrease time, at this stage, the low frequency elements would be dominated and the equivalent circuit of the layer winding model would almost behave inductively.

According to the analysis above, we could also know that no matter what magnitude of α is, if the waiting time is long enough, the voltage responses would distribute linearly along the layer winding model such as the imaginary line in figure 4, this concept also has been shown in [4].

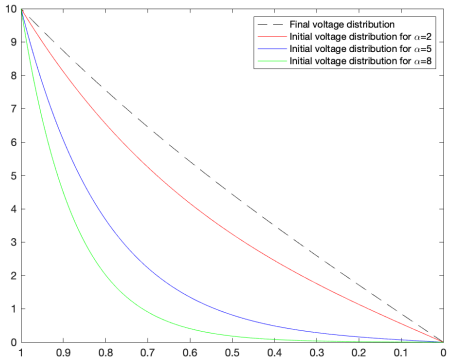

Figure 4. Grounded neutral disc winding

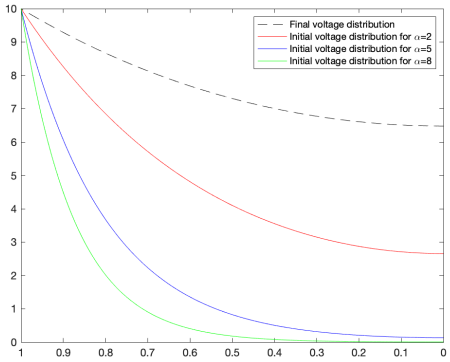

Figure 5. Floating neutral disc winding

5 The derivation processes for the general analytical formulas

In [6], the total series capacitance of the continuous disc pair model is $C_s = \frac{n}{6} * C_d + \frac{n-2}{n^2} * C_{tt}$. As for the disc pair model with one floating electrostatic inter-shield pair, the total series capacitance would become $C_s = \frac{n}{6} * C_d + \frac{n^2-n-2}{n^2} * C_{tt}$. With respect to the disc pair model with two floating electrostatic inter-shield pairs, the series capacitance would become $C_s = \frac{n}{6} * C_d + \frac{2n^2-7n+6}{n^2} * C_{tt}$. Moreover, n represents for the total number of transformer turns within the disc pair model.

Whereas, in [6], no derivation processes are present for the explanations about how to obtain those analytical formulas. Therefore, in this section, the derivation parts are added in order to make those analytical formulas more lucid. All of those analytical formulas above are obtained under the critical assumption from [1]–the voltage would only focus on the midpoint of the transformer turn or inter-shield wire and distribute linearly along the disc pair model at the frequency range of 1MHz.

5.1 The total series capacitance of the continuous disc pair

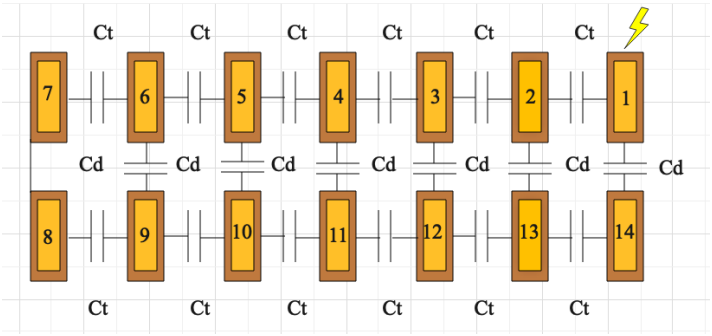

Figure 6. Capacitive continuous disc pair model

As for the capacitive continuous disc pair model shown in figure 6, only the influential capacitances: individual disc-disc series capacitances and adjacent turn-turn series capacitances should be taken into account. In order to precisely obtain the total disc-disc series capacitance C_{dr}, the micro-element method and the energy summation method should be applied. By means of these methods, the upper and bottom disc are assumed to be ideally divided into infinite transformer turns and the voltage drop per turn ΔV_{turn} should be equal. The derivation process is calculated mainly based on figure 7. Besides, d is the length of the upper or bottom disc. V is the magnitude of the input voltage applied to the disc pair model. x is the distance between the transformer turn under consideration and the turn attaches to the input lead.

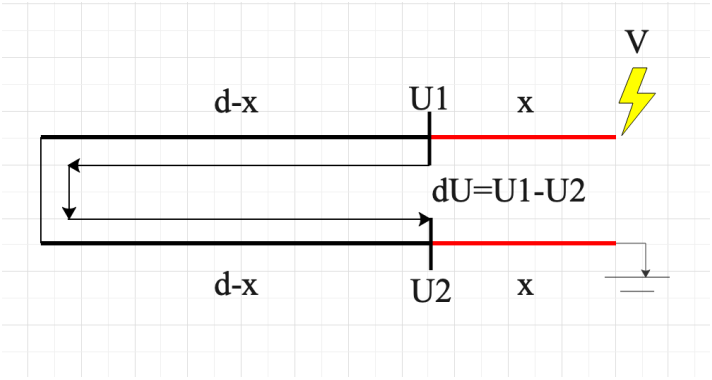

Figure 7. Micro-element method sketch

$$\Delta V = U_1 - U_2 = \frac{V}{2d} * (2d - 2x) = \frac{V}{d} * (d - x)$$

$$E_{tot_{disc-disc}} = \int_0^d \frac{1}{2} * C_d * \Delta V^2 * dx = (\frac{1}{2} * C_d * \frac{V^2}{d^2}) * \int_0^d (d^2 + x^2 - 2dx)dx = \frac{d}{6} * C_d * V^2$$

The analysis of the formula above: d could also represent for the number of transformer turns from one individual disc or coil and n indicates the total number of transformer turns from the disc pair model. Therefore, we could know $d = \frac{n}{2}$. As for the formulas below, $C_{dr} = \frac{n}{6} * C_d$.

$$E_{tot_{disc-disc}} = \frac{1}{2} * C_{dr} * V^2 = \frac{n}{12} * C_d * V^2$$
$$C_{series-dd} = C_{dr} = \frac{n}{6} * C_d$$

In order to obtain the analytical formula for the total turn-turn series capacitance C_{tr}, only the energy summation method needs to be taken into account. The critical assumption from [1] should be used again: the voltage drop per transformer turn should be equal and the voltages for the transformer turns would only focus at the midpoint. n is the total number of transformer turns from the disc pair model. There are actually (n-2) turn-turn series capacitance C_{tt} located within one disc pair model.

$$E_{tot_{turn-turn}} = \frac{1}{2} * C_{tr} * V^2 = (n-2) * \frac{1}{2} * C_{tt} * (\frac{V}{n})^2$$
$$C_{series-tt} = C_{tr} = \frac{n-2}{n^2} * C_{tt}$$

5.2 The series capacitance of disc pair model with one electrostatic inter-shield pair

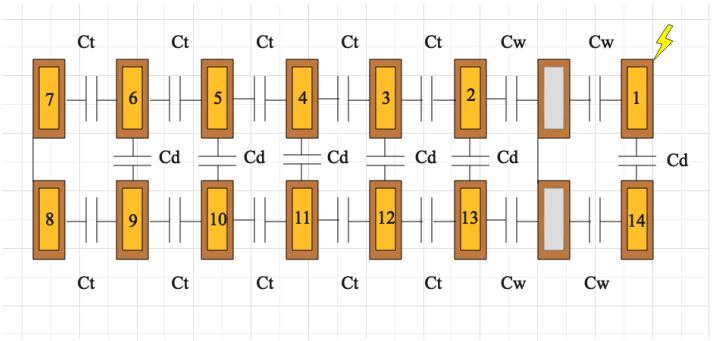

Figure 8. Disc pair model with one electrostatic inter-shield pair

According to figure 8, it is obvious that after applying one floating electrostatic inter-shield pair to the disc pair model, the number of the turn-turn series capacitance C_{tt} would become (n-4). Moreover, one electrostatic inter-shield pair would occupy two places for C_{tt} but bring another four turn-shield capacitances C_{ts} to the disc pair model. With respect to this case, the energy summation method should also be used to calculate the total series capacitance C_{s1}.

$$E_{tot_{turn-turn}} = \frac{1}{2} * C_{tt} * (\frac{V}{n})^2 * (n-4)$$
$$C_{series-tt} = \frac{n-4}{n^2} * C_{tt}$$

The voltage for the floating electrostatic inter-shield wire is actually $V_{sh} = \frac{V}{2}$, which could be verified through Comsol modelling. According to figure 10, if the magnitude of the input voltage is 2000V and that of the output voltage is 1000V, the resulted voltage of the inter-shield wire is around 1495.5V, which is almost the average value for the sum of the input and output voltage. For simplification, C_{tt} is assumed to be equal to C_{ts} and $C_t = C_{tt} = C_{ts}$.

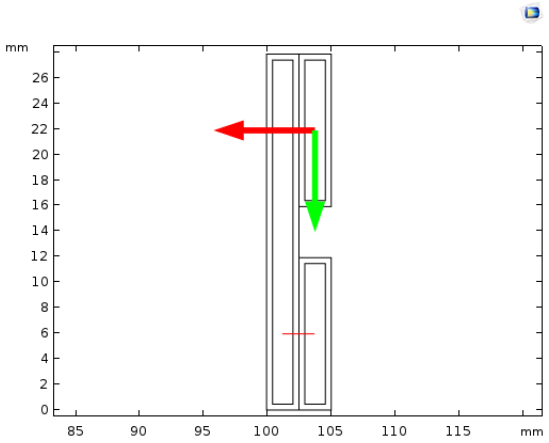

Figure 9. V-sh cut-lines

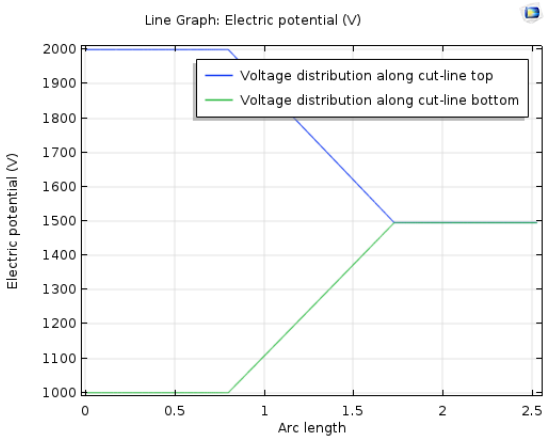

Figure 10. V-sh voltage distribution (mm)

$$E_{tot_{turn-shield}} = 2 * \frac{1}{2} * C_{ts} * (\frac{V}{2})^2 + 2 * \frac{1}{2} * C_{ts} * (\frac{V}{n} - \frac{V}{2})^2$$

$$C_{series-ts} = \frac{n^2 - 2n + 2}{n^2} * C_{ts}$$

$$C_{s1} = \frac{n^2 - n - 2}{n^2} * C_t + \frac{n}{6} * C_d$$

5.3 The series capacitance of disc pair model with two electrostatic inter-shield pairs

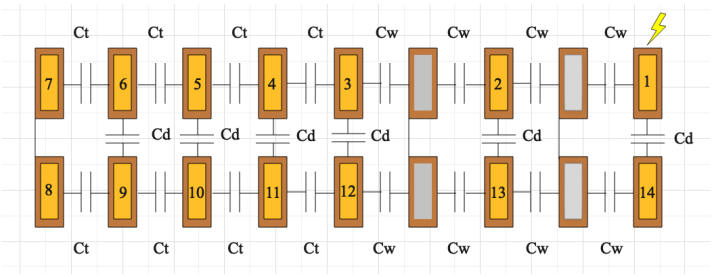

Figure 11. Disc pair model with two electrostatic inter-shield pairs

After introducing two floating electrostatic inter-shield pairs to the disc pair model shown in figure 11, the number of C_{tt}, which is the turn-turn series capacitance would become (n-6). Meanwhile, additional eight turn-shield series capacitance C_{ts} would be generated because every electrostatic inter-shield pair could consequently bring four turn-shield series capacitances.

$$E_{tot_{turn-turn}} = \frac{1}{2} * C_{tt} * (\frac{V}{n})^2 * (n - 6)$$

$$C_{series-tt} = \frac{n - 6}{n^2} * C_{tt}$$

The voltage for those floating electrostatic inter-shield wires is $V_{sh} = \frac{V}{2}$. For simplification, we could also assume that $C_{tt} = C_{ts} = C_t$. However, in [6], the total series capacitance of the disc pair model inter-shielded by two electrostatic inter-shield pairs C_s is derived as $C_s = \frac{2n^2-8n+6}{n^2} + \frac{n}{6} * C_d$, which is different from the outcome below.

$$E_{tot_{turn-shield}} = 2 * \frac{1}{2} * C_{ts} * (\frac{V}{2})^2 + 4 * \frac{1}{2} * C_{ts} * (\frac{V}{2} - \frac{V}{n})^2 + 2 * \frac{1}{2} * C_{ts} * (\frac{V}{2} - \frac{2V}{n})^2$$

$$C_{series-ts} = \frac{2n^2 - 8n + 12}{n^2} * C_{ts}$$

$$C_{s1} = \frac{2n^2 - 7n + 6}{n^2} * C_t + \frac{n}{6} * C_d$$

5.4 The series capacitance of the disc pair model with k electrostatic inter-shield pairs

Actually, k is the exact number of the electrostatic inter-shield pairs inserted inside the disc pair model. The magnitude of the voltage for the electrostatic shields is fixed, which is $V_{sh} = \frac{V}{2}$. The total electric energy stored in the disc pair model can be calculated by the equation below.

$$E_{tot} = E_{tot_{turn-turn}} + E_{tot_{turn-shield}} + E_{tot_{disc-disc}}$$

As for this case, the total electric energy stored in the capacitances between the discs is almost the same as that for the continuous disc pair, which is $C_{series-dd} = \frac{n}{6} * C_d$. The total electric energy stored in the turn-turn series capacitance C_{tt} depends on the number of that type of series capacitance. After introducing k electrostatic inter-shield pairs to the model, the number of C_{tt} would decrease from (n-2) to (n-2k-2). Additionally, the voltage drop per transformer turn should become $\Delta V = \frac{V}{n}$.

$$E_{tot_{turn-turn}} = \frac{1}{2} * C_{tt} * (\frac{V}{n})^2 * (n - 2 - 2k) = \frac{V^2}{2} * C_{tt} * \frac{n - 2 - 2k}{n^2}$$

$$C_{series-tt} = C_{tt} * \frac{n - 2k - 2}{n^2}$$

According to figure 12, if one electrostatic inter-shield pair is introduced to the disc pair model, four additional turn-shield capacitances C_{ts} would be generated. C_{ts-m} indicates the total series capacitance of the four C_{ts} generated by the m^{th} electrostatic inter-shield pair. Moreover, the energy summation method could be used to calculated the electric energy.

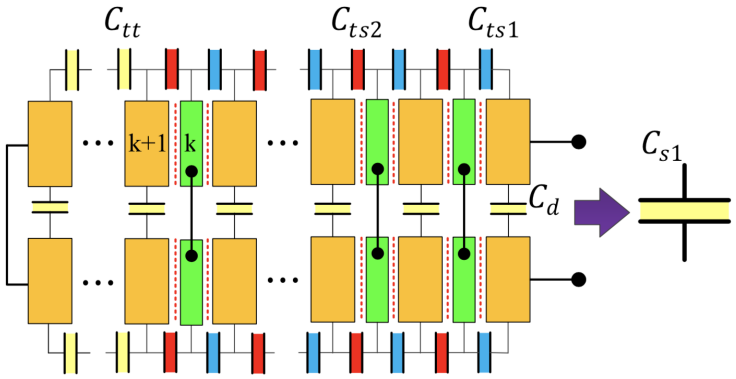

Figure 12. Disc pair model inter-shielded by k electrostatic shield pairs

$$E_{ts-m} = \frac{1}{2} * C_{ts} * ((V_{sh} - (V - \frac{m-1}{n} * V))^2 + (V_{sh} - (V - \frac{m}{n} * V))^2 + (V_{sh} - \frac{m-1}{n} * V)^2 + (V_{sh} - \frac{m}{n} * V)^2)$$

$$= \frac{1}{2} * C_{ts} * 2 * V^2 * ((\frac{n - 2m + 2}{2n})^2 + (\frac{n - 2m}{2n})^2)$$

$$C_{ts-m} = \frac{C_{ts}}{n^2} * \{(n - 2m + 2) * (n - 2m) + 2\}$$

The total electric energy stored in the series capacitances between electrostatic inter-shield wires and transformer turns $E_{tot_{turn-shield}}$ is given in the first formula below. The total series capacitance between the inter-shield wires and transformer turns $C_{series-ts}$ is given in the second formula below.

$$E_{tot_{turn-shield}} = \sum_{m=1}^{k} E_{ts-m} = \frac{1}{2} * C_{series-ts} * V^2$$

$$C_{series-ts} = \frac{C_{ts}}{n^2} * \sum_{m=1}^{k} \{(n-2m+2)*(n-2m)+2\}$$

The analytical formula for the total series capacitance of the disc pair model inter-shielded by k electrostatic shield pairs is shown as below. The inter-shielded disc pair model could be regarded as a capacitor which contains the same amount of electric energy as the disc pair model.

$$C_{s1} = C_{series-dd} + C_{series-tt} + C_{series-ts} = \frac{n}{6} * C_d + C_{tt} * \frac{n-2k-2}{n^2} + \frac{C_{ts}}{n^2} * \sum_{m=1}^{k} \{(n-2m+2)*(n-2m)+2\}$$

Theoretically, this section has provided us a general analytical formula for the total series capacitance with arbitrary number of the electrostatic inter-shield pairs. For k=1 and k=2, we could use this analytical formula to verify the results above.

5.5 The series capacitance of the disc pair model with k wound-in inter-shield pairs

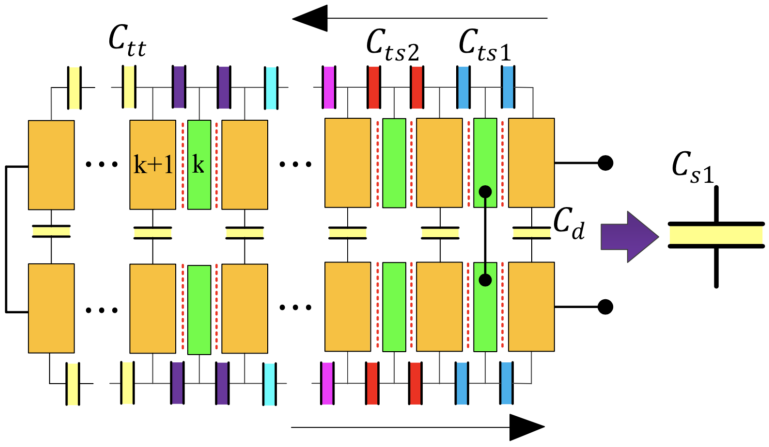

Figure 13. Disc pair model inter-shielded by k wound-in inter-shield pairs

As for the case with k wound-in inter-shield pairs, according to figure 13, it is obvious that the rightmost inter-shield wires from upper disc and bottom disc are bonded together at the cross-point. The voltage distribution trend for inter-shield wires from upper disc is considered to become the same as that for transformer turns. The same is also applicable to the inter-shield wires from the bottom disc, with the difference that for the bottom disc when the discs are made, the transformer turns and shield wires are wrapped from left to right.

As a result, the voltages for the inter-shield wires from upper transformer disc would decrease from rightmost to leftmost and the ones from bottom disc would increase from rightmost to leftmost. The voltage drop per inter-shield wire is $\Delta V_{shield} = \frac{V}{n}$. Furthermore, in case of the floating cross-point, the voltage for the cross-point is $V_{cross} = \frac{V}{2}$, which is the average value of the input and output voltage. If the cross-point is connected to the input lead of the top transformer disc, the voltage for the cross-point would then become $V_{cross} = V$, which is equal to the input voltage.

The total electric energy stored in the turn-shield capacitances C_{ts} introduced by the m^{th} wound-in inter-shield pair is shown as below and k is the total number of the wound-in inter-shield pairs.

$$
\begin{aligned}
E_{ts-m-upper} &= \frac{1}{2} * C_{ts} * \left\{ (V_{cross} - \frac{m-1}{n} * V) - (V - \frac{m-1}{n} * V) \right\}^2 \\
&+ \frac{1}{2} * C_{ts} * \left\{ (V_{cross} - \frac{m-1}{n} * V) - (V - \frac{m}{n} * V) \right\}^2 \\
E_{ts-m-bottom} &= \frac{1}{2} * C_{ts} * \left\{ (V_{cross} + \frac{m-1}{n} * V) - \frac{m-1}{n} * V \right\}^2 + \frac{1}{2} * C_{ts} * \left\{ (V_{cross} + \frac{m-1}{n} * V) - \frac{m}{n} * V \right\}^2 \\
E_{ts-m} &= E_{ts-m-upper} + E_{ts-m-bottom} \\
E_{ts-m} &= \frac{1}{2} * C_{ts} * \left\{ (V_{cross} - V)^2 + (V_{cross} - V + \frac{V}{n})^2 + V_{cross}^2 + (V_{cross} - \frac{V}{n})^2 \right\}
\end{aligned}
$$

From the analytical formulas above, it is quite clear that the electric energy E_{ts-m} is independent from m. Thus, the total electric energy stored in the turn-shield capacitance C_{ts} could be derived as below.

$$
E_{turn-shield} = k * \frac{1}{2} * C_{ts} * \left\{ (V_{cross} - V)^2 + (V_{cross} - V + \frac{V}{n})^2 + V_{cross}^2 + (V_{cross} - \frac{V}{n})^2 \right\}
$$

If the cross-point is connected to the input lead, then $V_{cross} = V$. Here, V_{cross} has the same value as the input voltage. The total electric energy stored in turn-shield capacitances $E_{turn-shield}$ and the total turn-shield series capacitance $C_{series-ts}$ could be derived as below.

$$
\begin{aligned}
E_{turn-shield} &= \frac{k}{2} * C_{ts} * \left\{ (\frac{V}{n})^2 + V^2 + (V - \frac{V}{n})^2 \right\} \\
C_{series-ts} &= k * \frac{2n^2 - 2n + 2}{n^2} * C_{ts}
\end{aligned}
$$

If the cross-point of the rightmost inter-shield pair is floating, then $V_{cross} = \frac{V}{2}$. Here, V_{cross} is equal to the average value of the input and output voltage of the inter-shielded disc pair model. The total electric energy stored in turn-shield capacitances $E_{turn-shield}$ and the total turn-shield series capacitance $C_{series-ts}$ could be derived as below.

$$
\begin{aligned}
E_{turn-shield} &= \frac{k}{2} * C_{ts} * 2 * \left\{ (\frac{V}{2})^2 + (\frac{V}{2} - \frac{V}{n})^2 \right\} \\
C_{series-ts} &= k * \frac{n^2 - 2n + 2}{n^2} * C_{ts}
\end{aligned}
$$

As a result, the analytical formula for the total series capacitance of the disc pair model inter-shielded by k wound-in shield pairs if the cross-point is connected to the input terminal C_{s1} is shown as the first equation below. Similarly, the analytical formula for the total series capacitance inter-shielded by k wound-in shield pairs if the cross-point is floating C_{s2} would be derived as the second equation below.

$$
\begin{aligned}
C_{s1} &= k * \frac{2n^2 - 2n + 2}{n^2} * C_{ts} + \frac{n - 2k - 2}{n^2} * C_{tt} + \frac{n}{6} * C_d \\
C_{s2} &= k * \frac{n^2 - 2n + 2}{n^2} * C_{ts} + \frac{n - 2k - 2}{n^2} * C_{tt} + \frac{n}{6} * C_d
\end{aligned}
$$

5.5.1 The general expression for E_{ts-m}

Actually, based on the analytical formulas above, we could know that the total series capacitances C_{s1} and C_{s2} are independent from the input and output voltage. Whereas, the derivation processes in the subsection 5.5 might cause some misunderstanding to the public, which is about whether these analytical formulas are only suitable for the disc pair model when the last transformer turn is grounded. Therefore, a more general derivation process for E_{ts-m} is needed.

With respect to the more general case, V_1 represents for the input voltage of the disc pair model and V_2 represents for the output voltage. Therefore, the entire voltage drop on the disc pair model is $V_1 - V_2$.

$$
\begin{aligned}
E_{ts-m-upper} &= \frac{1}{2} * C_{ts} * \left\{ (V_{cross} - \frac{m-1}{n} * (V_1 - V_2)) - (V_1 - \frac{m-1}{n} * (V_1 - V_2)) \right\}^2 \\
&+ \frac{1}{2} * C_{ts} * \left\{ (V_{cross} - \frac{m-1}{n} * (V_1 - V_2)) - (V_1 - \frac{m}{n} * (V_1 - V_2)) \right\}^2 \\
E_{ts-m-bottom} &= \frac{1}{2} * C_{ts} * \left\{ (V_{cross} + \frac{m-1}{n} * (V_1 - V_2)) - (V_2 + \frac{m-1}{n} * (V_1 - V_2)) \right\}^2 \\
&+ \frac{1}{2} * C_{ts} * \left\{ (V_{cross} + \frac{m-1}{n} * (V_1 - V_2)) - (V_2 + \frac{m}{n} * (V_1 - V_2)) \right\}^2 \\
E_{ts-m} &= E_{ts-m-upper} + E_{ts-m-bottom} = \frac{1}{2} * C_{series-ts} * (V_1 - V_2)^2 \\
E_{ts-m} &= \frac{1}{2} * C_{ts} * \left\{ (V_{cross} - V_1)^2 + (V_{cross} - V_1 + \frac{V_1 - V_2}{n})^2 + (V_{cross} - V_2)^2 + (V_{cross} - V_2 - \frac{V_1 - V_2}{n})^2 \right\} \\
&= \frac{1}{2} * C_{ts-m} * (V_1 - V_2)^2
\end{aligned}
$$

According to the last formula above, we could obtain the equation for C_{ts-m} with two variables V_1 and V_2. After typing that equation in Matlab and changing the values for V_1 and V_2, the magnitude for C_{ts-m} would remain constant. Thus, the results from the subsection 5.5 are rather convincing–the magnitudes of total series capacitance C_{s1} and C_{s2} are independent from input and output voltage.

6 The verification processes between the results calculated from analytical and numerical method

In chapter four, all of the analytical formulas are derived based on two critical assumptions mentioned in [1]. The first assumption is that the voltage would only focus on the midpoint of the transformer turn or inter-shield wire. The second assumption is that the voltage would distribute linearly along the disc pair model at the frequency range of 1MHz. Therefore, the voltage drop per transformer turn or inter-shield wire would become $\Delta V_{turn} = \Delta V_{shield} = \frac{V}{n}$ under this condition.

However, in Comsol, the voltage would focus on the surface of the transformer turn or inter-shield wire rather than the midpoint. Thus, the voltage drop per transformer turn or shield would then be modified to $\Delta V_{turn} = \Delta V_{shield} = \frac{V}{n-1}$. In order to deliver an accurate verification, the analytical formulas from chapter four should be re-derived as below.

6.1 Series capacitance with k electrostatic inter-shield pairs

The total electric energy stored in the turn-turn series capacitance C_{tt} could be derived as the first formula below. In addition, the total turn-turn series capacitance $C_{series-tt}$ could also be derived based on the formula related to the electric energy.

$$E_{tot_{turn-turn}} = \frac{1}{2} * C_{tt} * (\frac{V}{n-1})^2 * (n-2k-2) = \frac{V^2}{2} * C_{tt} * \frac{n-2k-2}{(n-1)^2}$$
$$C_{series-tt} = C_{tt} * \frac{n-2k-2}{(n-1)^2}$$

The electric energy stored in the turn-shield series capacitances C_{ts} brought by the m^{th} electrostatic inter-shield pair could be derived as the first formula below. The analytical formula of the total turn-shield series capacitance C_{ts-m} is shown as the second formula below.

$$E_{ts-m} = \frac{1}{2} * C_{ts} * (\left\{V_{sh} - (V - \frac{m-1}{n-1} * V)\right\}^2 + \left\{V_{sh} - (V - \frac{m}{n-1} * V)\right\}^2 + (V_{sh} - \frac{m-1}{n-1} * V)^2$$
$$+ (V_{sh} - \frac{m}{n-1} * V)^2) = \frac{1}{2} * C_{ts} * 2 * V^2 * \left\{\frac{(n-2m)^2 + 1}{2(n-1)^2}\right\}$$
$$C_{ts-m} = \frac{C_{ts}}{(n-1)^2} * \left\{(n-2m)^2 + 1\right\}$$

The total electric energy stored in the capacitances between electrostatic inter-shield wires and transformer turns $E_{tot_{turn-shield}}$ is given in the first formula below. The total series capacitance between the inter-shield wires and the transformer turns $C_{series-ts}$ is given in the second formula below.

$$E_{tot_{turn-shield}} = \sum_{m=1}^{k} E_{ts-m} = \frac{1}{2} * C_{series-ts} * V^2$$
$$C_{series-ts} = \frac{C_{ts}}{(n-1)^2} * \sum_{m=1}^{k} \left\{(n-2m)^2 + 1\right\}$$
$$C_{s1} = \frac{C_{ts}}{(n-1)^2} * \sum_{m=1}^{k} \left\{(n-2m)^2 + 1\right\} + C_{tt} * \frac{n-2k-2}{(n-1)^2} + \frac{n}{6} * C_d$$

6.2 Series capacitance with k wound-in shields under numerical condition

The total electric energy stored in the turn-shield series capacitances introduced by the m^{th} wound-in inter-shield pair is derived as below and k is the total number of the wound-in inter-shield pairs.

$$
\begin{aligned}
E_{ts-m-upper} &= \frac{1}{2} * C_{ts} * \left\{ (V_{cross} - \frac{m-1}{n-1} * V) - (V - \frac{m-1}{n-1} * V) \right\}^2 \\
&+ \frac{1}{2} * C_{ts} * \left\{ (V_{cross} - \frac{m-1}{n-1} * V) - (V - \frac{m}{n-1} * V) \right\}^2 \\
E_{ts-m-bottom} &= \frac{1}{2} * C_{ts} * \left\{ (V_{cross} + \frac{m-1}{n-1} * V) - \frac{m-1}{n-1} * V \right\}^2 + \frac{1}{2} * C_{ts} * \left\{ (V_{cross} + \frac{m-1}{n-1} * V) - \frac{m}{n-1} * V \right\}^2 \\
E_{ts-m} &= E_{ts-m-upper} + E_{ts-m-bottom} \\
E_{ts-m} &= \frac{1}{2} * C_{ts} * \left\{ (V_{cross} - V)^2 + (V_{cross} - V + \frac{V}{n-1})^2 + V_{cross}^2 + (V_{cross} - \frac{V}{n-1})^2 \right\}
\end{aligned}
$$

From the analytical formulas above, we could know that the electric energy E_{ts-m} is independent from m. Thus, the total electric energy stored in the turn-shield series capacitances C_{ts} could be derived as below.

$$
E_{turn-shield} = k * \frac{1}{2} * C_{ts} * \left\{ (V_{cross} - V)^2 + (V_{cross} - V + \frac{V}{n-1})^2 + V_{cross}^2 + (V_{cross} - \frac{V}{n-1})^2 \right\}
$$

If the cross-point is connected to the input terminal, then $V_{cross} = V$. Here, V_{cross} is equal to the input voltage. The total electric energy stored in turn-shield series capacitances $E_{turn-shield}$ and total series capacitance C_{s2} under this condition could be derived as below.

$$
\begin{aligned}
E_{turn-shield} &= \frac{k}{2} * C_{ts} * \left\{ (\frac{V}{n-1})^2 + V^2 + (V - \frac{V}{n-1})^2 \right\} \\
C_{series-ts} &= k * \frac{2n^2 - 6n + 6}{(n-1)^2} * C_{ts} \\
C_{s1} &= k * \frac{2n^2 - 6n + 6}{(n-1)^2} * C_{ts} + C_{tt} * \frac{n - 2k - 2}{(n-1)^2} + \frac{n}{6} * C_d
\end{aligned}
$$

If the cross-point of the rightmost inter-shield pair is floating, then $V_{cross} = \frac{V}{2}$. Here, V_{cross} is equal to the average value of the input and output voltage of the disc pair model. The total electric energy stored in the turn-shield series capacitances $E_{turn-shield}$ and total series capacitance $C_{series-ts}$ under this condition could be derived as the formulas below.

$$
\begin{aligned}
E_{turn-shield} &= \frac{k}{2} * C_{ts} * 2 * \left\{ (\frac{V}{2})^2 + (\frac{V}{2} - \frac{V}{n-1})^2 \right\} \\
C_{series-ts} &= k * \frac{n^2 - 4n + 5}{n - 1^2} * C_{ts} \\
C_{s2} &= k * \frac{n^2 - 4n + 5}{(n-1)^2} * C_{ts} + C_{tt} * \frac{n - 2k - 2}{(n-1)^2} + \frac{n}{6} * C_d
\end{aligned}
$$

6.2.1 The general expression for E_{ts-m}

With respect to the more general case, V_1 represents for the input voltage of the disc pair model and V_2 represents for the output voltage. Therefore, the total voltage drop on the disc pair model is $V_1 - V_2$.

$$E_{ts-m-upper} = \frac{1}{2} * C_{ts} * \left\{ (V_{cross} - \frac{m-1}{n-1} * (V_1 - V_2)) - (V_1 - \frac{m-1}{n-1} * (V_1 - V_2)) \right\}^2$$
$$+ \frac{1}{2} * C_{ts} * \left\{ (V_{cross} - \frac{m-1}{n-1} * (V_1 - V_2)) - (V_1 - \frac{m}{n-1} * (V_1 - V_2)) \right\}^2$$
$$E_{ts-m-bottom} = \frac{1}{2} * C_{ts} * \left\{ (V_{cross} + \frac{m-1}{n-1} * (V_1 - V_2)) - (V_2 + \frac{m-1}{n-1} * (V_1 - V_2)) \right\}^2$$
$$+ \frac{1}{2} * C_{ts} * \left\{ (V_{cross} + \frac{m-1}{n-1} * (V_1 - V_2)) - (V_2 + \frac{m}{n-1} * (V_1 - V_2)) \right\}^2$$
$$E_{ts-m} = E_{ts-m-upper} + E_{ts-m-bottom} = \frac{1}{2} * C_{series-ts} * (V_1 - V_2)^2$$
$$E_{ts-m} = \frac{1}{2} * C_{ts} * \left\{ (V_{cross} - V_1)^2 + (V_{cross} - V_1 + \frac{V_1 - V_2}{n-1})^2 + (V_{cross} - V_2)^2 + (V_{cross} - V_2 - \frac{V_1 - V_2}{n-1})^2 \right\}$$

6.3 Small scale continuous disc pair model with oil-impregnated paper shield

The verification between the results obtained from the numerical and analytical method could be done based on the critical assumption that the voltage would distribute linearly along the disc pair model at the frequency range of 1MHz. The voltage values for their corresponding transformer turns could be successfully calculated after the application of this assumption.

With respect to the disc pair model built in Comsol Multiphysics, the first transformer turn is connected to the input terminal whose voltage is V_1 and the last transformer turn is grounded. In addition, the transformer iron core is ungrounded, which could eliminate the influence of the ground capacitance C_g. After applying the voltage values to their corresponding transformer turns, the total series capacitance C_s could be directly calculated through the surface integration operation. From the numerical method, we could obtain the results that $C_{small-region} = 260.41pF$, $C_{large-region} = 322.83pF$. $C_{large-region}$ represents for the total series capacitance of the disc pair model that concludes the additional capacitance C_a caused by fringing effect and $C_{small-region}$ is the total series capacitance of the disc pair model that excludes C_a.

In fact, $C_{small-region}$ is calculated based on the total electric energy E_{small} stored in the integration box colored blue, which is shown in figure 14. Also, $C_{large-region}$ is calculated referring to the electric energy E_{large} stored in the entire region colored blue, which is shown in figure 15.

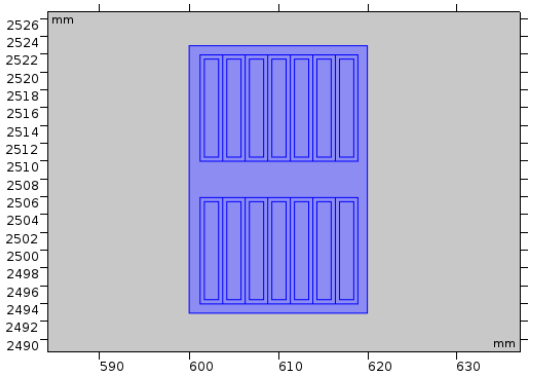

Figure 14. Figure for the small region

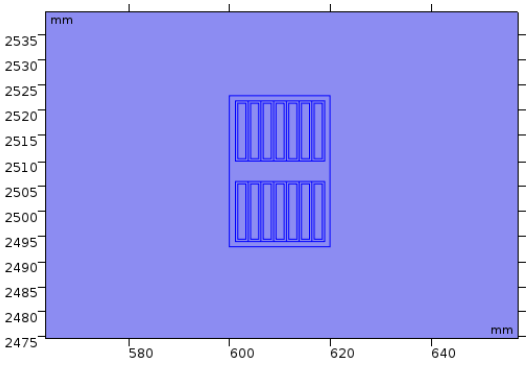

Figure 15. Figure for the large region

In Comsol, the voltage values are considered to concentrate on the surface of the transformer turns rather than the midpoint. Thus, in order to properly have the comparison of the results obtained from analytical and numerical method, the modified analytical formulas in the subsection 6.1 and 6.2 should be selected.

With respect to the geometry of the disc pair model, there are actually seven transformer turns per disc $n = 14$. The average radius of the disc pair model is $R_{ave} = 610.09mm$, the inner and outer radius are $R_{inner} = 601.235mm$ and $R_{outer} = 618.945mm$. The distance between two adjacent transformer turns is $\tau_c = 0.93mm$ and the distance between two discs is $d_{oil} = 5mm$, the height of the transformer turn is $h = 11mm$.

During the calculation of $C_{small-region}$ in Comsol Multiphysics, some fringing effect is still taken into account, because the integration box shown in figure 14 is a little away from the conductors (disc pair model). Therefore, if the analytical formulas are used to do the verification, during the calculation of C_{tt}, the height of the transformer turn should be replaced by $(h + \tau)$ in order to include some of C_a caused by fringing effect. Whereas, in [1], as for the analytical formula for the calculation of C_{tt}, the height of the transformer turn is considered to become $(h + 2 * \tau_c)$ in order to comprise all of the C_a. After the acquisition of those values, the total series capacitance calculated by the selected analytical formulas could be shown as below. C_{s1} is the total series capacitance that conclude the some of the additional capacitance C_a caused by fringing effect.

There is no doubt that the difference between the outcomes obtained from numerical and analytical method would always exists due to the presence of the other mutual capacitances. The results calculated by the analytical formulas only comprise the influential capacitances. Whereas, the results obtained from Comsol Multiphysics comprise the entire capacitance matrix.

$$
\begin{aligned}
C_{tt} &= \frac{2\pi * \varepsilon_0 * \varepsilon_{r-paper} * R_{ave} * (h + \tau_c)}{\tau_c} = 1741.530pF \\
C_{dd-tot} &= \frac{n}{2} * C_{dd} = \frac{\pi * \varepsilon_0 * (R_{outer}^2 - R_{inner}^2)}{\frac{\tau_c}{\varepsilon_{r-paper}} + \frac{d_{oil}}{\varepsilon_{r-oil}}} = 239.930pF \\
C_{series-dd} &= \frac{n}{6} * C_{dd} = \frac{1}{3} * C_{dd-tot} = 79.98pF \\
C_{series-tt} &= \frac{n-2}{(n-1)^2} * C_{tt} = 123.66pF \\
C_{s1} &= C_{series-tt} + C_{series-dd} = 203.64pF
\end{aligned}
$$

After having the values for analytical and numerical method, we could observe the capacitance difference due to the presence of the other mutual capacitance from $\Delta C_1 = 56.77pF$. Moreover, the total additional capacitance C_a generated by the fringing effect could be calculated through $C_a = C_{large-region} - C_{small-region} = 62.42pF$

$$
\begin{aligned}
\Delta C_1 &= C_{small-region} - C_{s1} = 260.41 - 203.64 = 56.77pF \\
C_a &= C_{large-region} - C_{small-region} = 322.83 - 260.41 = 62.42pF
\end{aligned}
$$

6.4 Large scale continuous disc pair model covered by oil-impregnated paper shield

As for the disc pair model shown in figure 16, there are 60 transformer turns per disc $n = 120$ and the transformer iron core is ungrounded. Therefore, the total series capacitance of the disc pair model C_s could be directly obtained through the surface integration operation. Based on the numerical analysis, we could obtain that $C_{small-region} = 916.9pF$ and $C_{large-region} = 1005.8pF$. It is worth mentioning that $C_{small-region}$ just comprises of a fraction of C_a generated by the fringing effect but $C_{large-region}$ concludes the total C_a.

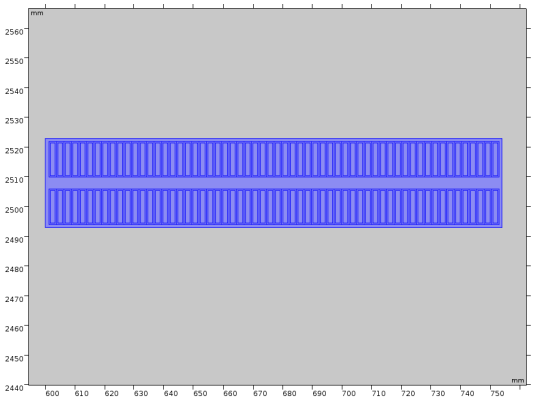

Figure 16. Disc pair model–60 turns per disc

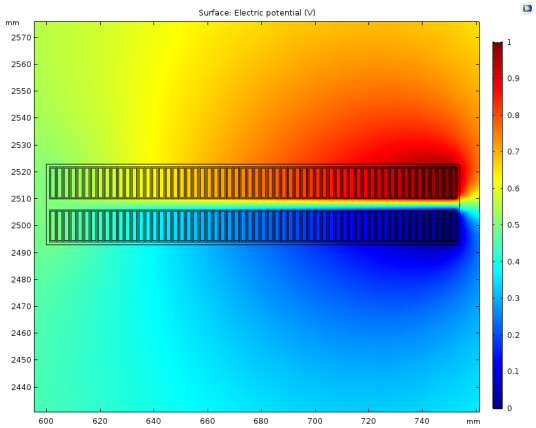

Figure 17. Electric potential distribution

With respect to the analytical method, the basic electric parameters are shown as follows: $R_{outer} = 753.035mm$, $R_{inner} = 601.235mm$, $R_{ave} = 677.135mm$, $\tau_c = 0.93mm$, $d_{oil} = 5mm$ and $h = 11mm$.

$$C_{tt} = \frac{2\pi * \varepsilon_0 * \varepsilon_{r-paper} * R_{ave} * (h + \tau_c)}{\tau_c} = 1932.91pF$$
$$C_{dd-tot} = \frac{n}{2} * C_{dd} = \frac{\pi * \varepsilon_0 * (R_{outer}^2 - R_{inner}^2)}{\frac{\tau_c}{\varepsilon_{r-paper}} + \frac{d_{oil}}{\varepsilon_{r-oil}}} = 2282.544pF$$
$$C_{series-dd} = \frac{n}{6} * C_{dd} = \frac{1}{3} * C_{dd-tot} = 760.85pF$$
$$C_{series-tt} = \frac{n-2}{(n-1)^2} * C_{tt} = 16.11pF$$
$$C_{s1} = C_{series-dd} + C_{series-tt} = 776.96pF$$

After having the outcomes obtained from analytical and numerical method, we could observe the capacitance difference due to the existence of the other mutual capacitance from ΔC_1. The total additional capacitance C_a generated by the fringing effect for the model shown in figure 16 could be calculated through $C_a = C_{large-region} - C_{small-region} = 88.90pF$.

$$\Delta C_1 = C_{small-region} - C_{s1} = 916.9 - 776.96 = 139.94pF$$
$$C_a = C_{large-region} - C_{small-region} = 1005.8 - 916.9 = 88.90pF$$

6.5 20 turns per continuous disc without paper shield

With respect to the disc pair model shown in figure 18, the total number of the transformer turns within this model is $n = 40$. After applying the voltage values to their corresponding transformer turns, the total series capacitance could be finally obtained through the surface integration operation: $C_{small-region} = 307.46pF$ and $C_{large-region} = 380.21pF$.

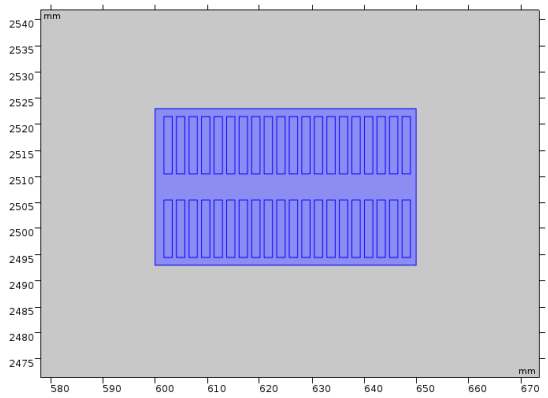

Figure 18. Disc pair model–20 turns per disc

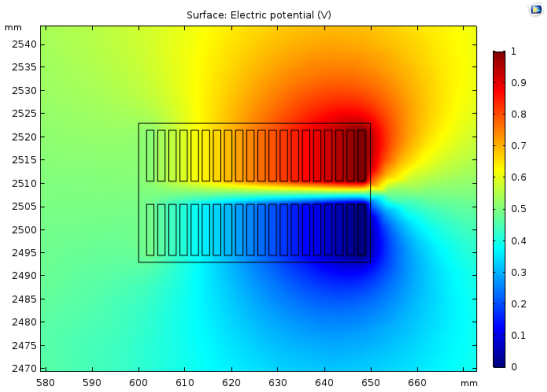

Figure 19. Electric potential distribution

The basic electric parameters of this case are shown as follows: $R_{outer} = 648.9mm$, $R_{inner} = 601.7mm$, $R_{ave} = 625.3mm$ and $d_{oil} = 5mm$ and $\tau = 0.8mm$. It is worth mentioning that the results obtained from analytical method don't consider the other series capacitances (Only the series capacitances between adjacent transformer turns C_{tt} and the individual disc-disc series capacitances C_{dd} are taken into account). However, the results obtained from the numerical method comprise of the entire capacitance matrix.

$$C_{tt} = \frac{2\pi * \varepsilon_0 * \varepsilon_{r-oil} * R_{ave} * (h+\tau)}{\tau} = 1128.81pF$$
$$C_{dd-tot} = \frac{n}{2} * C_{dd} = \frac{\pi * (R_{outer}^2 - R_{inner}^2) * \varepsilon_0 * \varepsilon_{r-oil}}{d_{oil}} = 722.44pF$$
$$C_{series-dd} = \frac{n}{6} * C_{dd} = \frac{1}{3} * C_{dd-tot} = 240.81pF$$
$$C_{series-tt} = \frac{n-2}{(n-1)^2} * C_{tt} = 28.20pF$$
$$C_{s1} = C_{series-tt} + C_{series-dd} = 269.01pF$$

After having the results obtained from analytical and numerical method, we could observe the capacitance difference ΔC due to the presence of the other mutual capacitance from ΔC_1 and the total additional capacitance C_a induced by the fringing effect.

$$\Delta C_1 = C_{small-region} - C_{s1} = 307.46 - 269.01 = 38.45pF$$
$$C_a = C_{large-region} - C_{small-region} = 380.21 - 307.46 = 72.75pF$$

6.6 30 turns per continuous disc without paper shield

As for the disc pair model shown in figure 20, the total number of the transformer turns inside the disc pair model is $n = 60$. After applying the voltage values to their corresponding transformer turns manually, the total series capacitance C_{s1} could be successfully obtained through the surface integration: $C_{small-region} = 444.10pF$ and $C_{large-region} = 509.96pF$.

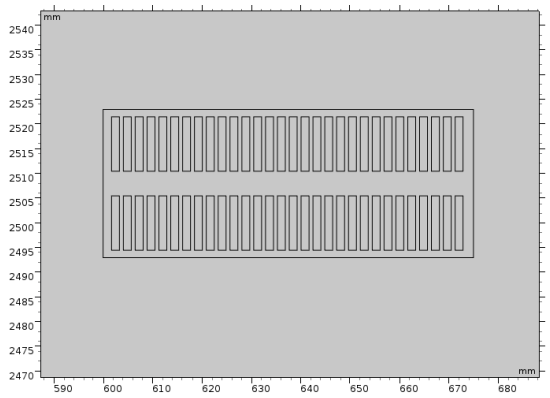

Figure 20. Disc pair model–30 turns per disc

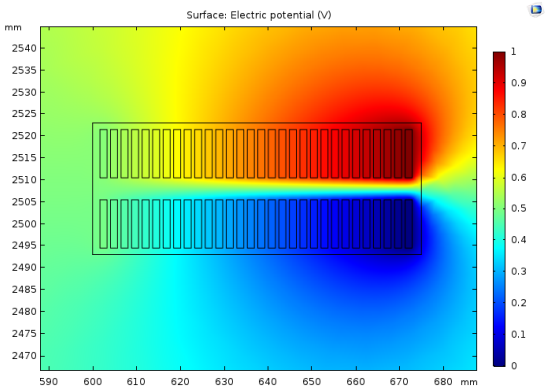

Figure 21. Electric potential distribution

The electric parameters of this disc pair model are shown as follows: $R_{outer} = 672.9mm$, $R_{inner} = 601.7mm$, $R_{ave} = 637.3mm$ and $d_{oil} = 5mm$. Moreover, the distance between two adjacent transformer turns is considered to become $\tau = 0.8mm$.

$$C_{tt} = \frac{2\pi * \varepsilon_0 * \varepsilon_{r-oil} * R_{ave} * (h+\tau)}{\tau} = 1150.48pF$$
$$C_{dd-tot} = \frac{n}{2} * C_{dd} = \frac{\pi * (R_{outer}^2 - R_{inner}^2) * \varepsilon_0 * \varepsilon_{r-oil}}{d_{oil}} = 1110.7pF$$
$$C_{series-dd} = \frac{n}{6} * C_{dd} = \frac{1}{3} * C_{dd-tot} = 370.23pF$$
$$C_{series-tt} = \frac{n-2}{(n-1)^2} * C_{tt} = 19.17pF$$
$$C_{s1} = C_{series-tt} + C_{series-dd} = 389.40pF$$

After having the outcomes for the analytical and numerical method, we could observe the magnitude of the capacitance difference due to the presence of the other mutual capacitance from ΔC_1 below.

$$\Delta C_1 = C_{small-region} - C_{s1} = 444.10 - 389.40 = 54.70pF$$
$$C_a = C_{large-region} - C_{small-region} = 509.96 - 444.10 = 65.86pF$$

6.7 60 turns per continuous disc without paper shield

With respect to the disc pair model shown in figure 22, the distance between the upper disc and lower disc is considered to become $d_{oil=5mm}$ and the distance between two adjacent transformer turns is set to be $\tau = 0.8mm$. The transformer tank is filled with transformer oil $\varepsilon_{r-oil} = 2.2$. Through the surface integration in Comsol Multiphysics, we could know that $C_{small-region} = 873.31pF$ and $C_{large-region} = 958.43pF$.

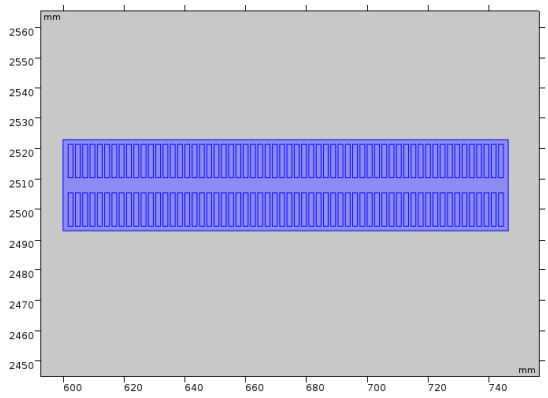

Figure 22. Disc pair model–60 turns per disc

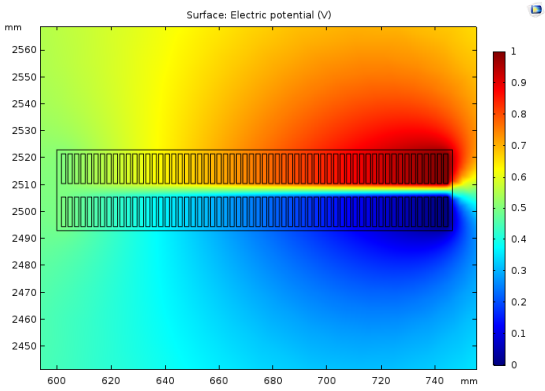

Figure 23. Electric potential distribution

In case of calculating the total series capacitance C_{s1} based on the analytical method, the necessary electric parameters are shown as follows: $R_{outer} = 744.9mm$, $R_{inner} = 601.7mm$ and $R_{ave} = 673.3mm$.

$$C_{tt} = \frac{2\pi * \varepsilon_0 * \varepsilon_{r-oil} * R_{ave} * (h + \tau)}{\tau} = 1215.47pF$$
$$C_{dd-tot} = \frac{n}{2} * C_{dd} = \frac{\pi * (R_{outer}^2 - R_{inner}^2) * \varepsilon_0 * \varepsilon_{r-oil}}{d_{oil}} = 2360.06pF$$
$$C_{series-dd} = \frac{n}{6} * C_{dd} = \frac{1}{3} * C_{dd-tot} = 786.69pF$$
$$C_{series-tt} = \frac{n-2}{(n-1)^2} * C_{tt} = 10.13pF$$
$$C_{s1} = C_{series-tt} + C_{series-dd} = 796.82pF$$

After having the values obtained from analytical and numerical method, we could observe the capacitance difference due to the presence of the other mutual capacitance from ΔC_1.

$$\Delta C_1 = C_{small-region} - C_{s1} = 873.31 - 796.82 = 76.49pF$$
$$C_a = C_{large-region} - C_{small-region} = 958.43 - 873.31 = 85.12pF$$

7 The fringing effect among different disc pair scales

The concept of the fringing effect: Ideally, between two parallel plates, the electric field lines are considered to distribute uniformly. Thus, the capacitance could be calculated as: $C = \frac{\varepsilon_0 * \varepsilon_r * S}{d}$. However, in reality, there would be more electric field lines located at the edge of the parallel plates, which could enlarge the total electric charge Q, $C = \frac{Q}{V}$. Due to the fringing effect, the resulted capacitance in reality is larger than the capacitance calculated by the original formula.

According to the parameters obtained from Royal Smit Transformers, the radius of the transformer core is 532.5mm and the distance between transformer core and hv disc winding is 70mm. In order to find out how the disc pair scale would influence the fringing effect, all of the transformer turns from upper disc should be connected to the high voltage terminal and all of the ones from bottom disc should be connected to ground.

The expected result is that if the number of transformer turns per disc is increased (the scale of the parallel plates is enlarged), the additional capacitance difference rate $C_a\%$ should decrease. The additional capacitance difference rate $C_a\%$ is actually equal to the additional capacitance C_a generated by the fringing effect divided by the total series capacitance $C_{small-region}$.

In this chapter, four types of disc pair scales (5, 20, 30 and 60 transformer turns per disc) are shown in figure 24, figure 26, figure 28 and figure 30 respectively. All of the results are obtained from numerical method. $C_{small-region}$ is the total series capacitance of the disc pair model that ignore most of the influence of fringing effect and $C_{large-region}$ is the total series capacitance obtained when we consider the fringing effect. The value of additional capacitance caused by the fringing effect is equal to $C_a = C_{large-region} - C_{small-region}$.

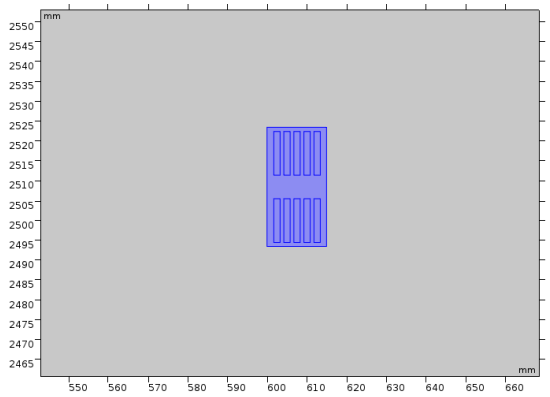

Figure 24. Geometry–5 transformer turns per disc

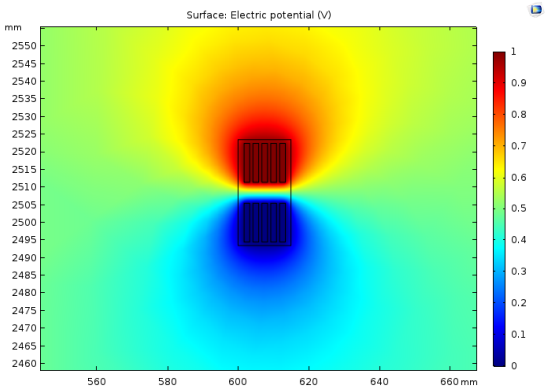

Figure 25. Electric potential distribution

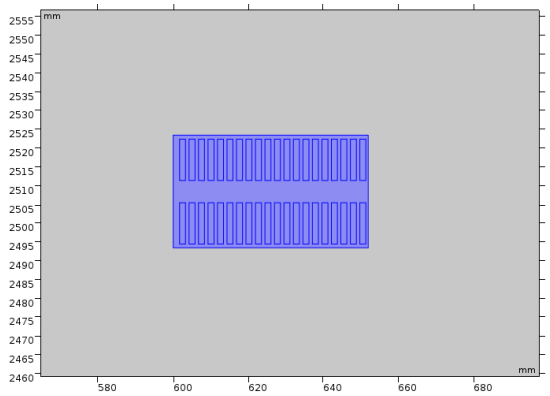

Figure 26. Geometry–20 transformer turns per disc

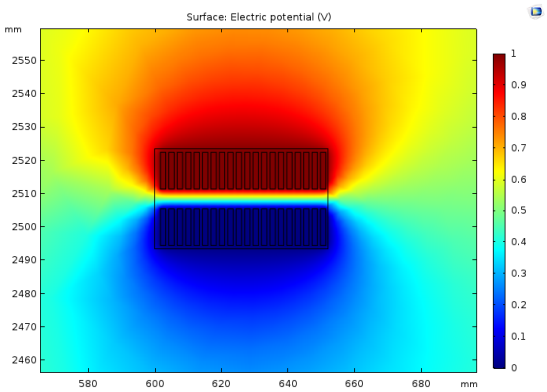

Figure 27. Electric potential distribution

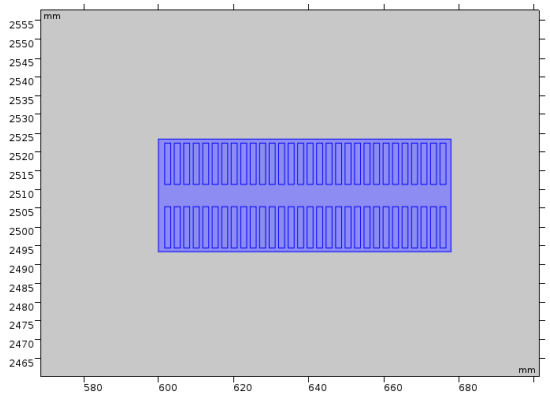

Figure 28. Geometry–30 transformer turns per disc

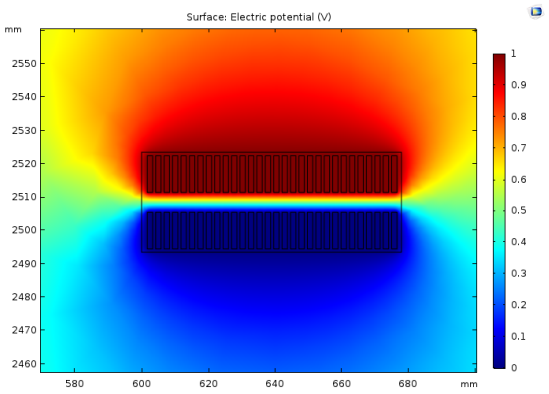

Figure 29. Electric potential distribution

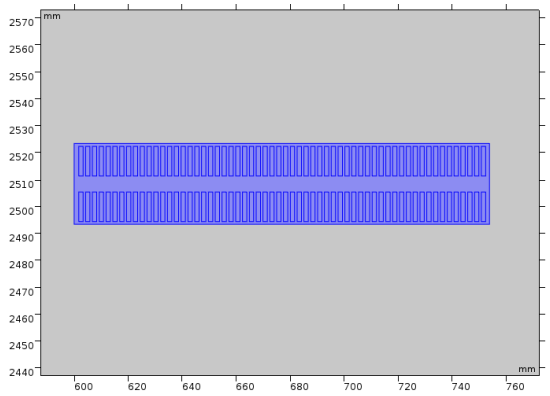

Figure 30. Geometry–60 transformer turns per disc

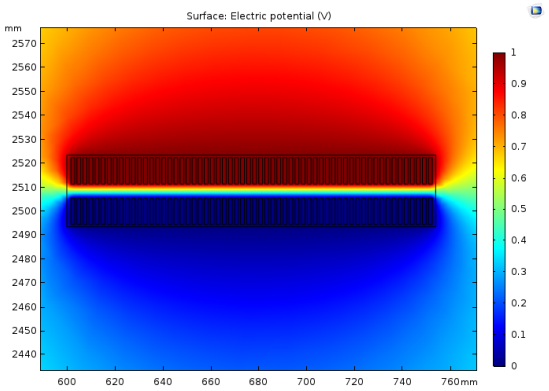

Figure 31. Electric potential distribution

Number of turns per disc	$C_{small-region}$	$C_{large-region}$	C_a	C_a% (compared to $C_{small-region}$)
5 turns	198.69pF	302.14pF	103.45pF	52.07%
20 turns	672.82pF	813.90pF	141.08pF	20.97%
30 turns	1023.7pF	1165.9pF	142.20pF	13.89%
60 turns	2126.6pF	2293.6pF	167.0pF	7.85%

Table 1. The table related to the fringing effect

According to table 1, it is quite obvious that as the number of transformer turns per disc is increased, the additional capacitance generated by the fringing effect C_a would also slightly increase. However, the additional capacitance difference rate C_a% would decrease significantly.

8 The total series capacitance of the interleaved disc pair model

Theoretically, the transformer turns from the disc pair model could be interleaved to increase the total series capacitance C_s and in [3], several types of turn-interleaved methods are provided. Here, only the most original turn-interleaved geometry are considered, which is shown in figure 32. However, nowadays, the large power transformer companies such as Royal Smit Transformers only have the technique to interleave the discs. Figure 33 illustrates the geometry of the disc-interleaved winding and the discs that consider to be interleaved are covered by the transparent integration box. In order to achieve the disc-interleaving method, first of all, the number of disc pairs that needs to be interleaved should be determined. Secondly, those determined disc pairs should be interleaved. Finally, the residual disc pairs are decided to wind in continuous connection.

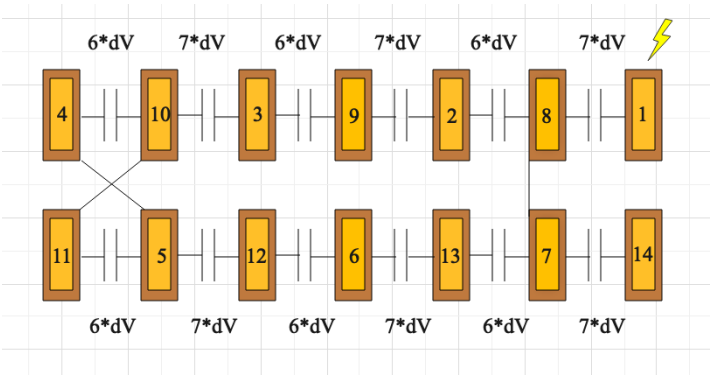

Figure 32. Turn-interleaved disc pair model drawing

When we use the analytical method to calculate the total series capacitance of the turn-interleaved disc pair model C_s, there are actually two cases that need to be taken into account. The first case is that the number of transformer turns per disc is odd and the second case is that the number of turns per disc is even. As for the odd case, the number of C_{tt} under the voltage difference $\Delta V_1 = \left\{\frac{V}{n-1} * (\frac{n}{2} - 1)\right\}$ is $(\frac{n}{2} - 1)$ and the number of C_{tt} under the voltage difference $\Delta V_2 = \left\{\frac{V}{n-1} * \frac{n}{2}\right\}$ is also $(\frac{n}{2} - 1)$. As for the even case, the number of C_{tt} under voltage difference $\Delta V_1 = \left\{\frac{V}{n-1} * (\frac{n}{2} - 1)\right\}$ is $(\frac{n}{2} - 2)$ and the number of C_{tt} under the voltage difference $\Delta V_2 = \left\{\frac{V}{n-1} * \frac{n}{2}\right\}$ is $\frac{n}{2}$.

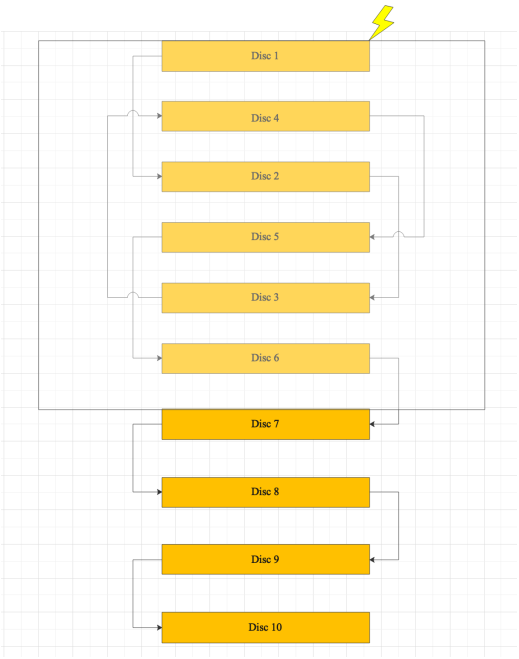

Figure 33. Disc-interleaved disc winding drawing

8.1 The number of transformer turns per disc is even

The analytical formulas for C_{s1} is derived when the voltage is considered to focus on the surface of the transformer turn based on the energy summation method. Firstly, the total electric energy located within the disc pair $E_{turn-turn}$ is calculated and then C_{s1} could be obtained based on the equation $C_{s1} = \frac{2*E_{turn-turn}}{V^2}$. Furthermore, the analytical formula for C_{s2} is directly obtained from reference [5], which could also calculate the total series capacitance of the turn-interleaved disc pair model.

$$E_{turn-turn} = \frac{1}{2} * C_{series-tt} * V^2 = \frac{1}{2} * C_{tt} * (\frac{V}{n-1} * \frac{n}{2})^2 * \frac{n}{2} + \frac{1}{2} * C_{tt} * \left\{ \frac{V}{n-1} * (\frac{n}{2} - 1) \right\}^2 * (\frac{n}{2} - 2)$$

$$C_{series-tt} = C_{tt} * \frac{1}{(n-1)^2} * \left\{ (\frac{n}{2})^3 + (\frac{n}{2} - 1)^3 - (\frac{n}{2} - 1)^2 \right\}$$

$$C_{s1} = \frac{1}{3} * C_{d-tot} + C_{tt} * \frac{1}{(n-1)^2} * \left\{ (\frac{n}{2})^3 + (\frac{n}{2} - 1)^3 - (\frac{n}{2} - 1)^2 \right\}$$

$$C_{s2} = \frac{E * (\frac{n}{2} - 1) * C_{tt}}{4}$$

The turn-interleaving method could significantly enlarge the total series capacitance C_s through increasing the voltage difference of each turn-turn series capacitance C_{tt}, which demands thicker turn-turn isolation. Moreover, the analytical formulas above are derived when we consider that the voltage would focus on the surface of the transformer turn. However, if the voltage is considered to focus at the midpoint of the transformer turn, the formula for C_{s1} should be modified to the equation below.

$$C_{s1} = \frac{1}{3} * C_{d-tot} + C_{tt} * \frac{1}{n^2} * \left\{ (\frac{n}{2})^3 + (\frac{n}{2} - 1)^3 - (\frac{n}{2} - 1)^2 \right\}$$

In [6], the authors provided another analytical formula $C_{s2} = \frac{E*(\frac{n}{2}-1)*C_{tt}}{4}$ to calculate the total series capacitance of the interleaved case. E is introduced as the number of the discs which are determined to be interleaved. n is the total number of the transformer turns. $\frac{n}{2}$ is the number of transformer turns per disc.

8.1.1 The number of transformer turns per disc is 8

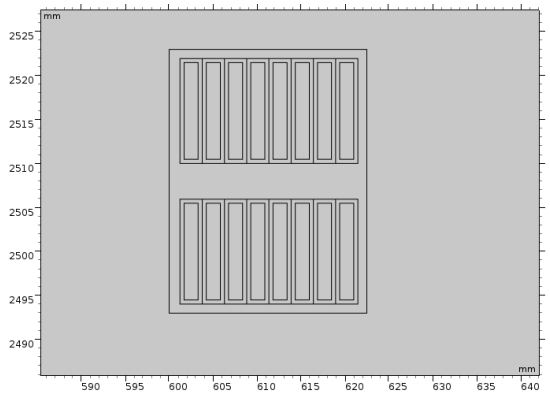

Figure 34. Geometry of turn-interleaved disc pair

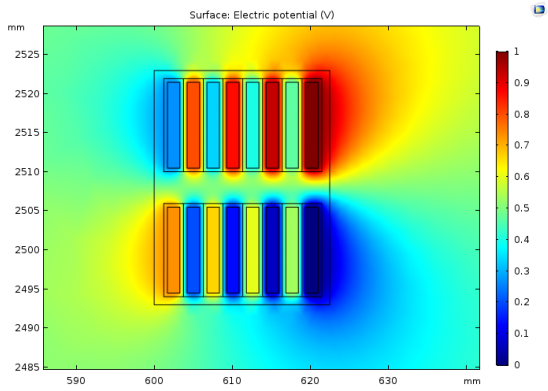

Figure 35. Electric potential distribution

Figure 35 illustrates the electric potential distribution of the turn-interleaved disc pair model shown in figure 34. The basic electric parameters are shown as follows: $R_{outer} = 621.475mm$, $R_{inner} = 601.235mm$, $R_{ave} = 611.355mm$, $\tau_c = 0.93mm$, $d_{oil} = 5mm$ and $h = 11mm$. Through the numerical method, the values for the total series capacitance could be directly obtained from the surface integration operation: $C_{small-region} = 6372.40pF$ and $C_{large-region} = 6445.90pF$. According to those electric parameters, the total series capacitance could also be calculated with the aid of the analytical formulas shown in subsection 8.1.

$$C_{tt} = \frac{2 * \pi * \varepsilon_0 * \varepsilon_{r-paper} * (h + \tau_c) * R_{ave}}{\tau_c} = 1745.14pF$$

$$C_{dd-tot} = \frac{\pi * (R_{outer}^2 - R_{inner}^2) * \varepsilon_0}{\frac{\tau_c}{\varepsilon_{r-paper}} + \frac{d_{oil}}{\varepsilon_{r-oil}}} = 274.77pF$$

$$C_{s1} = \frac{1}{3} * C_{dd-tot} + C_{tt} * \frac{1}{(n-1)^2} * \left\{ (\frac{n}{2})^3 + (\frac{n}{2} - 1)^3 - (\frac{n}{2} - 1)^2 \right\} = 6343.07pF$$

$$C_{s2} = \frac{E * (\frac{n}{2} - 1) * C_{tt}}{4} = \frac{2 * (8-1) * 1745.14}{4} = 6107.99pF$$

8.1.2 The number of transformer turns per disc is 60

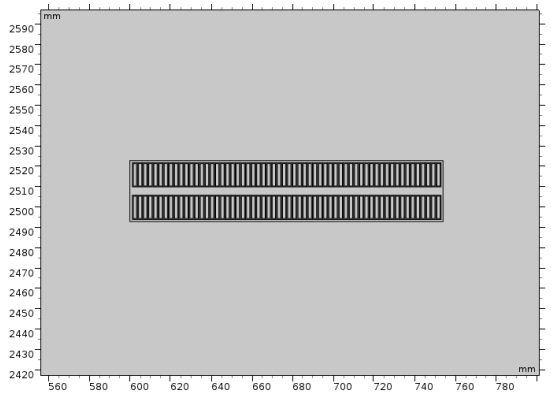

Figure 36. Geometry of turn-interleaved disc pair

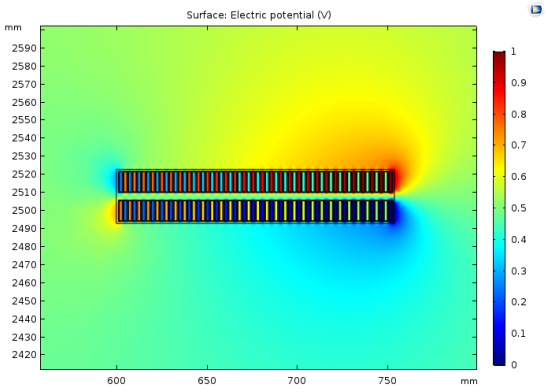

Figure 37. Electric potential distribution

Figure 37 illustrates the electric potential distribution of the turn-interleaved disc pair model shown in figure 36. The basic electric parameters of this interleaved case in subsection 8.1.2 are shown as follows: $R_{outer} = 753.035mm$, $R_{inner} = 601.235mm$, $R_{ave} = 677.135mm$, $\tau_c = 0.93mm$, $d_{oil} = 5mm$ and $h = 11mm$. Through the numerical method, we could acquire the values for total series capacitance: $C_{small-region} = 57640pF$, $C_{large-region} = 57768pF$ from the surface integration operation. According to those obtained electric parameters, the total series capacitance could also be calculated based on the analytical formulas shown in subsection 8.1.

$$C_{tt} = \frac{2 * \pi * \varepsilon_0 * \varepsilon_{r-paper} * (h + \tau_c) * R_{ave}}{\tau_c} = 1932.91pF$$

$$C_{dd-tot} = \frac{\pi * (R_{outer}^2 - R_{inner}^2) * \varepsilon_0}{\frac{\tau_c}{\varepsilon_{r-paper}} + \frac{d_{oil}}{\varepsilon_{r-oil}}} = 2282.545pF$$

$$C_{s1} = \frac{1}{3} * C_{dd-tot} + C_{tt} * \frac{1}{(n-1)^2} * \left\{ (\frac{n}{2})^3 + (\frac{n}{2} - 1)^3 - (\frac{n}{2} - 1)^2 \right\} = 57801.96pF$$

$$C_{s2} = \frac{E * (\frac{n}{2} - 1) * C_{tt}}{4} = \frac{2 * (60-1) * 1932.91}{4} = 57020.85pF$$

8.2 The number of transformer turns per disc is odd

The analytical formula for C_{s1} is derived when the voltage is considered to focus on the surface of the transformer turn based on the energy summation method. Firstly, the total electric energy located within the disc pair model is calculated and then C_{s1} could be obtained based on the equation: $C_{s1} = \frac{2 * E_{turn-turn}}{V^2}$.

$$E_{turn-turn} = \frac{1}{2} * C_{series-tt} * V^2 = \frac{1}{2} * C_{tt} * (\frac{V}{n-1} * \frac{n}{2})^2 * (\frac{n}{2} - 1) + \frac{1}{2} * C_{tt} * \left\{ \frac{V}{n-1} * (\frac{n}{2} - 1) \right\}^2 * (\frac{n}{2} - 1)$$

$$C_{series-tt} = C_{tt} * \frac{1}{(n-1)^2} * \left\{ (\frac{n}{2})^3 + (\frac{n}{2} - 1)^3 - (\frac{n}{2})^2 \right\}$$

$$C_{s1} = \frac{1}{3} * C_{d-tot} + C_{tt} * \frac{1}{(n-1)^2} * \left\{ (\frac{n}{2})^3 + (\frac{n}{2} - 1)^3 - (\frac{n}{2})^2 \right\}$$

$$C_{s2} = \frac{E * (\frac{n}{2} - 1) * C_{tt}}{4}$$

Actually, the analytical formulas above are derived based on the assumption that the voltage would only focus on the surface of the transformer turn. However, if the voltage is considered to focus at the midpoint of the transformer turn, the formula for C_{s1} should be re-derived as below.

$$C_{s1} = \frac{1}{3} * C_{d-tot} + C_{tt} * \frac{1}{n^2} * \left\{ (\frac{n}{2})^3 + (\frac{n}{2} - 1)^3 - (\frac{n}{2})^2 \right\}$$

8.2.1 The number of transformer turns per disc is 7

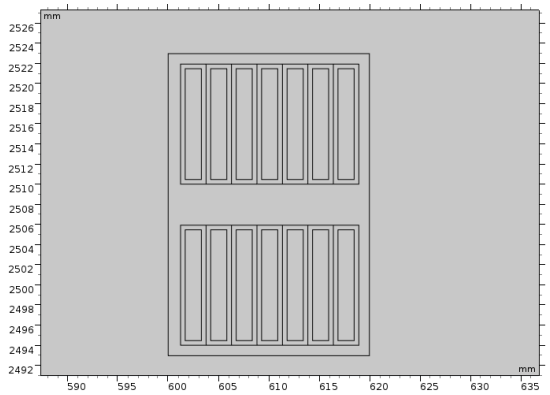

Figure 38. Geometry of turn-interleaved disc pair

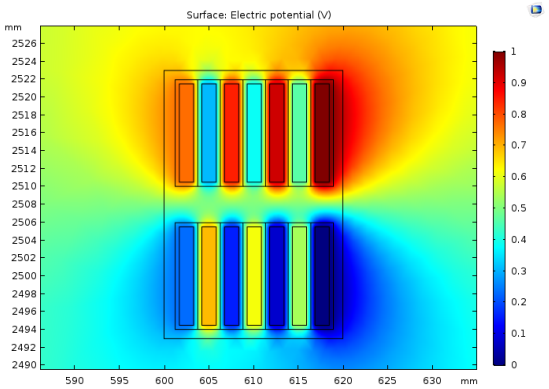

Figure 39. Electric potential distribution

With respect to the disc pair model that needs to be turn-interleaved shown in figure 38, the electric potential distribution of the turn-interleaved disc pair model is shown in figure 39 and the voltage values for anywhere within the disc pair model could be evaluated according to the color bar.

Moreover, the electric parameters for the turn-interleaved disc pair model are shown as follows: $R_{outer} = 618.945mm$, $R_{inner} = 601.235mm$, $R_{ave} = 610.09mm$, $d = \tau_c = 0.93mm$ and $h = 11mm$. Through the numerical method, we could obtain the series capacitance values $C_{small-region} = 5370.8pF$ and $C_{large-region} = 5441.4pF$ from surface integration operation. Based on those electric parameters, the total series capacitance could also be calculated by the analytical formula shown in subsection 8.2.

$$C_{tt} = \frac{2 * \pi * \varepsilon_0 * \varepsilon_{r-paper} * (h + \tau_c) * R_{ave}}{\tau_c} = 1741.53pF$$

$$C_{dd-tot} = \frac{\pi * (R_{outer}^2 - R_{inner}^2) * \varepsilon_0}{\frac{\tau_c}{\varepsilon_{r-paper}} + \frac{d_{oil}}{\varepsilon_{r-oil}}} = 239.93pF$$

$$C_{s1} = \frac{1}{3} * C_{dd-tot} + C_{tt} * \frac{1}{(n-1)^2} * \left\{ (\frac{n}{2})^3 + (\frac{n}{2} - 1)^3 - (\frac{n}{2})^2 \right\} = 5335.48pF$$

$$C_{s2} = \frac{E * (\frac{n}{2} - 1) * C_{tt}}{4} = \frac{2 * (7 - 1) * 1741.53}{4} = 5224.59pF$$

8.2.2 The number of transformer turns per disc is 9

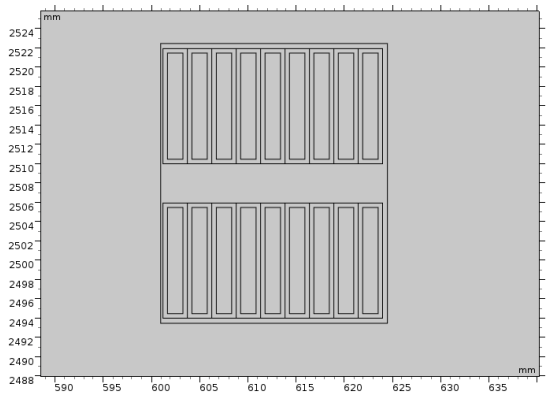

Figure 40. Geometry of turn-interleaved disc pair

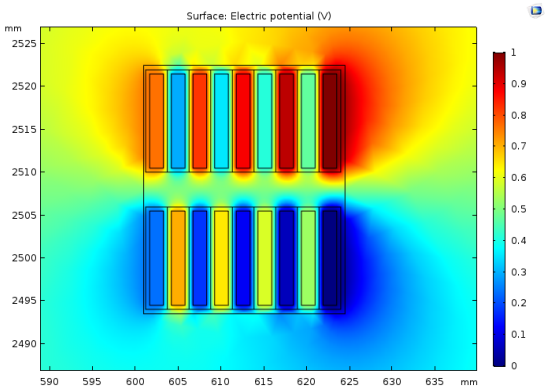

Figure 41. Electric potential distribution

Figure 41 illustrates the electric potential distribution of the turn-interleaved disc pair model shown in figure 40. Through the numerical method, the series capacitance values $C_{small-region} = 7124.5pF$ and $C_{large-region} = 7226.9pF$ could be directly obtained by means of the surface integration operation. Moreover, the electric parameters of the interleaved disc pair are shown as follows: $R_{outer} = 624.005mm$, $R_{inner} = 601.235mm$, $R_{ave} = 612.620mm$, $d = \tau_c = 0.93mm$ and $h = 11mm$. Based on those electric parameters, the total series capacitance of the turn-interleaved disc pair could be calculated based on the analytical formula shown in subsection 8.2.

$$C_{tt} = \frac{2 * \pi * \varepsilon_0 * \varepsilon_{r-paper} * (h + \tau_c) * R_{ave}}{\tau_c} = 1748.75pF$$

$$C_{dd-tot} = \frac{\pi * (R_{outer}^2 - R_{inner}^2) * \varepsilon_0}{\frac{\tau_c}{\varepsilon_{r-paper}} + \frac{d_{oil}}{\varepsilon_{r-oil}}} = 309.76pF$$

$$C_{s1} = \frac{1}{3} * C_{dd-tot} + C_{tt} * \frac{1}{(n-1)^2} * \left\{ (\frac{n}{2})^3 + (\frac{n}{2} - 1)^3 - (\frac{n}{2})^2 \right\} = 7122.46pF$$

$$C_{s2} = \frac{E * (\frac{n}{2} - 1) * C_{tt}}{4} = \frac{2 * (9 - 1) * 1748.75}{4} = 6995.00pF$$

	C_{s1} (analytical)	C_{s2} (analytical)	$C_{small-region}$	ΔC_{s1}	ΔC_{s2}	$C_{large-region}$
7 turns	$5335.48pF$	$5224.59pF$	$5370.80pF$	$35.32pF$	$146.21pF$	$5441.40pF$
8 turns	$6343.07pF$	$6107.99pF$	$6372.40pF$	$29.33pF$	$264.41pF$	$6445.90pF$
9 turns	$7122.46pF$	$6995.00pF$	$7124.50pF$	$2.04pF$	$129.50pF$	$7226.90pF$
60 turns	$57801.96pF$	$57020.85pF$	$57640.00pF$	$161.96pF$	$619.15pF$	57768.00

Table 2. The comparison between the results obtained from numerical and analytical method

According to table 2, the capacitance difference ΔC_{s1} and ΔC_{s2} are defined as $\Delta C_{s1} = C_{small-region} - C_{s1}$ and $\Delta C_{s2} = C_{small-region} - C_{s2}$ respectively. Although the results obtained from the analytical method are not accurate, the outcomes calculated based on formula C_{s1} are relatively better compared with those obtained from formula C_{s2}.

$C_{small-region}$ comprises of a fraction of additional capacitance C_a generated by the fringing effect. In order to have the comparison under same condition, during the calculation of C_{tt} by means of analytical method, $(h + 2 * \tau_c)$ should be replaced by $(h + \tau_c)$.

In reality, the number of transformer turns per disc for almost all of the large power transformers is even. Because in case of manufacturing the turn-interleaved disc pair model, two transformer turn wires ought to wind together.

9 Calculation of the series capacitance improvement factor λ in the case of disc pair model with electrostatic inter-shield wires using numerical method

9.1 The total series capacitance of the inter-shielded disc pair model

With respect to the disc pair model inter-shielded by the electrostatic shield pairs, in order to make the improvement factor λ more realistic, there should be 60 transformer turns per disc or coil and $n = 120$. If the magnitude of the input voltage is V_1 and that for the output voltage is V_2, then the voltage value for every electrostatic inter-shield wire would become $V_{sh} = \frac{V_1+V_2}{2}$.

According to the critical assumption in [1], the voltage would distribute linearly along the disc pair at the frequency range of 1MHz. The total voltage drop for the disc pair would become $\Delta V_{tot} = V_1 - V_2$ and the voltage drop per transformer turn would become $\Delta V_{turn} = \frac{V_1-V_2}{n-1}$. Moreover, the voltage value for the k^{th} transformer turn ought to become $U_k = V_1 - \frac{k-1}{n-1} * (V_1 - V_2)$.

If there are no electrostatic inter-shield pairs inserted in the disc pair model, during the Comsol simulation, the unoccupied gaps should be filled with transformer oil. As a result, this case ought to behave as the reference. Figure 42 illustrates the exact places for the transformer oil gaps and figure 43 indicates the electric potential distribution of the reference disc pair model.

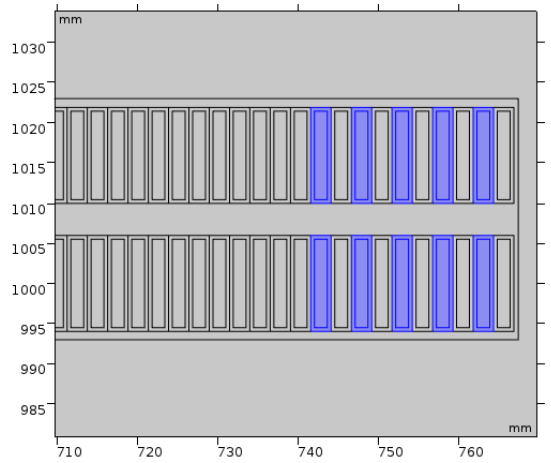

Figure 42. Geometry–oil-gap pairs

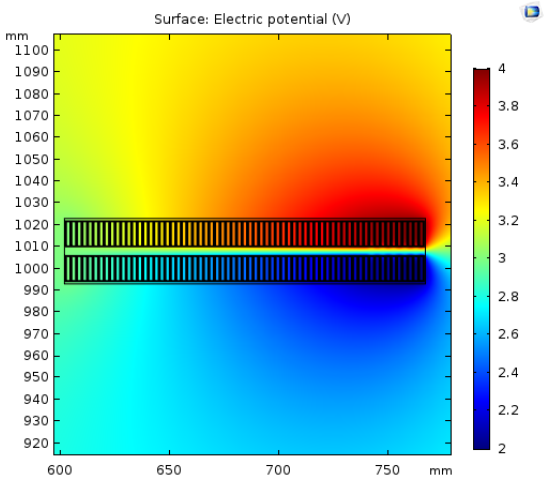

Figure 43. Voltage distribution–without shield pairs

During Comsol simulation, we use surface integration from derived values section to calculate the total series capacitance C_{s1}. First of all, the total electric energy stored in the disc pair model E_{tot} should be calculated. Then, the magnitude of C_{s1} could be obtained based on the formula: $E_{tot} = \frac{1}{2} * C_{s1} * \Delta V_{tot}^2$. After studying the Comsol mph file, we could know that $C_{s0} = 1.18nF$.

If there are five floating electrostatic inter-shield pairs inserted in the disc pair model, during the Comsol simulation, all of the transformer oil-gap pairs are replaced by the floating inter-shield pairs covered by paper shield. Figure 44 illustrates the places for those five floating inter-shield pairs and figure 45 shows the electric potential distribution of the disc pair model inter-shielded by those five shield pairs.

Similarly, with respect to this geometry, the surface integration operation is used to calculate the total electric energy located within the inter-shielded disc pair E_{tot-5}. The total series capacitance C_{s5} could be calculated according to the formula: $C_{s5} = \frac{2}{(V_1-V_2)^2} * E_{tot-5} = 9.64nF$. Thus, the series capacitance improvement factor λ_5 should become $\lambda_5 = \frac{C_{s5}}{C_{s0}} = 8.17$.

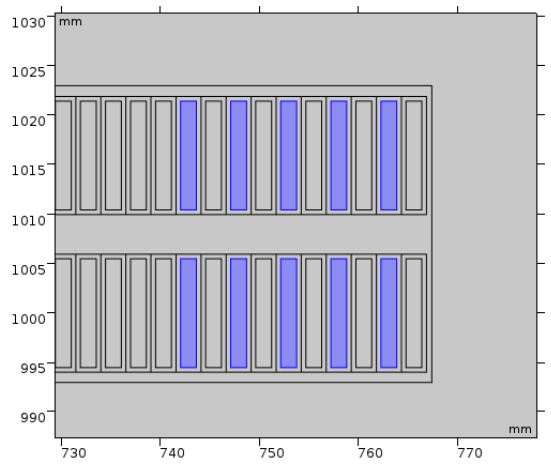

Figure 44. Geometry–five floating shield pairs

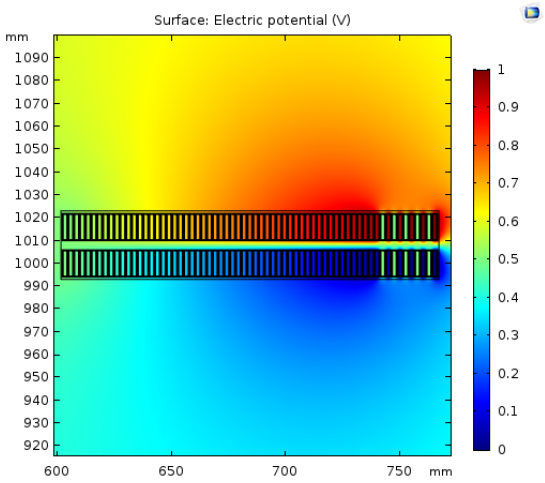

Figure 45. Voltage distribution–five shield pairs

If four floating electrostatic inter-shield pairs are present within the disc pair model, during Comsol simulation, one oil-gap pair is left untouched and the residual ones are replaced by the floating inter-shield wires covered by paper shield. Figure 46 illustrates the places for those floating inter-shield wires and figure 47 indicates the electric potential distribution for the inter-shielded disc pair model.

As for the geometry with four inter-shield pairs, the surface integration operation should be used to calculate the total electric energy E_{tot-4} stored in the disc pair model. The total series capacitance C_{s4} could then be calculated based on the formula: $C_{s4} = \frac{2}{(V_1-V_2)^2} * E_{tot-4} = 8.09nF$. Thus, the series capacitance improvement factor λ_4 should become $\lambda_4 = \frac{C_{s4}}{C_{s0}} = 6.86$.

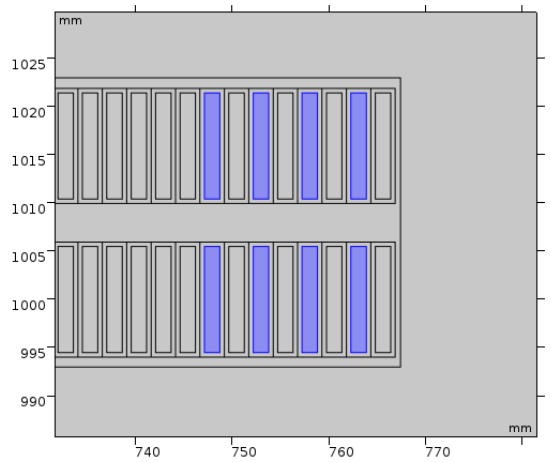

Figure 46. Geometry–four floating shield pairs

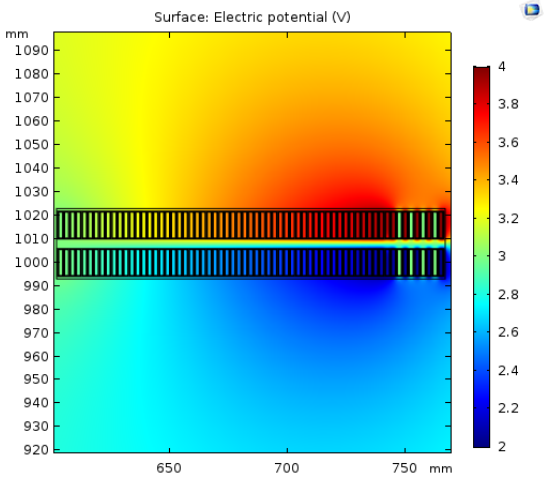

Figure 47. Voltage distribution–four shield pairs

If three floating electrostatic shield pairs are inserted in the disc pair model, during Comsol simulation, two oil-gap pairs are left untouched and the residual ones are replaced by the floating inter-shield pairs covered by paper shield. Figure 48 illustrates the places for those floating inter-shield wires, which are colored by blue and figure 49 shows the electric potential distribution of the disc pair model with three electrostatic inter-shield pairs.

Similarly, as for the geometry with three floating inter-shield pairs, the total electric energy E_{tot-3} stored in the disc pair model could be calculated through the surface integration operation. The value for the total series capacitance C_{s3} could be obtained based on the formula: $C_{s3} = \frac{2}{(V_1-V_2)^2} * E_{tot-3} = 6.47nF$. Thus, the series capacitance improvement factor λ_3 would become $\lambda_3 = \frac{C_{s3}}{C_{s0}} = 5.48$.

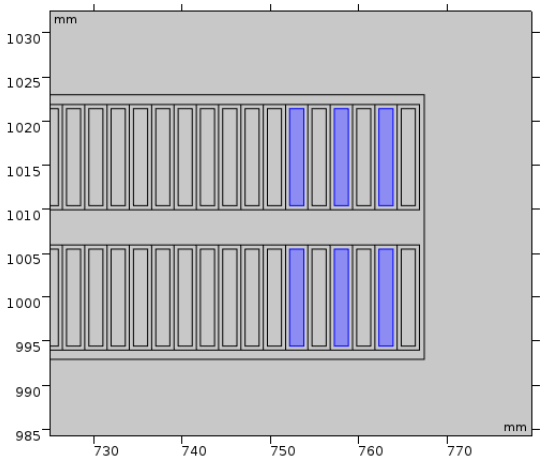

Figure 48. Geometry–three floating shield pairs

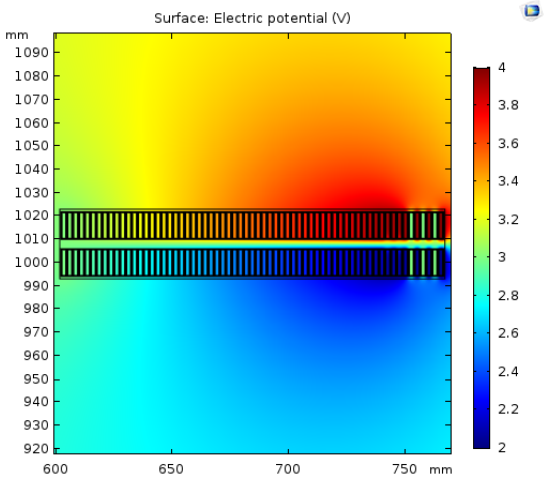

Figure 49. Voltage distribution–three shield pairs

Number of the floated shield wires	Series capacitance C_s	Improvement factor λ (within one disc pair)
N=0	$C_{s0} = 1.18nF$	λ_0=1.00
N=1	$C_{s1} = 3.02nF$	λ_1=2.56
N=2	$C_{s2} = 4.78nF$	λ_2=4.05
N=3	$C_{s3} = 6.47nF$	λ_3=5.48
N=4	$C_{s4} = 8.09nF$	λ_4=6.86
N=5	$C_{s5} = 9.64nF$	λ_5=8.17

Table 3. Improvement of series capacitance of the disc pair model inter-shielded by different number of electrostatic shield pairs

So far, in this subsection, the calculation processes for the improvement factor λ in case of three, four and five floating electrostatic inter-shield wires have been explained thoroughly. After using the same numerical method, C_{s2} and λ_2, C_{s1} and λ_1 could also be successfully obtained. All of those obtained results are listed in the table 3.

9.2 The series capacitance between adjacent disc pairs

When we calculate the total series capacitance C_s between adjacent disc pairs, the number of floating electrostatic inter-shield wires from upper disc ($N = k$) may become unequal to that from lower disc ($N = k - r$). Thus, the analytical formulas in chapter 5 should be changed as below.

$$C_{series-ts} = \frac{C_{ts}}{n^2} * \sum_{m=1}^{k-r} \{(n-2m) * (n-2m+2) + 2\} + \frac{C_{ts}}{2n^2} * \sum_{m=k-r+1}^{k} \{(n-2m) * (n-2m+2) + 2\}$$

$$C_{series-tt} = C_{tt} * \frac{(n-2k) + (r-2)}{n^2}$$

$$C_s = \frac{C_{ts}}{n^2} * \sum_{m=1}^{k-r} \{(n-2m) * (n-2m+2) + 2\} + \frac{C_{ts}}{2n^2} * \sum_{m=k-r+1}^{k} \{(n-2m) * (n-2m+2) + 2\} + C_{tt} * \frac{(n-2k) + (r-2)}{n^2} + \frac{n}{6} * C_d$$

Actually, the upper disc comprises of k floating electrostatic inter-shield wires and the bottom disc concludes (k-r) inter-shield wires. Moreover, the total series capacitance of the upper disc pair is C_{s-top} and that of the bottom disc pair is $C_{s-bottom}$. The analytical formulas for C_{s-top} and $C_{s-bottom}$ are shown as below.

$$C_{s-top} = \frac{C_{ts}}{n^2} * \sum_{m=1}^{k-r} \{(n-2m)*(n-2m+2)+2\} + \frac{C_{ts}}{n^2} * \sum_{m=k-r+1}^{k} \{(n-2m)*(n-2m+2)+2\}$$
$$+ C_{tt} * \frac{(n-2k)-2}{n^2} + \frac{n}{6} * C_d$$
$$C_{s-bottom} = \frac{C_{ts}}{n^2} * \sum_{m=1}^{k-r} \{(n-2m)*(n-2m+2)+2\} + C_{tt} * \frac{(n-2k)+(2r-2)}{n^2} + \frac{n}{6} * C_d$$
$$C_s = \{C_{s-top} + C_{s-bottom}\} * \frac{1}{2}$$

As a result, the magnitude of the series capacitance between adjacent disc pairs C_s is the average value of series capacitance from upper disc pair C_{s-top} together with series capacitance from bottom disc pair $C_{s-bottom}$. In order to make the analytical result more convincing, we should use the numerical method for verification.

With respect to the inter-shielded disc pair model shown in figure 50, there are basically three floating inter-shield wires located in the upper disc and two floating inter-shield wires located in the lower disc. The total series capacitance of this inter-shielded disc pair model is named as C_{23}. According to table 3 shown in subsection 9.1, we could know that $C_{s3} = 6.47nF$ and $C_{s2} = 4.78nF$. Thus, based on the analytical formulas derived in this subsection, the magnitude of the total series capacitance is expected to become $C_{23} = \frac{1}{2} * (6.47 + 4.78) = 5.625nF$.

After studying the corresponding Comsol file, the electric potential distribution of the inter-shielded disc pair is shown in figure 51. Also, the precise value for the series capacitance of the geometry shown in figure 50 could be obtained: $C_{23} = 5.6232nF$, which is really close to the expected value. Thus, the predicted result is proved to be convincing.

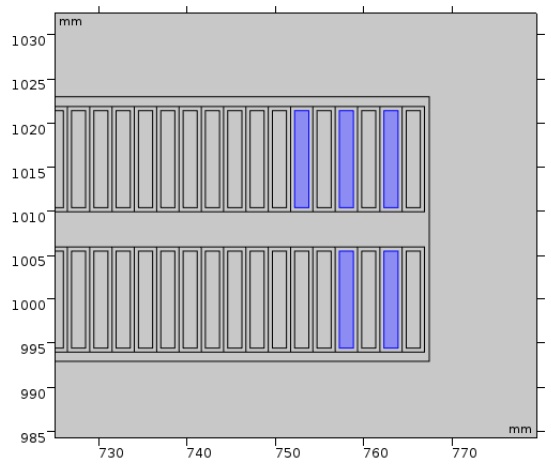

Figure 50. Geometry–floating inter-shield wires

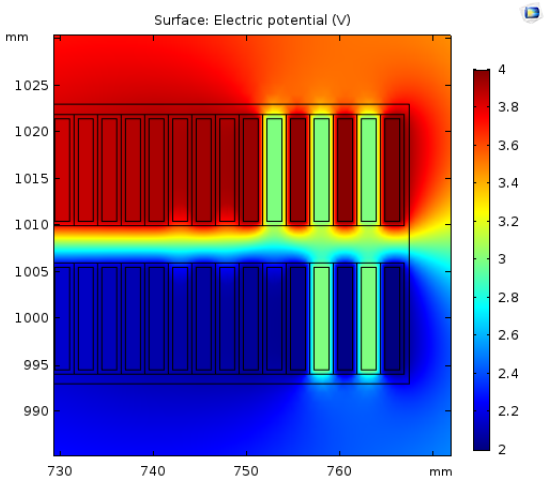

Figure 51. Electric potential distribution

Number of the floated shield wires	Numerical series capacitance C_s	Analytical series capacitance C_s
N=0, N=1	$C_{s01} = 2.0979nF$	$C_{s01} = 2.1006nF$
N=1, N=2	$C_{s12} = 3.8984nF$	$C_{s12} = 3.9010nF$
N=2, N=3	$C_{s23} = 5.6232nF$	$C_{s23} = 5.6257nF$
N=3, N=4	$C_{s34} = 7.2771nF$	$C_{s34} = 7.2795nF$
N=4, N=5	$C_{s45} = 8.8623nF$	$C_{s45} = 8.8646nF$

Table 4. The comparison between the C_s obtained from numerical method and analytical method

9.3 The disc-to-ground series capacitance C_g calculation using the numerical method

Based on the formulas below, each of the equivalent transformer disc ought to be applied to a voltage whose magnitude is one Volt. After collecting all of the electric charges accumulated on the disc winding, the total ground capacitance could be obtained. Normally, the ground series capacitances for top and bottom disc would become much larger than those for intermediate discs. Here, c_{1i} represents for the i^{th} capacitance coefficient.

$$Q_1 = \sum_{i=1}^{n} c_{1i} * U_i = c_{11} * U_1 + c_{12} * U_2 + c_{13} * U_3 + c_{14} * U_4 + c_{15} * U_5 + c_{16} * U_6 + ... + c_{1n} * U_n$$

$$C_{g1} = \sum_{i=1}^{n} c_{1i} = c_{11} + c_{12} + c_{13} + c_{14} + c_{15} + c_{16} + ... + c_{1n}$$

In order to preciously calculate the ground capacitances, first of all, an equivalent disc pair model should be built in Comsol and the total ground capacitances C_{tot-1} for two sides(C_{g1} and C_{g12}) could be acquired through line integration operation. Then, a disc winding model with 12 discs should be built and the total ground capacitance of these 12 discs C_{tot-2} could also be obtained.

$$C_{tot-1} = C_{g1} + C_{g12} = 306.23pF$$

$$C_{tot-2} = \sum_{i=1}^{12} c_{gi} = 491.80pF$$

Normally, the values for ground capacitances in the middle could be regarded as equal $C_{g-middle} = 18.557pF$. Moreover, the ground capacitances for two sides also have the same value $C_{g1} = C_{g12} = 153.115pF$.

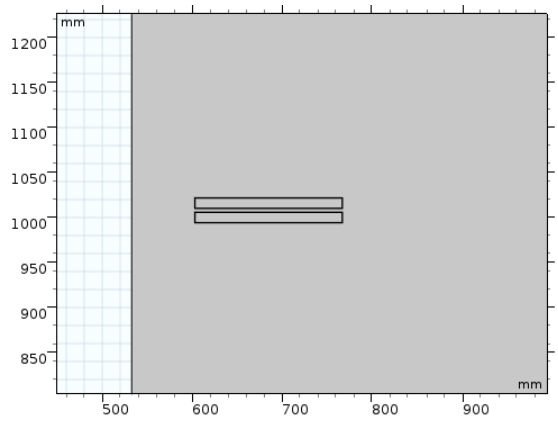

Figure 52. Geometry of the equivalent disc pair

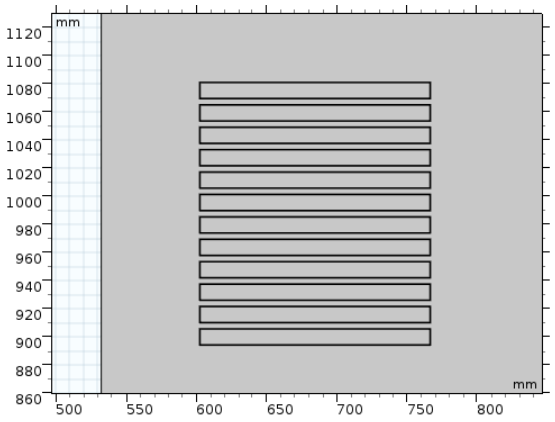

Figure 53. Geometry of the equivalent disc winding

10 Calculation of the series capacitance improvement factor λ with wound-in inter-shield wires and turn-interleaved disc pair

10.1 The cross-point of the first wound-in shield pair is floating

When the cross-point of the first (rightmost) wound-in inter-shield pair is floating, the voltage for both of the rightmost inter-shield turns is considered to become $V_{sh} = \frac{V_1+V_2}{2}$. Here, V_1 represents for the input voltage and V_2 represents for the output voltage of the disc pair model. Besides, the voltage drop per wound-in inter-shield ΔV_{shield} is equal to the voltage drop per transformer turn ΔV_{turn}. The improvement factors for different cases are shown in table 5.

$$\Delta V_{shield} = \Delta V_{turn} = \frac{V_1 - V_2}{n-1}$$

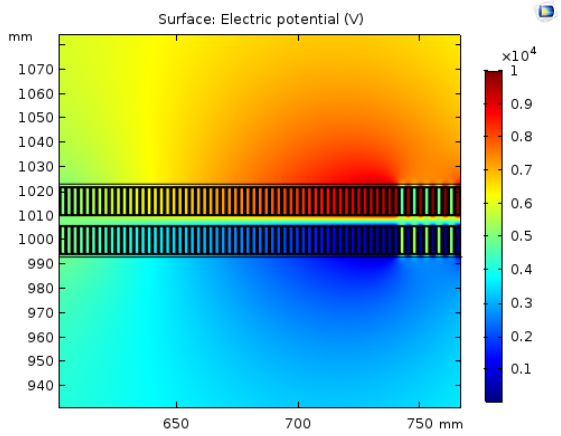

Figure 54. Voltage distribution–five shield pairs

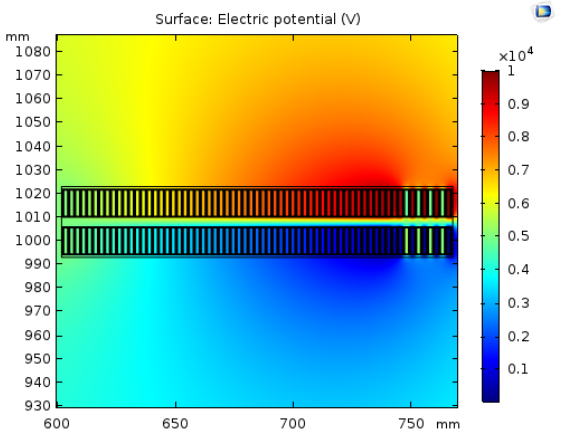

Figure 55. Voltage distribution–four shield pairs

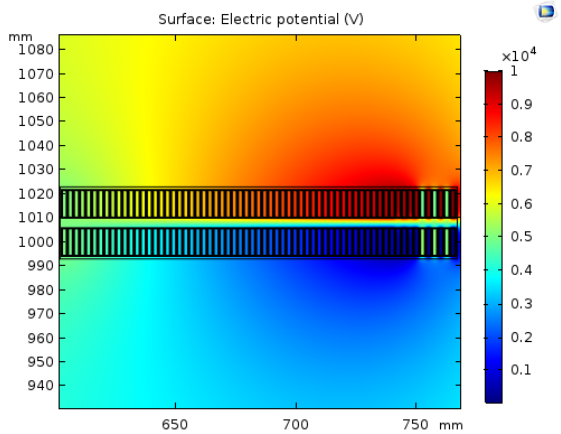

Figure 56. Voltage distribution–three shield pairs

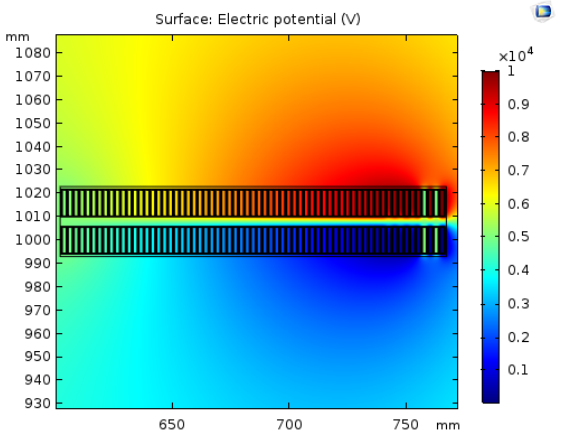

Figure 57. Voltage distribution–two shield pairs

Number of wound-in shield wires	Series capacitance C_s	Improvement factor λ (within one disc pair)
N=0	$C_{s0} = 1.18nF$	λ_0=1.00
N=1	$C_{s1} = 3.02nF$	λ_1=2.56
N=2	$C_{s2} = 4.84nF$	λ_2=4.10
N=3	$C_{s3} = 6.66nF$	λ_3=5.64
N=4	$C_{s4} = 8.46nF$	λ_4=7.17
N=5	$C_{s5} = 10.25nF$	λ_5=8.69

Table 5. Improvement of the total series capacitance of the disc pair model for different number of wound-in inter-shield pairs–the cross-point is floating

Figure 58, 59, 60 and 61 illustrate the electric potential distribution for two discs from adjacent disc pairs. After the surface integration operation in Comsol Multiphysics, the total series capacitance C_s between two adjacent disc pairs could be obtained. The values for those series capacitances are shown in table 6. As a result, according to table 5 and table 6, the improvement factors λ of this case are slightly larger those with floating electrostatic inter-shield pairs.

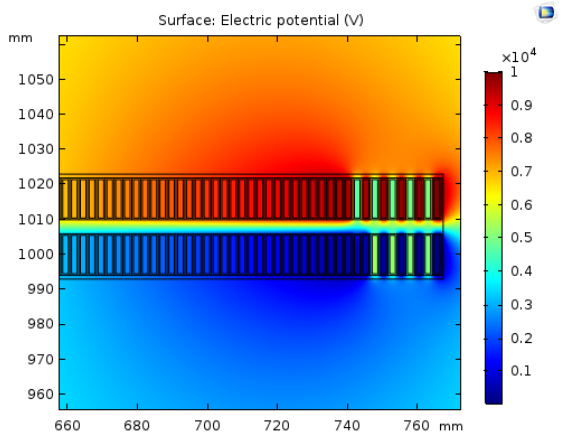

Figure 58. Electric potential distribution–5,4

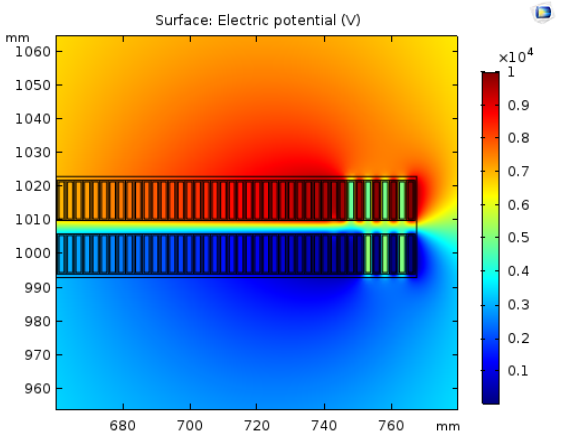

Figure 59. Electric potential distribution–4,3

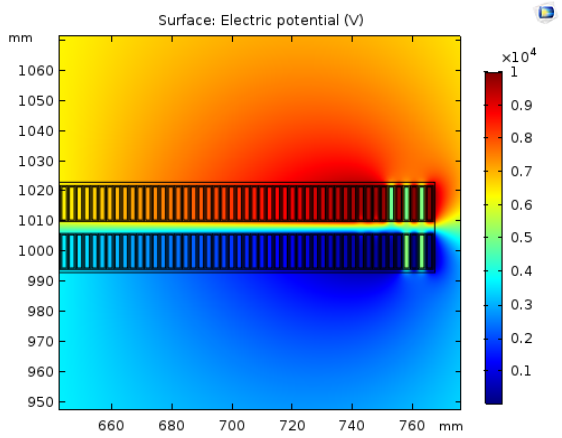

Figure 60. Electric potential distribution–3,2

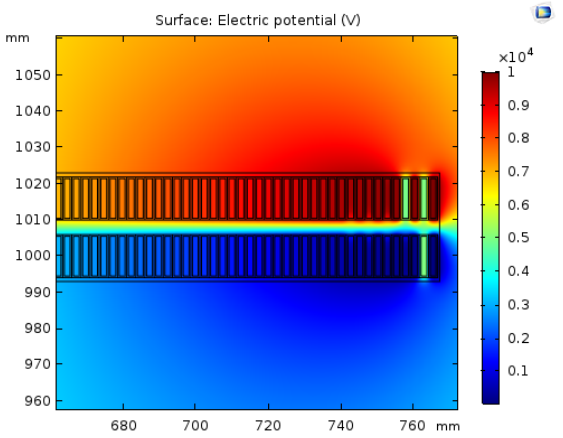

Figure 61. Electric potential distribution–2,1

Number of the floated shield wires	Numerical series capacitance C_s	Analytical series capacitance
N=0, N=1	$C_{s01} = 2.0979nF$	$C_{s01} = 2.1006nF$
N=1, N=2	$C_{s12} = 3.9296nF$	$C_{s12} = 3.9323nF$
N=2, N=3	$C_{s23} = 5.7472nF$	$C_{s23} = 5.7499nF$
N=3, N=4	$C_{s34} = 7.5537nF$	$C_{s34} = 7.5564nF$
N=4, N=5	$C_{s45} = 9.3492nF$	$C_{s45} = 9.3520nF$

Table 6. The total series capacitance C_s between two adjacent disc pairs with different number of wound-in inter-shields–the cross-point is floating

10.2 The cross-point of the first wound-in inter-shield pair is connected to the input terminal

If the cross-point of the rightmost wound-in inter-shield pair is connected to the high voltage terminal, the voltage for both of the rightmost inter-shield turns is considered to become $V_{sh} = V_1$. Moreover, the voltage drop per wound-in inter-shield ΔV_{shield} is equal to the voltage drop per transformer turn ΔV_{turn}. The improvement factors λ_i for different cases are shown in table 7. Furthermore, figure 62, 63, 64 and 65 illustrate the electric potential distribution of the disc pair model with different number of inter-shield pairs.

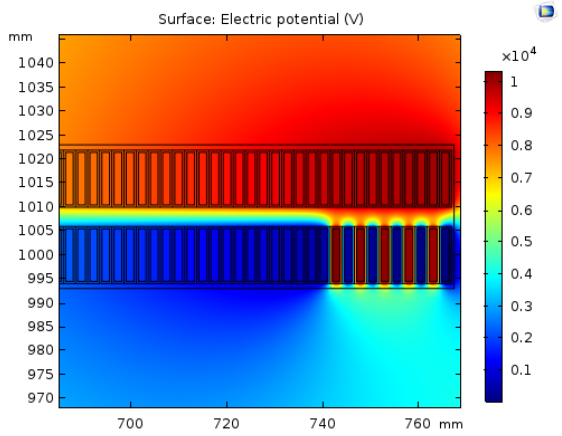

Figure 62. Voltage distribution–five shield pairs

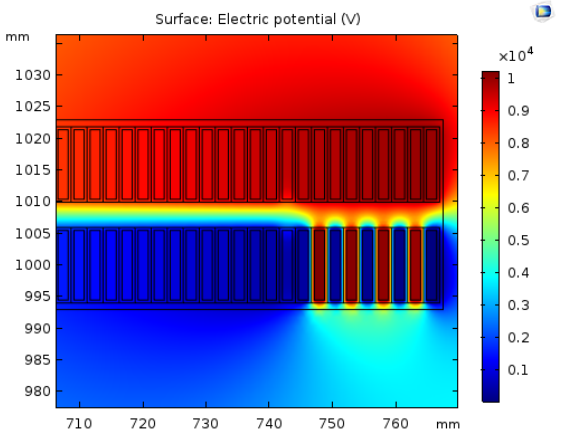

Figure 63. Voltage distribution–four shield pairs

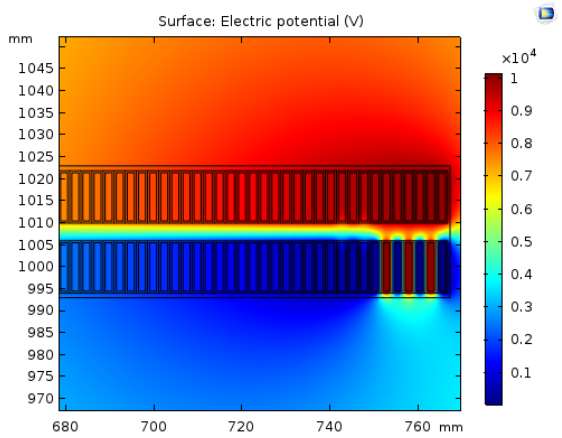

Figure 64. Voltage distribution–three shield pairs

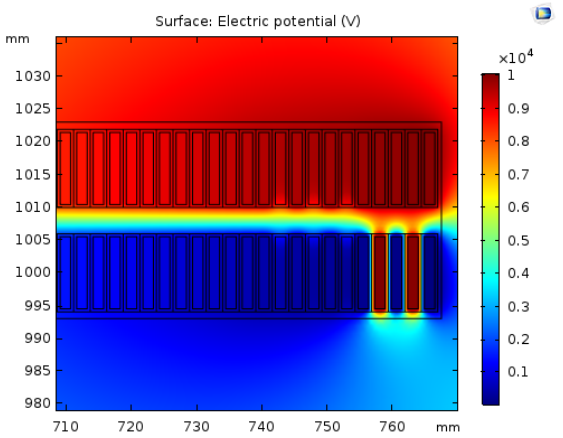

Figure 65. Voltage distribution–two shield pairs

Number of wound-in shield wires	Series capacitance C_s	Improvement factor λ (within one disc pair)
N=0	$C_{s0} = 1.18nF$	λ_0=1.00
N=1	$C_{s1} = 4.96nF$	λ_1=4.20
N=2	$C_{s2} = 8.70nF$	λ_2=7.37
N=3	$C_{s3} = 12.42nF$	λ_3=10.53
N=4	$C_{s4} = 16.11nF$	λ_4=13.65
N=5	$C_{s5} = 19.77nF$	λ_5=16.75

Table 7. Improvement of the total series capacitance of the disc pair model for different number of wound-in inter-shield pairs–the cross-point is connected to the input terminal

After the calculation of the total series capacitance C_s between two adjacent disc pairs, the obtained results shown in table 8 are quite close to the total series capacitance of the disc pair model that comprises of the bottom disc.

Number of wound-in shield wires	Series capacitance C_s	Improvement factor λ (between adjacent disc pairs)
N=0, N=1	$C_{s01} = 1.1868nF$	λ_{01}=1.0054
N=1, N=2	$C_{s12} = 4.9676nF$	λ_{12}=4.2084
N=2, N=3	$C_{s23} = 8.7058nF$	λ_{23}=7.3753
N=3, N=4	$C_{s34} = 12.420nF$	λ_{34}=10.522
N=4, N=5	$C_{s45} = 16.109nF$	λ_{45}=13.647

Table 8. Improvement of the total series capacitance between two adjacent disc pairs with different number of wound-in inter-shields–the cross-point is connected to the input terminal

10.3 All of the transformer turns within the disc pair model are interleaved

Normally, it is complicated for the manufacturing company to produce the turn-interleaved disc pair due to the higher labour cost. However, several disc pairs close to high voltage connections need to be turn-interleaved when the transformer places at the stormy region. In order to have a coordination of inter-shielding and turn-interleaving disc pairs in one winding, the turn-interleaved disc pairs ought to have five oil-gap pairs, which are shown in figure 66 and figure 68.

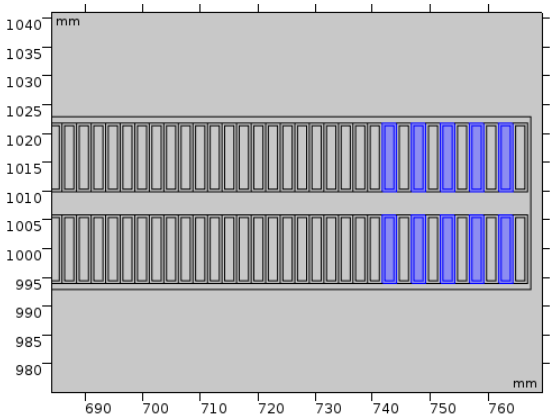

Figure 66. Oil-gap pairs–turn-interleaved disc pair

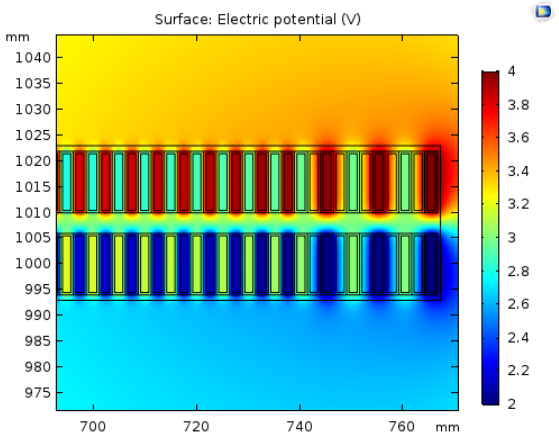

Figure 67. Electric potential distribution

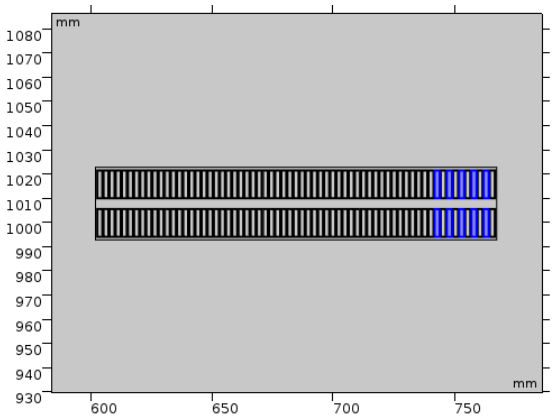

Figure 68. Oil-gap pairs–zoom out

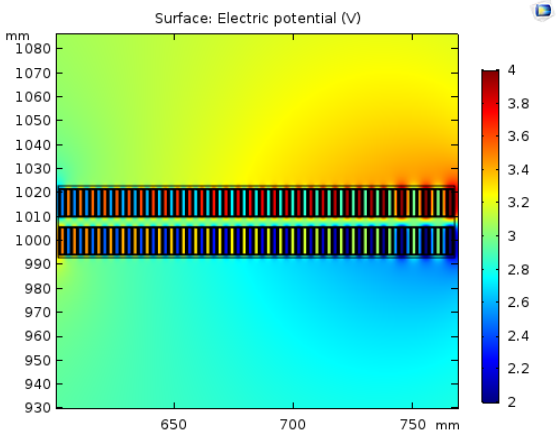

Figure 69. Voltage distribution–zoom out

After the surface integration operation in Comsol, we could know that the total series capacitance C_s of the interleaved disc pair is $C_s = 47.228nF$ and the improvement factor of the turn-interleaved disc pair model is $\lambda_{interleaved} = 40.01$.

11 The verification of the critical assumption mentioned in [1]

In [1], the authors have already provided a critical assumption that the voltage would distribute uniformly along the disc pair model at the frequency range of 1MHz. Our analytical formulas related to the calculation of the total series capacitance C_s are derived based on this. Therefore, it is necessary to verify whether this assumption is valid or not.

Actually, all of the electric potential distribution figures shown in following pages are obtained under the following assumptions made in Comsol: First of all, the voltage responses are considered to distribute capacitively, which means that only the capacitance matrix is present in the disc or disc pair model. Secondly, the voltage would distribute under infinitely high frequency level.

11.1 Voltage response distribution along the disc model with grounded iron core

Based on figure 72, 74 and 76 shown in next page, it is clear that the voltage would distribute non-linearly along the cut-line, especially for the disc model in large scale (such as 60 transformer turns per disc). Normally, the magnitude of the i^{th} turn-ground capacitance C_{gi} is much smaller than turn-turn series capacitance C_{tt} and $X_{gi} = \frac{1}{\omega C_{gi}} \approx 100 * \frac{1}{\omega C_{tt}} = 100 * X_{tt}$. The i^{th} ground-capacitive current I_{gi} which would flow through C_{gi} could be calculated as the following equation which could be derived based on the sketch 70: $I_{gi} = \frac{U_{input}}{X_{gi}+(i-1)*X_{tt}}$. Because X_{tt} is much smaller than X_{gi}, the values for all of I_{gi} are regarded as the same: $I_{g1} \approx I_{g2} \approx I_{g3} \approx ... \approx I_{gn}$.

When the disc model is in large scale (such as 60 transformer turns per disc), the intensity of the ground-capacitive current I_g flowing through the C_{tt} nearby high voltage connection is much larger than that close to the end. Also, the voltage drop across the C_{tt} adjacent to high voltage terminal ΔV_{front} is much larger than that close to the end ΔV_{end} because more capacitive currents would flow through C_{tt} nearby the input lead. Therefore, under this situation, the voltage distribution line would become fairly non-linear, which is the same as figure 76 in this subsection.

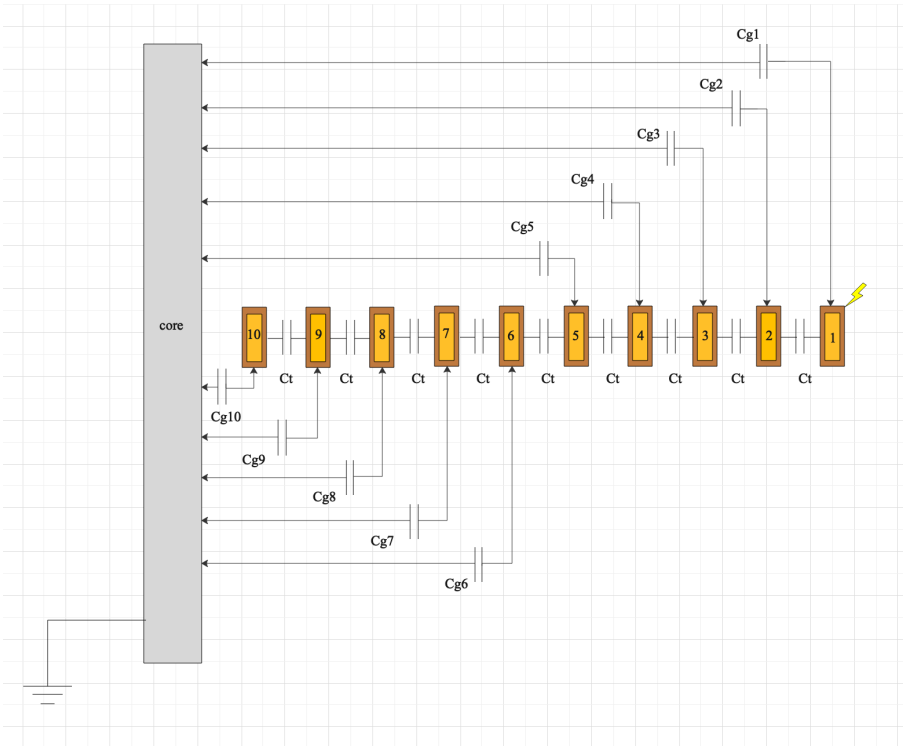

Figure 70. Equivalent capacitive disc model

In order to make the voltage value for everywhere inside the transformer turn (conductor) remain constant, the relative permittivity of copper is considered to become 10^8. Figure 71, 73 and 75 illustrate the cut-lines for different scales of the disc model and figure 72, 74 and 76 represent for the voltage distribution along their corresponding cut-line. The voltage would distribute following the direction of the red arrow.

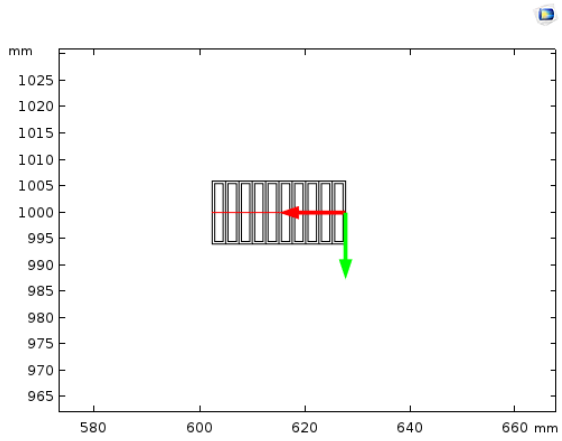

Figure 71. Cut-line 10 turns per disc

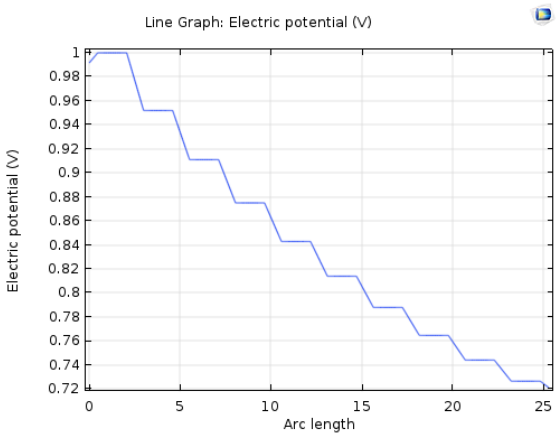

Figure 72. Voltage distribution 10 turns per disc

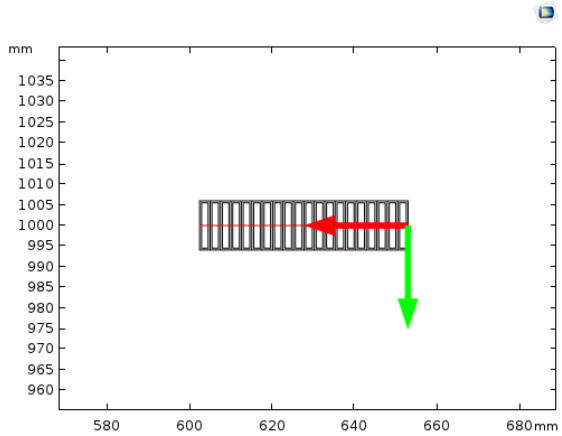

Figure 73. Cut-line 20 turns per disc

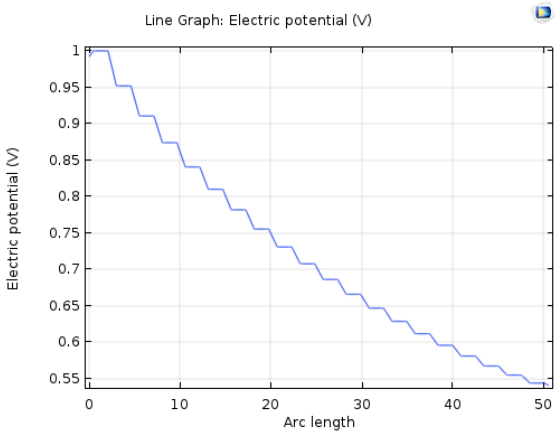

Figure 74. Voltage distribution 20 turns per disc

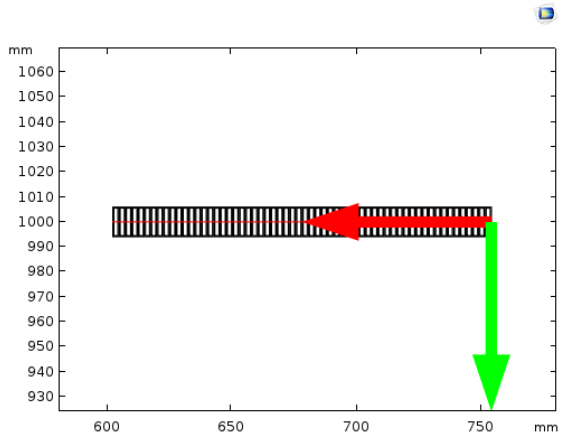

Figure 75. Cut-line 60 turns per disc

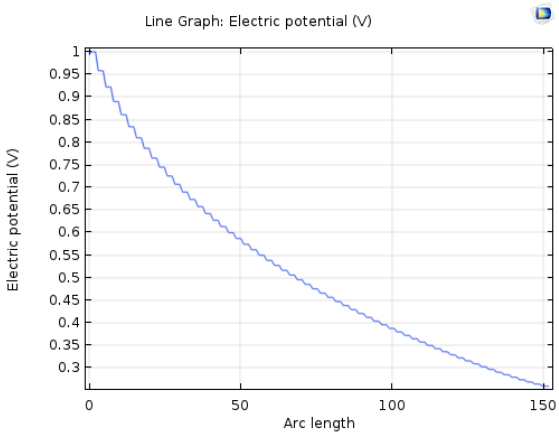

Figure 76. Voltage distribution 60 turns per disc

11.2 Voltage response distribution along disc pair with ungrounded iron core

With respect to the disc pair model, the transformer iron core is ungrounded, the last turn of the disc pair model is connected to ground and the first turn is connected to the high voltage terminal. Based on figure 78, 80 and 82, it is quite obvious that as the number of transformer turns per disc increases, the voltage response distribution would become more non-linear. All of the cases are simulated under capacitive voltage distribution. Therefore, the results in this subsection behave as the proof that at extremely high frequency level, the critical assumption mentioned in [1] is not correct.

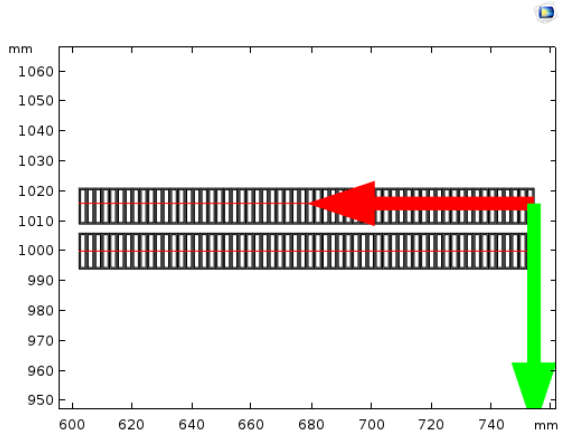

Figure 77. Cut-line 60 turns per disc

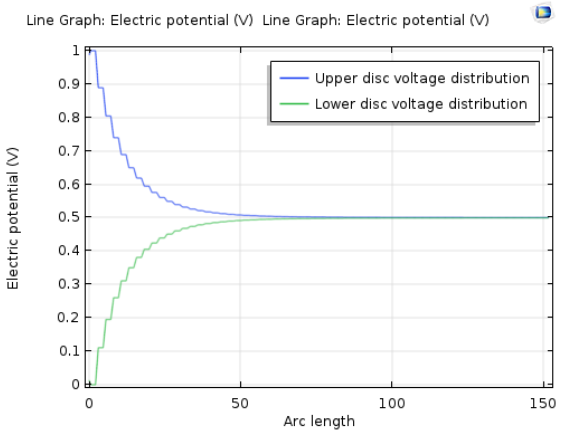

Figure 78. Voltage distribution 60 turns per disc

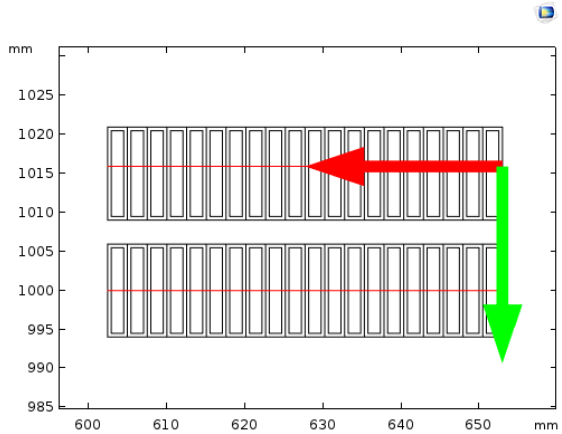

Figure 79. Cut-line 20 turns per disc

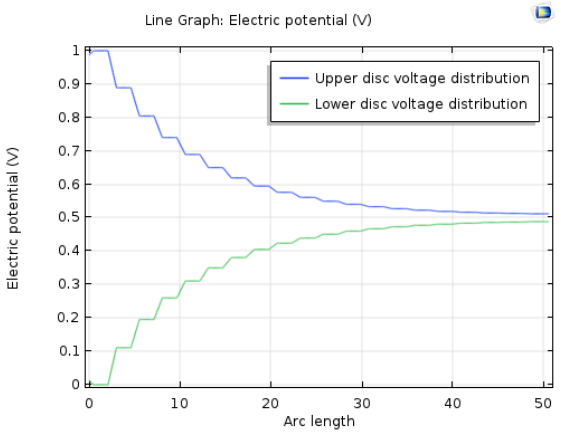

Figure 80. Voltage distribution 20 turns per disc

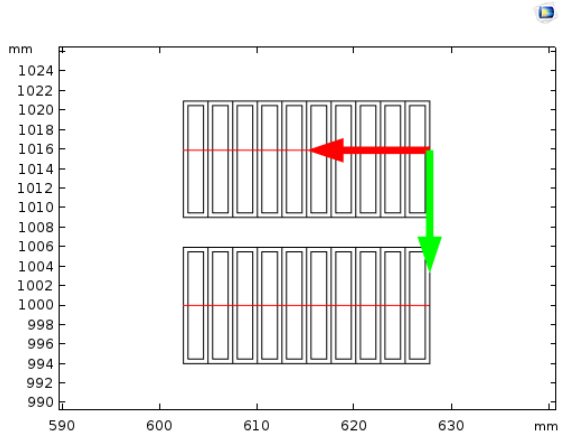

Figure 81. Cut-line 10 turns per disc

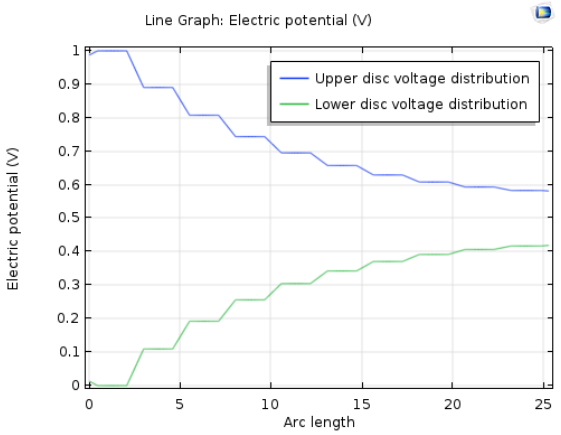

Figure 82. Voltage distribution 10 turns per disc

11.3 The explanation of the assumption

Based on all of the figures from the front page, we could know that at high frequency level, the voltage responses would distribute non-uniformly along the disc pair model when the influential capacitances dominate the voltage distribution. However, normally, when the frequency level is reduced to around 1MHz, not only the capacitance but also the inductance would start to play an important role in voltage distribution and the impedance of the inductance would gradually become dominant.

From the theoretical analysis, we could know that at the frequency range of 1MHz, if the mutual inductance between adjacent transformer turns is $L_{tt} = 0.126\mu H$, the impedance would then become $X_L = j\omega L_{tt} = j0.792\Omega$ and if the turn-turn series capacitance is $C_{tt} = 1752.36pF$, the impedance would then become $X_c = \frac{1}{j\omega C_{tt}} = -j570.66\Omega$. Because the impedance X_c and X_L are in parallel condition, the final result $R = X_L//X_c = 0.791\Omega$ would become similar to the impedance of the inductance. Thus, the impedance of the inductance would play an important role in the voltage distribution at the frequency range of 1MHz. If the voltage distribute inductively, the waveform would become more linear when we ideally consider that the LC resonances are not existing.

In reality, the resistance and the inductance matrix for disc winding are frequency dependent. If we change the frequency of the voltage source such as sinusoidal voltage source or surge overvoltages, the resistance matrix of the disc winding would vary a lot but the inductance matrix would have a slightly change. Therefore, when we do the verification in Matlab, for simplification, we could regard the magnitude of the inductance and resistance as fixed values.

In order to do the verification of the critical assumption mentioned in [1], we need to use the Matlab codes mentioned in the appendix. The derivation processes of those Matlab codes are explained thoroughly in chapter 13, 14 and 15. From the results of the Matlab codes, the figures for the crest voltage distribution and the voltage responses under different frequencies could be acquired. Actually, there are 15 transformer turns per disc.

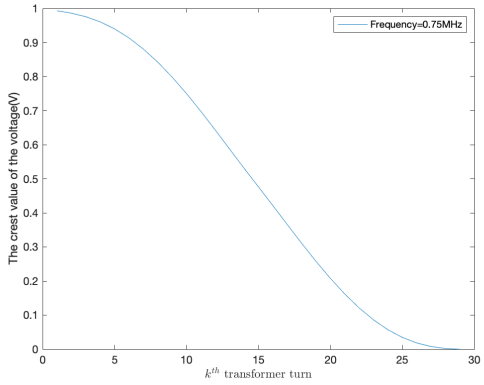

Figure 83. Crest voltage distribution f=0.75MHz

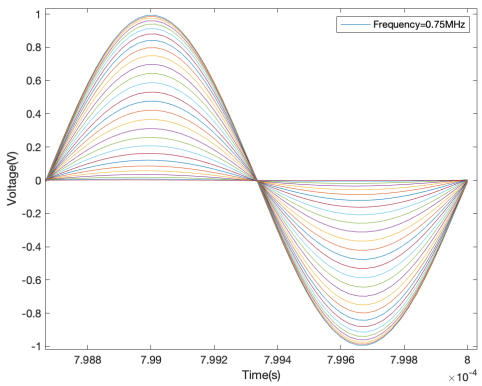

Figure 84. Voltage responses f=0.75MHz

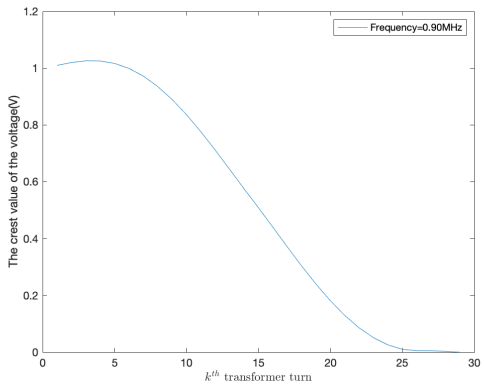

Figure 85. Crest voltage distribution f=0.90MHz

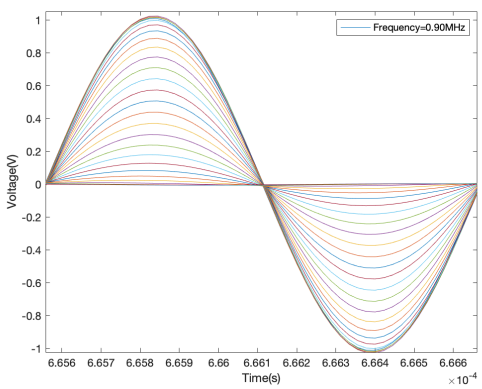

Figure 86. Voltage responses f=0.90MHz

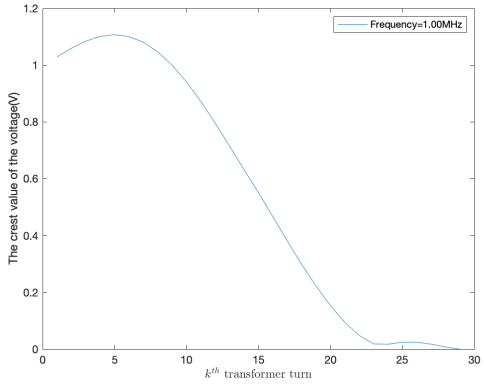

Figure 87. Crest voltage distribution f=1.00MHz

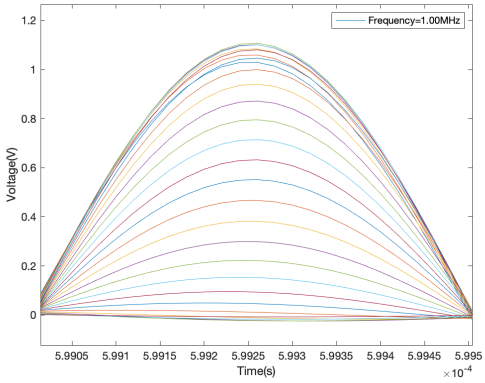

Figure 88. Voltage responses f=1.00MHz

According to the figure 83, when the frequency of the sinusoidal voltage source is considered to be $f = 0.75MHz$, the positive crest voltages for the voltage responses of the transformer turn would distribute linearly along the disc pair model. Whereas, when the frequency is increased to $f = 0.90MHz$, the positive crest voltage distribution line would be slightly distorted by LC resonances, which could be shown in figure 85. If the frequency climbs to $1MHz$, based on figure 87, it is obvious that the resonances would be more severe, but the shape of crest voltage distribution line could still be regarded as linear.

Indeed, the reason for this phenomenon is that when the frequency of the sinusoidal voltage source is more close to the smallest undamped network frequency $f_1 = 1.35MHz$, the LC resonances would become more severe and the voltage distribution line would be seriously distorted.

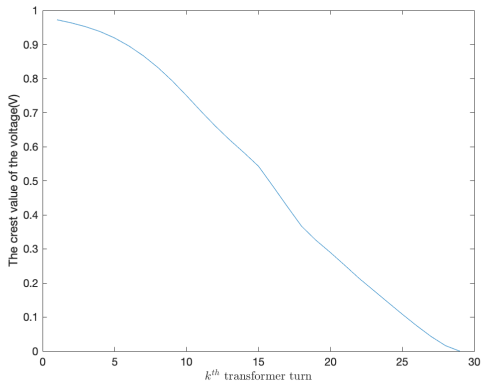

Figure 89. Crest voltage distribution lightning impulse

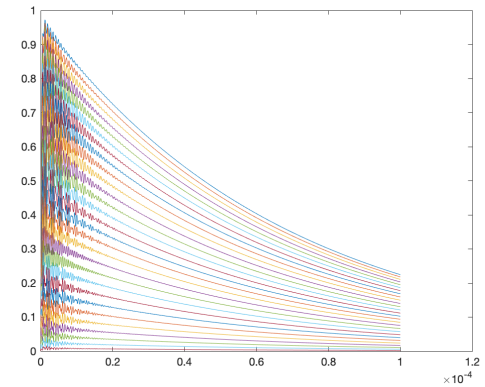

Figure 90. Voltage responses standard lightning impulse

As for figure 89 and 90, when the voltage source is a standard lightning impulse ($1.2\mu s/50\mu s$), the crest voltages for the voltage responses of the transformer turns would distribute linearly along the the disc pair shown in figure 89, which is the most convincing prove of the critical assumption. As a standard surge impulse strikes the disc pair, the voltage would almost distribute linearly along the disc pair model.

12 Voltage response distribution of the layer or disc winding

12.1 The case with grounded iron core and floating neutral

In [16], the authors provided us an equivalent capacitive circuit of the layer winding model shown in figure 91 and the real layer winding model. Similarly, the equivalent capacitive circuit for the disc winding model could also be drawn based on the same approach shown in figure 92. Under transient stage, the voltage would distribute non-linearly due to the presence of the disc-ground series capacitance C_{gi} as well as disc-disc series capacitance C_{si}. Actually, $X_g \approx 60 * X_s$ and $I_{gi} = \frac{U_{in}}{X_g + i * X_s}$. As a result, $I_{g1} \approx I_{g2} \approx I_{g3} \approx ... = I_g$ and $I_{ci} = (n - i) * I_g$ (n is the total number of discs).

Because of the existence of the disc-ground series capacitance C_{gi}, more ground capacitive currents I_c would flow through the disc-disc series capacitance C_s located nearby the top than that close to the bottom. The size of the red arrow in figure 92 indicates the intensity of the capacitive current I_c following through C_s, which would decrease from the top series capacitance to the bottom series capacitance. This would result in the unequal voltage drop $\Delta V_{disc-disc} = X_s * I_c$.

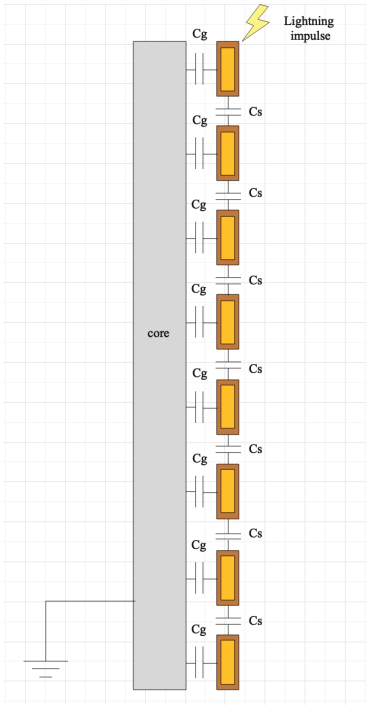

Figure 91. Layer winding model

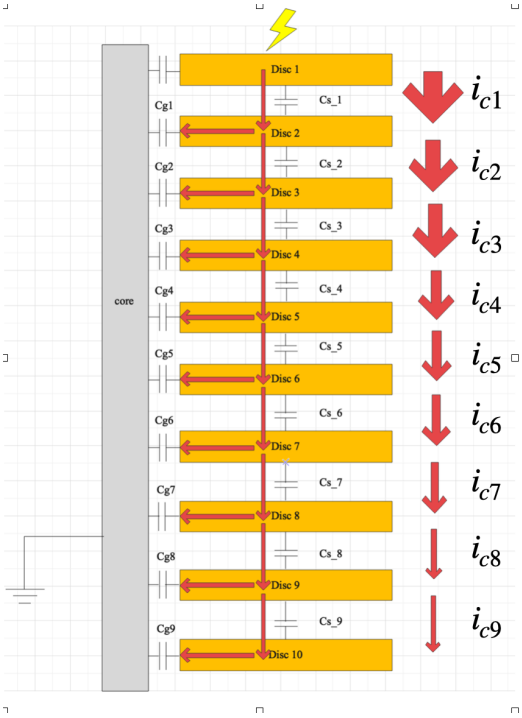

Figure 92. Equivalent disc winding model

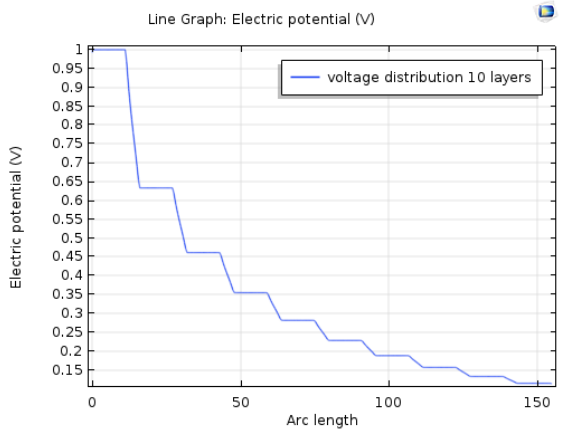

Figure 93. Voltage distribution 10 layers

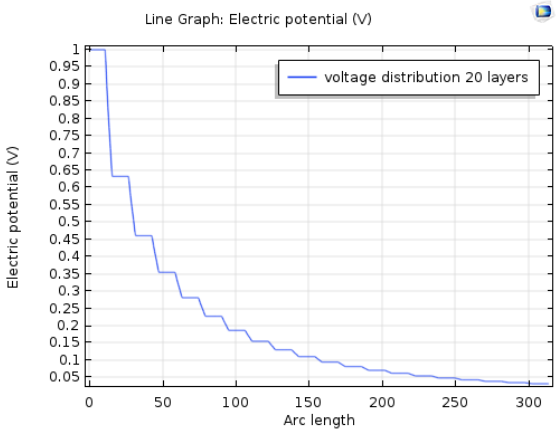

Figure 94. Voltage distribution 20 layers

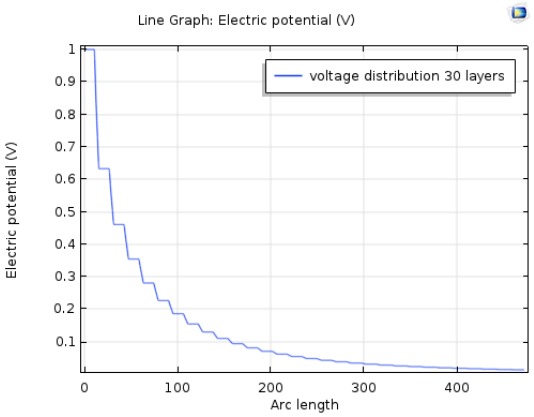

Figure 95. Voltage distribution 30 layers

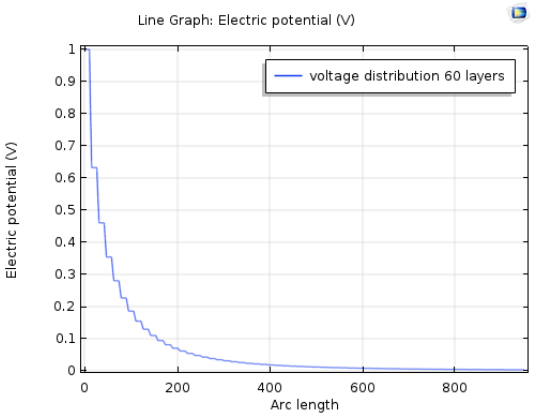

Figure 96. Voltage distribution 60 layers

12.2 The case with ungrounded iron core and floating neutral

With respect to the case when the transformer iron core is ungrounded but the last turn (layer) is grounded, the voltage distribution from top turn to intermediate turn and from intermediate turn to bottom turn would become symmetrical. The reason of the non-linear trend is that the mutual capacitance and capacitive currents would play an important role in the voltage distribution. Compared with the mutual capacitance, although the series capacitance would be much larger, the mutual capacitance could still distort the linear distribution line. If the mutual capacitance could be ideally removed, the voltage distribution would become linear.

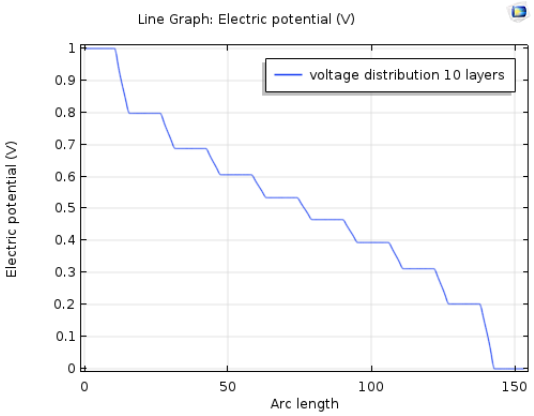

Figure 97. Voltage distribution 10 layers

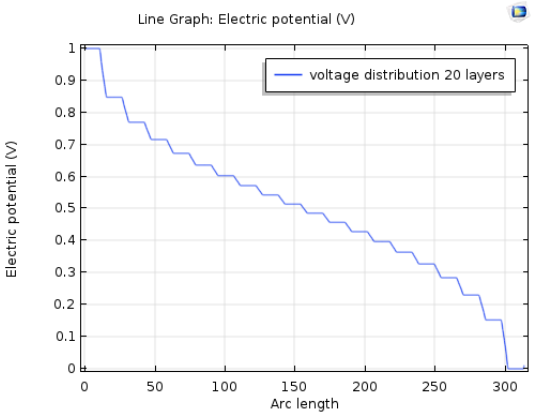

Figure 98. Voltage distribution 20 layers

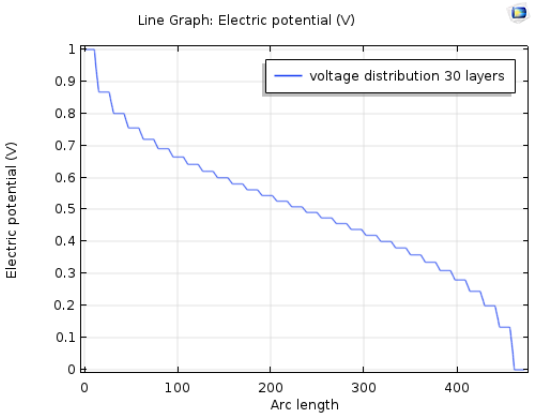

Figure 99. Voltage distribution 30 layers

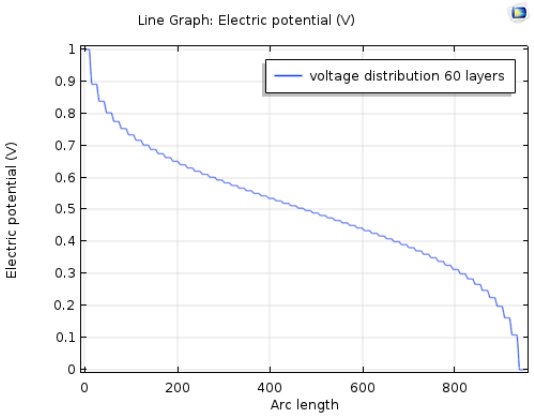

Figure 100. Voltage distribution 60 layers

13 The calculation of sinusoidal voltage distribution for transformer windings

From [2], according to C.Kroon's method, we could eventually acquire the voltage distribution formulas in the case of the standard lightning impulse ($1.2\mu s/50\ \mu s$) under three different situations. (However, in the original paper, there is an error in the condition that $\omega_i = \frac{\delta}{2}$.) In this chapter, we could also obtain the voltage distribution formulas in the case of sinusoidal wave under those three conditions after applying the same method. The derivation processes are explained in detail.

The following ordinary equation could be obtained from [1], which is the equation 13 in that reference and my derivation process would start from here: $[s(s+\delta) * C^* + L^{*-1}] * U^1 = [s(s+\delta) * N + M]$. In order to acquire the U^1 matrix, the Kramer's law should be introduced and after that, we could get the voltage distribution of the k^{th} turn with respect to earth in frequency domain.

$$U_k^1(s) = \frac{Det|s(s+\delta) * C_k^* + L_k^{*-1}|}{Det|s(s+\delta) * C^* + L^{*-1}|} = \frac{Det|s(s+\delta) * C_k^* + L_k^{*-1}|}{Det|C^*| * \prod_{i=1}^{m}[(s+\frac{\delta}{2})^2 + \omega_i^2 - (\frac{\delta}{2})^2]}$$

As for the equation above, C_k^* is obtained from the matrix C^* by replacing the k^{th} column by matrix N and L_k^{*-1} is obtained from the matrix L^{*-1} by replacing the k^{th} column by matrix M. Moreover, after using Preiniger's method, the voltage distribution of each transformer turn with respect to earth in time domain could be finally derived as the following equations.

$$\begin{aligned}
f(s) &= u * (\frac{b}{s^2+b^2}) \\
U_k^1(s) &= \frac{f(s)}{Det|C^*|} * [Det|C_k^*| + \sum_{i=1}^{m} \frac{a_{ik}}{(s+\frac{\delta}{2})^2 + \omega_i^2 - (\frac{\delta}{2})^2}] \\
a_{ik} &= \frac{Det|L_k^{*-1} - \omega_i^2 * C_k^*|}{\prod_{j=1}^{i-1}(\omega_j^2 - \omega_i^2) * \prod_{j=i+1}^{m}(\omega_j^2 - \omega_i^2)}
\end{aligned}$$

When the value of the undamped natural frequency ω_i is larger than $\frac{\delta}{2}$, the value of ω_i^* would become a real number. We could get the formula for the voltage of the k^{th} turn in the case of sinusoidal wave in time domain under this condition. The process of the derivation could be shown as below. $\omega_i^* = \sqrt{|\omega_i^2 - (\frac{\delta}{2})^2|}$

$$\begin{aligned}
U_k^1(t) &= \frac{u}{Det|C^*|} * [Det|C_k^*| * sin(b*t) + M(t)] \\
M(s) &= \sum_{i=1}^{m}(\frac{b}{s^2+b^2}) * \frac{a_{ik}}{(s+\frac{\delta}{2})^2 + \omega_i^{*2}} \\
N(s) &= \frac{1}{s^2+b^2} * \frac{1}{(s+\frac{\delta}{2})^2 + \omega_i^{*2}} = \frac{As+C}{s^2+b^2} + \frac{Bs+D}{(s+\frac{\delta}{2})^2 + \omega_i^{*2}} \\
A &= \frac{-\delta}{(\omega_i^2 - b^2)^2 + b^2 * \delta^2} \\
B &= \frac{\delta}{(\omega_i^2 - b^2)^2 + b^2 * \delta^2} \\
C &= \frac{\omega_i^2 - b^2}{(\omega_i^2 - b^2)^2 + b^2 * \delta^2} \\
D &= \frac{\delta^2 - (\omega_i^2 - b^2)}{(\omega_i^2 - b^2)^2 + b^2 * \delta^2}
\end{aligned}$$

$$M(t) = \sum_{i=1}^{m} \frac{b * a_{ik}}{(\omega_i^2 - b^2)^2 + b^2 * \delta^2} * [(-\delta) * cos(b * t) + (\frac{\omega_i^2 - b^2}{b}) * sin(b * t) + \delta * e^{-\frac{\delta}{2}t} * cos(\omega_i^* * t)$$
$$+ \frac{\frac{\delta^2}{2} - (\omega_i^2 - b^2)}{\omega_i^*} * e^{-\frac{\delta}{2}t} * sin(\omega_i^* * t)]$$
$$U_k^1(t) = \frac{u}{Det|C^*|} * (Det|C_k^*| * sin(b * t) + \sum_{i=1}^{m} \frac{b * a_{ik}}{(\omega_i^2 - b^2)^2 + b^2 * \delta^2} * [(-\delta) * cos(b * t) + (\frac{\omega_i^2 - b^2}{b}) * sin(b * t)$$
$$+ \delta * e^{-\frac{\delta}{2}t} * cos(\omega_i^* * t) + \frac{\frac{\delta^2}{2} - (\omega_i^2 - b^2)}{\omega_i^*} * e^{-\frac{\delta}{2}t} * sin(\omega_i^* * t)])$$

In order to calculate the Inverse Laplacian Transformation of N(s), that equation should be splited into two parts. The small fractions which are splited from N(s) are much easier to be transformed. After determining the elements: A, B, C and D, we could obtain M(t) ultimately.

When the value of the undamped natural network frequency ω_i is equal to $\frac{\delta}{2}$, then the value of ω_i^* would become zero at this condition. The voltage response of the k^{th} turn at this situation could be derived as below.

$$M(s) = \sum_{i=1}^{m} (\frac{b}{s^2 + b^2}) * \frac{a_{ik}}{(s + \frac{\delta}{2})^2}$$
$$N(s) = \frac{1}{s^2 + b^2} * \frac{1}{(s + \frac{\delta}{2})^2} = \frac{As + C}{s^2 + b^2} + \frac{B}{(s + \frac{\delta}{2})^2} + \frac{D}{s + \frac{\delta}{2}}$$
$$A = \frac{-16 * \delta}{(\delta^2 + 4 * b^2)^2}$$
$$B = \frac{4 * (\delta^2 + 4 * b^2)}{(\delta^2 + 4 * b^2)^2}$$
$$C = \frac{4 * (\delta^2 - 4 * b^2)}{(\delta^2 + 4 * b^2)^2}$$
$$D = \frac{16 * \delta}{(\delta^2 + 4 * b^2)^2}$$
$$M(t) = \sum_{i=1}^{m} \frac{4b * a_{ik}}{(\delta^2 + 4b^2)^2} * [(-4\delta) * cos(b * t) + (\frac{1}{b}) * (\delta^2 - 4b^2) * sin(b * t) + (\delta^2 + 4b^2) * t * e^{-\frac{\delta}{2} * t} + 4 * \delta * e^{-\frac{\delta}{2} * t}]$$
$$U_k^1(t) = \frac{u}{Det|C^*|} * (Det|C_k^*| * sin(b * t) + \sum_{i=1}^{m} \frac{4b * a_{ik}}{(\delta^2 + 4b^2)^2} * [(-4\delta) * cos(b * t) + (\frac{1}{b}) * (\delta^2 - 4b^2) * sin(b * t)$$
$$+ (\delta^2 + 4b^2) * t * e^{-\frac{\delta}{2} * t} + 4 * \delta * e^{-\frac{\delta}{2} * t}])$$

When the magnitude of the undamped natural frequency ω_i is smaller than $\frac{\delta}{2}$, the value of ω_i^* would become an imaginary number. Hence, at this situation, ω_i^* in the first condition should be replaced by $i * \omega_i^*$. The voltage response of the k^{th} turn at this situation would be derived as below.

$$M(s) = \sum_{i=1}^{m} (\frac{b}{s^2 + b^2}) * \frac{a_{ik}}{(s + \frac{\delta}{2})^2 - \omega_i^{*2}}$$
$$M(t) = \sum_{i=1}^{m} \frac{b * a_{ik}}{(\omega_i^2 - b^2)^2 + b^2 * \delta^2} * [(-\delta) * cos(b * t) + (\frac{\omega_i^2 - b^2}{b}) * sin(b * t) + \delta * e^{-\frac{\delta}{2}t} * cos(i * \omega_i^* * t)$$
$$+ \frac{\frac{\delta^2}{2} - (\omega_i^2 - b^2)}{i * \omega_i^*} * e^{-\frac{\delta}{2}t} * sin(i * \omega_i^* * t)]$$
$$U_k^1(t) = \frac{u}{Det|C^*|} * (Det|C_k^*| * sin(b * t) + \sum_{i=1}^{m} \frac{b * a_{ik}}{(\omega_i^2 - b^2)^2 + b^2 * \delta^2} * [(-\delta) * cos(b * t) + (\frac{\omega_i^2 - b^2}{b}) * sin(b * t)$$
$$+ \delta * e^{-\frac{\delta}{2}t} * cos(i * \omega_i^* * t) + \frac{\frac{\delta^2}{2} - (\omega_i^2 - b^2)}{i * \omega_i^*} * e^{-\frac{\delta}{2}t} * sin(i * \omega_i^* * t)])$$

The Matlab code for the voltage response distribution in the case of sinusoidal wave under those three conditions is shown in the first appendix. This Matlab code actually has some constraints: The Matlab code ought to be used when the neutral or last turn is grounded. Besides, this code should only be used in disc pair model and layer winding model (one turn per disc).

During the derivation process, there are indeed three scenarios for the voltage distribution of the k^{th} transformer turn: the first scenario is $\omega_i > \frac{\delta}{2}$, the second scenario is $\omega_i = \frac{\delta}{2}$ and the third scenario is $\omega_i < \frac{\delta}{2}$. Those three scenarios would also be mentioned in chapter 14 and 15.

14 The calculation of the step voltage distribution for transformer windings

In this chapter, we could obtain the formula for the voltage of the k^{th} transformer turn with respect to earth in the case of step voltage source under those three scenarios after applying the same derivation method as professor C.Kroon's. The derivation processes are shown as below.

Firstly, if the value of the undamped natural network frequency ω_i is larger than $\frac{\delta}{2}$, the value of ω_i^* ought to be a real number. The voltage of the k^{th} turn in the case of step voltage under this scenario in time domain could be derived as follows.

$$
\begin{aligned}
U_k^1(s) &= \frac{u}{Det|C^*|} * (Det|C_k^*| * \frac{1}{s} + \frac{1}{s} * \sum_{i=1}^{m} \frac{a_{ik}}{(s+\frac{\delta}{2})^2 + \omega_i^{*2}}) \\
U_k^1(t) &= \frac{u}{Det|C^*|} * (Det|C_k^*| * 1 + M(t)) \\
M(s) &= \sum_{i=1}^{m} a_{ik} * [\frac{1}{s} * \frac{1}{(s+\frac{\delta}{2})^2 + \omega_i^{*2}}] \\
N(s) &= \frac{1}{s} * \frac{1}{(s+\frac{\delta}{2})^2 + \omega_i^{*2}} = \frac{A}{s} + \frac{Bs + C}{(s+\frac{\delta}{2})^2 + \omega_i^{*2}} \\
A &= \frac{1}{\omega_i^2} \\
B &= \frac{-1}{\omega_i^2} \\
C &= \frac{-\delta}{\omega_i^2} \\
M(t) &= \sum_{i=1}^{m} (\frac{a_{ik}}{\omega_i^2}) * [1 - cos(\omega_i^* * t) * e^{-\frac{\delta}{2} * t} - \frac{\delta}{2 * \omega_i^*} * sin(\omega_i^* * t) * e^{-\frac{\delta}{2} * t}] \\
U_k^1(t) &= \frac{u}{Det|C^*|} * (Det|C_k^*| * 1 + \sum_{i=1}^{m} (\frac{a_{ik}}{\omega_i^2}) * [1 - cos(\omega_i^* * t) * e^{-\frac{\delta}{2} * t} - \frac{\delta}{2 * \omega_i^*} * sin(\omega_i^* * t) * e^{-\frac{\delta}{2} * t}])
\end{aligned}
$$

When the magnitude of the natural network frequency ω_i is equal to $\frac{\delta}{2}$, the value of ω_i^* is zero. The voltage of the k^{th} transformer turn in the case of step voltage under this scenario in time domain could be derived as below.

$$
\begin{aligned}
U_k^1(s) &= \frac{u}{Det|C^*|} * (Det|C_k^*| * \frac{1}{s} + \frac{1}{s} * \sum_{i=1}^{m} \frac{a_{ik}}{(s+\frac{\delta}{2})^2}) \\
U_k^1(t) &= \frac{u}{Det|C^*|} * (Det|C_k^*| * 1 + M(t)) \\
M(s) &= \sum_{i=1}^{m} a_{ik} * [\frac{1}{s} * \frac{1}{(s+\frac{\delta}{2})^2}] \\
N(s) &= \frac{1}{s} * \frac{1}{(s+\frac{\delta}{2})^2} = \frac{A}{s} + \frac{B}{(s+\frac{\delta}{2})^2} + \frac{C}{(s+\frac{\delta}{2})} \\
A &= \frac{4}{\delta^2} \\
B &= \frac{-2}{\delta} \\
C &= \frac{-4}{\delta^2}
\end{aligned}
$$

$$
\begin{aligned}
M(t) &= \sum_{i=1}^{m} a_{ik} * (\frac{4}{\delta^2}) * [1 - \frac{\delta}{2} * t * e^{-\frac{\delta}{2} * t} - e^{-\frac{\delta}{2} * t}] \\
U_k^1(t) &= \frac{u}{Det|C^*|} * (Det|C_k^*| * 1 + \sum_{i=1}^{m} a_{ik} * (\frac{4}{\delta^2}) * [1 - \frac{\delta}{2} * t * e^{-\frac{\delta}{2} * t} - e^{-\frac{\delta}{2} * t}])
\end{aligned}
$$

When the value of the natural network frequency ω_i is smaller than $\frac{\delta}{2}$, then the value of ω_i^* should be an imaginary number. ω_i^* should be replaced by $i * \omega_i^*$ from the first case. The voltage of the k^{th} transformer turn in the case of step voltage under this scenario in time domain could be derived as below.

$$U_k^1(s) = \frac{u}{Det|C^*|} * (Det|C_k^*| * \frac{1}{s} + \frac{1}{s} * \sum_{i=1}^{m} \frac{a_{ik}}{(s+\frac{\delta}{2})^2 - \omega_i^{*2}})$$

$$U_k^1(t) = \frac{u}{Det|C^*|} * (Det|C_k^*| * 1 + M(t))$$

$$M(s) = \sum_{i=1}^{m} a_{ik} * [\frac{1}{s} * \frac{1}{(s+\frac{\delta}{2})^2 - \omega_i^{*2}}]$$

$$M(t) = \sum_{i=1}^{m} (\frac{a_{ik}}{\omega_i^2}) * [1 - cos(i * \omega_i^* * t) * e^{-\frac{\delta}{2} * t} - \frac{\delta}{2 * i * \omega_i^*} * sin(i * \omega_i^* * t) * e^{-\frac{\delta}{2} * t}]$$

$$U_k^1(t) = \frac{u}{Det|C^*|} * (Det|C_k^*| * 1 + \sum_{i=1}^{m} (\frac{a_{ik}}{\omega_i^2}) * [1 - cos(i * \omega_i^* * t) * e^{-\frac{\delta}{2} * t} - \frac{\delta}{2 * i * \omega_i^*} * sin(i * \omega_i^* * t) * e^{-\frac{\delta}{2} * t}])$$

The Matlab code for the voltage distribution in the case of this step voltage source under those three scenarios is shown in the second appendix. This Matlab code is suitable for the disc pair model (last turn grounded) and ordinary layer winding (There is only one transformer turn per disc).

15 The calculation of the surge voltage distribution for the transformer windings

In [2], C.Kroon has already provided his analytical formula for the voltage of the k^{th} turn with respect to earth both in frequency domain and time domain, described as the equation 15 and equation 18 respectively in the reference. Nonetheless, he overlooked the process of the inverse Laplacian transformation from the frequency domain to time domain in the reference paper. Therefore, in this chapter, the derivation process is added.

If the value of the natural network frequency ω_i is larger than $\frac{\delta}{2}$, then the value of ω_i^* ought to be a real number. The voltage of the k^{th} transformer turn in the case of surge voltage under this scenario in time domain could ultimately be derived as the equations below.

$$U_k^1(s) = \frac{u}{Det|C^*|} * (Det|C_k^*| * (\frac{1}{s+\alpha_1} - \frac{1}{s+\alpha_2}) + (\frac{1}{s+\alpha_1} - \frac{1}{s+\alpha_2}) * \sum_{i=1}^{m} \frac{a_{ik}}{(s+\frac{\delta}{2})^2 + \omega_i^{*2}})$$

$$M_1(s) = \frac{1}{s+\alpha_1} * \sum_{i=1}^{m} \frac{a_{ik}}{(s+\frac{\delta}{2})^2 + \omega_i^{*2}} = \sum_{i=1}^{m} a_{ik} * N_1(s)$$

$$M_2(s) = \frac{1}{s+\alpha_2} * \sum_{i=1}^{m} \frac{a_{ik}}{(s+\frac{\delta}{2})^2 + \omega_i^{*2}} = \sum_{i=1}^{m} a_{ik} * N_2(s)$$

$$N_1(s) = \frac{A_1}{s+\alpha_1} + \frac{B_1 * s + C_1}{(s+\frac{\delta}{2})^2 + \omega_i^{*2}}$$

$$N_2(s) = \frac{A_2}{s+\alpha_2} + \frac{B_2 * s + C_2}{(s+\frac{\delta}{2})^2 + \omega_i^{*2}}$$

$$A_1 = \frac{1}{\alpha_1 * (\alpha_1 - \delta) + \omega_i^2}$$

$$B_1 = \frac{-1}{\alpha_1 * (\alpha_1 - \delta) + \omega_i^2}$$

$$C_1 = \frac{\alpha_1 - \delta}{\alpha_1 * (\alpha_1 - \delta) + \omega_i^2}$$

$$A_2 = \frac{1}{\alpha_2 * (\alpha_2 - \delta) + \omega_i^2}$$

$$B_2 = \frac{-1}{\alpha_2 * (\alpha_2 - \delta) + \omega_i^2}$$

$$C_2 = \frac{\alpha_2 - \delta}{\alpha_2 * (\alpha_2 - \delta) + \omega_i^2}$$

$$N_1(t) = A_1 * e^{-\alpha_1 * t} + B_1 * e^{-\frac{\delta}{2} * t} * cos(\omega_i^* * t) + \frac{C_1 - \frac{\delta}{2} * B_1}{\omega_i^*} * e^{-\frac{\delta}{2} * t} * sin(\omega_i^* * t)$$

$$N_2(t) = A_2 * e^{-\alpha_2 * t} + B_2 * e^{-\frac{\delta}{2} * t} * cos(\omega_i^* * t) + \frac{C_2 - \frac{\delta}{2} * B_2}{\omega_i^*} * e^{-\frac{\delta}{2} * t} * sin(\omega_i^* * t)$$

$$M_1(t) = \sum_{i=1}^{m} \frac{a_{ik}}{\alpha_1 * (\alpha_1 - \delta) + \omega_i^2} * (e^{-\alpha_1 * t} - e^{-\frac{\delta}{2} * t} * cos(\omega_i^* * t) + \frac{\alpha_1 - \frac{\delta}{2}}{\omega_i^*} * e^{-\frac{\delta}{2} * t} * sin(\omega_i^* * t))$$

$$M_2(t) = \sum_{i=1}^{m} \frac{a_{ik}}{\alpha_2 * (\alpha_2 - \delta) + \omega_i^2} * (e^{-\alpha_2 * t} - e^{-\frac{\delta}{2} * t} * cos(\omega_i^* * t) + \frac{\alpha_2 - \frac{\delta}{2}}{\omega_i^*} * e^{-\frac{\delta}{2} * t} * sin(\omega_i^* * t))$$

$$X_1(t) = cos(\omega_i^* * t) - \frac{\alpha_1 - \frac{\delta}{2}}{\omega_i^*} * sin(\omega_i^* * t)$$

$$X_2(t) = cos(\omega_i^* * t) - \frac{\alpha_2 - \frac{\delta}{2}}{\omega_i^*} * sin(\omega_i^* * t)$$

$$M_1(t) = \sum_{i=1}^{m} \frac{a_{ik}}{\alpha_1 * (\alpha_1 - \delta) + \omega_i^2} * (e^{-\alpha_1 * t} - X_1(t) * e^{-\frac{\delta}{2} * t})$$

$$M_2(t) = \sum_{i=1}^{m} \frac{a_{ik}}{\alpha_1 * (\alpha_1 - \delta) + \omega_i^2} * (e^{-\alpha_1 * t} - X_1(t) * e^{-\frac{\delta}{2} * t})$$

$$U_k^1(t) = \frac{u}{Det|C^*|} * (Det|C_k^*| * (e^{-\alpha_1 * t} - e^{-\alpha_2 * t}) + \sum_{i=1}^{m} \frac{a_{ik}}{\alpha_1 * (\alpha_1 - \delta) + \omega_i^2} * (e^{-\alpha_1 * t} - X_1(t) * e^{-\frac{\delta}{2} * t})$$
$$- \sum_{i=1}^{m} \frac{a_{ik}}{\alpha_2 * (\alpha_2 - \delta) + \omega_i^2} * (e^{-\alpha_2 * t} - X_2(t) * e^{-\frac{\delta}{2} * t}))$$

Moreover, if the value of the natural network frequency ω_i is equal to $\frac{\delta}{2}$, then the value of ω_i^* would become zero. The voltage of the k^{th} transformer turn in the case of surge voltage under this scenario in time domain could be derived as the formulas below.

$$M_1(s) = \frac{1}{s + \alpha_1} * \sum_{i=1}^{m} \frac{a_{ik}}{(s + \frac{\delta}{2})^2} = \sum_{i=1}^{m} a_{ik} * N_1(s)$$

$$M_2(s) = \frac{1}{s + \alpha_2} * \sum_{i=1}^{m} \frac{a_{ik}}{(s + \frac{\delta}{2})^2} = \sum_{i=1}^{m} a_{ik} * N_2(s)$$

$$N_1(s) = \frac{1}{s + \alpha_1} * \frac{1}{(s + \frac{\delta}{2})^2}$$

$$N_2(s) = \frac{1}{s + \alpha_2} * \frac{1}{(s + \frac{\delta}{2})^2}$$

$$N_1(s) = \frac{A_1}{s + \alpha_1} + \frac{B_1}{(s + \frac{\delta}{2})^2} + \frac{C_1}{s + \frac{\delta}{2}} = \frac{A_1}{s + \alpha_1} + \frac{B_1 + C_1 * (s + \frac{\delta}{2})}{(s + \frac{\delta}{2})^2}$$

$$N_2(s) = \frac{A_2}{s + \alpha_2} + \frac{B_2}{(s + \frac{\delta}{2})^2} + \frac{C_2}{s + \frac{\delta}{2}} = \frac{A_2}{s + \alpha_2} + \frac{B_2 + C_2 * (s + \frac{\delta}{2})}{(s + \frac{\delta}{2})^2}$$

$$A_1 = \frac{1}{(\alpha_1 - \frac{\delta}{2})^2}$$

$$B_1 = \frac{1}{\alpha_1 - \frac{\delta}{2}}$$

$$C_1 = \frac{-1}{(\alpha_1 - \frac{\delta}{2})^2}$$

$$A_2 = \frac{1}{(\alpha_2 - \frac{\delta}{2})^2}$$

$$B_2 = \frac{1}{\alpha_2 - \frac{\delta}{2}}$$

$$C_2 = \frac{-1}{(\alpha_2 - \frac{\delta}{2})^2}$$

$$N_1(s) = \frac{1}{(\alpha_1 - \frac{\delta}{2})^2} * (e^{-\alpha_1 * t} + (\alpha_1 - \frac{\delta}{2}) * t * e^{-\frac{\delta}{2} * t} - e^{-\frac{\delta}{2} * t})$$

$$N_2(s) = \frac{1}{(\alpha_2 - \frac{\delta}{2})^2} * (e^{-\alpha_2 * t} + (\alpha_2 - \frac{\delta}{2}) * t * e^{-\frac{\delta}{2} * t} - e^{-\frac{\delta}{2} * t})$$

$$X_1(t) = 1 - (\alpha_1 - \frac{\delta}{2}) * t$$

$$X_2(t) = 1 - (\alpha_2 - \frac{\delta}{2}) * t$$

$$N_1(s) = \frac{1}{(\alpha_1 - \frac{\delta}{2})^2} * (e^{-\alpha_1 * t} - X_1(t) * e^{-\frac{\delta}{2} * t}) = \frac{1}{\alpha_1 * (\alpha_1 - \delta) + \omega_i^2} * (e^{-\alpha_1 * t} - X_1(t) * e^{-\frac{\delta}{2} * t})$$

$$N_2(s) = \frac{1}{(\alpha_2 - \frac{\delta}{2})^2} * (e^{-\alpha_2 * t} - X_2(t) * e^{-\frac{\delta}{2} * t}) = \frac{1}{\alpha_2 * (\alpha_2 - \delta) + \omega_i^2} * (e^{-\alpha_2 * t} - X_2(t) * e^{-\frac{\delta}{2} * t})$$

$$U_k^1(t) = \frac{u}{Det|C^*|} * (Det|C_k^*| * (e^{-\alpha_1 * t} - e^{-\alpha_2 * t}) + \sum_{i=1}^{m} \frac{a_{ik}}{\alpha_1 * (\alpha_1 - \delta) + \omega_i^2} * (e^{-\alpha_1 * t} - X_1(t) * e^{-\frac{\delta}{2} * t}) - \sum_{i=1}^{m} \frac{a_{ik}}{\alpha_2 * (\alpha_2 - \delta) + \omega_i^2} * (e^{-\alpha_2 * t} - X_2(t) * e^{-\frac{\delta}{2} * t}))$$

When the value of the natural network frequency ω_i is smaller than $\frac{\delta}{2}$, then the value of ω_i^* ought to become an imaginary number. Therefore, ω_i^* should be replaced by $i * \omega_i^*$ from the first scenario. Compared with the first case, only $X_1(t)$ and $X_2(t)$ should be modified. The voltage of the k^{th} transformer turn in the case of surge voltage under this scenario in time domain could be finally derived as below.

$$X_1(t) = cos(i * \omega_i^* * t) - \frac{\alpha_1 - \frac{\delta}{2}}{i * \omega_i^*} * sin(i * \omega_i^* * t)$$

$$X_2(t) = cos(i * \omega_i^* * t) - \frac{\alpha_2 - \frac{\delta}{2}}{i * \omega_i^*} * sin(i * \omega_i^* * t)$$

$$U_k^1(t) = \frac{u}{Det|C^*|} * (Det|C_k^*| * (e^{-\alpha_1 * t} - e^{-\alpha_2 * t}) + \sum_{i=1}^{m} \frac{a_{ik}}{\alpha_1 * (\alpha_1 - \delta) + \omega_i^2} * (e^{-\alpha_1 * t} - X_1(t) * e^{-\frac{\delta}{2} * t}) - \sum_{i=1}^{m} \frac{a_{ik}}{\alpha_2 * (\alpha_2 - \delta) + \omega_i^2} * (e^{-\alpha_2 * t} - X_2(t) * e^{-\frac{\delta}{2} * t}))$$

In fact, the undamped natural network frequency ω_i is one of the eigenvalues of the matrix $C^{*^{-1}} L^{*^{-1}}$. Thus, the value of ω_i is only dependent on the inductance matrix and capacitance matrix. Moreover, ω_i could also determine the shape of the voltage response.

For instance, in [11], as for the geometry of the layer winding when the neutral is isolated, the voltage responses along the layer winding with the laminated iron core are different from those without laminated iron core. The reason of this phenomenon is that the value of inductance would reduce significantly when we remove the iron core from the transformer winding because the relative permeability of iron is 4000 but that of air is only 1. The natural network frequency ω_i would vary a lot. Thus, the voltage responses with the core are different from the voltage responses without the core when the neutral is isolated.

In fact, there is an error in [2], as for the second scenario, when the value of natural network frequency ω_i is equal to $\frac{\delta}{2}$, then $X_1(t)$ should become $\left\{1 - (\alpha_1 - \frac{\delta}{2}) * t\right\}$ rather than $\left\{1 + (\alpha_1 - \frac{\delta}{2}) * t\right\}$, which is shown in the reference paper. Meanwhile, $X_2(t)$ should become $\left\{1 - (\alpha_2 - \frac{\delta}{2}) * t\right\}$ rather than $\left\{1 + (\alpha_2 - \frac{\delta}{2}) * t\right\}$.

The Matlab code of the voltage responses in the case of surge voltage source under those three scenarios is shown in the third appendix. Additionally, there are some constrains for the application of this Matlab code: the code is suitable for the disc pair model when the last transformer turn is grounded as well as the layer winding model that there are only one turn per disc.

16 Negative mutual resistance discussion

According to [17], we could know that it is rather reasonable to have negative mutual resistances during the numerical calculation. The resistances could bring some damping to the voltage responses and result in the active power losses.

As for the active power losses P_{loss} in the geometry of two adjacent conductors, AC current I_1 would flow in the first conductor and current I_2 would flow in the second conductor. Moreover, I_1 and I_2 are the peak values for AC currents. The equation of P_{loss} would be shown as follow:

$$P_{loss} = \frac{1}{2} * R_{11} * |I_1|^2 + \frac{1}{2} * R_{22} * |I_2|^2 + R_{12} * Re(I_1 * I_2^*)$$

When both of I_1 and I_2 are positive real values, we could know that a negative value of R_{12} would indicate that the total power dissipation with both current sources active is lower than it would be if we choose to add up the power values calculated with each one turned on by itself. Moreover, we have to pay attention that the total power dissipation could not be the negative value, which means that P_{loss} should always become a positive value.

As for the layer winding model in Comsol, the distance between layer winding and the transformer core is set to be 70mm and the distance between adjacent layers is 0.3mm. It is worth mentioning that there is only one turn per layer in the layer winding. According to the consequence analysis, when the number of effective layers is larger than 8 (ignore the grounded turn), the negative mutual resistances would start to emerge. In addition, as we increase the number of the layers, the number of the negative resistances would increase exponentially. The table below provided 7 cases corresponding to the position of the negative resistances and the total number of the negative resistances.

Number of effective layers (without grounded turn)	Position of the negative resistances (half)
7	None negative values
8	None negative values
9	R_{15}, R_{16}
10	R_{14}, R_{15}, R_{16}, R_{17}, R_{18}
11	R_{14}, R_{15}, R_{16}, R_{17}, R_{18}, R_{19}, R_{27}, R_{28}
12	R_{14}, R_{15}, R_{16}, R_{17}, R_{18}, R_{19}, R_{110}, R_{26}, R_{27}, R_{28}, R_{29}, R_{210}
13	R_{14}, R_{15}, R_{16}, R_{17}, R_{18}, R_{19}, R_{110}, R_{111}, R_{112}, R_{26}, R_{27}, R_{28}, R_{29}, R_{210}, R_{211}, R_{38}, R_{39}, R_{310}
20	Half of the resistances from the resistance matrix are negative

Table 9. The positions for the negative resistances

17 The reshape of the basic transformer geometry in Comsol

17.1 The reshape of the geometry with transformer iron core

According to [11], A. Miki and T. Hosoya mentioned that the main magnetic flux Φ_{hv} generated by high voltage winding inside the transformer iron core will be cancelled by the magnetic flux Φ_{sc} caused from the short-circuited low voltage winding which is not energized. Therefore, only leakage flux contributes to the voltage responses inside the winding.

Based on figure 101, the fast alternating excitation currents represented by dashed blue arrowlines in hv winding would cause the fast-variation magnetic flux inside the transformer iron core. The fast alternating magnetic flux would induce the opposite currents represented by the dashed red arrowline inside the non-impulsed lv winding, if the distance between those windings are not large, through the right-hand screw rule, the magnetic flux inside the transformer iron core would almost been totally cancelled.

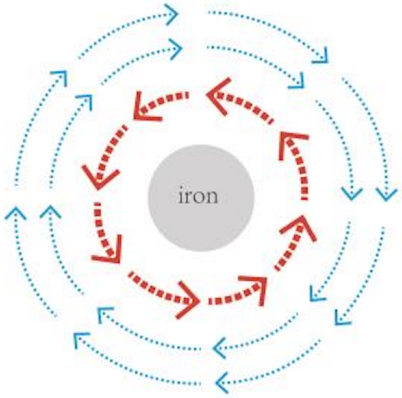

Figure 101. current distribution–iron core

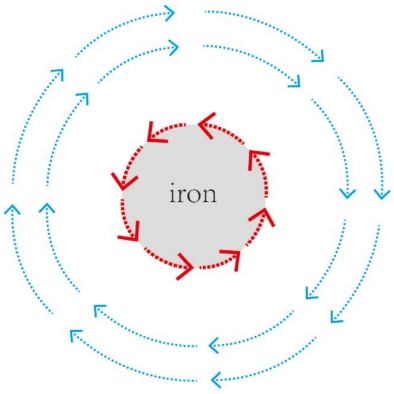

Figure 102. current distribution–iron core

Based on figure 102, if the short-circuited lv winding is removed, at higher frequency level ranging from 100kHz to 1MHz, the eddy currents represented by the dashed red arrowlines I_{eddy} would be induced on the surface of the transformer iron core due to the severe skin effect. Actually, the eddy currents could then be regarded as the induced currents flowing within the short-circuited lv winding in figure 101. Thus, under this condition, the main magnetic flux generated by the excitation currents inside a transformer iron core $\Phi_{excitation}$ would also been canceled by the opposite flux generated by the eddy currents Φ_{eddy}. As a result, the inductance of a transformer winding with an iron core is similar to that of a winding without an iron core. In case of building a disc winding model in Comsol, the transformer iron core could be removed.

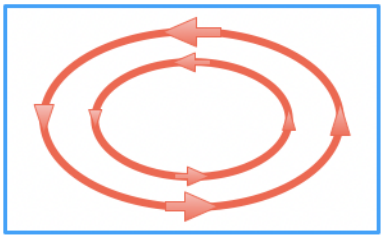

Figure 103. Eddy currents–solid iron core

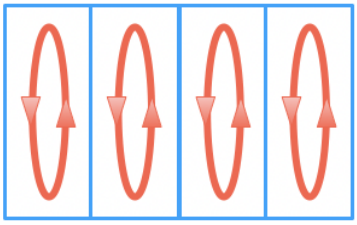

Figure 104. Eddy currents–laminated iron core

In reality, the laminated iron core is widely used in the large power transformer. During normal operation $f = 50Hz$, the thickness of the laminated component $\tau_{thickness} = 0.2mm$ is still far larger than the skin depth $\delta_{skin} \approx 0.4\mu m$. The intensity of the eddy current density at the normal stage $f = 50Hz$ is far smaller than that at the transient stage $f = 1MHz$ according to figure 113 and figure 114. After the application of the laminated transformer iron core, eddy currents would be divided into a number of fractions and effectively limited because the total flowing path of the induced eddy currents would be enlarged significantly, which could be seen in figure 103 and 104. Thus, the total eddy currents

would face more resistance and the intensity would reduce significantly. Due to these good properties, the transformer designers choose to use the laminated iron core.

Whereas, at transient stage $f = 1MHz$, based on figure 115, the induced eddy currents would only flow on the surface of the laminated iron core and the intensity of the eddy currents would become more than $1500(A/m^2)$. Due to the large intensity of the eddy currents, even though the total flowing path is enlarged through lamination, the eddy currents couldn't be limited effectively, which would have the same performance as the solid iron core. Thus, as a result, in order to simplify the geometry of the hv disc winding model and save the simulation time in Comsol simulation, the solid iron transformer core is selected.

In [11], A. Miki and T. Hosoya thought that the transformer iron core could be replaced by an air core. However, in Comsol simulation, according to figure 107, the flux linkages could penetrate the air core freely, which is in contrary to the results obtained from the case with solid iron core shown in figure 108. Theoretically, the position of solid iron core should be empty because figure 105 has similar magnetic flux density as figure 106.

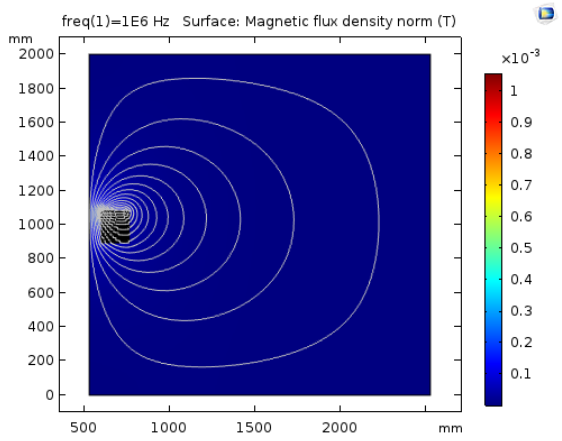

Figure 105. Magnetic flux density-empty

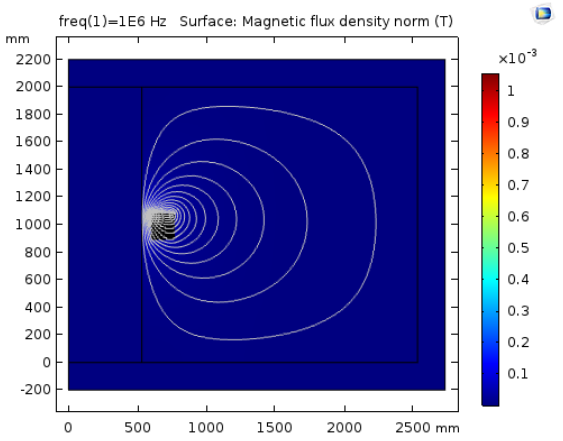

Figure 106. Magnetic flux density with iron core

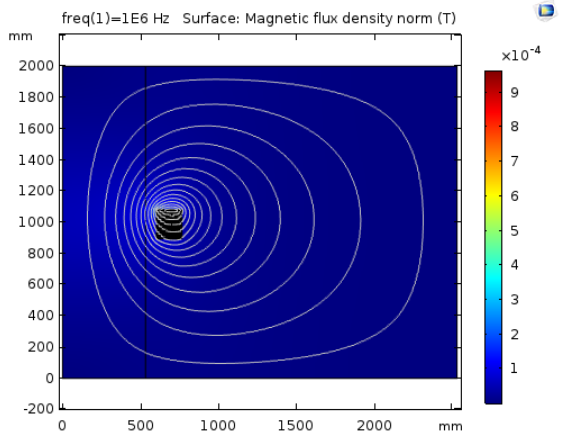

Figure 107. Magnetic flux density with air core

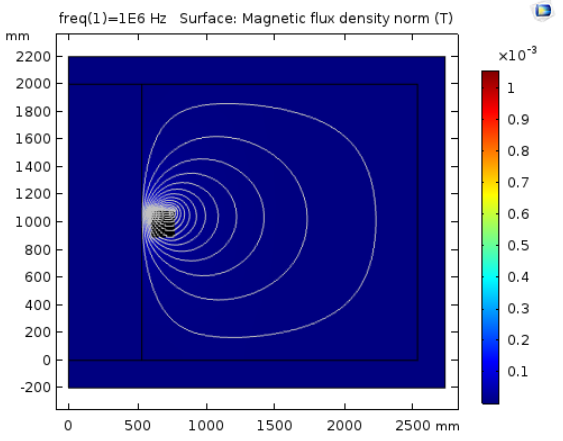

Figure 108. Magnetic flux density with iron core

17.2 The reshape of the geometry with ferrite F transformer core

In this chapter, the original transformer iron core is considered to be replaced by the ferrite F core. Actually, ferrite F is a kind of non-magnetic material with really low conductivity $\sigma = 10^{-12} S/m$ and high relative permeability $\mu_r = 3000$. Therefore, at higher frequency level, the skin effect could be eliminated due to the extremely small σ and all of the flux linkages could freely penetrate the transformer iron core.

With respect to the disc pair model, if the outer iron shield is removed and the material of the transformer core is set to become ferrite F, the mutual inductance between the disc pair L_s under different frequency levels could be acquired through numerical methods, which could be shown in the second column from table 10. If the outer iron shield is reserved, the magnitudes of the mutual inductance between disc pair L_s under a range of frequencies could also be obtained, which is shown in the third column from table 10.

Frequency	Mutual inductance without iron outer shield	Mutual inductance with iron outer shield
f=1Hz	$L_s = 0.017584H$	$L_s = 0.020955H$
f=10Hz	$L_s = 0.017584H$	$L_s = 0.017743H$
f=100Hz	$L_s = 0.017584H$	$L_s = 0.017587H$
f=1kHz	$L_s = 0.017592H$	$L_s = 0.017592H$
f=10kHz	$L_s = 0.017565H$	$L_s = 0.017565H$
f=100kHz	$L_s = 0.017501H$	$L_s = 0.017501H$
f=1MHz	$L_s = 0.017486H$	$L_s = 0.017486H$

Table 10. Mutual inductance comparison between two geometries under different frequencies

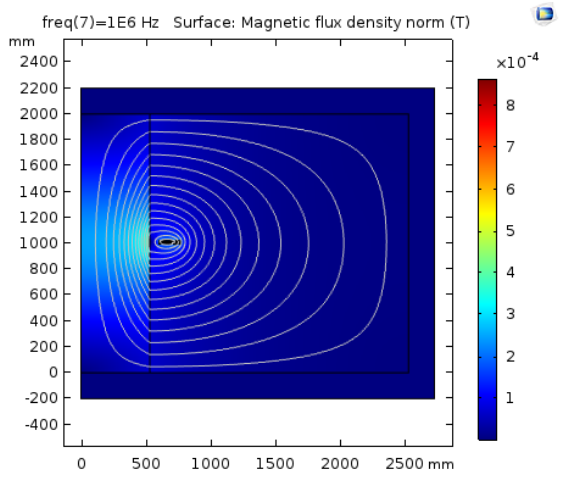

Figure 109. Ferrite core–with outer iron shield

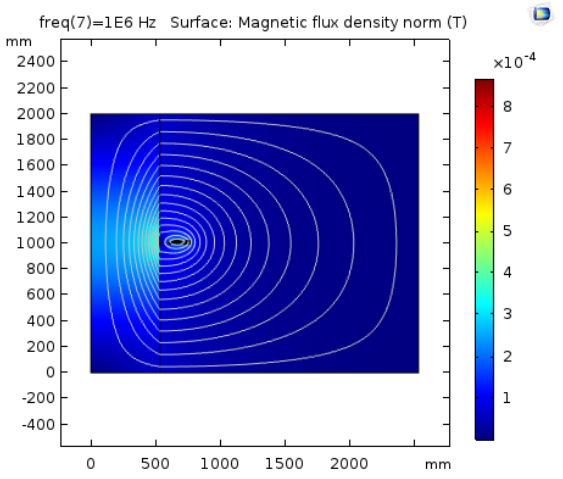

Figure 110. Ferrite core–without outer iron shield

Frequency	Mutual resistance without iron outer shield	Mutual resistance with iron outer shield
f=1Hz	$R_s = 3.0834 * 10^{-8}\Omega$	$R_s = 0.11374\Omega$
f=10Hz	$R_s = 3.0409 * 10^{-6}\Omega$	$R_s = 0.14606\Omega$
f=100Hz	$R_s = -3.6081 * 10^{-5}\Omega$	$R_s = 0.14948\Omega$
f=1kHz	$R_s = 1.4327 * 10^{-4}\Omega$	$R_s = 0.15138\Omega$
f=10kHz	$R_s = 2.6887\Omega$	$R_s = 2.8400\Omega$
f=100kHz	$R_s = 14.773\Omega$	$R_s = 14.924\Omega$
f=1MHz	$R_s = 52.877\Omega$	$R_s = 53.209\Omega$

Table 11. Mutual resistance comparison between two geometries under different frequencies

According to table 10 and table 11, it is quite obvious that at higher frequency level such as 100kHz and 1MHz, the values for the mutual resistance and mutual inductance between the disc pair model with or without the outer iron shield would almost become the same. Therefore, the outer iron shield could be removed for faster numerical calculation.

18 Mutual inductance and resistance calculations in Comsol

$I_1 = 1A$ is the excitation current that has been applied to each of the transformer turns from the first disc. In Comsol, it is very important that the coil group checkbox should be clicked. There are basically N transformer turns per disc inside the disc pair Comsol geometry. If all of the excitation currents are DC currents, there would be no eddy currents induced inside the solid iron transformer core. Thus, the flux linkages could easily penetrate the iron core and there is no skin effect at DC condition.

If the excitation currents I_1 from the first disc are AC currents, thus, inside the transformer core, the eddy currents generated by the variation of the original magnetic fields would occur. However, at high frequency level, due to the presence of eddy currents, skin effect would play an important role in the magnetic field density distribution inside the solid iron core. Because of the skin effect, the eddy currents would only concentrate within the narrow area nearby the surface. Moreover, the magnitude of the induced eddy current is proportional to the original current variation rate.(σ represents for the conductivity of the transformer core and μ represents for the product of μ_0 and relative permeability μ_r.)

$$\delta_{skin} = \sqrt{\frac{2}{\omega * \sigma * \mu}}$$

The magnetic fields generated by the eddy currents would always oppose the variation of the original magnetic fields. In other words, the magnetic fields produced by eddy currents would always hinder the change of the original magnetic fields. Whereas, at high frequency level, the magnetic fields generated by eddy currents would cancel the original magnetic fields. Because if the variation of the original magnetic field is fast enough, eddy currents would always produce the opposite magnetic fields compared with the original magnetic fields.

When the frequency increases, the skin depth δ_{skin} would decrease significantly according to the formula above. However, the magnitude of the eddy currents density would increase drastically. Therefore, a larger amount of eddy currents are forced to flow within thinner region nearby the surface, which could be shown in figure 113.

Because higher eddy currents induce higher opposite magnetic fields, the flux linkages inside transformer iron core could be totally canceled at high frequency level. If the intensity of the eddy currents is not severe, the opposite fields produced by eddy currents could not completely cancel the original field. Therefore, there are still some magnetic linkages or magnetic flux density remained inside the iron core, which could also be shown in figure 111.

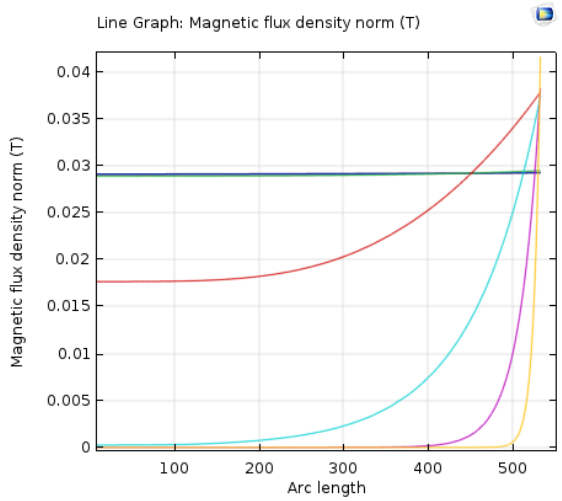

Figure 111. Magnetic flux density–frequencies

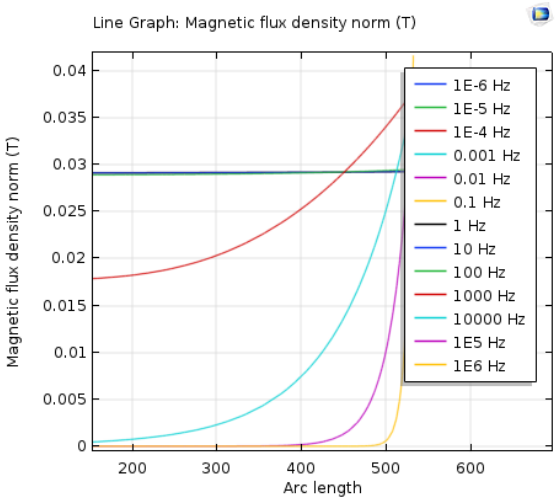

Figure 112. Legend for magnetic flux density

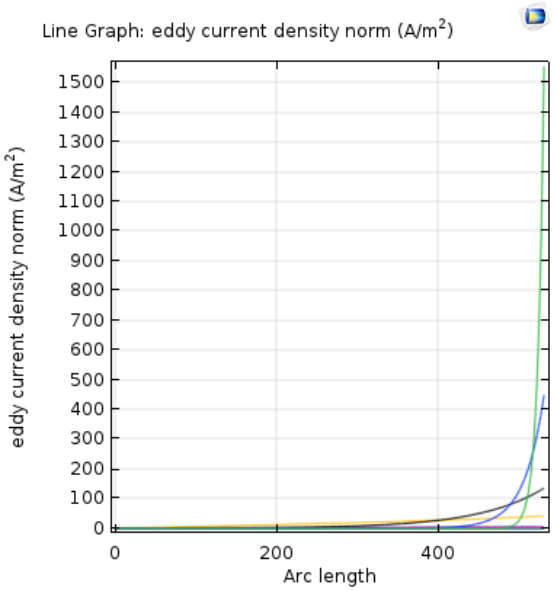

Figure 113. Eddy current density–frequencies

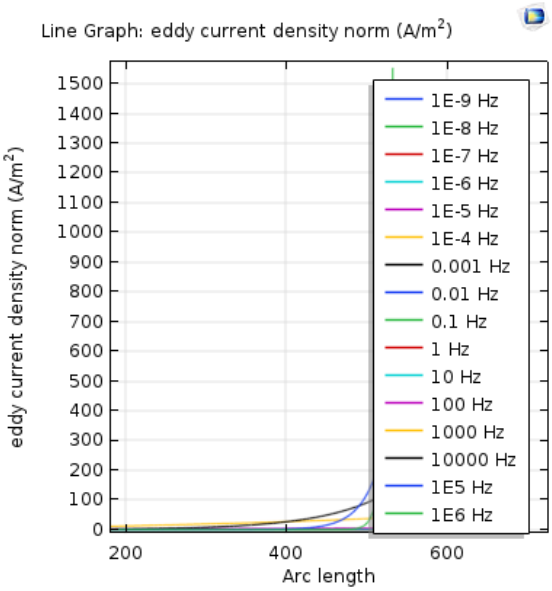

Figure 114. Legend for eddy current density

18.1 Iron transformer core

The inductance is actually a geometry parameter, which should be independent from the frequency. However, when we apply a solid iron core to the transformer disc pair model in Comsol, we have introduced another conductor to the geometry because the iron core could generate eddy currents. Therefore, there are three conductors inside the model: two transformer discs and one solid iron core. The iron core would change the mutual inductance between the two discs.

The magnetic energy would be transmitted from the the energized transformer disc to the non-energized disc through the flux linkages. Nonetheless, at higher frequency level, the flux linkages inside the transformer core would be canceled a lot due to the opposite magnetic flux generated by the eddy currents. Therefore, only a small part of magnetic energy could reach the non-energized disc and the resulted mutual inductance would be really small compare with the mutual inductance at DC stage.

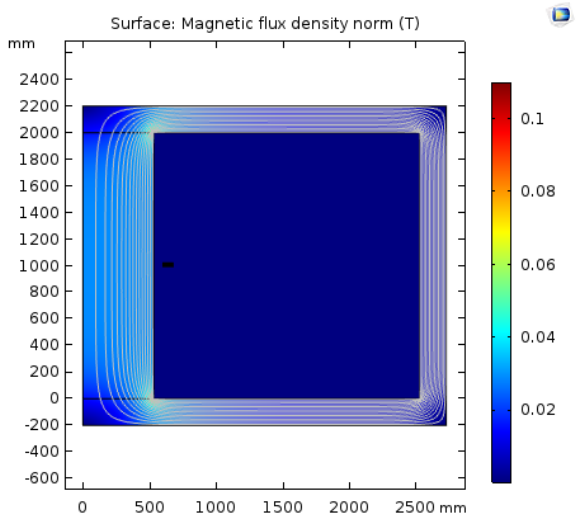

Figure 115. Magnetic flux density DC iron core

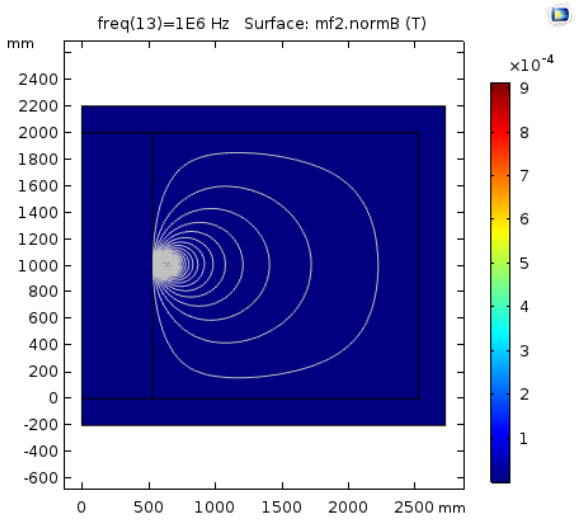

Figure 116. Magnetic flux density f=1MHz iron core

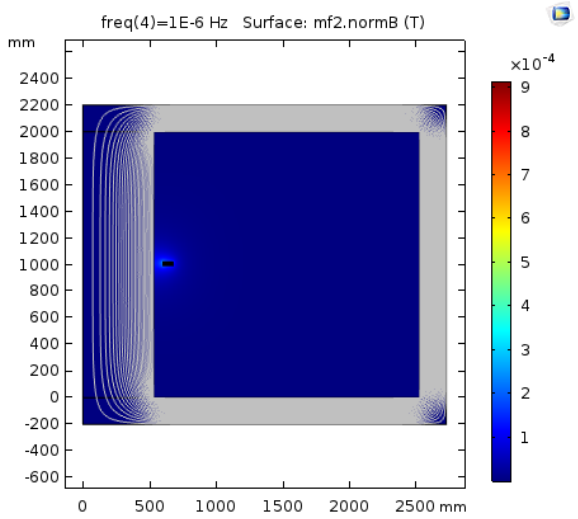

Figure 117. Magnetic flux density $f = 10^{-6}Hz$

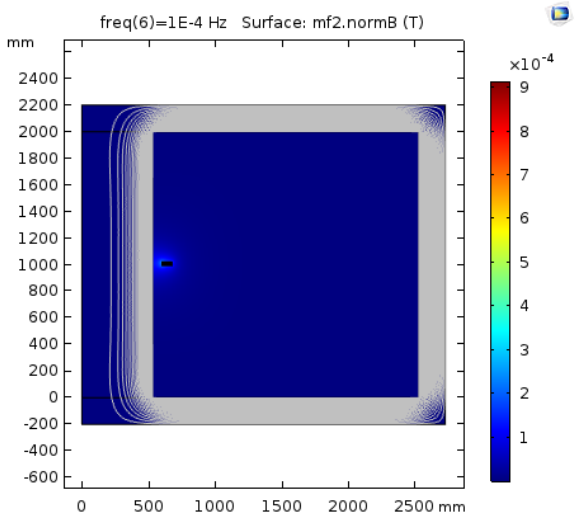

Figure 118. Magnetic flux density $f = 10^{-4}Hz$

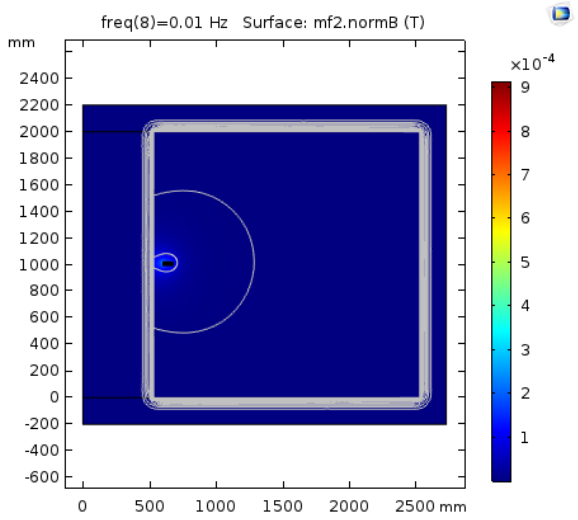

Figure 119. Magnetic flux density f=0.01Hz

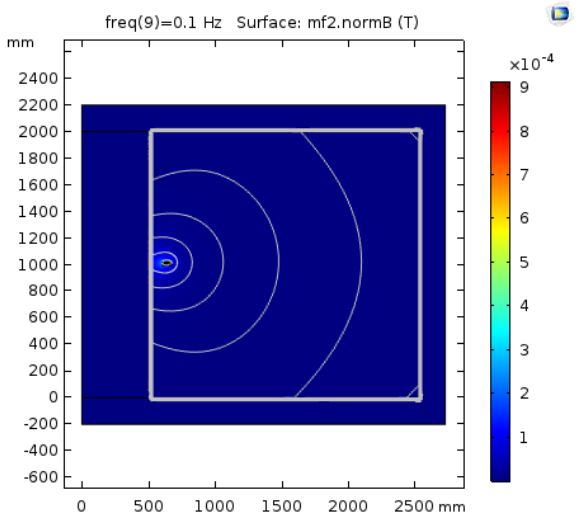

Figure 120. Magnetic flux density f=0.1Hz

According to figures from 117 to 120, it is quite obvious that the penetration depth would reduce significantly when the frequency of the excitation currents is increased. At high frequency level, due to the extremely thin skin depth which is in the order of nanometer, the flux linkages could not penetrate the core and the eddy currents could be regarded as only flowing on the surface of the iron core. Thus, whatever inside the transformer core would be canceled by eddy currents and the solid iron core could be empty, which has been mentioned in the subsection 17.1.

Honestly, the results of the case for the solid iron transformer core are actually not accurate. Because at higher frequency level such as 1MHz, the skin depth of the solid iron core would be around 2.67 nanometer, which is too thin for Comsol to capture. In order to capture that extremely thin skin depth, the maximum element size for mesh of the surface region should be at least one third of the skin depth, which is too precious for Comsol to calculate. Thus, the magnetic field energy located within the skin depth would be neglected by Comsol. The consequence of the mutual inductance calculated by Comsol would be smaller than the real mutual inductance.

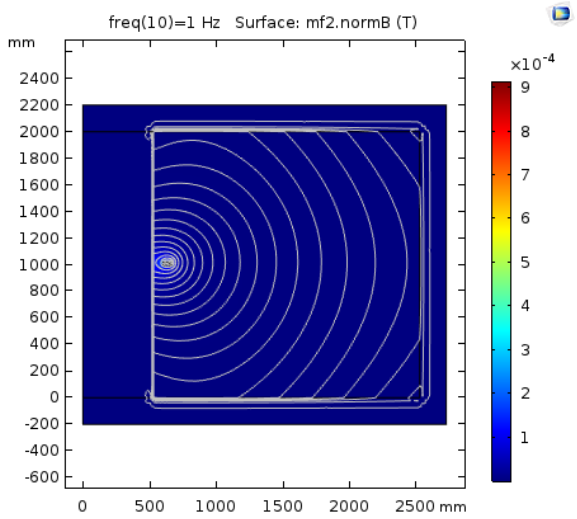

Figure 121. Magnetic flux density f=1Hz

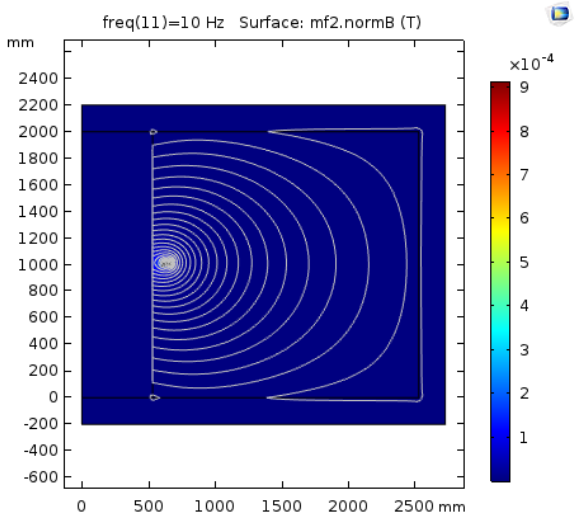

Figure 122. Magnetic flux density f=10Hz

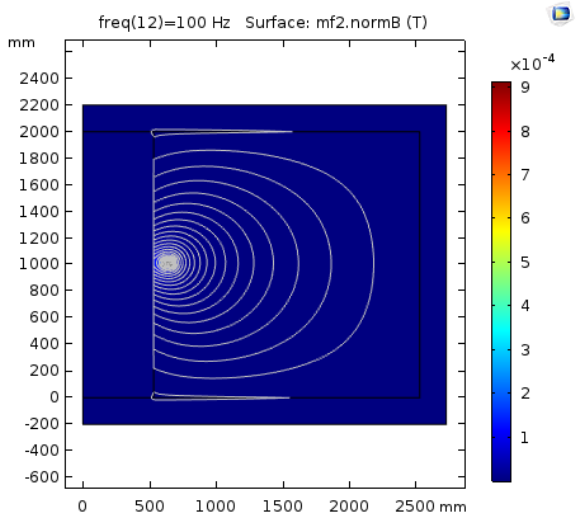

Figure 123. Magnetic flux density f=100Hz

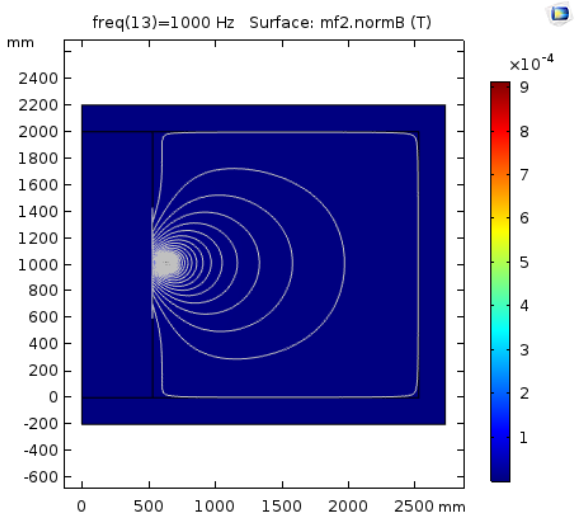

Figure 124. Magnetic flux density f=1kHz

In order to reduce the eddy currents that could generate more energy loss and cancel the original magnetic fields, we choose to use the laminated iron core. The reason why the laminated iron core could have the ability to reduce the eddy currents is that the total flowing path for the eddy currents would be expanded significantly and the eddy currents would face more resistance. However, if the width of the laminated layer is still larger than the skin depth, the skin effect should also be taken into account. Thus, at higher frequency level, some of the flux linkages inside the laminated transformer core would also be canceled.

As for the laminated iron core, the elements are not electrically connected and there would be some insulation material between the elements so that the electrons cannot flow from one element to another. If we are able to ideally laminate the solid iron core, the eddy currents could be regarded as negligible, thus, the mutual inductance is independent from the frequency and the magnetic field lines could penetrate easily into the core.

If we choose to use the solid iron core in Comsol, the mutual resistances between the transformer discs would become really large at higher frequency level. Due to the skin effect, all of the induced eddy currents would flow within the very narrow region, thus, the eddy currents would need more energy to flow. The energized disc provides the energy for the eddy currents and therefore, the energized coil feels a lot of resistances. Compared with the air core, the solid iron core would result a lot of damping for the voltage responses.

18.2 Ferrite transformer core

In order to let the flux linkages easily penetrate into the transformer core and get rid of the induced eddy currents, the material named ferrite F needs to be selected. Ferrite F has really high relative permeability $\mu_r = 3000$ but extremely low conductivity $\sigma = 10^{-12} S/m$, which is comparable with the most of insulators. Therefore, at higher frequency level such as 1MHz, the skin depth of ferrite F would be still large and all of the flux linkages could freely flow inside the transformer core. The magnetic flux density at the frequency of 0.01Hz and 1MHz could be seen as the figures below.

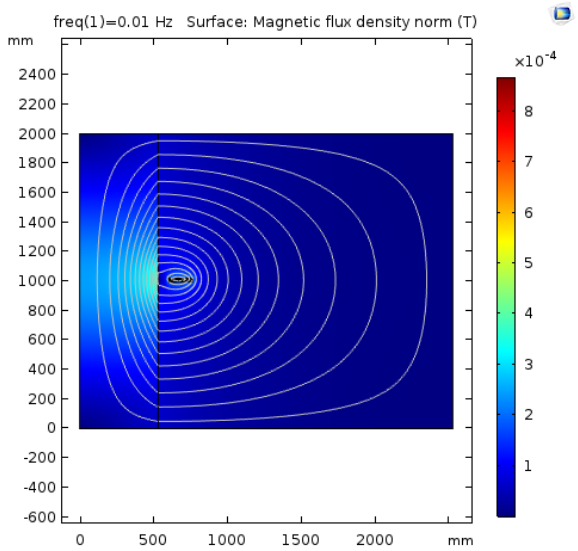

Figure 125. Magnetic flux density at f=0.01Hz

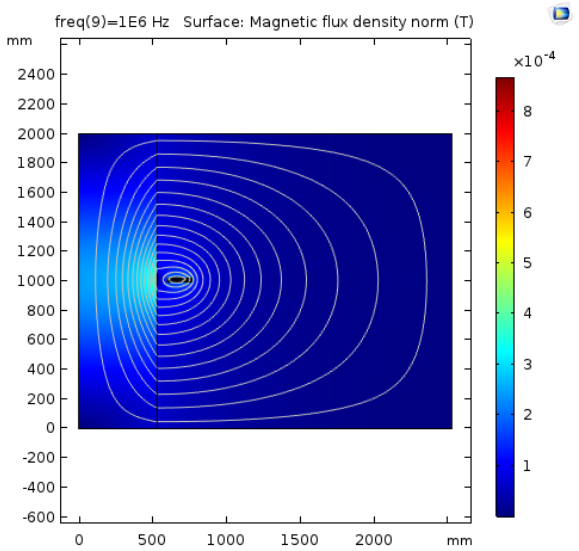

Figure 126. Magnetic flux density at f=1MHz

According to figure 127, it is quite obvious that there would be almost no eddy currents inside the ferrite core when the frequency of the original currents range from $10^{-2} Hz$ to 100kHz. Nonetheless, if the frequency reaches 1MHz, the eddy currents would increase non-linearly from the center of the core to the outer boundary of the core. The reason of that phenomenon is probably because of the saturation of the ferrite F core caused by the B-H curve. At higher frequency level, the relative permeability μ_r would decrease significantly, as we increase the frequency.

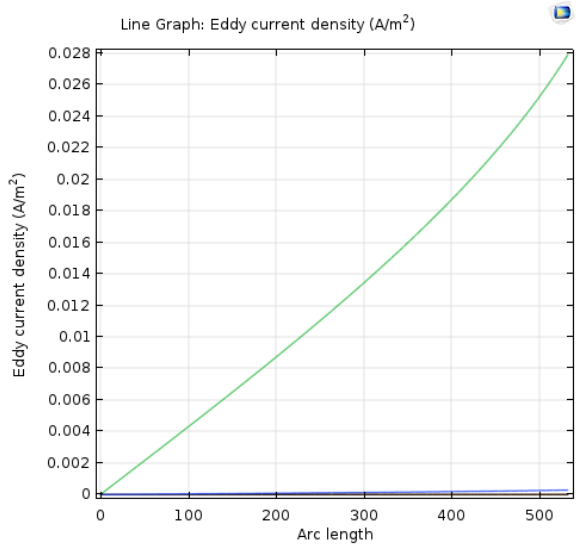

Figure 127. Eddy current density–frequencies

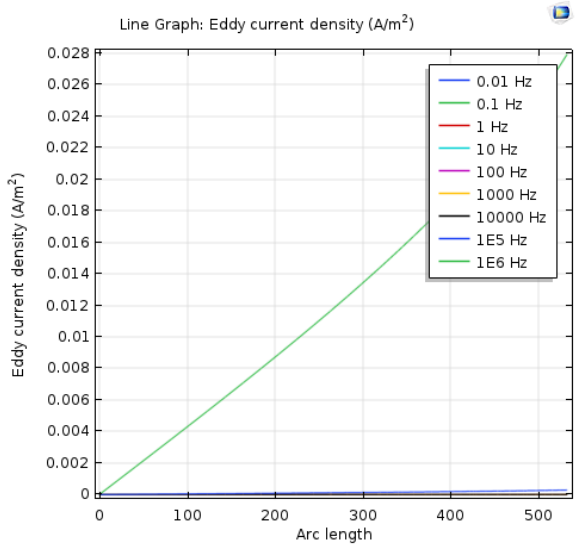

Figure 128. Legend for eddy current density

As for figure 129, when the frequency ranges from 100kHz to 1MHz, the eddy current density would increase drastically as the frequency goes up. Moreover, the eddy currents densities at their corresponding frequencies would increase along the cut-line of the ferrite core under this condition. However, when the frequency ranges from 10kHz to 100kHz shown in figure 130, the total eddy current density increments are rather tiny. Thus, we could regard that there would be no eddy currents under this phenomenon.

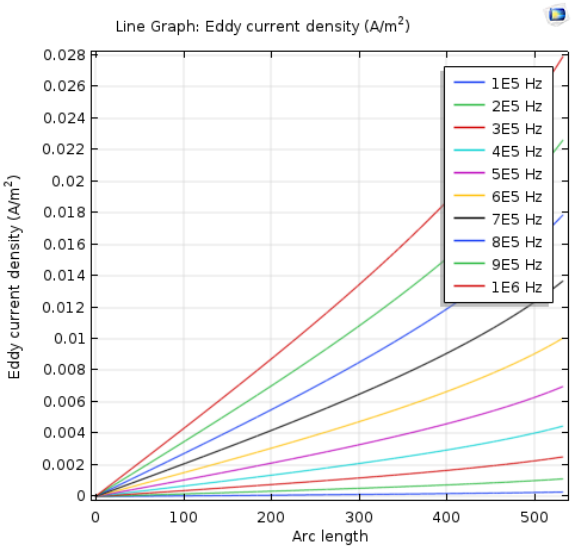

Figure 129. Eddy current density–frequencies

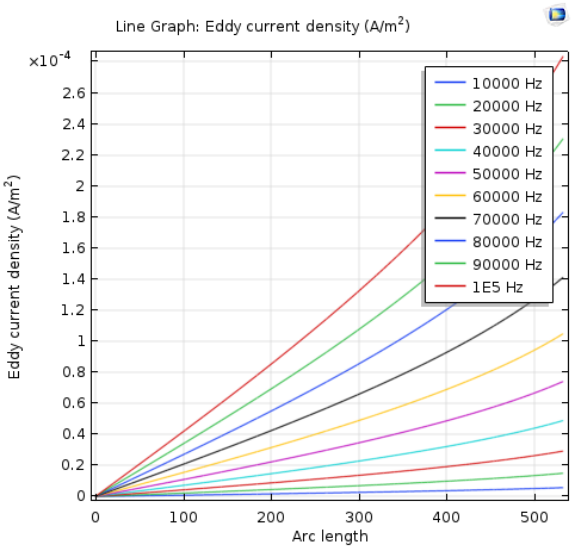

Figure 130. Eddy current density–frequencies

Figure 132 illustrates that if all of the frequency ranges are beneath 100kHz, the magnetic flux densities inside the ferrite F core would almost become the same. Additionally, along the cut-line shown in figure 131, the magnitudes of the magnetic flux density would gradually increase from the center of the core to the edge. The reason why the eddy current is less inside is because the opposite eddy currents flows on the region of the core that are closer to the outside boundary already cancel some of the magnetic flux. Therefore, less eddy currents would be present deep inside of the core than a little inside the core.

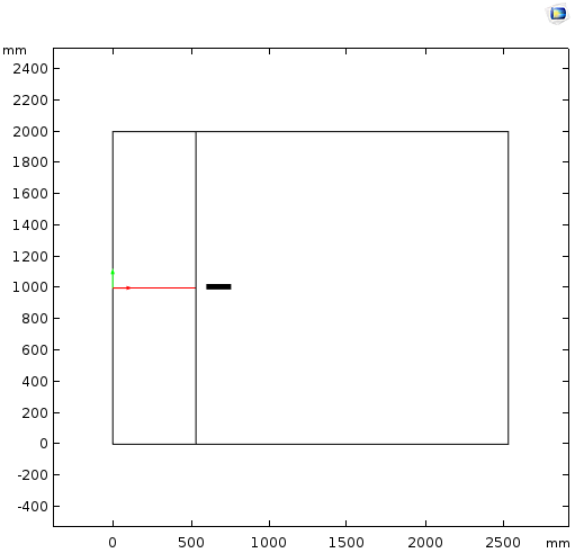

Figure 131. Cut-line of the transformer core

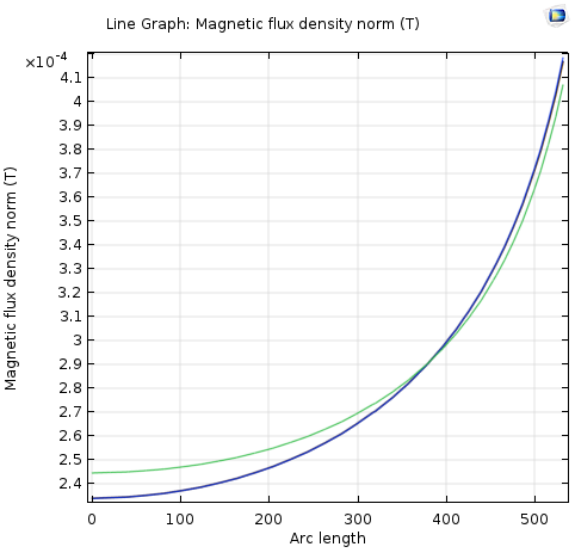

Figure 132. Magnetic flux density frequencies

19 The influence of the mutual inductance after adding inter-shield wires to the disc pair model

With respect to those reference papers, only series capacitances C_s are mentioned to increased when the inter-shield wires are applied to the disc pair model and the magnitude of the mutual inductances are considered to be fixed. Whereas, in reality, the mutual inductance would also change after the inter-shielding operation, which has been verified through numerical methods.

First of all, during the calculation of the mutual inductance of the disc pair model, the modified geometry mentioned in chapter 16 ought to be used. The transformer iron core and outer shield should be removed and nothing would be placed at that place. Besides, in contrary to the transformer turns, the inter-shield wires should not be energized.

19.1 The reference mutual inductance for the disc pair model

If there are no shield wires inserted in the disc pair model, the result obtained from this case $L_{s0} = 0.0052775H$ should behave as the reference value and decrease factor is $\eta_0 = 1.000$. Normally, the mutual inductance L_s of the disc pair model should be calculated at 1MHz. Whereas, in order to observe the current density, we need to run the file at 100Hz to reduce the influence of the skin effect.

Figure 133 and 134 illustrate the current density for the continuous disc pair model under 100Hz and that under 1MHz respectively. As for the figure at high frequency level, due to the severe skin effect, the skin depth would become around 2.5nm, which almost exceeds the resolution of Comsol Multiphysics. Thus, the current density is really complex for the software to capture. That is the most fundamental reason why you could hardly observe the current density in the figure for 1MHz.

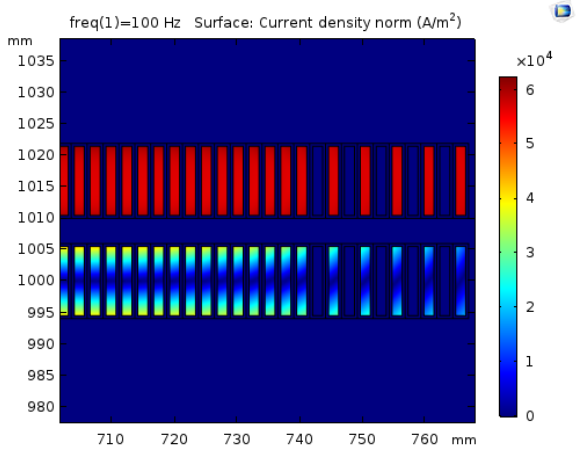

Figure 133. Current density at 100Hz

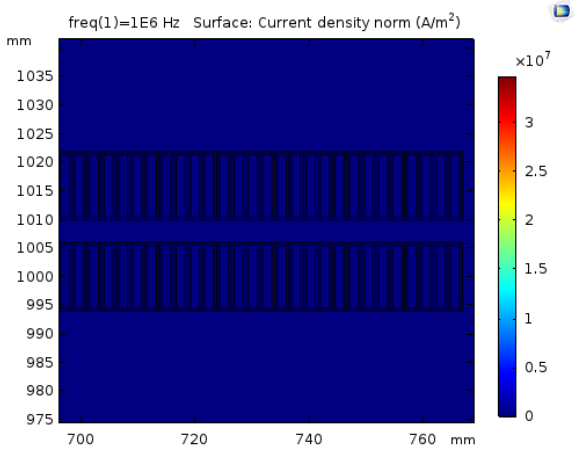

Figure 134. Current density at 1MHz

With respect to figure 133, the currents from upper disc are the excitation currents and the currents from lower disc are actually the induced currents generated by the fast-alternating magnetic flux. Figure 135 and figure 136 basically illustrate the magnetic flux density under the frequency of 100Hz and 1MHz respectively.

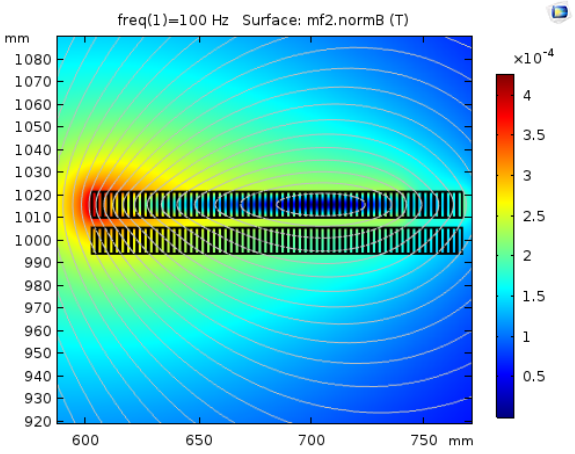

Figure 135. Magnetic flux density at 100Hz

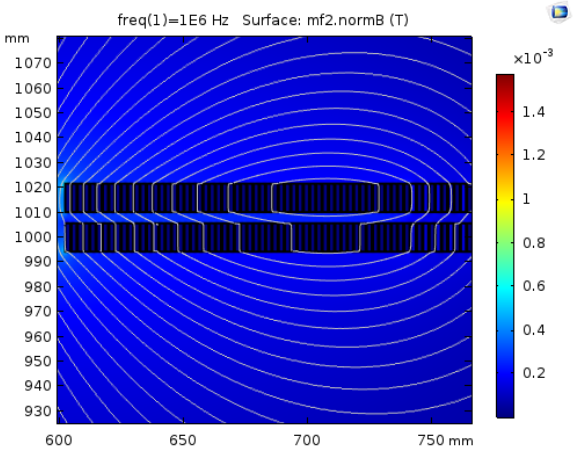

Figure 136. Magnetic flux density at 1MHz

As for the case when the frequency of the voltage source is considered to be 1MHz, in general, it is hard to observe the current density and magnetic flux density for the disc pair model due to the serve skin effect. However, when we zoom in the model for several times, we could find out that most of the current density and magnetic flux density are located at the corner of the transformer turns, which could be seen in figure 137 and figure 138.

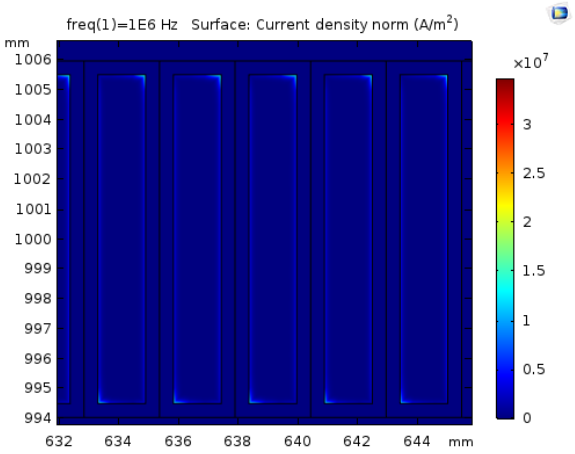

Figure 137. Current density 1MHz–zoom in

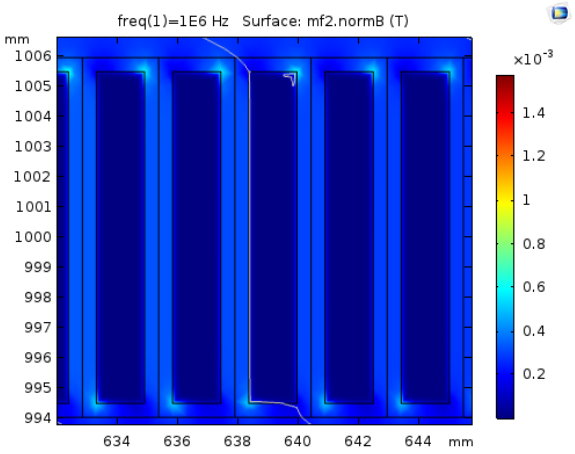

Figure 138. Magnetic flux density 1MHz–zoom in

19.2 The mutual inductance decrease factor η calculation in the case of disc pair model with inter-shield pairs

As for the figures from 139 to 144, it is clear that when we introduce the non-energized inter-shield pairs to the disc pair model, opposite induced currents with higher current density would be generated inside those inter-shield wires. Due to the presence of those opposite induced currents, a fraction of the magnetic flux generated by the excitation currents $\phi_{excitation}$ would be canceled. Therefore, the calculated mutual inductance would be smaller than the reference. As the number of the applied inter-shield pairs increases, the decrease factor η of the mutual inductance would be smaller.

Moreover, in order to reduce the skin effect, all of the figures from 139 to 144 are obtained at the frequency of 100Hz and the magnitude of the mutual inductance between disc pair should be calculated at the frequency of 1MHz.

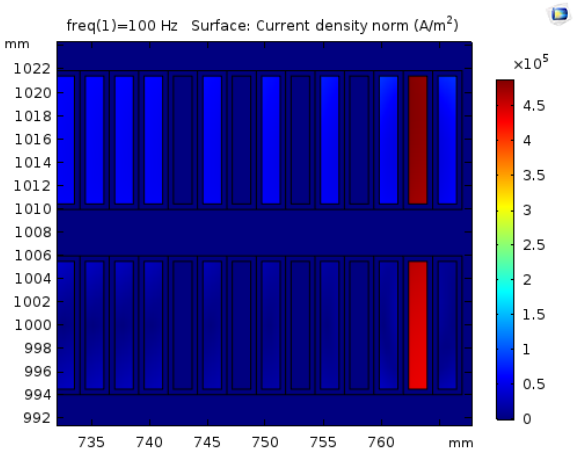

Figure 139. Current density one shield pair

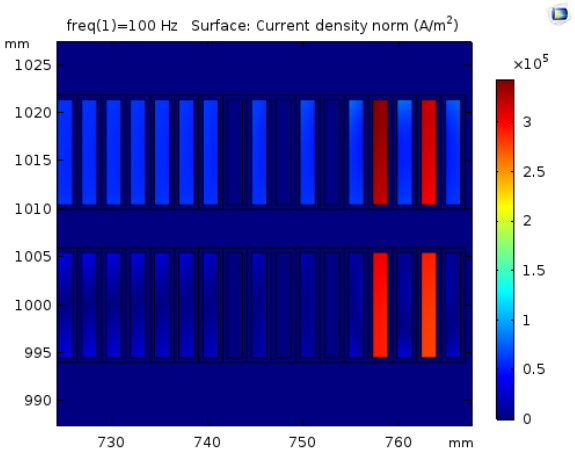

Figure 140. Current density two shield pairs

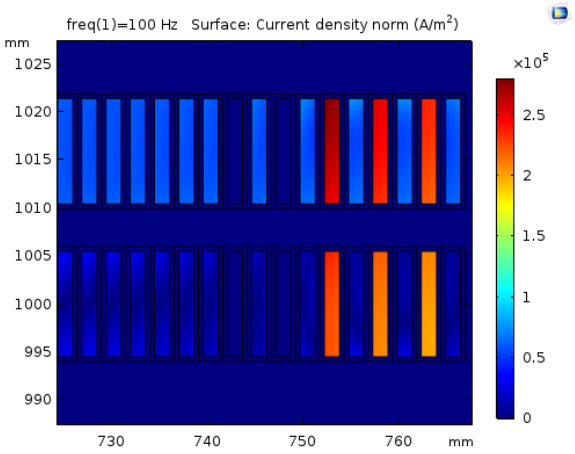

Figure 141. Current density three shield pairs

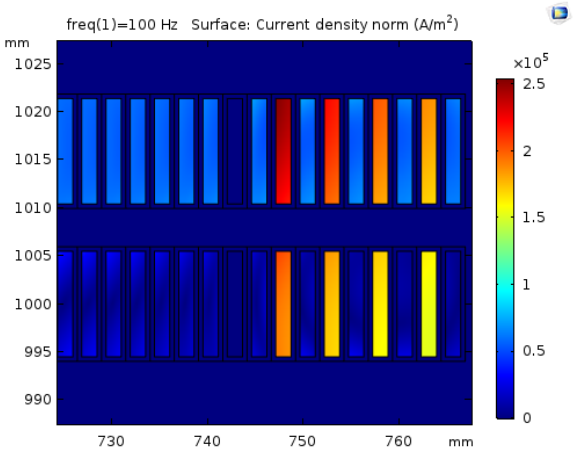

Figure 142. Current density four shield pairs

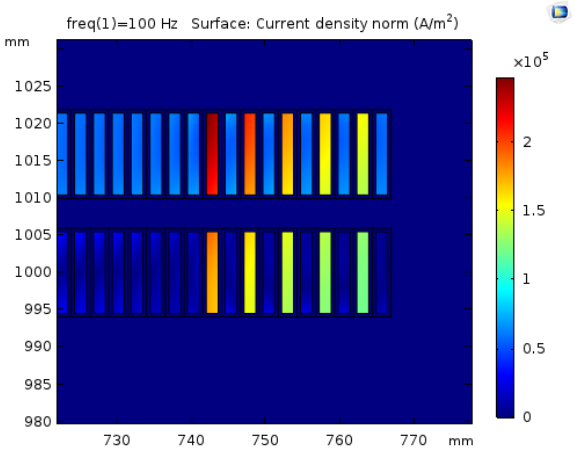

Figure 143. Current density five shield pairs

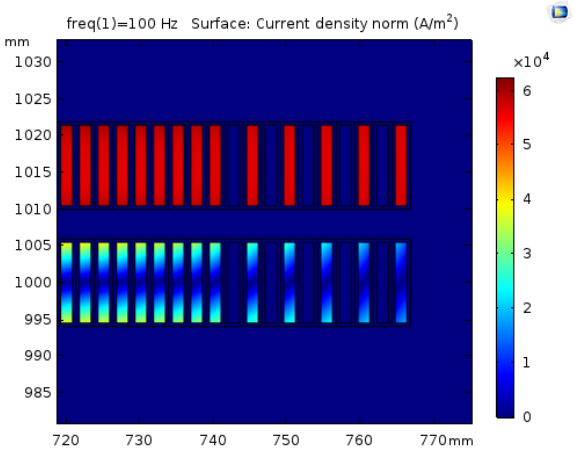

Figure 144. Current density no shield pairs

Figure 145 and 146 are actually the simplified aerial view of the energized hv disc pair model with certain number of inter-shield wires. Based on the right-hand screw rule, the induced currents $I_{inter-shield}$ represented by dashed red arrowlines would generate opposite magnetic flux compared with that generated by the excitation currents I_{turn} represented by dashed blue arrowlines.

Indeed, the flux linkages are the medium that could transmit the magnetic energy from the energized disc to the non-energized disc. Because of the cancellation of some flux linkages, the total mutual inductance between the discs would decrease. It is worth mentioning that the decrease factor η table is obtained in case of the hv disc winding model with transformer iron core through Comsol simulation.

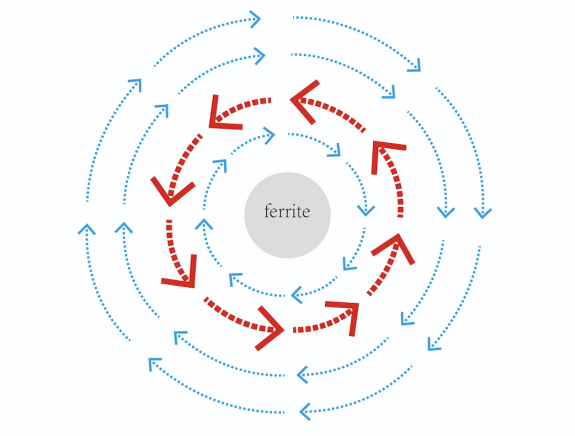

Figure 145. current distribution ferrite core

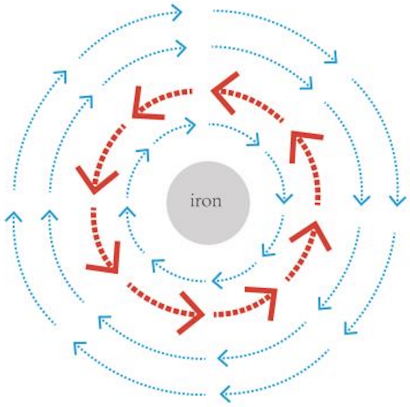

Figure 146. current distribution iron core

According to the figures from the front page, the intensity of the opposite induced currents inside the inter-shield wires would decrease from the leftmost shield wire to rightmost one. With respect to a certain inter-shield pair, the shield wire from the energised disc has higher current density than the other. Although the color for the excitation current density is not the same under different cases, all of the excitation current densities are proved to show the same value through Comsol verification.

Number of inserted shield wires	Mutual inductance L_s	Decrease factor η (within one disc pair)
N=0	$L_{s0} = 0.0052775H$	η_0=1.0000
N=1	$L_{s1} = 0.0031473H$	η_1=0.5964
N=2	$L_{s2} = 0.0029363H$	η_2=0.5564
N=3	$L_{s3} = 0.0027218H$	η_3=0.5157
N=4	$L_{s4} = 0.0024941H$	η_4=0.4726
N=5	$L_{s5} = 0.0022355H$	η_5=0.4236

Table 12. Mutual inductance between disc pair and decrease factor η with different number of inter-shield pairs

Table 12 shows the decrease factors η for the disc pair model with different number of inter-shields at the frequency of 1MHz. Whereas, with respect to one case, if the frequency is reduced from 1MHz to 100Hz, the decrease factor would be improved and the magnitude of the mutual inductance between disc pair would become larger. The reason for this phenomenon is that as the frequency of the initial currents reduces, the intensity of the opposite induced currents would also decrease. Thus, the amount of magnetic flux canceled by the induced currents inside the shield wires would be reduced and more flux linkages would be reserved.

As for the disc pair model without inter-shield pairs (reference case), the magnitude of the mutual inductance between disc pair Ls under different frequency levels would almost remain the same, which could be seen in the second column in table 13. In case of the disc pair with five inter-shield pairs, the intensity of the opposite induced currents is proportional to the variation of the excitation currents. Thus, when the frequency is increased, the magnitude of the mutual inductance would be reduced, which could be seen in the third column in table 13. Figure 147 and figure 148 illustrate the mutual inductance variation with the increase of the excitation current frequency.

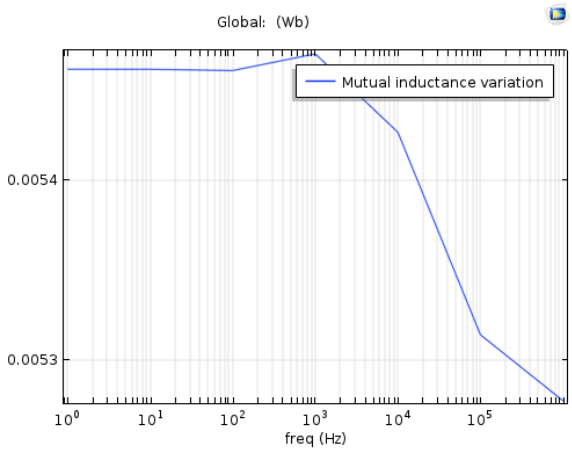

Figure 147. Mutual inductance variation reference

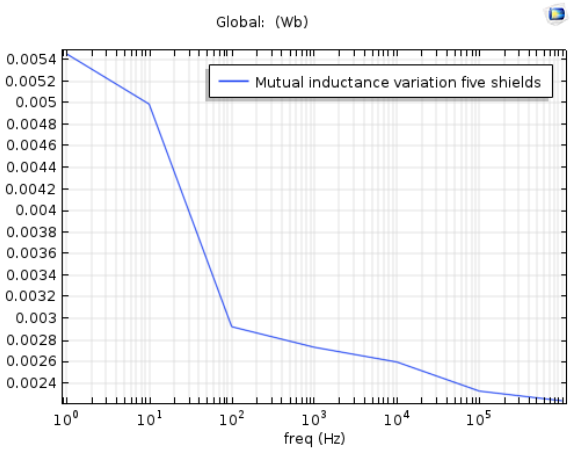

Figure 148. Mutual inductance variation 5 shields

Frequency	Mutual inductance without inter-shield pairs	Mutual inductance with five inter-shield pairs
f=1Hz	$L_{00} = 0.0054617H$	$L_{05} = 0.0054559H$
f=10Hz	$L_{10} = 0.0054617H$	$L_{15} = 0.0049894H$
f=100Hz	$L_{20} = 0.0054610H$	$L_{25} = 0.0029229H$
f=1kHz	$L_{30} = 0.0054703H$	$L_{35} = 0.0027324H$
f=10kHz	$L_{40} = 0.0054266H$	$L_{45} = 0.0025953H$
f=100kHz	$L_{50} = 0.0053141H$	$L_{55} = 0.0023252H$
f=1MHz	$L_{60} = 0.0052775H$	$L_{65} = 0.0022355H$

Table 13. Mutual inductance variation under different frequency levels

20 The selection for the inter-shielding or interleaving method that could provide the best voltage response performance

The main purpose of chapter 20 is to find out the best optimized method that could improve the voltage response distribution and save the manufacturing cost. In reality, a real hv disc winding would comprise of around 50 disc pairs (100 discs in total), but only the top several 6 or 8 disc pairs nearby the high voltage connections are required to be inter-shielded or interleaved in order to reduce the cost, which could be shown in the figure below. Therefore, with respect to this thesis project, the disc winding model built in Simulink (Matlab) and Comsol only concludes those 6 disc pairs (12 discs in total) which need to be improved. Under this condition, the last disc from the model should be floating.

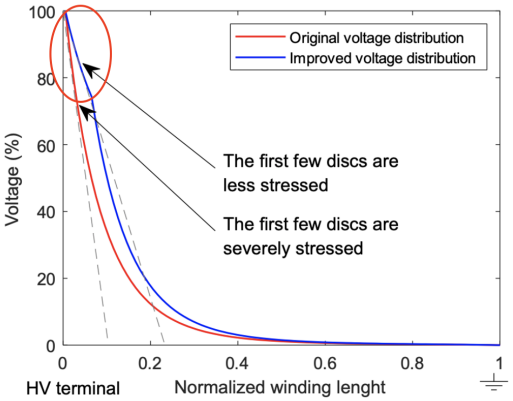

Figure 149. Voltage response distribution–disc winding

In fact, there is no doubt that the turn-interleaved method could definitely bring us the best voltage response performance due to the fairly large improvement factor $\lambda_{interleaved} = 40.010$. Based on figure 151 and 152, it is clear that all of the voltage drops between the discs are really small. Furthermore, the best voltage response performance should comprise of three properties: least LC resonance distortion, most linear voltage distribution and least cost for manufacturing.

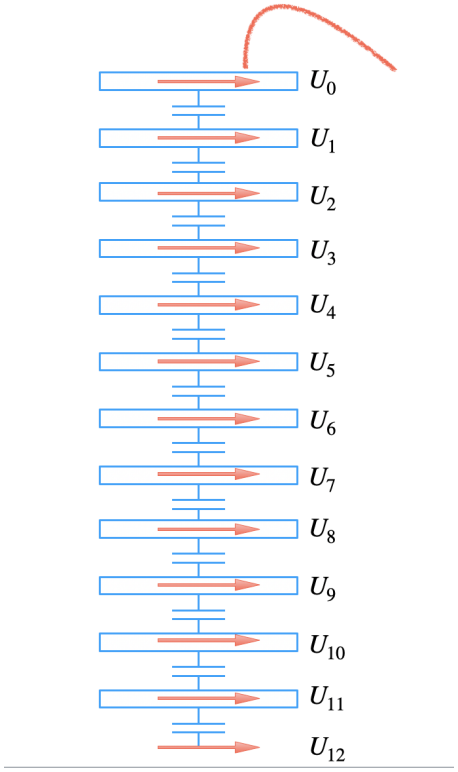

Figure 150. Legend explanations for U_i in following figures

According to figure 151 and 152, the total voltage drop on those 6 turn-interleaved disc pairs ΔV_{total} is only ten percent of the crest value of the impulse voltage source. Thus, it is quite obvious that through the application of the turn-interleaved method, the voltage drop between discs $\Delta_{disc-disc}$ nearby high voltage connections could be reduced significantly.

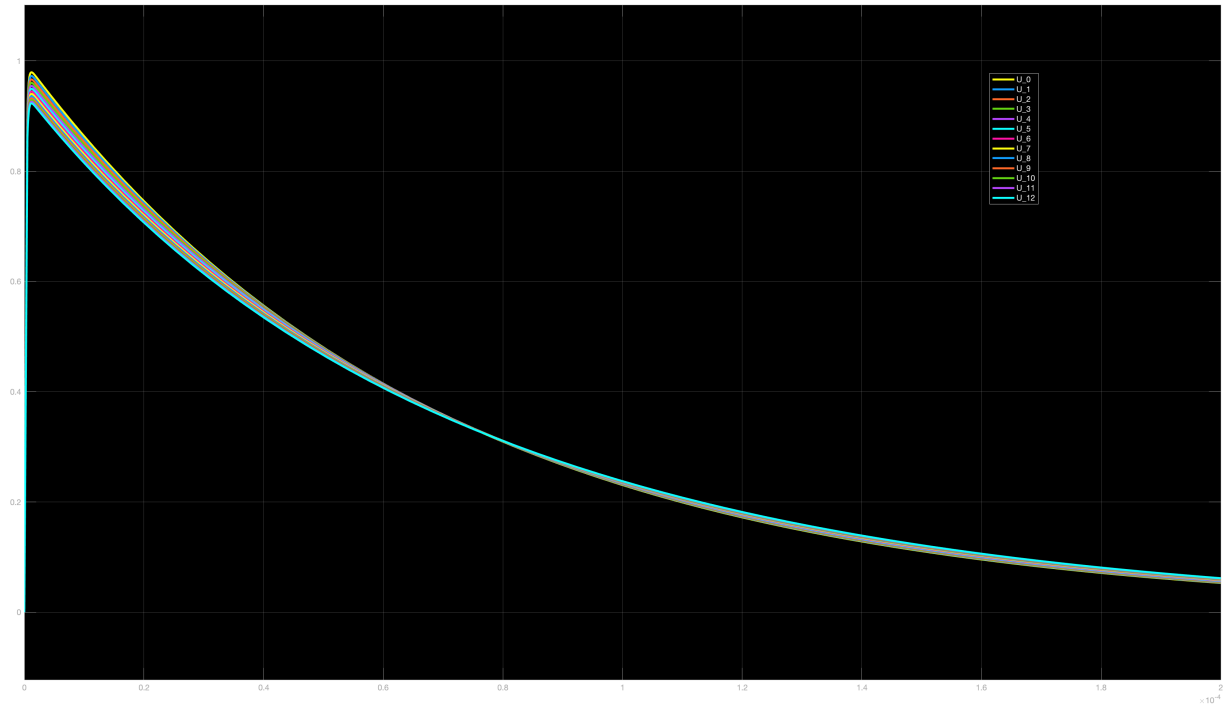

Figure 151. Voltage response distribution turn-interleaved $T_{period} = 200\mu s$

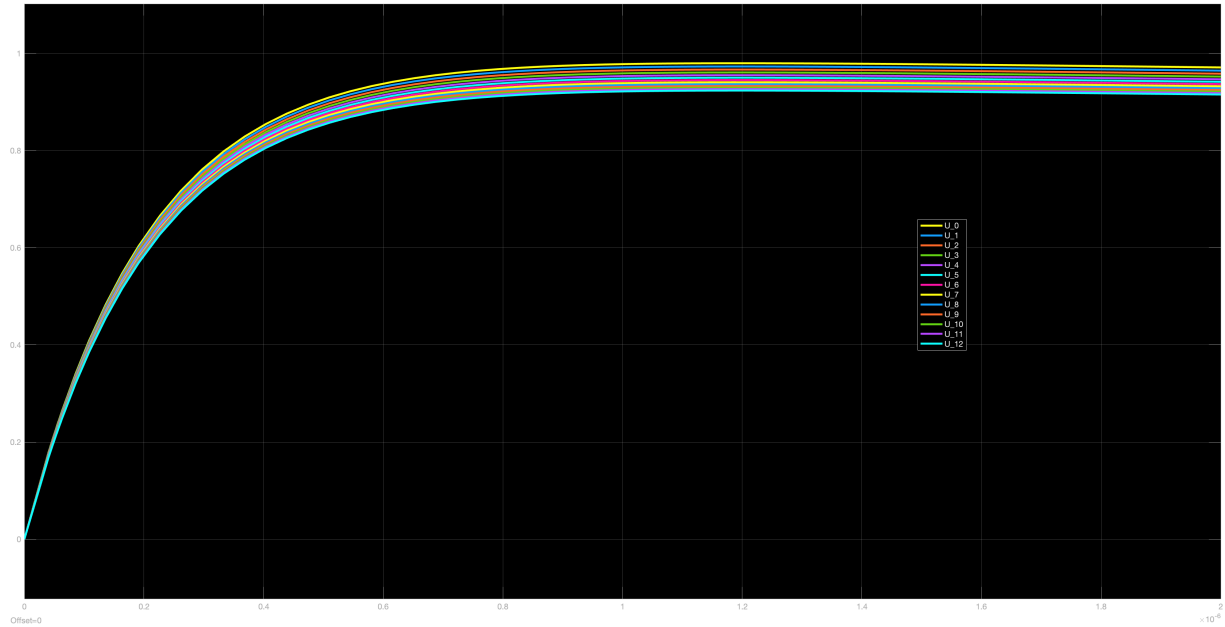

Figure 152. Voltage response distribution turn-interleaved $T_{period} = 2\mu s$

Furthermore, after the application of the inter-shielding method, the geometry of the disc winding model is considered to be built as follows: the first disc pair has five inter-shield pairs, the second disc pair has four inter-shield pairs, the third disc pair comprises of three inter-shield pairs, the forth and fifth disc pair have two and one inter-shield pairs respectively and the last disc pair doesn't have any inter-shield wires.

Figure 153 illustrates the voltage responses of the disc winding model inter-shielded by electrostatic shield pairs. Compared with the results obtained from the continuous disc winding shown in figure 154, the intensity of the LC resonances and the voltage drop between adjacent discs have been reduced significantly after introducing the electrostatic inter-shield wires to the disc winding.

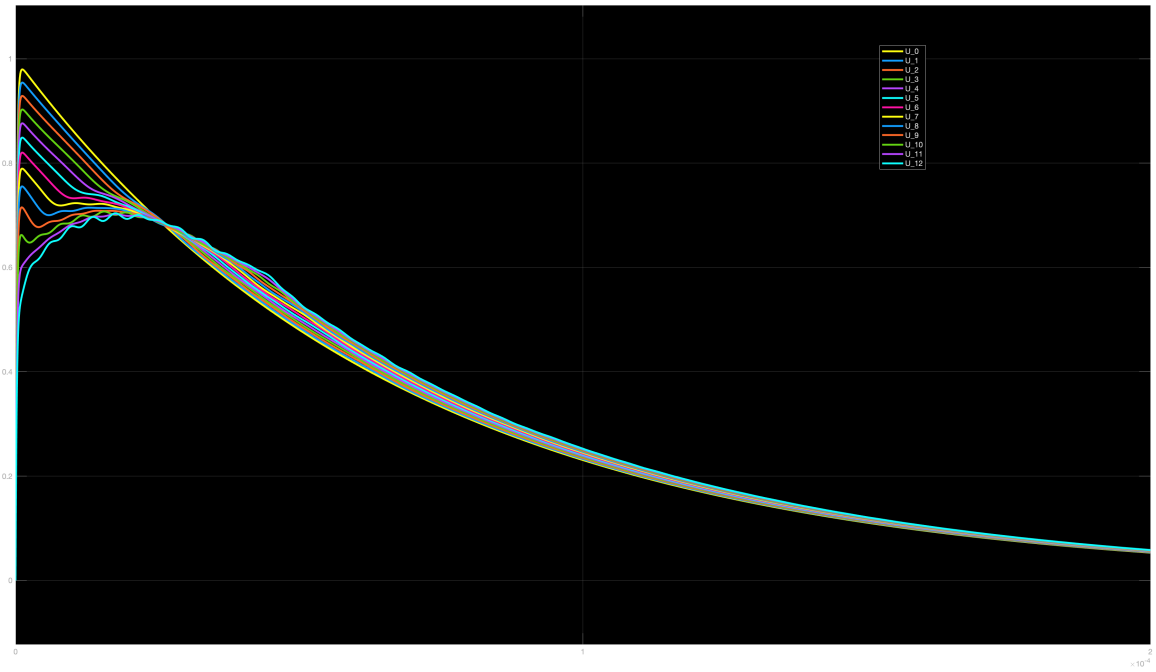

Figure 153. Voltage response distribution–electrostatic inter-shield pairs

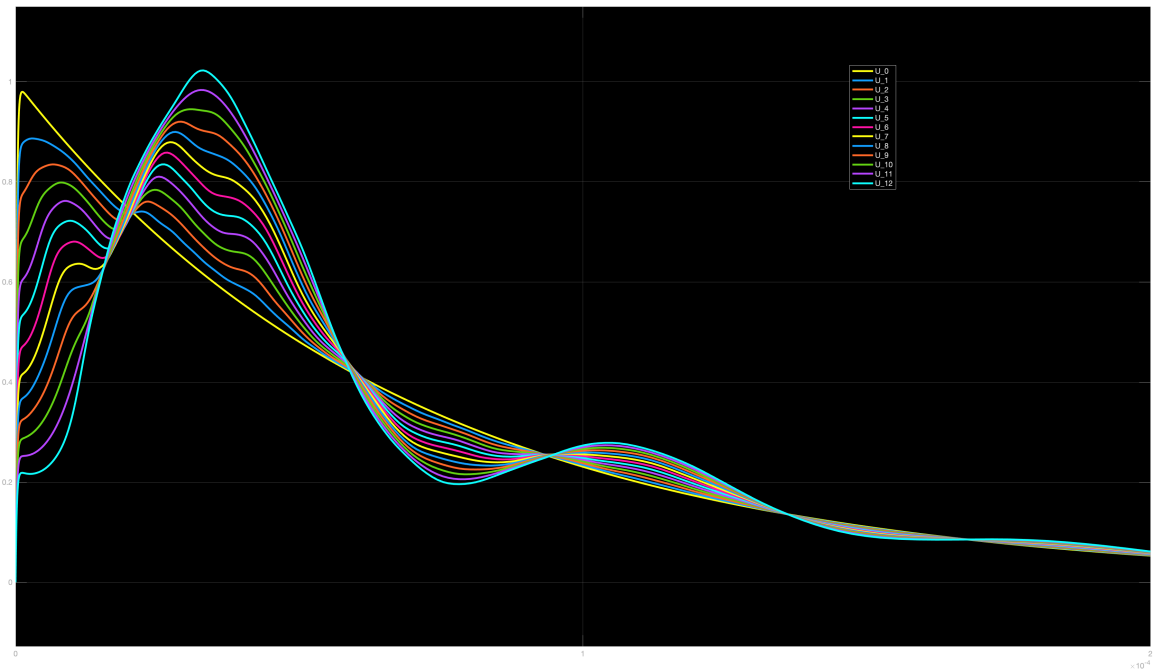

Figure 154. Voltage response distribution–without inter-shield pairs

Actually, figure 155 and figure 156 illustrate the voltage response distribution for the disc winding model inter-shielded by wound-in shield pairs when the cross-point is floating and connected to the input terminal respectively. To sum up, the voltage response distribution for the case with wound-in inter-shields in case of the floating cross-point is less distorted by the LC resonances compare with case that the cross-point is connected to the high voltage terminals. The voltage distribution of this case is almost the same as that for the case with electrostatic inter-shield pairs. Thus, the case with electrostatic shield wires is proposed in order to save some labour cost, because it is relatively hard to add the wound-in inter-shields to the disc pair.

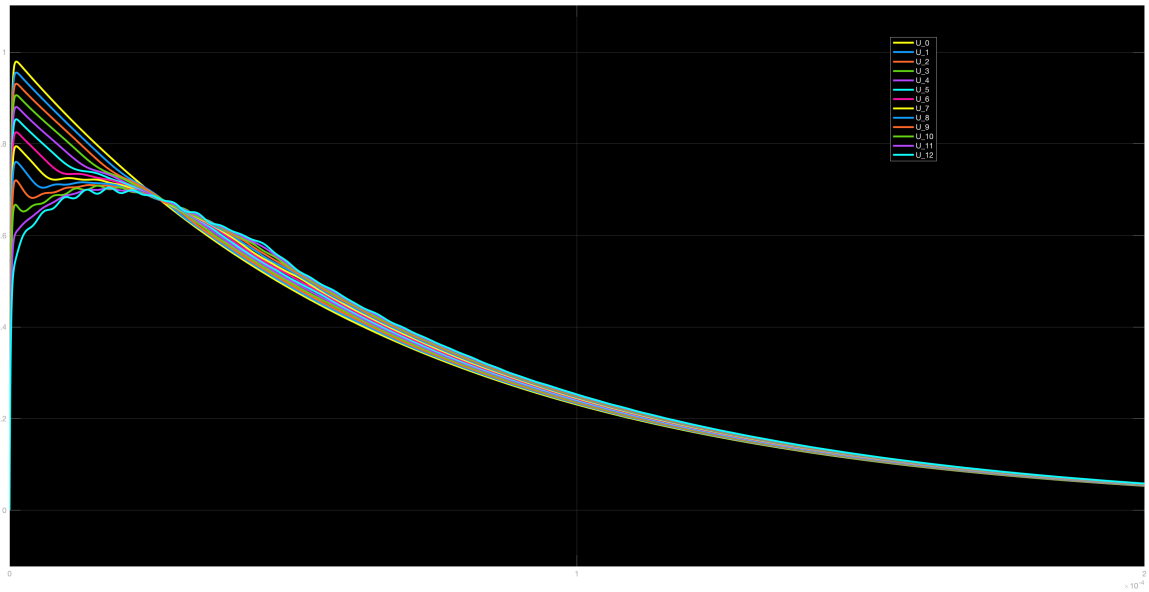

Figure 155. Voltage response distribution wound-in inter-shields–cross-point floating

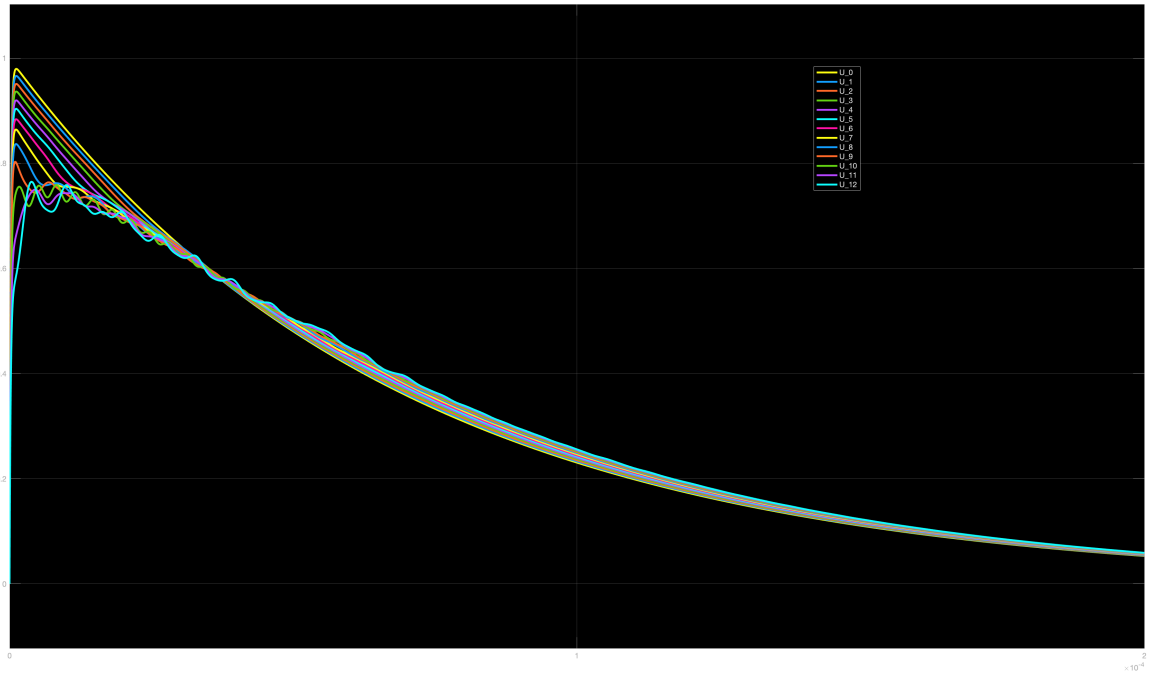

Figure 156. Voltage response distribution wound-in inter-shields–cross-point is connected to voltage terminal

21 The voltage responses comparison between the disc winding model with ferrite core and iron core

21.1 The voltage responses of the case without inter-shield wires–reference (forth) configuration

Based on the results obtained from chapter 20, after introducing the electrostatic inter-shield pairs to the disc winding model, a better voltage response performance could be obtained. In this chapter, the designed disc winding model would comprise of 8 disc pairs. Figure 157 and figure 158 illustrate the geometry of the winding with no inter-shield wires.

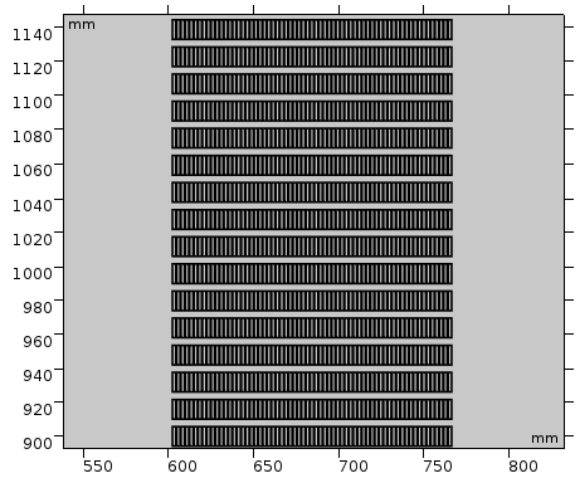

Figure 157. Disc winding model without shields

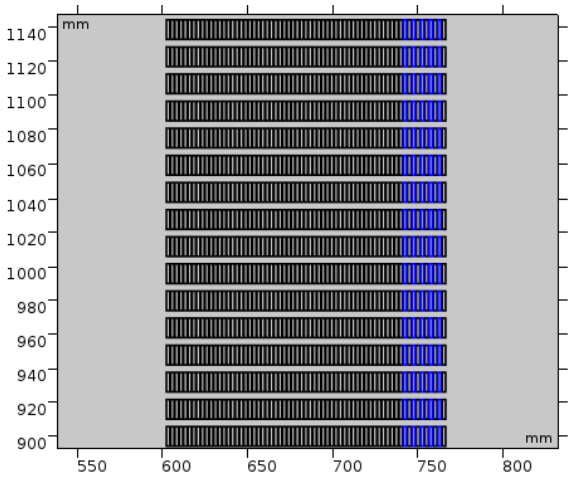

Figure 158. Oil-gap pairs colored blue

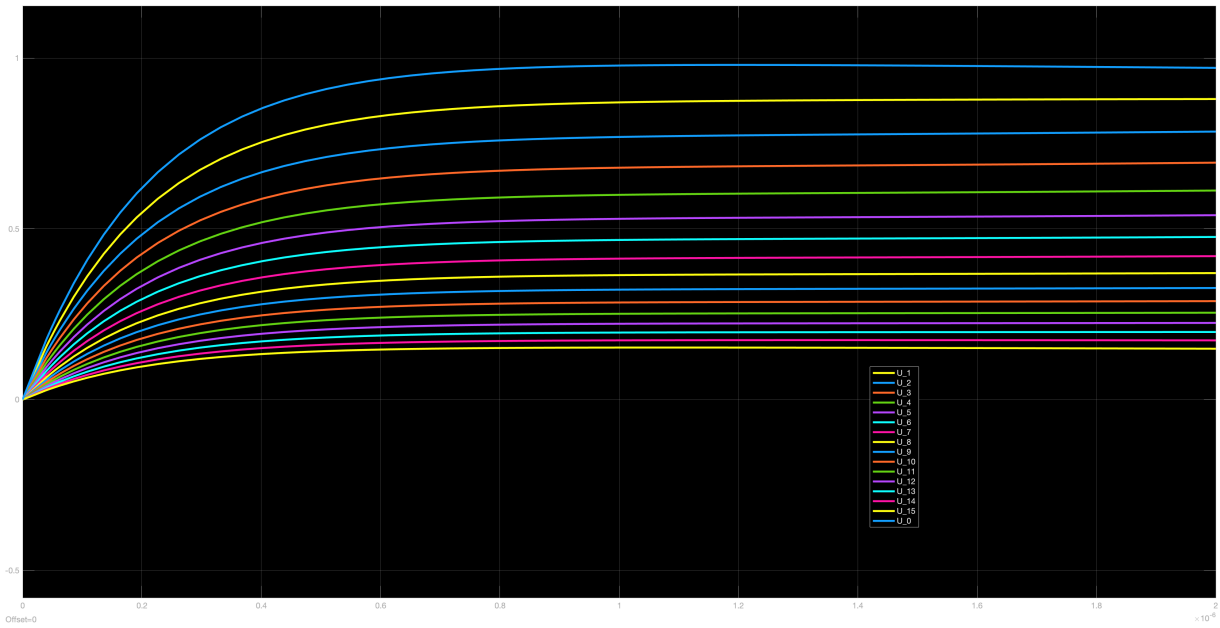

Figure 159. Voltage response distribution ferrite F core $T_{period} = 2\mu s$

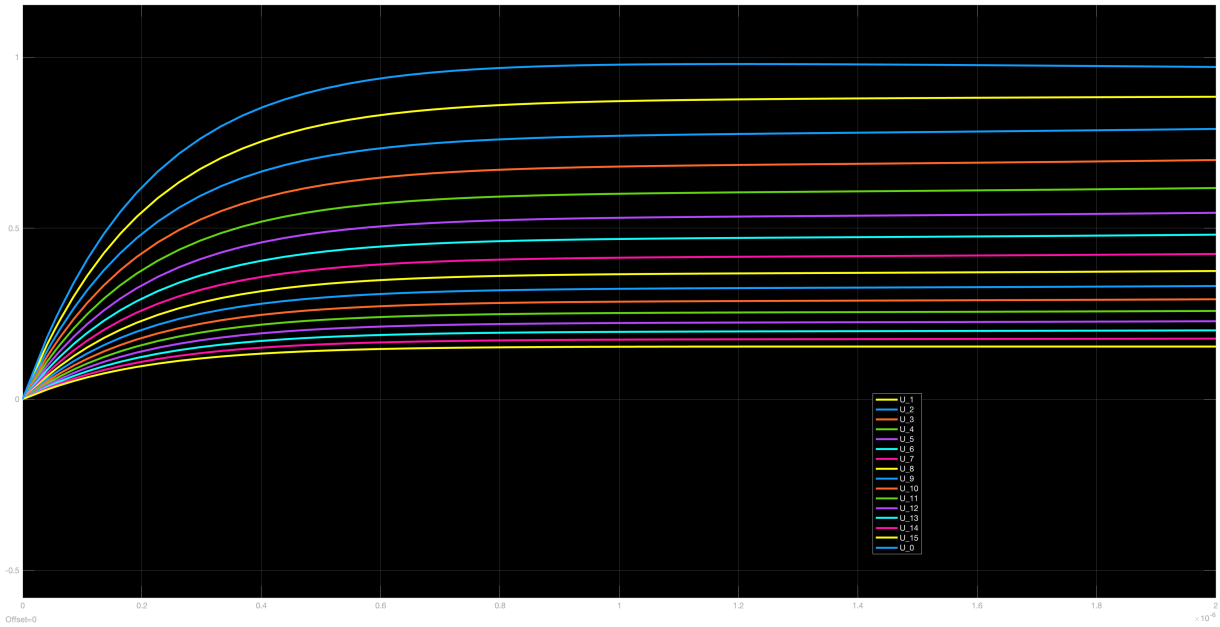

Figure 160. Voltage response distribution iron core $T_{period} = 2\mu s$

Figure 159 and figure 160 illustrate that when the lightning impulse strikes a reference hv transformer winding with iron core or ferrite core, the voltage responses would distribute non-linearly from the top disc to the bottom disc. Meanwhile, this phenomenon is also a quite convincing prove for the consequences acquired from the Greenwood book.

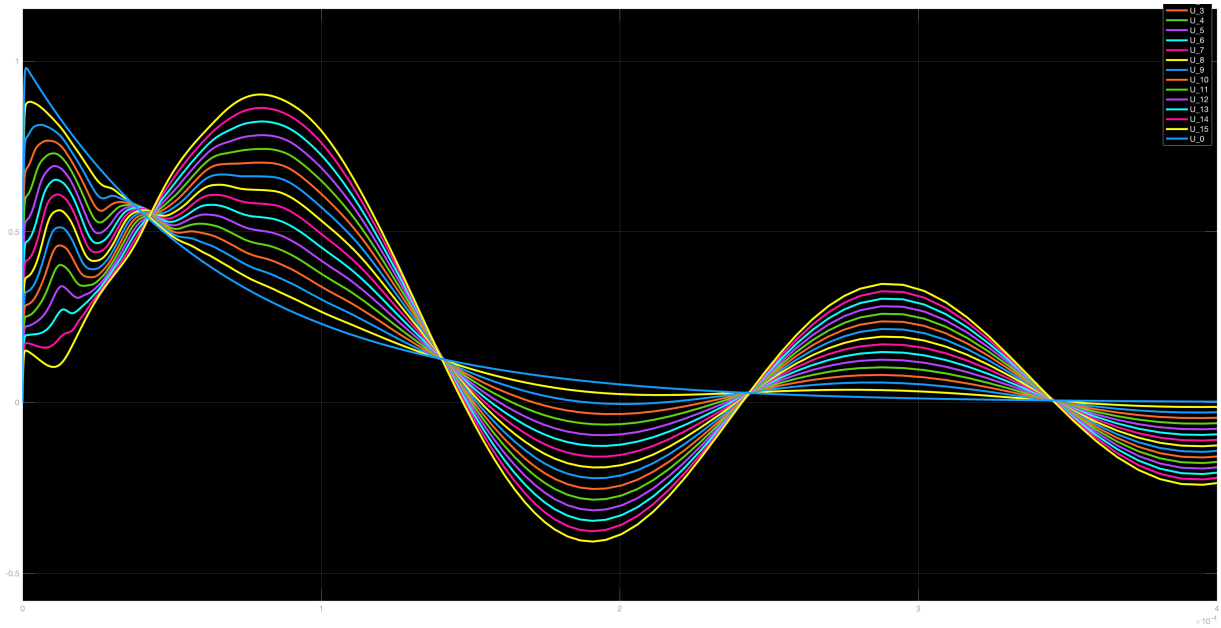

Figure 161. Voltage response distribution ferrite core $T_{period} = 400\mu s$

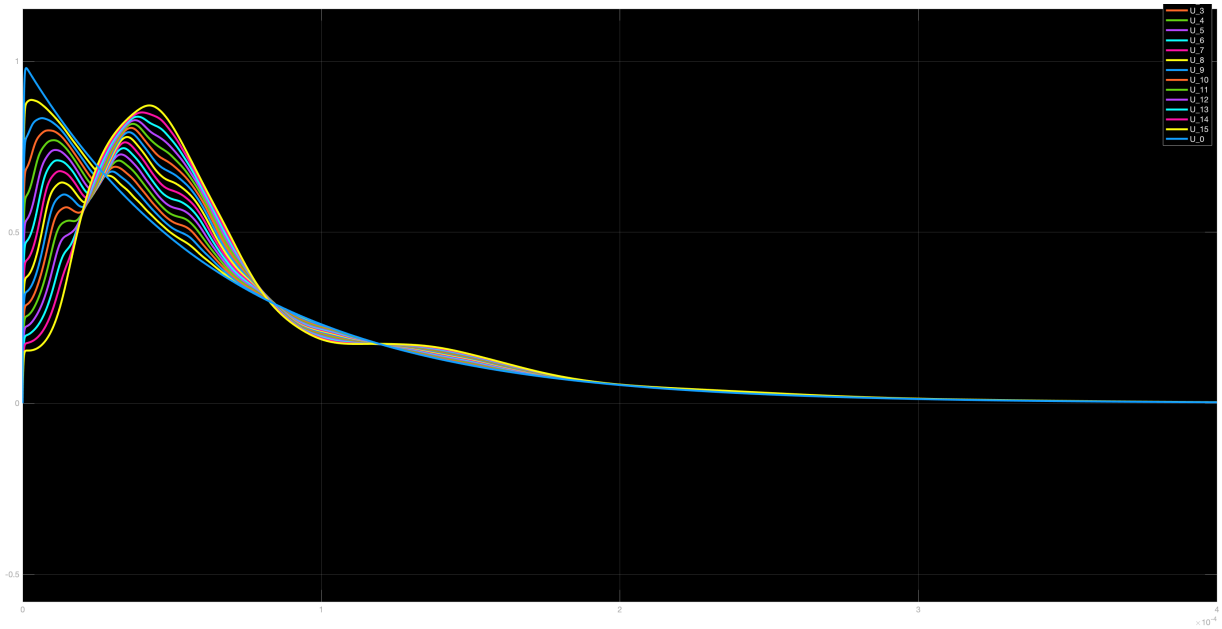

Figure 162. Voltage response distribution iron core $T_{period} = 400\mu s$

According to figure 161 and figure 162, if there are no electrostatic inter-shield wires inserted in the disc winding model, severe LC resonances would start to emerge and distort the voltage response waves and the undamped natural network frequencies f_i would have a relatively large range. The natural network frequencies could be calculated as:

$$f_i = \frac{\omega_i}{2\pi} = \frac{1}{2\pi * \sqrt{LC}}$$

Therefore, because the magnitude of the inductance matrix for the case with ferrite core is larger than that for the case with iron core, the duty cycle of the resonance for the ferrite case is also larger than that for iron case. Actually, based on figure 161 and figure 162, it is evident that the case with ferrite core has less damping than the case with iron core. In general, as for the continuous disc winding, the case with iron core would have better voltage response performance.

21.2 The voltage responses with ferrite F transformer core–configuration one

With respect to the geometry of the disc winding model, the material of the transformer core is set to become ferrite F and the outer iron shield is removed. Moreover, there are 8 disc pairs located inside the disc winding model: the first disc pair model comprises of five electrostatic inter-shield pairs and the second one has four electrostatic inter-shield pairs, the third one has three inter-shield pairs, the forth has two, the fifth has one and the rest three disc pairs have no shield wires. Figure 163 and figure 164 illustrate the geometry of the configuration one.

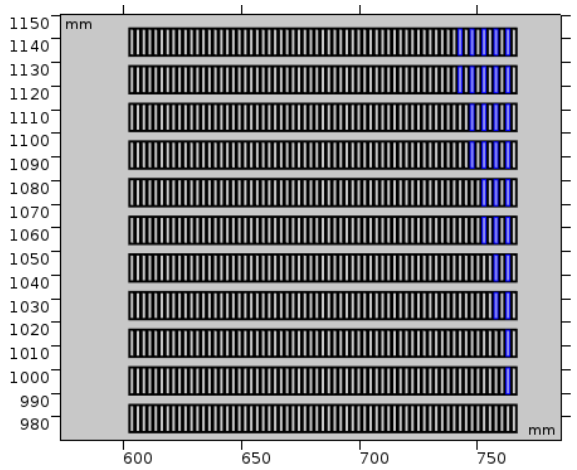

Figure 163. Electrostatic shield wires colored blue

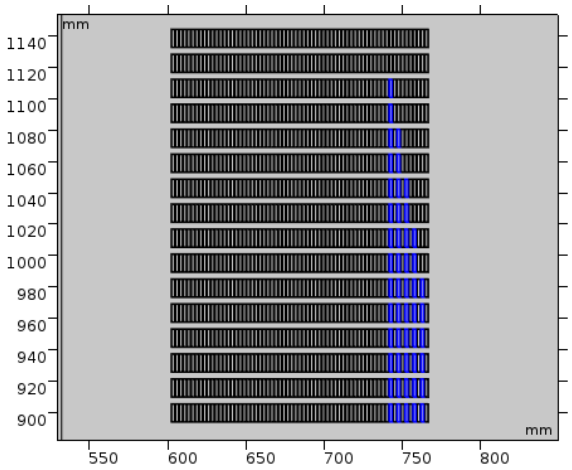

Figure 164. Oil-gap pairs colored blue

Through numerical calculation, the inductance and resistance matrix could be finally obtained. Moreover, the series capacitance C_s between adjacent discs could be obtained from table in chapter 9. All of those basic electric parameters should be put into the Simulink model. The computation time periods for the Simulink model are considered to become $100\mu s$, $400\mu s$ and $2\mu s$. Figure 165, 166 and 167 illustrate the voltage response distribution for configuration one.

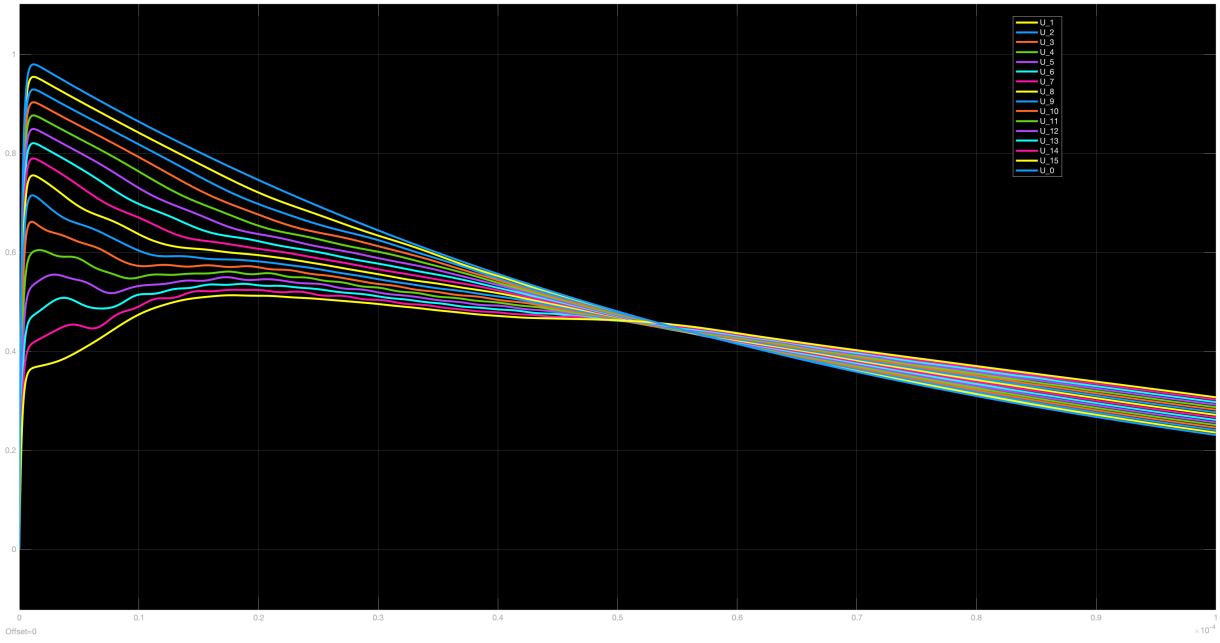

Figure 165. Voltage response distribution ferrite core $T_{period} = 100\mu s$

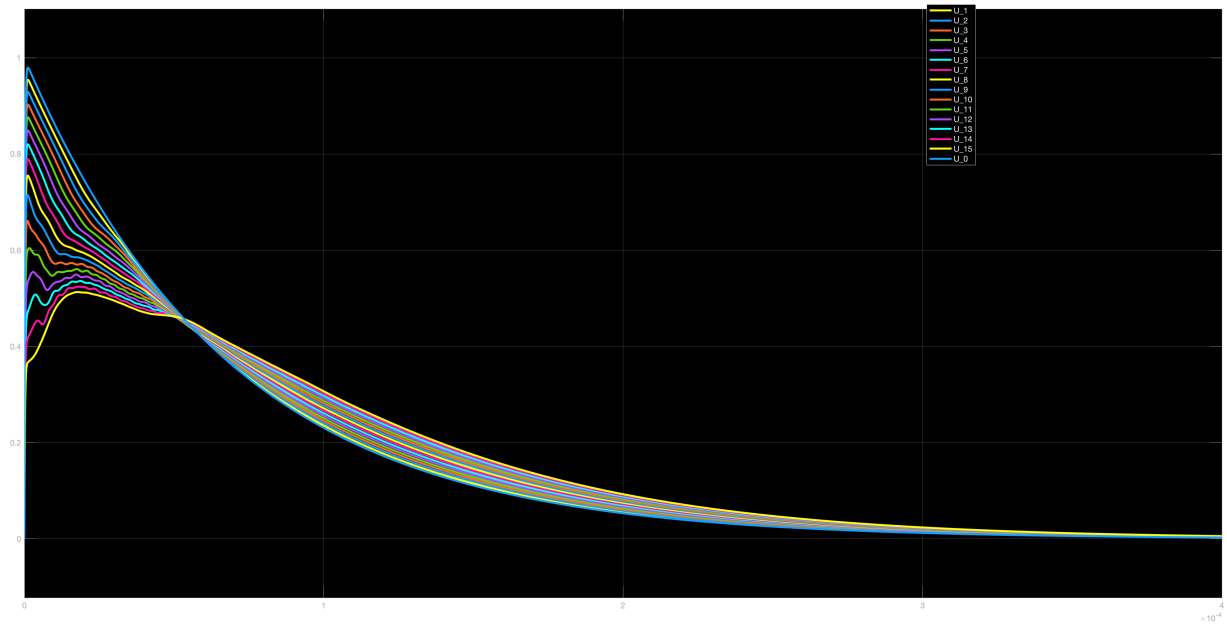

Figure 166. Voltage response distribution ferrite core $T_{period} = 400\mu s$

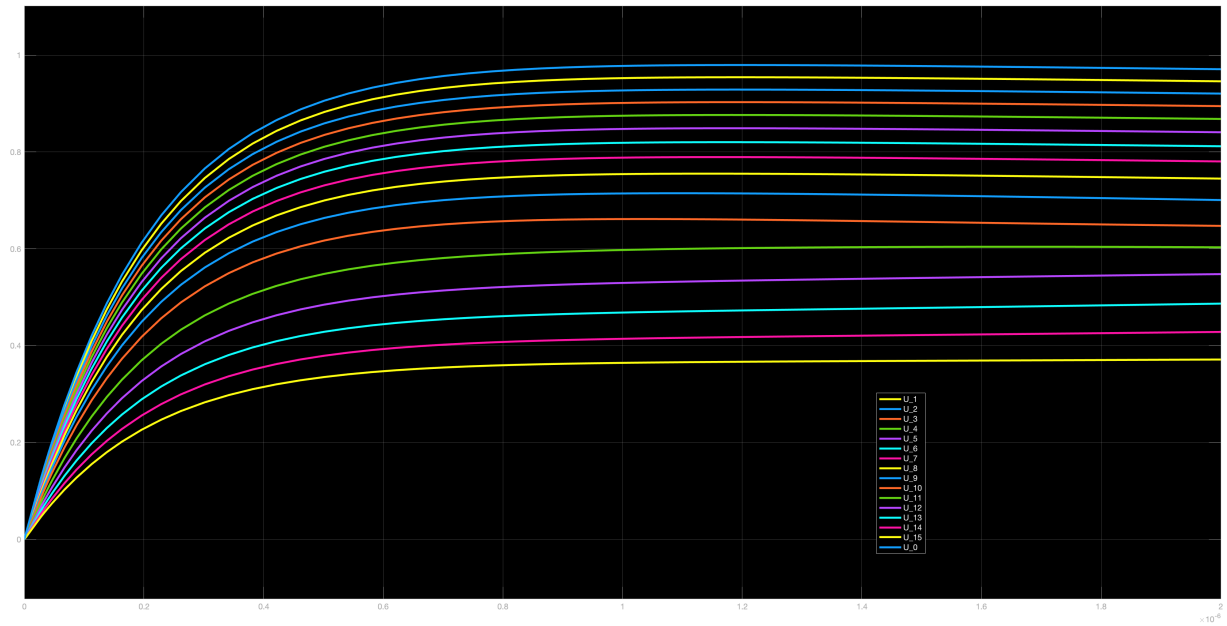

Figure 167. Voltage response distribution ferrite core $T_{period} = 2\mu s$

According to figure 167, the voltage drops between the discs nearby the bottom are relatively larger than those close to the top. In order to solve this problem, another configuration needs to be implemented: a certain number of electrostatic inter-shield wires should also be added into the disc pairs nearby the bottom. Moreover, based on figure 165 and figure 166, it is obvious that the intensity of the LC resonances has be sufficiently reduced through the application of electrostatic inter-shield pairs.

21.3 The voltage responses with iron core–configuration one

Normally, the laminated iron core has been widely used in large power transformers due to its lower material cost. The ferrite F transformer cores are mostly used in low voltage application rather than high voltage applications. In this subsection, we would like to find out whether the case with ferrite F core has better voltage response performance than the case with iron core or not. Besides, the magnetic flux density of the case with ferrite core and that with iron core are shown as figure 168 and figure 169.

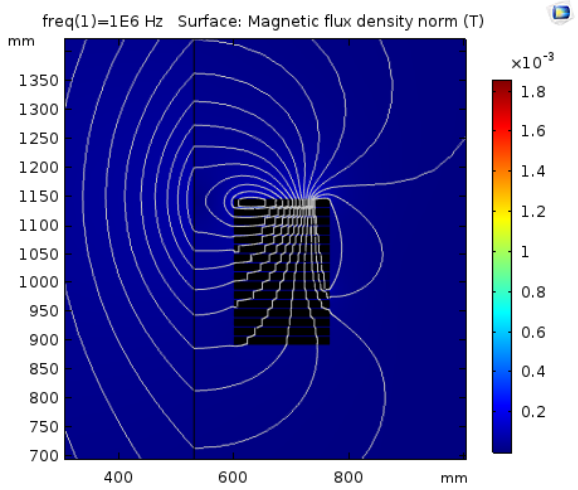

Figure 168. Ferrite core configuration one

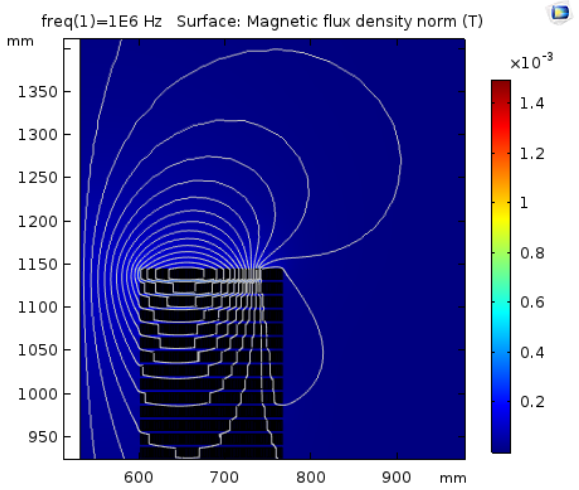

Figure 169. Iron core configuration one

Based on the figures for $T_{period} = 100\mu s$ and $T_{period} = 400\mu s$, it is quite obvious that the voltage responses for the case with iron core have relatively more severe resonances than those with ferrite F core. Moreover, because the case with laminated iron core has larger natural network frequency f_i range than the case with ferrite F core, the resonances of the iron case would start much earlier than those of ferrite case. Thus, as a result, the case with ferrite F core has better voltage response performance.

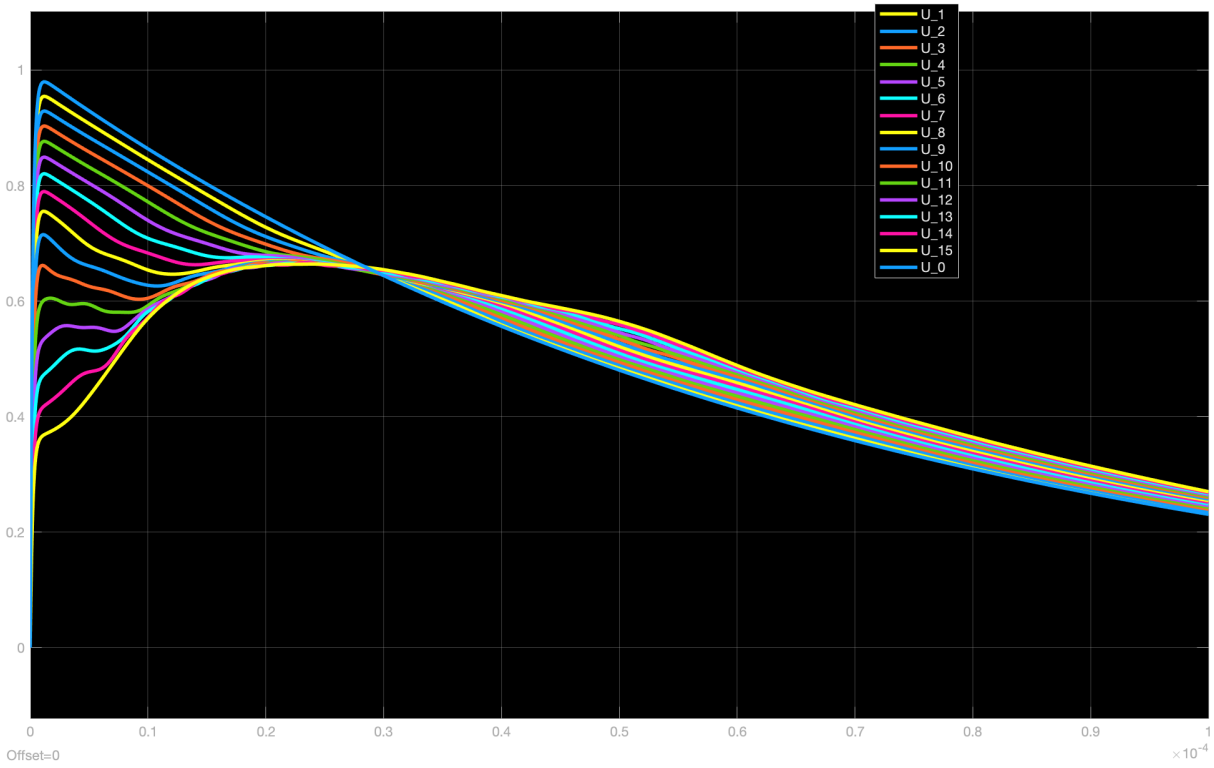

Figure 170. Voltage response distribution iron core $T_{period} = 100\mu s$

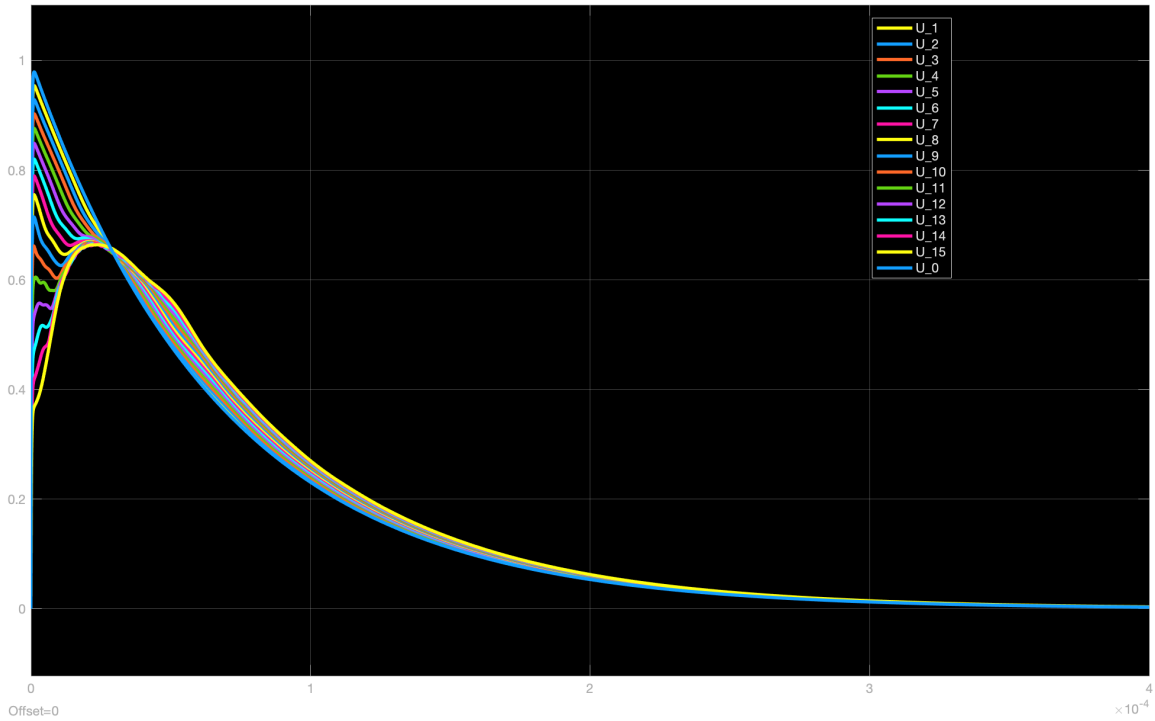

Figure 171. Voltage response distribution iron core $T_{period} = 400\mu s$

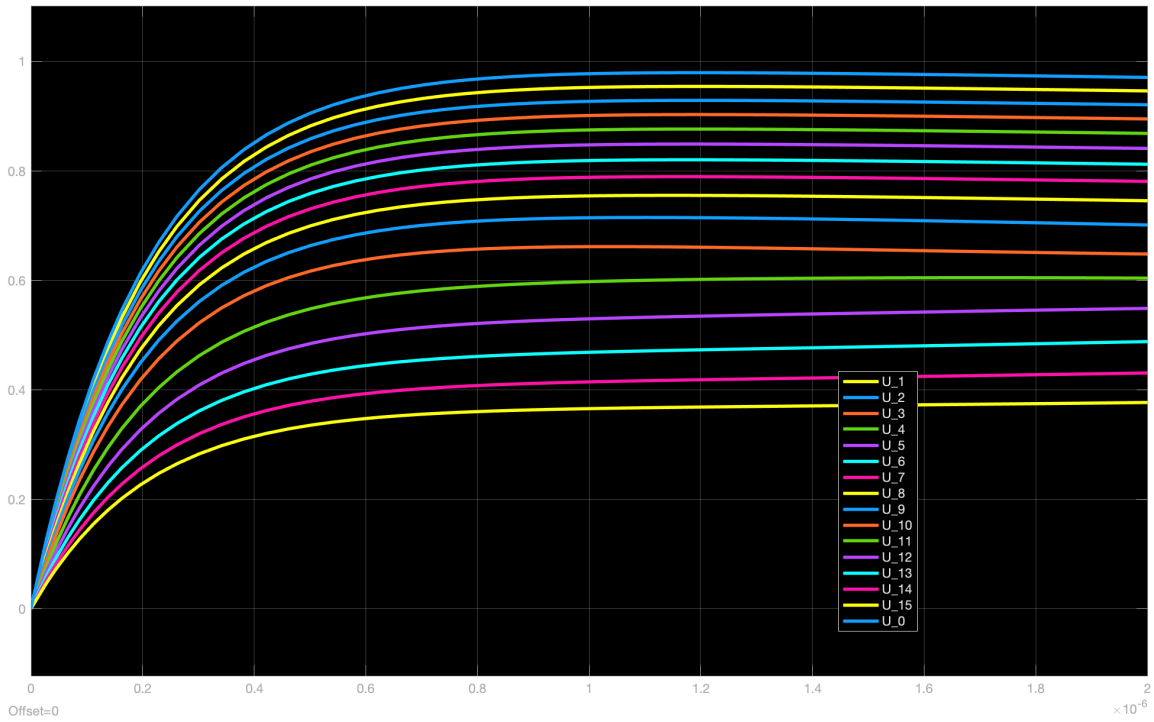

Figure 172. Voltage response distribution iron core $T_{period} = 2\mu s$

With respect to the figure for $T_{period} = 2\mu s$, after introducing the electrostatic inter-shield wires to the disc winding model, it is obvious that the voltage drop between adjacent discs nearby the high voltage terminals has been reduced significantly but that nearby the bottom is still kind of large. Therefore, the number of inter-shield wires for each disc pair from the disc winding needs to be optimized in order to obtain the better voltage response distribution. Compared with the figures for $T_{period} = 400\mu s$ in 20.2 and 20.3, the voltage responses for the case with ferrite core are less distorted by the LC resonances compared with those for the case with iron core.

21.4 The voltage responses with ferrite F core–configuration two

In order to solve the problem from configuration one, the second disc winding configuration has been designed: there are also 8 disc pairs present inside the model: the first disc pair comprises of five electrostatic inter-shield pairs, the second one has four inserted shield pairs, the third and forth disc pair have three inserted shield pairs, the fifth and sixth disc pair have two shield pairs and the seventh and eighth disc pair comprises of one inter-shield pair. The figures of the new geometry are shown as figure 173 and figure 174.

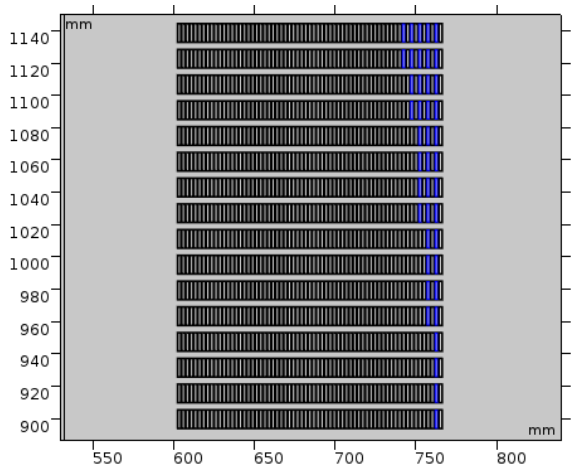

Figure 173. Electrostatic inter-shields colored blue

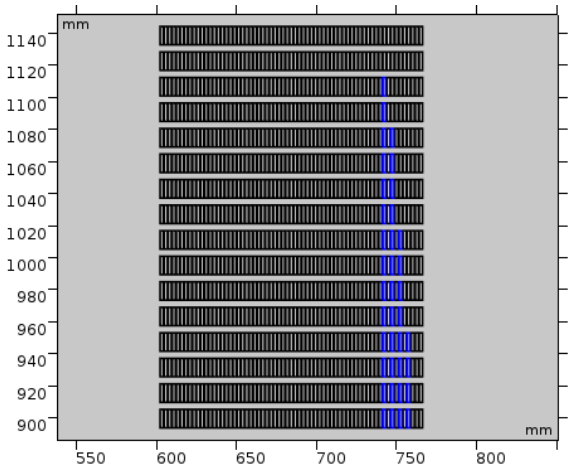

Figure 174. Oil gaps colored blue

With respect to the figures for $T_{period} = 100\mu s$ and $T_{period} = 400\mu s$, if the material of the transformer core is ferrite F, configuration two would have better voltage response performance than configuration one due to the less severe LC resonance distortion. According to the figure for $T_{period} = 2\mu s$, we could know that the electric stress between adjacent discs nearby the bottom are also much smaller. Whereas, configuration two would need six more electrostatic inter-shield pairs, which would result in more material cost.

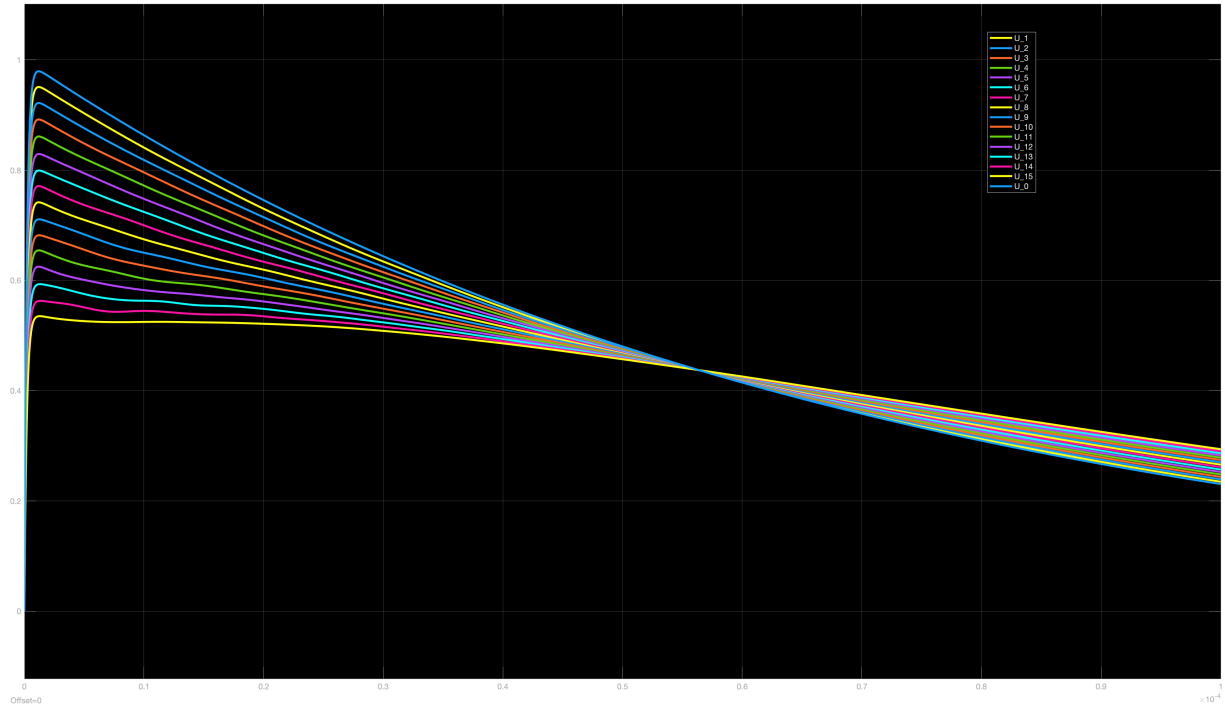

Figure 175. Voltage response distribution ferrite core $T_{period} = 100\mu s$

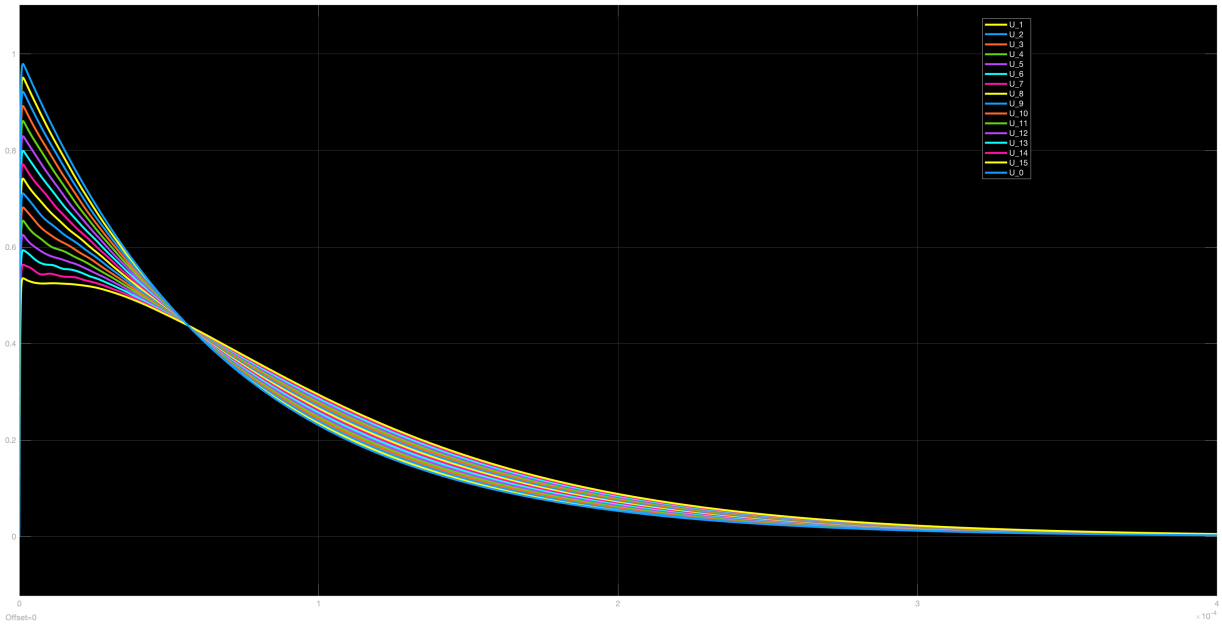

Figure 176. Voltage response distribution ferrite core $T_{period} = 400\mu s$

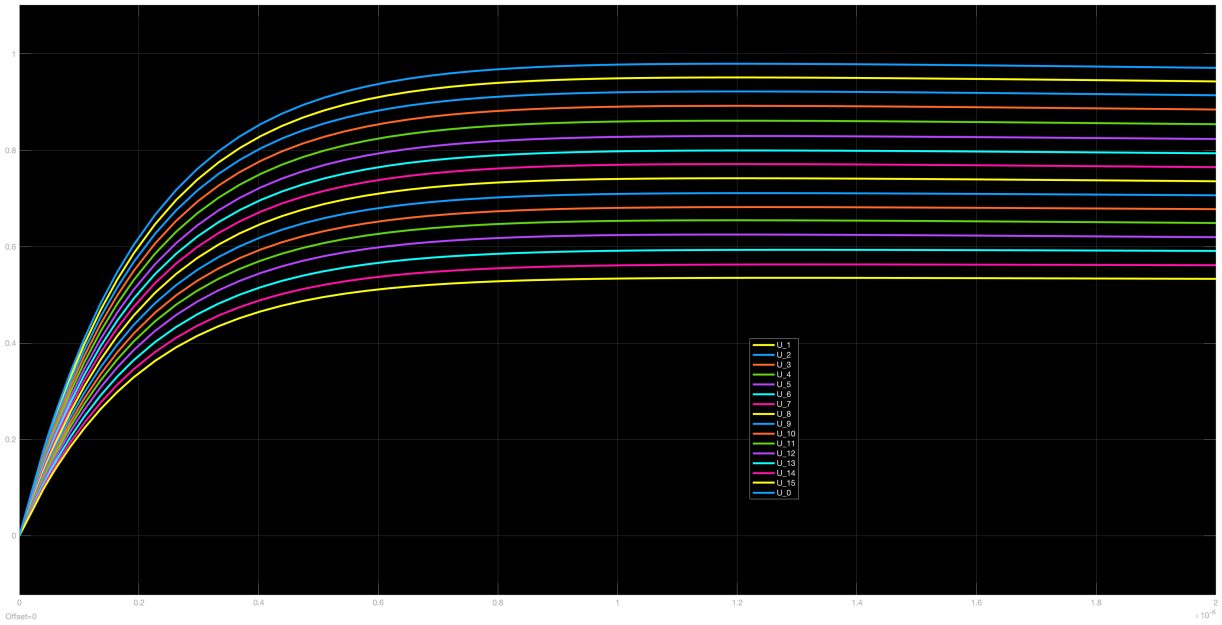

Figure 177. Voltage response distribution ferrite core $T_{period} = 2\mu s$

With respect to the figures obtained after the application of configuration two, the intensity of the LC resonances has been significantly reduced compared with that of configuration one. Meanwhile, the response waves are also more smooth than configuration one. Based on the figure for $T_{period} = 2\mu s$ the voltage responses would distribute linearly from the top disc to the bottom disc.

As for the figures located in this subsection, the lines with different colors represent the voltage response waveforms of their corresponding disc. The x-axis is on behalf of the computation time in the order of second(s), y-axis is on behalf of the voltage value in the order of volts(V).

21.5 The voltage responses with iron core–configuration two

According to the figures for $T_{period} = 100\mu s$ and $T_{period} = 400\mu s$ shown in subsection 21.4, it is evident that there are still some LC resonances present in each of the voltage response, but the amplitudes or intensities for the resonances are much smaller than those for configuration one. Based on the figure for $T_{period} = 2\mu s$ in this subsection, through the application of the second configuration, the voltage would distribute linearly from the top disc to bottom disc, which is the same as the case with ferrite F core. However, we have to pay attention that the second configuration is more costly than the first configuration.

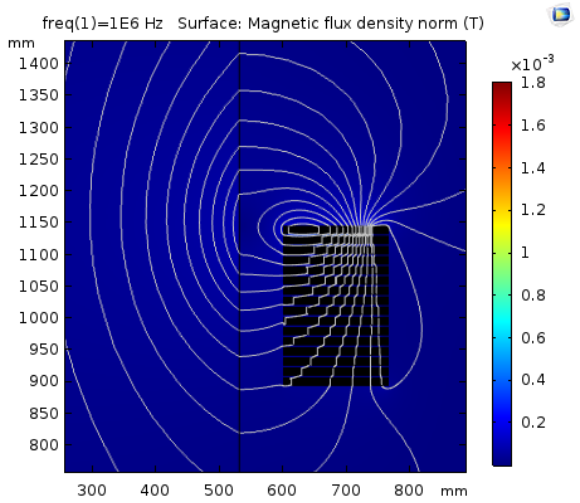

Figure 178. Ferrite core–configuration two

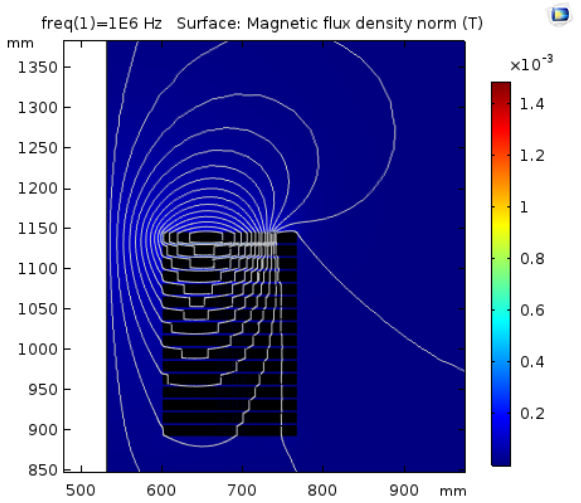

Figure 179. Iron core–configuration two

Figure 178 and figure 179 illustrate the magnetic flux density for the disc winding designed in the second configuration with ferrite F core and iron core respectively. According to figure 180, 181 and 182, the intensity of the LC resonances decreases drastically due to the implementation of configuration two and the electric stress between adjacent discs has been reduced a lot. Therefore, the flash-overs are not easy to occur when the lightning impulse strikes the transformer.

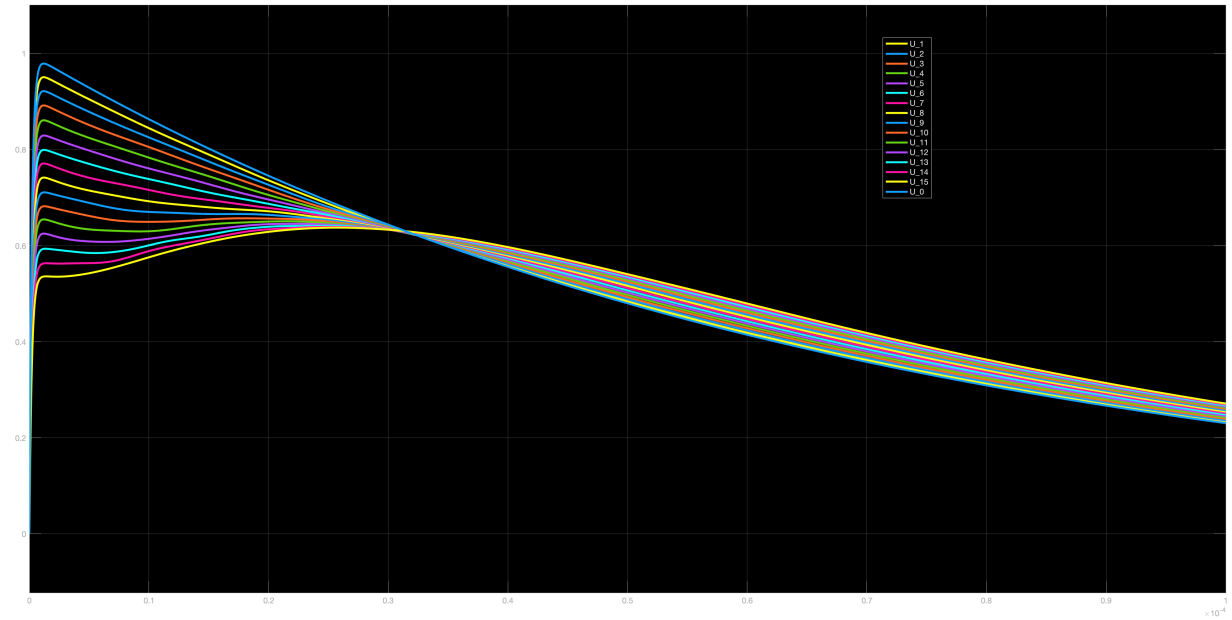

Figure 180. Voltage response distribution iron core $T_{period} = 100\mu s$

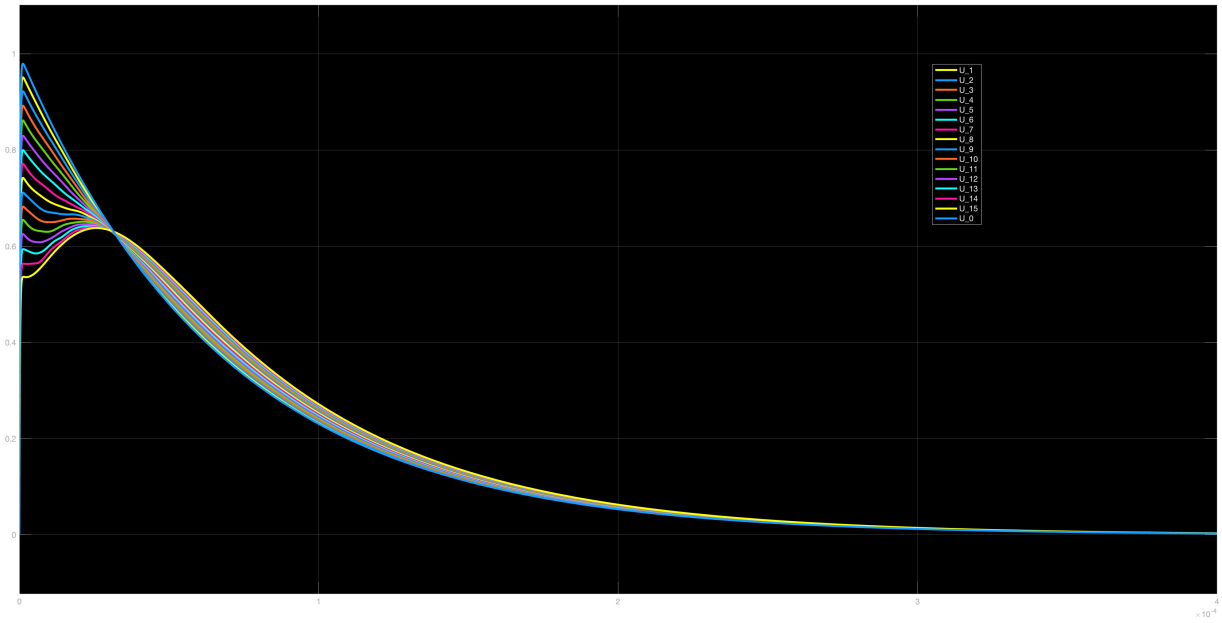

Figure 181. Voltage response distribution iron core $T_{period} = 400\mu s$

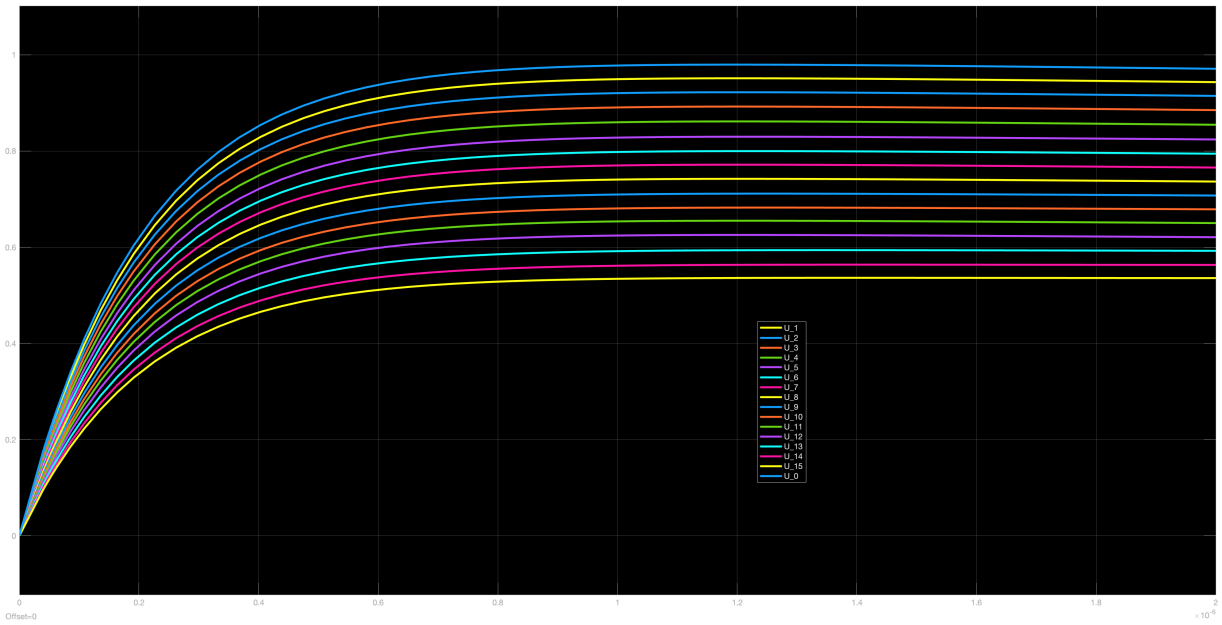

Figure 182. Voltage response distribution iron core $T_{period} = 2\mu s$

21.6 The voltage responses with ferrite F core–configuration three

Generally, it is clear that the second configuration could contribute to a better voltage response distribution, but it could also result in more material cost due to the application of 6 additional electrostatic inter-shield pairs. In order to reduce the cost and keep the good response performance, configuration three has been designed: the first disc pair has four inter-shield pairs, the second and third disc pair comprise of three inter-shield pairs, the following three disc pairs have two inter-shields pairs and the last two disc pairs comprise of one inter-shield pair. Figure 183 and figure 184 illustrate the geometry of the disc winding model designed in the third configuration.

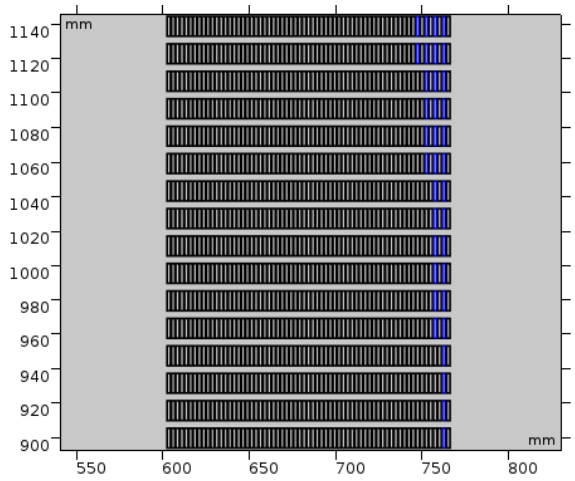

Figure 183. Electrostatic shield wires colored blue

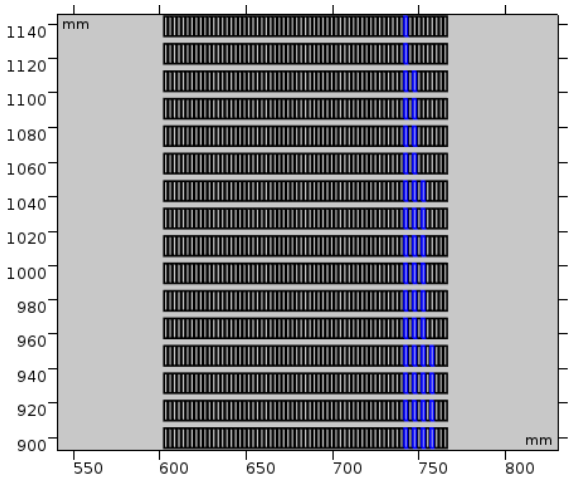

Figure 184. Oil gaps colored blue

As for the figures for $T_{period} = 100\mu s$ and $T_{period} = 400\mu s$ shown as below, the voltage response distribution of the third configuration is almost the same as that of the second configuration. Compared with the second configuration, three additional electrostatic inter-shield pairs have been saved. Thus, the material cost could be reduced. As a result, the third configuration could have a perfect balance between the cost and the response performance.

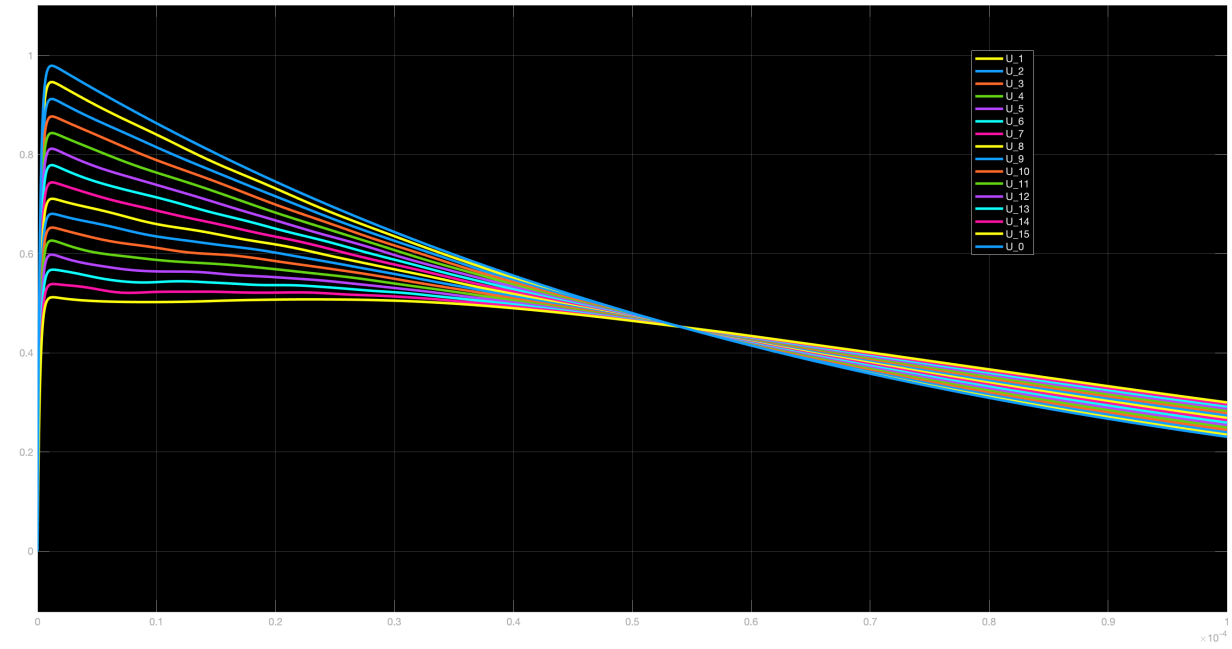

Figure 185. Voltage response distribution ferrite core $T_{period} = 100\mu s$

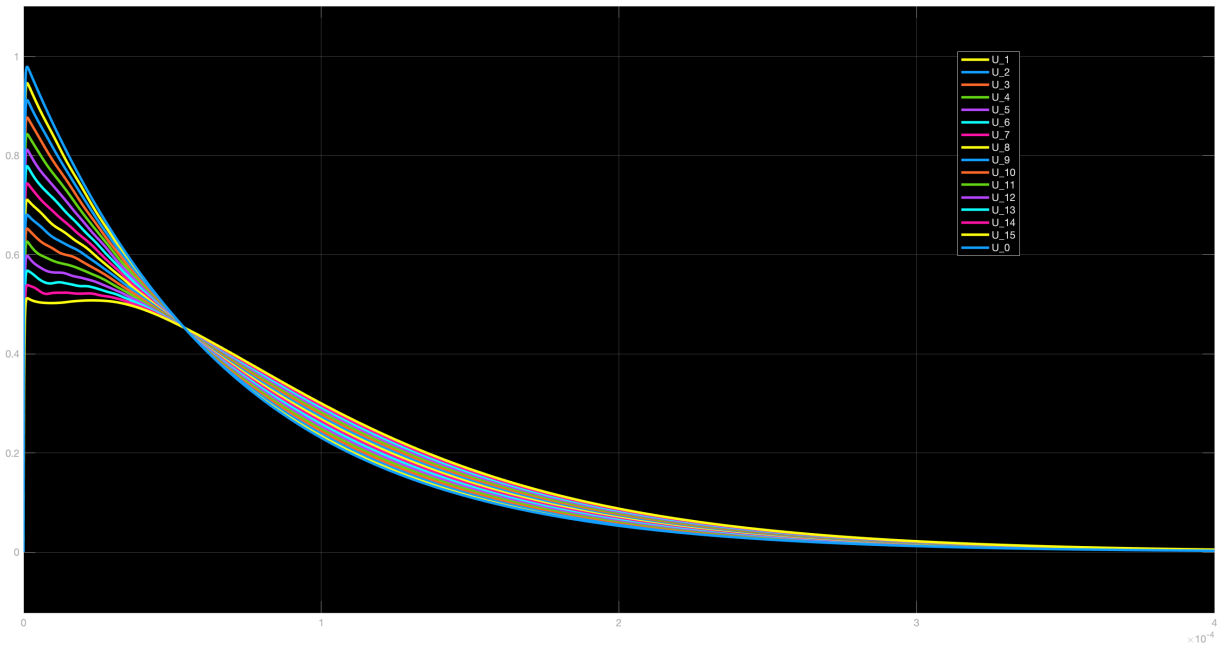

Figure 186. Voltage response distribution ferrite core $T_{period} = 400\mu s$

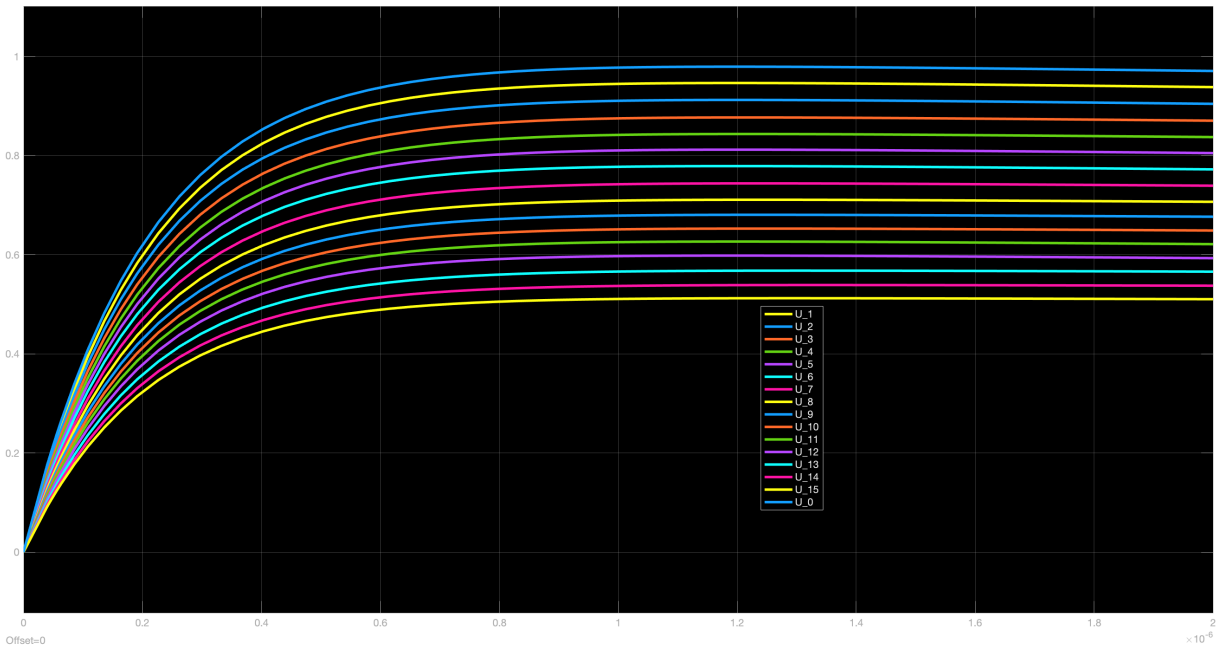

Figure 187. Voltage response distribution ferrite core $T_{period} = 2\mu s$

Based on figure 187, it is quite evident that the voltage responses would still distribute linearly along the disc winding. Meanwhile, the LC resonances have been significantly limited through the coordination of the disc pairs inter-shielded by optimized number of electrostatic shield wires. It is really important that the results obtained from the case designed in the third configuration are quite similar to those for the case designed in the second configuration, which proves that the third configuration could be regarded as acceptable.

21.7 The voltage responses with iron core–configuration three

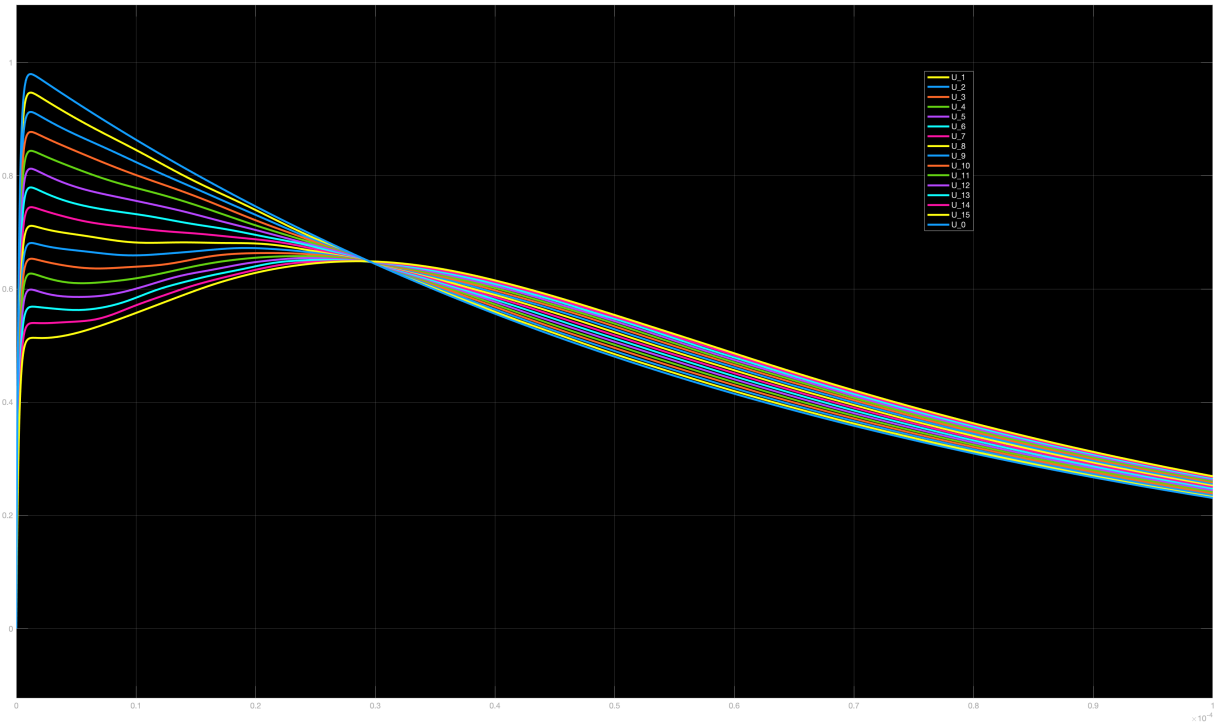

Figure 188. Voltage response distribution iron core $T_{period} = 100\mu s$

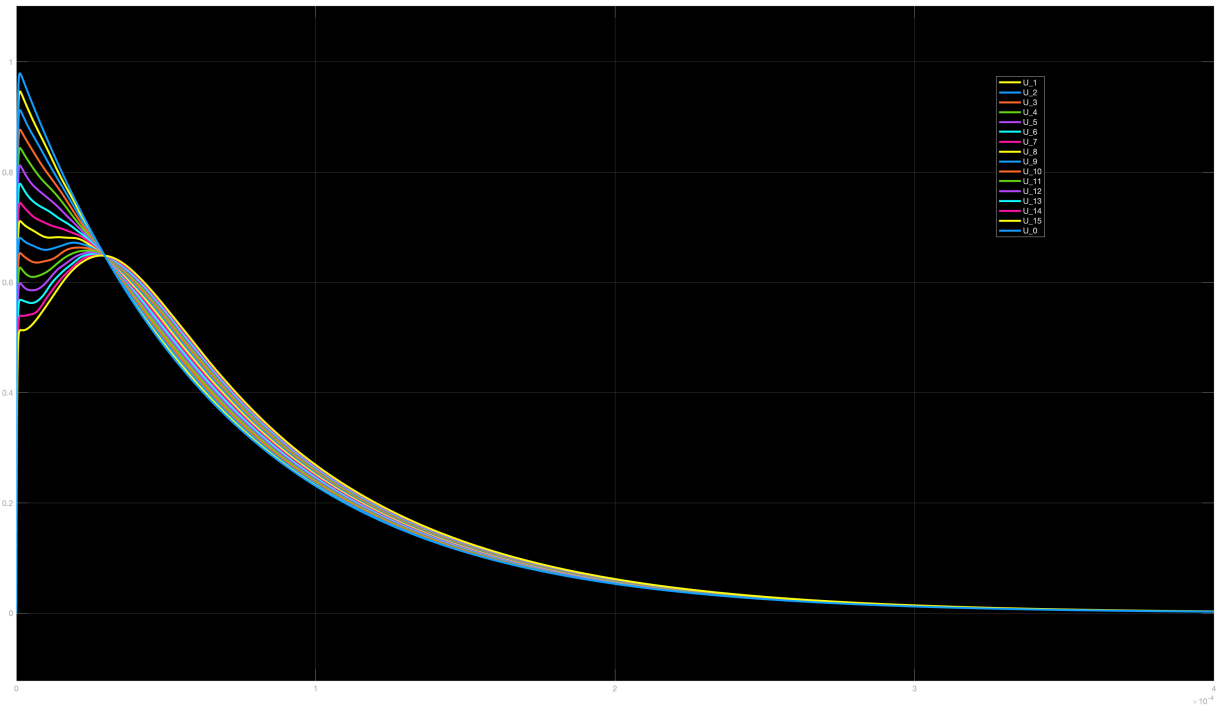

Figure 189. Voltage response distribution iron core $T_{period} = 400\mu s$

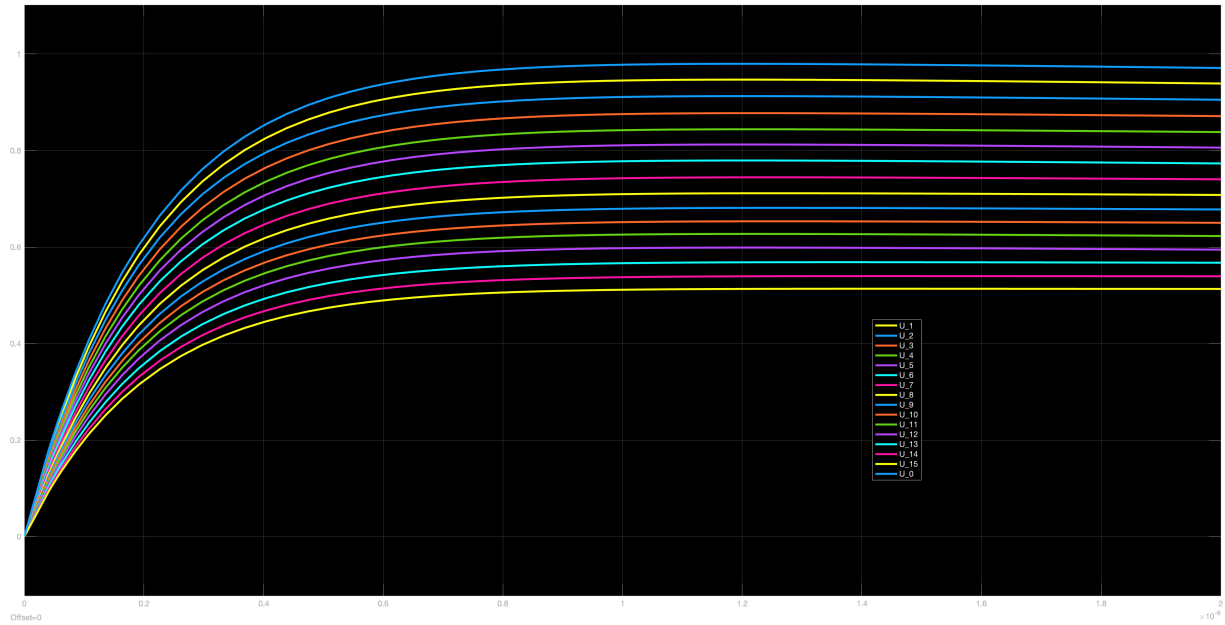

Figure 190. Voltage response distribution iron core $T_{period} = 2\mu s$

According to figure 190, if the material of the transformer core is iron, the voltage responses would distribute linearly along the disc winding model after the implementation of the third configuration. The LC resonances have been effectually limited according to the figures for $T_{period} = 100\mu s$ and $T_{period} = 400\mu s$. Also, the range for natural network frequencies f_i has been reduced through the coordination of the disc pairs with different number of electrostatic inter-shield pairs.

To sum up, the hv disc winding model with iron core designed in configuration three is the best option for the transformer manufacturing company. Moreover, after the application of the third configuration, the voltage responses would distribute linearly along the winding and the goal of the thesis project could be achieved. Ferrite F core would be used in the high frequency layer winding transformers and the results obtained from the cases with ferrite F core are only used for the results comparison.

21.8 The optimization of the geometry for the disc winding transformer

As for the geometry of the disc winding model designed before, the distance between two adjacent disc pairs d_1 is considered to be equal to the distance between the discs from individual disc pair d_2. Whereas, according to figure 191 and figure 192, we could know that d_1 ought to become around three times of d_2 in some real large power transformers. In order to obtain the precious voltage responses for different configurations, the geometry needs to be modified.

Figure 191. Transformer figure one

Figure 192. Transformer figure two

Figure 193 and figure 194 illustrate the geometry of the improved disc winding model with iron core in the third configuration, which is expected to become the best option. Here, d_1 is set to become 12mm and d_2 is 4mm. Moreover, the values for total series capacitance of each disc pair would not change, but the values of the series capacitances between adjacent disc pairs would become different.

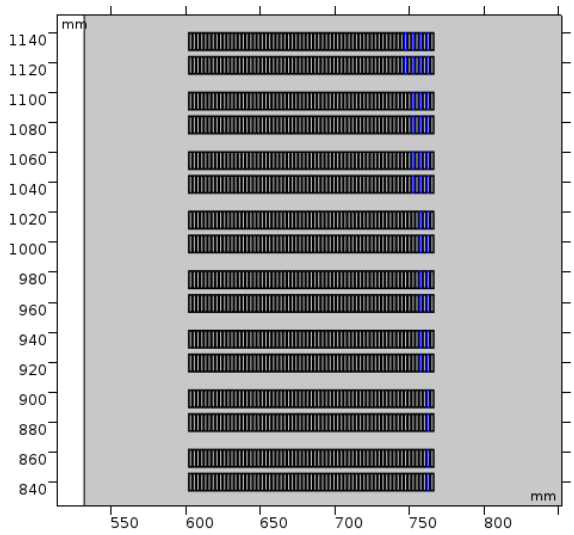

Figure 193. Inserted electrostatic shield wires

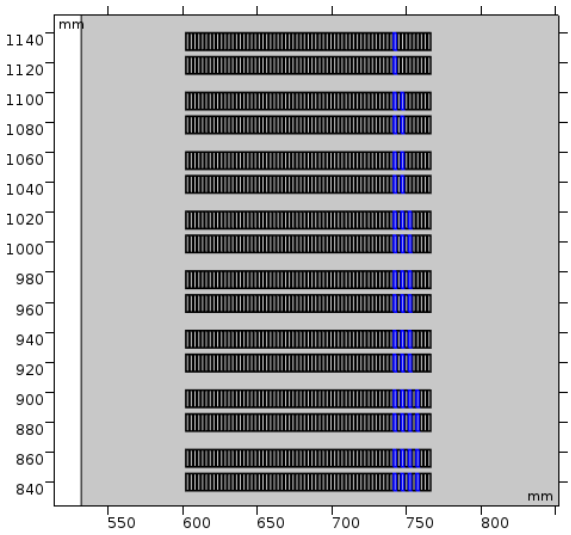

Figure 194. Inserted oil gaps

The tables below comprises the new improvement factors λ_{new} and series capacitances C_{s-new} when the distance between two discs has been increased to 12mm. All of the results mentioned are also obtained through the Comsol simulation.

Number of inserted electrostatic shield wires	Series capacitance C_{s-new}	Improvement factor λ_{new}
N=0	$C_{s0-new} = 0.4586nF$	$\lambda_{0-new} = 1.000$
N=1	$C_{s1-new} = 2.3393nF$	$\lambda_{1-new} = 5.101$
N=2	$C_{s2-new} = 4.1351nF$	$\lambda_{2-new} = 9.017$
N=3	$C_{s3-new} = 5.8574nF$	$\lambda_{3-new} = 12.772$
N=4	$C_{s4-new} = 7.5086nF$	$\lambda_{4-new} = 16.373$
N=5	$C_{s5-new} = 9.0908nF$	$\lambda_{5-new} = 19.823$
$N_1 = 0, N_2 = 0$	$C_{s00-new} = 0.4586nF$	$\lambda_{00-new} = 1.000$
$N_1 = 1, N_2 = 0$	$C_{s10-new} = 1.3983nF$	$\lambda_{10-new} = 3.049$
$N_1 = 2, N_2 = 1$	$C_{s21-new} = 3.2367nF$	$\lambda_{21-new} = 7.058$
$N_1 = 3, N_2 = 2$	$C_{s32-new} = 4.9958nF$	$\lambda_{32-new} = 10.894$
$N_1 = 4, N_2 = 3$	$C_{s43-new} = 6.6825nF$	$\lambda_{43-new} = 14.572$
$N_1 = 5, N_2 = 4$	$C_{s54-new} = 8.2993nF$	$\lambda_{54-new} = 18.097$

Table 14. Improvement of the series capacitance for different number of electrostatic inter-shield wires

After extracting the values of series capacitances C_s we expected from the tables 3, table 4 and table 14, we could finally obtain the new voltage responses of this modified disc winding geometry in configuration three. Moreover, the inductance matrix together with the resistance matrix should also be re-calculated.

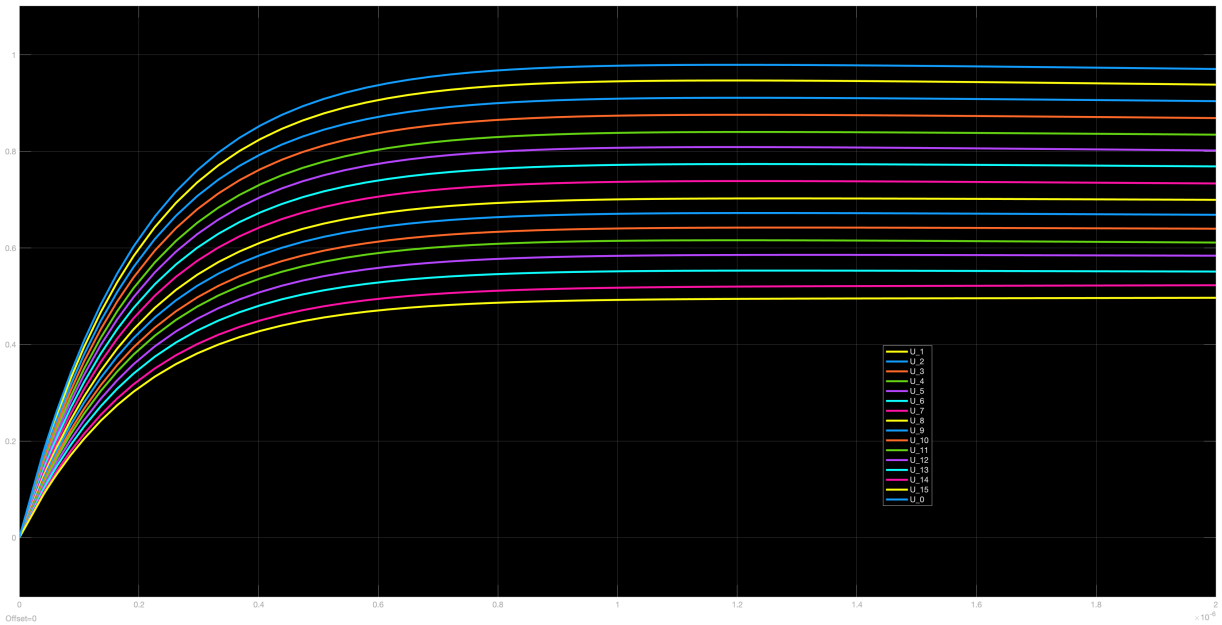

Figure 195. Voltage response distribution iron core $2\mu s$

According to figure for $2\mu s$ shown above and the figures for $100\mu s$ and $400\mu s$ shown below, the voltage responses still distribute linearly from top disc to bottom disc when the geometry of the disc winding has been slightly modified. In reality, these voltage response distribution lines are almost the same as those for the initial geometry. Thus, the third configuration with iron core is still the best option for the transformer company.

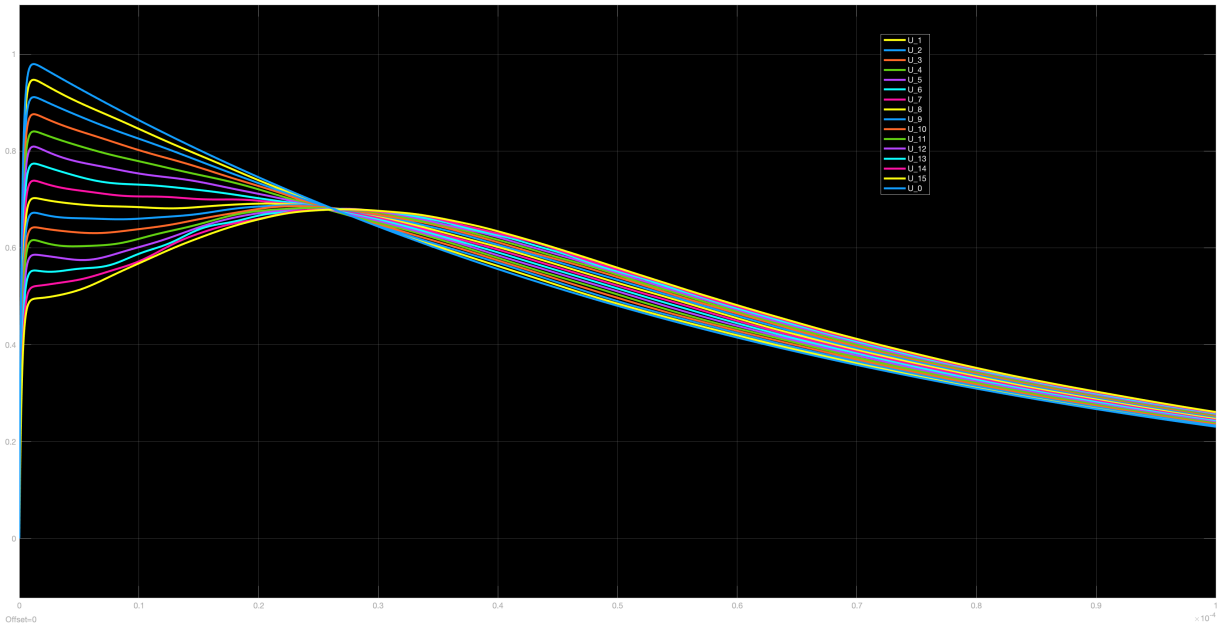

Figure 196. Voltage response distribution iron core $100\mu s$

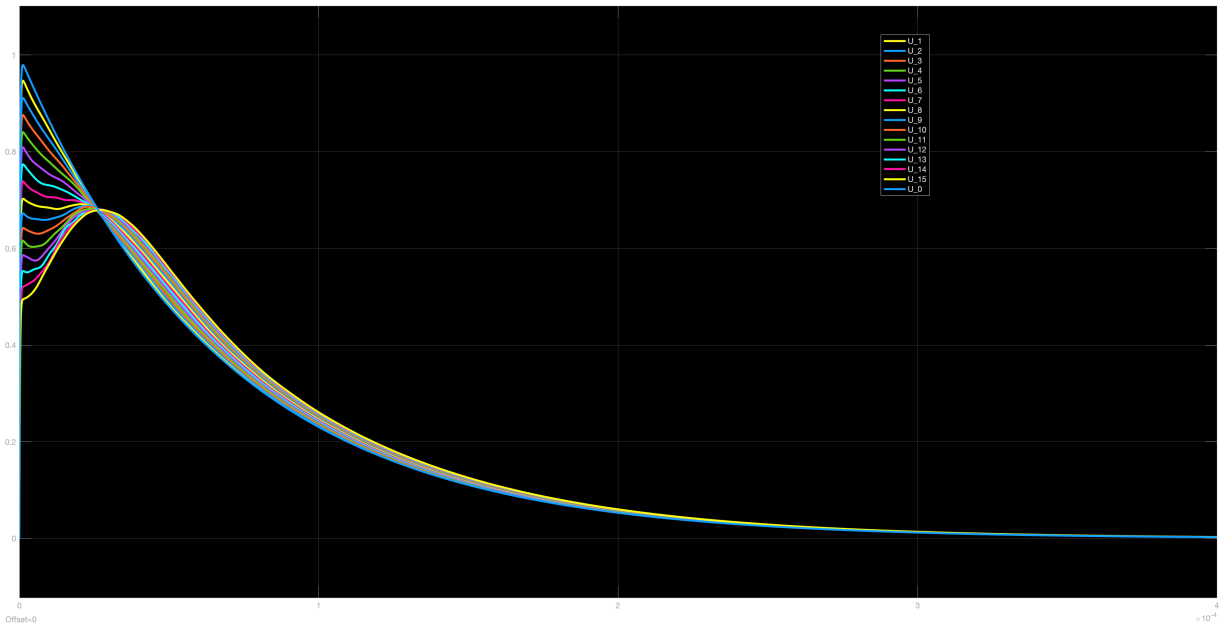

Figure 197. Voltage response distribution iron core $400\mu s$

22 Conclusions and recommendations

22.1 Conclusions

This practical thesis topic is in collaboration with Royal Smit Transformers. Through the literature review, the number of the useful references related to this thesis topic are quite limited. With respect to the acquired references, the resulted analytical formulas are not general and lack of derivation processes, which is really complex for the readers to understand. After the re-derivation, some errors could even be found out in those reference papers. In this thesis report, those errors are indicated and corrected.

In order to obtain the voltage response waveforms for the hv disc winding, first of all, the winding ought to be represented by an simplified electric network which comprises of the mutual inductances, mutual resistances and the influential capacitances. Secondly, the simplified electric network should be built in Simulink. These two steps are achieved after reading reference [2] and [9]. The most critical step is to simulate the disc winding model in Comsol. Through the Comsol modelling, the values for inductance and resistance matrix together with the influential capacitances of a certain configuration could be obtained.

The main objective of this master thesis has been successfully achieved by the application of the third configuration with optimized number of electrostatic inter-shield wires mainly based on Comsol modelling and the general analytical formula derivations.

1) From this thesis report, the general analytical formulas for the total series capacitance C_s of the disc pair model with k inserted electrostatic shield wires or with k would-in shield wires are obtained. Meanwhile, the analytical formula of the total series capacitance for the continuous disc pair model together with the turn-interleaved disc pair model are also capable to be obtained. These analytical formulas are proved to be correct through the numerical verification. These formulas are also existing in reference [7], which will be published in 2020 IEEE International Conference on High Voltage Engineering and Application.

2) The question about how to properly calculate the total series capacitance of a disc pair model with different number of inter-shield wires through numerical method could be solved through Comsol modeling. It is also worth mentioning that the results calculated from those analytical formulas are basically the approximate values. They are not accurate but still meaningful and reasonable.

3) The improvement factor λ tables of the total series capacitance C_s for different type of inter-shield wires are acquired. The values for λ are really practical and reasonable because the scale of the disc pair is really close to that from real hv transformer winding.

4) The critical assumption has been successfully proved based on the Matlab codes derived from [2]. The verification of this assumption is necessary because so far the designers from Royal Smit Transformers would directly accept and use it for manufacturing and we cannot find any explanations related to the correctness of this assumption. After running the Matlab codes, the voltage response distribution inside the disc pair model could be approximately observed and it is also very easy to switch the voltage sources for the model.

5) After knowing how to calculate the total mutual inductance L_s between two discs or coils in Comsol Multiphysics, the decrease factor η table for the mutual inductance of the disc pair with different number of inter-shield wires could be obtained and reason why L_s would decrease after the application of shield wires is also thoroughly explained.

22.2 Recommendations

1) Real measurements for the individual turn-turn series capacitance C_{tt}, turn-shield capacitance C_{ts} and the total mutual inductance L_s between two adjacent discs are required to be done in order to verify the simulation results.

2) The voltage distribution in reaction to the impulse voltage source or chopped voltage source would be test in real hv transformer disc winding model in order to make the verification of the assumption in [1] more convincing.

3) Theoretically, the third configuration could cause the linear voltage distribution and the influence of the LC resonances could be limited. However, this should also be investigated by means of real testing.

References

[1] R. Del Vecchio, B. Poulin, and R. Ahuja, "Calculation and measurement of winding disk capacitances with wound-in-shields", *IEEE Transactions on Power delivery*, vol. 13, no. 2, pp. 503–509, 1998.

[2] C. Kroon, *Digital computer calculation of surge voltage distribution in transformer windings*. Royal Smit Transformers, Nijmegen.

[3] R. Van Nuys, "Interleaved high-voltage transformer windings", *IEEE Transactions on Power Apparatus and Systems*, no. 5, pp. 1946–1954, 1978.

[4] R. A. Hinton, K. W. Doughty, and W. N. Kennedy, *Electrostatic shielding of disc windings*, US Patent 4,042,900, Aug. 1977.

[5] M. Bagheri, A. Hekmati, R. Heidarzadeh, and M. S. Naderi, "Impulse voltage distribution in intershield disk winding vs interleaved and continuous disk winding in power transformer", in *2008 IEEE 2nd International Power and Energy Conference*, IEEE, 2008, pp. 387–392.

[6] M. Bagheri, M. Vakilian, A. Hekmati, and R. Heidarzadeh, "Influence of electrostatic shielding of disc winding on increasing the series capacitance in transformer", in *2007 IEEE Lausanne Power Tech*, IEEE, 2007, pp. 1780–1784.

[7] M. G. Niasar and W. Zhao, "Impulse voltage distribution on disk winding: Calculation of disk series capacitances using analytical method", 2020.

[8] G. E. Sauer, *Impulse voltage distribution improving partial-turn electrostatic shields for disc windings*, US Patent 4,017,815, Apr. 1977.

[9] J. Smajic, T. Steinmetz, M. Rüegg, Z. Tanasic, R. Obrist, J. Tepper, B. Weber, and M. Carlen, "Simulation and measurement of lightning-impulse voltage distributions over transformer windings", *IEEE transactions on magnetics*, vol. 50, no. 2, pp. 553–556, 2014.

[10] O. Moreau, P. Guuinic, R. Dorr, and Q. Su, "Comparison between the high frequency characteristics of transformer interleaved and ordinary disk windings", in *2000 IEEE Power Engineering Society Winter Meeting. Conference Proceedings (Cat. No. 00CH37077)*, IEEE, vol. 3, 2000, pp. 2187–2192.

[11] A. Miki, T. Hosoya, and K. Okuyama, "A calculation method for impulse voltage distribution and transferred voltage in transformer windings", *IEEE Transactions on Power Apparatus and Systems*, no. 3, pp. 930–939, 1978.

[12] K. Wirgau, "Inductance calculation of an air-core disk winding", *IEEE Transactions on Power Apparatus and Systems*, vol. 95, no. 1, pp. 394–400, 1976.

[13] J. A. Martinez-Velasco, *Power system transients: parameter determination*. CRC press, 2017.

[14] W. Zhao, *Study on the lightning voltage distribution in the next generation of transformers and reactors*. Technical University of Delft, Electrical Sustainable Energy Department, Delft, The Netherlands, 2020.

[15] A. Greenwood, *Electrical transients in power systems*. New York, NY (USA); John Wiley and Sons Inc., 1991.

[16] H. Masdi, N. Mariun, A. Mohamed, and N. I. A. Wahab, "Study of impulse voltage distribution in transformer windings", in *2010 IEEE International Conference on Power and Energy*, IEEE, 2010, pp. 379–383.

[17] J. E. Bracken, "Mutual resistance in spicelink", *Ansoft Corporation, Pittsburgh, PA*, 2000.

23 Appendices

23.1 The Matlab code in the case of Sinusoidal wave

```
%% Voltage response of the kth transformer turn with respect to earth—disc pair model
    —sinusoidal voltage sources
clc
close all
clear
%%
load 'L_1.txt'
load 'R_1.txt'
R_1(1)=[];
L_1(1)=[];
R_1=transpose(R_1);
L_1=transpose(L_1);
%%
load 'L_2.txt'
load 'R_2.txt'
R_2(1)=[];
L_2(1)=[];
R_2=transpose(R_2);
L_2=transpose(L_2);
%%
load 'L_3.txt'
load 'R_3.txt'
R_3(1)=[];
L_3(1)=[];
R_3=transpose(R_3);
L_3=transpose(L_3);
%%
load 'L_4.txt'
load 'R_4.txt'
R_4(1)=[];
L_4(1)=[];
R_4=transpose(R_4);
L_4=transpose(L_4);
%%
load 'L_5.txt'
load 'R_5.txt'
R_5(1)=[];
L_5(1)=[];
R_5=transpose(R_5);
L_5=transpose(L_5);
%%
load 'L_6.txt'
load 'R_6.txt'
R_6(1)=[];
L_6(1)=[];
R_6=transpose(R_6);
L_6=transpose(L_6);
%%
load 'L_7.txt'
load 'R_7.txt'
R_7(1)=[];
L_7(1)=[];
R_7=transpose(R_7);
L_7=transpose(L_7);
%%
load 'L_8.txt'
load 'R_8.txt'
R_8(1)=[];
L_8(1)=[];
R_8=transpose(R_8);
```

```
60 L_8=transpose(L_8);
61 %%
62 load 'L_9.txt'
63 load 'R_9.txt'
64 R_9(1)=[];
65 L_9(1)=[];
66 R_9=transpose(R_9);
67 L_9=transpose(L_9);
68 %%
69 load 'L_10.txt'
70 load 'R_10.txt'
71 R_10(1)=[];
72 L_10(1)=[];
73 R_10=transpose(R_10);
74 L_10=transpose(L_10);
75 %%
76 load 'L_11.txt'
77 load 'R_11.txt'
78 R_11(1)=[];
79 L_11(1)=[];
80 R_11=transpose(R_11);
81 L_11=transpose(L_11);
82 %%
83 load 'L_12.txt'
84 load 'R_12.txt'
85 R_12(1)=[];
86 L_12(1)=[];
87 R_12=transpose(R_12);
88 L_12=transpose(L_12);
89 %%
90 load 'L_13.txt'
91 load 'R_13.txt'
92 R_13(1)=[];
93 L_13(1)=[];
94 R_13=transpose(R_13);
95 L_13=transpose(L_13);
96 %%
97 load 'L_14.txt'
98 load 'R_14.txt'
99 R_14(1)=[];
100 L_14(1)=[];
101 R_14=transpose(R_14);
102 L_14=transpose(L_14);
103 %%
104 load 'L_15.txt'
105 load 'R_15.txt'
106 R_15(1)=[];
107 L_15(1)=[];
108 R_15=transpose(R_15);
109 L_15=transpose(L_15);
110 %%
111 load 'L_16.txt'
112 load 'R_16.txt'
113 R_16(1)=[];
114 L_16(1)=[];
115 R_16=transpose(R_16);
116 L_16=transpose(L_16);
117 %%
118 load 'L_17.txt'
119 load 'R_17.txt'
120 R_17(1)=[];
121 L_17(1)=[];
122 R_17=transpose(R_17);
```

```
123 L_17=transpose(L_17);
124 %%
125 load 'L_18.txt'
126 load 'R_18.txt'
127 R_18(1)=[];
128 L_18(1)=[];
129 R_18=transpose(R_18);
130 L_18=transpose(L_18);
131 %%
132 load 'L_19.txt'
133 load 'R_19.txt'
134 R_19(1)=[];
135 L_19(1)=[];
136 R_19=transpose(R_19);
137 L_19=transpose(L_19);
138 %%
139 load 'L_20.txt'
140 load 'R_20.txt'
141 R_20(1)=[];
142 L_20(1)=[];
143 R_20=transpose(R_20);
144 L_20=transpose(L_20);
145 %%
146 load 'L_21.txt'
147 load 'R_21.txt'
148 R_21(1)=[];
149 L_21(1)=[];
150 R_21=transpose(R_21);
151 L_21=transpose(L_21);
152 %%
153 load 'L_22.txt'
154 load 'R_22.txt'
155 R_22(1)=[];
156 L_22(1)=[];
157 R_22=transpose(R_22);
158 L_22=transpose(L_22);
159 %%
160 load 'L_23.txt'
161 load 'R_23.txt'
162 R_23(1)=[];
163 L_23(1)=[];
164 R_23=transpose(R_23);
165 L_23=transpose(L_23);
166 %%
167 load 'L_24.txt'
168 load 'R_24.txt'
169 R_24(1)=[];
170 L_24(1)=[];
171 R_24=transpose(R_24);
172 L_24=transpose(L_24);
173 %%
174 load 'L_25.txt'
175 load 'R_25.txt'
176 R_25(1)=[];
177 L_25(1)=[];
178 R_25=transpose(R_25);
179 L_25=transpose(L_25);
180 %%
181 load 'L_26.txt'
182 load 'R_26.txt'
183 R_26(1)=[];
184 L_26(1)=[];
185 R_26=transpose(R_26);
```

```
L_26=transpose(L_26);
%%
load 'L_27.txt'
load 'R_27.txt'
R_27(1)=[];
L_27(1)=[];
R_27=transpose(R_27);
L_27=transpose(L_27);
%%
load 'L_28.txt'
load 'R_28.txt'
R_28(1)=[];
L_28(1)=[];
R_28=transpose(R_28);
L_28=transpose(L_28);
%%
load 'L_29.txt'
load 'R_29.txt'
R_29(1)=[];
L_29(1)=[];
R_29=transpose(R_29);
L_29=transpose(L_29);
%% Inductance matrix & Resistance matrix
L=[L_1 L_2 L_3 L_4 L_5 L_6 L_7 L_8 L_9 L_10 L_11 L_12 L_13 L_14 L_15 L_16 L_17 L_18
    L_19 L_20 L_21 L_22 L_23 L_24 L_25 L_26 L_27 L_28 L_29];
R=[R_1 R_2 R_3 R_4 R_5 R_6 R_7 R_8 R_9 R_10 R_11 R_12 R_13 R_14 R_15 R_16 R_17 R_18
    R_19 R_20 R_21 R_22 R_23 R_24 R_25 R_26 R_27 R_28 R_29];
%%
v_a=29;  %the total number of the transformer turns
v_b=28;
%% Capacitance matrix
load 'capacitance_matrix.txt'
C=capacitance_matrix*10^(-12); %unit has been transformed into pF
A=[zeros(1,v_b) 0; eye(v_b) zeros(v_b,1)];
%% p_0 has been simplified as a v_b*v_b matrix
A1=transpose(A);
C_star=A1*C*A;
C_star(:,v_a)=[];
C_star(v_a,:)=[];
p_0=C_star;
%% l_0 has been simplified as a v_b*v_b matrix
E=eye(v_a);
L_star=(A-E)^(-1)*L*(A1-E)^(-1);
l_0=L_star^(-1);
l_0(:,v_a)=[];
l_0(v_a,:)=[];
%% D has been simplified as a v_b*v_b matrix
Delta=9.1e4;
D=Delta*E;
D(:,v_a)=[];
D(v_a,:)=[];
%%
DD=(A1-E)*(L^(-1))*R*((A1-E)^(-1)); %provide some hints to Delta
%% The calculation of the eigenvalues—— natural frequency of the network
P=C_star^(-1)*l_0;
e=eig(P);
f0=(sqrt(e)/1e6)/(2*pi); %unit in MHz
%% The constant value part
F=[1;zeros(v_b,1)];
K_star=(-A1)*C;
N=K_star*F;
N(v_a,:)=[];%N is a v_b*1 matrix
M=(E-A1)*L^(-1)*F;
```

```
247 M(v_a,:) =[];%M is a v_b*1 matrix
248 %% Kramer's rule
249 l= zeros(v_b,v_b,v_b);
250 for v=1:v_b
251     l(:,:,v)=l_0;
252     l(:,v,v)=M;
253 end
254
255 p= zeros(v_b,v_b,v_b);
256 for v=1:v_b
257     p(:,:,v)=p_0;
258     p(:,v,v)=N;
259 end
260 %%
261 a=zeros(v_b,v_b);  %a_ik
262 de=zeros(v_b,v_b); %the upper part of a_ik
263
264 for k=1:v_b
265     for v=1:v_b
266         de(v,k)=det(l(:,:,k)-e(v)*p(:,:,k));
267         b=e-e(v);
268         b(v)=[];
269
270         a(v,k)=de(v,k);
271         for mm=1:1:length(b)
272             a(v,k)=a(v,k)/b(mm);
273         end
274
275     end
276 end
277 %% Sinusoidal voltage wave
278 V=1; % the magnitude of the sine wave
279 f=1e6; %unit in MHz
280 b=2*pi*f;
281 step=100;
282 t=0:(1/(f*step)):(100/f);
283 ttt=length(t);
284 V_source=V*sin(b*t);
285 %%
286 w=sqrt(abs(e-(Delta/2)^2));
287 %% U
288 z_1=zeros(v_b,v_b,ttt);
289 z_0=zeros(v_b,1,ttt);
290 U=zeros(v_b,ttt);
291
292 for k=1:v_b
293    for v=1:v_b
294        if e(v)>(0.5*Delta)^2
295
296            for j=1:ttt
297                z_1(k,v,j)=((b*a(v,k))/((e(v)-b^2)^2+(b*Delta)^2))*((-Delta)*cos(b*t(j))
                        +((e(v)-b^2)/b)*sin(b*t(j))+Delta*exp(-0.5*Delta*t(j))*cos(w(v)*t(j))
                        +((0.5*Delta^2-(e(v)-b^2))/w(v))*exp(-0.5*Delta*t(j))*sin(w(v)*t(j)))
                        ;
298
299                z_0(k,1,j)=det(p(:,:,k))*sin(b*t(j));
300            end
301
302        elseif e(v)==(0.5*Delta)^2
303
304             for j=1:ttt
305                z_1(k,v,j)=((4*b*a(v,k))/(Delta^2+4*b^2)^2)*((-4*Delta)*cos(b*t(j))+((
                        Delta^2-4*b^2)/b)*sin(b*t(j))+(Delta^2+4*b^2)*t(j)*exp(-0.5*Delta*t(j
```

```
                    ))+4*Delta*exp(-0.5*Delta*t(j)));
306
307                 z_0(k,1,j)=det(p(:,:,k))*sin(b*t(j));
308             end
309
310         elseif e(v)<(0.5*Delta)^2
311
312             for j=1:ttt
313                 z_1(k,v,j)=((b*a(v,k))/((e(v)-b^2)^2+(b*Delta)^2))*((-Delta)*cos(b*t(j))
                        +((e(v)-b^2)/b)*sin(b*t(j))+Delta*exp(-0.5*Delta*t(j))*cos((1i)*w(v)*
                        t(j))+((0.5*Delta^2-(e(v)-b^2))/((1i)*w(v)))*exp(-0.5*Delta*t(j))*sin
                        ((1i)*w(v)*t(j)));
314
315                 z_0(k,1,j)=det(p(:,:,k))*sin(b*t(j));
316             end
317
318         end
319     end
320 end
321
322 ele_1=sum(z_1,2);
323 ele_0=z_0;
324 U=V*(ele_0+ele_1)/det(C_star);
325 %%
326 U =reshape(U, [v_b, ttt]);
327 U_1=U(1,:);
328 U_2=U(2,:);
329 U_3=U(3,:);
330 U_4=U(4,:);
331 U_5=U(5,:);
332 U_6=U(6,:);
333 U_7=U(7,:);
334 U_8=U(8,:);
335 U_9=U(9,:);
336 U_10=U(10,:);
337 U_11=U(11,:);
338 U_12=U(12,:);
339 U_13=U(13,:);
340 U_14=U(14,:);
341 U_15=U(15,:);
342 U_16=U(16,:);
343 U_17=U(17,:);
344 U_18=U(18,:);
345 U_19=U(19,:);
346 U_20=U(20,:);
347 U_21=U(21,:);
348 U_22=U(22,:);
349 U_23=U(23,:);
350 U_24=U(24,:);
351 U_25=U(25,:);
352 U_26=U(26,:);
353 U_27=U(27,:);
354 U_28=U(28,:);
355 %% The voltage responses made by Matlab code
356 figure()
357 plot(t,U_1)
358 hold on
359 plot(t,U_2)
360 hold on
361 plot(t,U_3)
362 hold on
363 plot(t,U_4)
364 hold on
```

```
365 plot(t,U_5)
366 hold on
367 plot(t,U_6)
368 hold on
369 plot(t,U_7)
370 hold on
371 plot(t,U_8)
372 hold on
373 plot(t,U_9)
374 hold on
375 plot(t,U_10)
376 hold on
377 plot(t,U_11)
378 hold on
379 plot(t,U_12)
380 hold on
381 plot(t,U_13)
382 hold on
383 plot(t,U_14)
384 hold on
385 plot(t,U_15)
386 hold on
387 plot(t,U_16)
388 hold on
389 plot(t,U_17)
390 hold on
391 plot(t,U_18)
392 hold on
393 plot(t,U_19)
394 hold on
395 plot(t,U_20)
396 hold on
397 plot(t,U_21)
398 hold on
399 plot(t,U_22)
400 hold on
401 plot(t,U_23)
402 hold on
403 plot(t,U_24)
404 hold on
405 plot(t,U_25)
406 hold on
407 plot(t,U_26)
408 hold on
409 plot(t,U_27)
410 hold on
411 plot(t,U_28)
412 xlabel('Time');
413 ylabel('Voltage(V)');
414 legend('Freq=XMHz');
415 addToolbarExplorationButtons(gcf)
416 %% The positive crest value distribution
417 pp=2; %the number of the duty cycle under consideration
418 aa0=max(V_source);
419 aa1=max(U_1(ttt-step*pp:ttt));
420 aa2=max(U_2(ttt-step*pp:ttt));
421 aa3=max(U_3(ttt-step*pp:ttt));
422 aa4=max(U_4(ttt-step*pp:ttt));
423 aa5=max(U_5(ttt-step*pp:ttt));
424 aa6=max(U_6(ttt-step*pp:ttt));
425 aa7=max(U_7(ttt-step*pp:ttt));
426 aa8=max(U_8(ttt-step*pp:ttt));
427 aa9=max(U_9(ttt-step*pp:ttt));
```

```
aa10=max(U_10(ttt-step*pp:ttt));
aa11=max(U_11(ttt-step*pp:ttt));
aa12=max(U_12(ttt-step*pp:ttt));
aa13=max(U_13(ttt-step*pp:ttt));
aa14=max(U_14(ttt-step*pp:ttt));
aa15=max(U_15(ttt-step*pp:ttt));
aa16=max(U_16(ttt-step*pp:ttt));
aa17=max(U_17(ttt-step*pp:ttt));
aa18=max(U_18(ttt-step*pp:ttt));
aa19=max(U_19(ttt-step*pp:ttt));
aa20=max(U_20(ttt-step*pp:ttt));
aa21=max(U_21(ttt-step*pp:ttt));
aa22=max(U_22(ttt-step*pp:ttt));
aa23=max(U_23(ttt-step*pp:ttt));
aa24=max(U_24(ttt-step*pp:ttt));
aa25=max(U_25(ttt-step*pp:ttt));
aa26=max(U_26(ttt-step*pp:ttt));
aa27=max(U_27(ttt-step*pp:ttt));
aa28=max(U_28(ttt-step*pp:ttt));
aa29=0;
%%
figure();
qq=1:1:30;
aa=[aa0 aa1 aa2 aa3 aa4 aa5 aa6 aa7 aa8 aa9 aa10 aa11 aa12 aa13 aa14 aa15 aa16 aa17
    aa18 aa19 aa20 aa21 aa22 aa23 aa24 aa25 aa26 aa27 aa28 aa29 aa29];
plot(qq,aa)
xlabel('Number of layers');
ylabel('Voltage(V)');
legend('Freq=XMHz');
addToolbarExplorationButtons(gcf)
```

23.2 The Matlab code in the case of the step wave

```
%% voltage response distribution of the kth transformer turn with respect to earth in time domain—Step voltage source
clc
close all
clear
%%
load 'L_1.txt'
load 'R_1.txt'
R_1(1)=[];
L_1(1)=[];
R_1=transpose(R_1);
L_1=transpose(L_1);
%%
load 'L_2.txt'
load 'R_2.txt'
R_2(1)=[];
L_2(1)=[];
R_2=transpose(R_2);
L_2=transpose(L_2);
%%
load 'L_3.txt'
load 'R_3.txt'
R_3(1)=[];
L_3(1)=[];
R_3=transpose(R_3);
L_3=transpose(L_3);
%%
load 'L_4.txt'
load 'R_4.txt'
R_4(1)=[];
L_4(1)=[];
R_4=transpose(R_4);
L_4=transpose(L_4);
%%
load 'L_5.txt'
load 'R_5.txt'
R_5(1)=[];
L_5(1)=[];
R_5=transpose(R_5);
L_5=transpose(L_5);
%%
load 'L_6.txt'
load 'R_6.txt'
R_6(1)=[];
L_6(1)=[];
R_6=transpose(R_6);
L_6=transpose(L_6);
%%
load 'L_7.txt'
load 'R_7.txt'
R_7(1)=[];
L_7(1)=[];
R_7=transpose(R_7);
L_7=transpose(L_7);
%%
load 'L_8.txt'
load 'R_8.txt'
R_8(1)=[];
L_8(1)=[];
R_8=transpose(R_8);
L_8=transpose(L_8);
%%
```

```
load 'L_9.txt'
load 'R_9.txt'
R_9(1)=[];
L_9(1)=[];
R_9=transpose(R_9);
L_9=transpose(L_9);
%%
load 'L_10.txt'
load 'R_10.txt'
R_10(1)=[];
L_10(1)=[];
R_10=transpose(R_10);
L_10=transpose(L_10);
%%
load 'L_11.txt'
load 'R_11.txt'
R_11(1)=[];
L_11(1)=[];
R_11=transpose(R_11);
L_11=transpose(L_11);
%%
load 'L_12.txt'
load 'R_12.txt'
R_12(1)=[];
L_12(1)=[];
R_12=transpose(R_12);
L_12=transpose(L_12);
%%
load 'L_13.txt'
load 'R_13.txt'
R_13(1)=[];
L_13(1)=[];
R_13=transpose(R_13);
L_13=transpose(L_13);
%%
load 'L_14.txt'
load 'R_14.txt'
R_14(1)=[];
L_14(1)=[];
R_14=transpose(R_14);
L_14=transpose(L_14);
%%
load 'L_15.txt'
load 'R_15.txt'
R_15(1)=[];
L_15(1)=[];
R_15=transpose(R_15);
L_15=transpose(L_15);
%%
load 'L_16.txt'
load 'R_16.txt'
R_16(1)=[];
L_16(1)=[];
R_16=transpose(R_16);
L_16=transpose(L_16);
%%
load 'L_17.txt'
load 'R_17.txt'
R_17(1)=[];
L_17(1)=[];
R_17=transpose(R_17);
L_17=transpose(L_17);
%%
```

```
125 load 'L_18.txt'
126 load 'R_18.txt'
127 R_18(1)=[];
128 L_18(1)=[];
129 R_18=transpose(R_18);
130 L_18=transpose(L_18);
131 %%
132 load 'L_19.txt'
133 load 'R_19.txt'
134 R_19(1)=[];
135 L_19(1)=[];
136 R_19=transpose(R_19);
137 L_19=transpose(L_19);
138 %%
139 load 'L_20.txt'
140 load 'R_20.txt'
141 R_20(1)=[];
142 L_20(1)=[];
143 R_20=transpose(R_20);
144 L_20=transpose(L_20);
145 %%
146 load 'L_21.txt'
147 load 'R_21.txt'
148 R_21(1)=[];
149 L_21(1)=[];
150 R_21=transpose(R_21);
151 L_21=transpose(L_21);
152 %%
153 load 'L_22.txt'
154 load 'R_22.txt'
155 R_22(1)=[];
156 L_22(1)=[];
157 R_22=transpose(R_22);
158 L_22=transpose(L_22);
159 %%
160 load 'L_23.txt'
161 load 'R_23.txt'
162 R_23(1)=[];
163 L_23(1)=[];
164 R_23=transpose(R_23);
165 L_23=transpose(L_23);
166 %%
167 load 'L_24.txt'
168 load 'R_24.txt'
169 R_24(1)=[];
170 L_24(1)=[];
171 R_24=transpose(R_24);
172 L_24=transpose(L_24);
173 %%
174 load 'L_25.txt'
175 load 'R_25.txt'
176 R_25(1)=[];
177 L_25(1)=[];
178 R_25=transpose(R_25);
179 L_25=transpose(L_25);
180 %%
181 load 'L_26.txt'
182 load 'R_26.txt'
183 R_26(1)=[];
184 L_26(1)=[];
185 R_26=transpose(R_26);
186 L_26=transpose(L_26);
187 %%
```

```
load 'L_27.txt'
load 'R_27.txt'
R_27(1)=[];
L_27(1)=[];
R_27=transpose(R_27);
L_27=transpose(L_27);
%%
load 'L_28.txt'
load 'R_28.txt'
R_28(1)=[];
L_28(1)=[];
R_28=transpose(R_28);
L_28=transpose(L_28);
%%
load 'L_29.txt'
load 'R_29.txt'
R_29(1)=[];
L_29(1)=[];
R_29=transpose(R_29);
L_29=transpose(L_29);
%% Inductance matrix & Resistance matrix
L=[L_1 L_2 L_3 L_4 L_5 L_6 L_7 L_8 L_9 L_10 L_11 L_12 L_13 L_14 L_15 L_16 L_17 L_18
    L_19 L_20 L_21 L_22 L_23 L_24 L_25 L_26 L_27 L_28 L_29];
R=[R_1 R_2 R_3 R_4 R_5 R_6 R_7 R_8 R_9 R_10 R_11 R_12 R_13 R_14 R_15 R_16 R_17 R_18
    R_19 R_20 R_21 R_22 R_23 R_24 R_25 R_26 R_27 R_28 R_29];
%%
v_a=30; %the total number of the layers
v_b=29;
%% Capacitance matrix & Adjacent matrix
load 'capacitance_matrix.txt'
C=capacitance_matrix*10^(-12); %unit has been transformed into pF
A=[zeros(1,v_b) 0; eye(v_b) zeros(v_b,1)];
%% p_0 has been simplified as a v_b*v_b matrix---C_star
A1=transpose(A);
C_star=A1*C*A;
C_star(:,v_a)=[];
C_star(v_a,:)=[];
p_0=C_star;
%% l_0 has been simplified as a v_b*v_b matrix---L_star^(-1)
E=eye(v_a);
L_star=(A-E)^(-1)*L*(A1-E)^(-1);
l_0=L_star^(-1);
l_0(:,v_a)=[];
l_0(v_a,:)=[];
%% D has been simplified as a v_b*v_b matrix
Delta= 2.1e5;
D=Delta*E;
D(:,v_a)=[];
D(v_a,:)=[];
%%
DD=(A1-E)*(L^(-1))*R*((A1-E)^(-1)); %provide some hints to Delta
%% The calculation of the eigenvalues---natural network frequencies
P=C_star^(-1)*l_0;
e=eig(P);
f0=(sqrt(e)/1e6)/(2*pi); %unit in MHz
%% The constant value part
F=[1;zeros(v_b,1)];
K_star=(-A1)*C;
N=K_star*F;
N(v_a,:)=[];%N is a v_b*1 matrix
M=(E-A1)*L^(-1)*F;
M(v_a,:)=[];%M is a v_b*1 matrix
%% Kramer's rule
```

```
l= zeros(v_b,v_b,v_b);
for v=1:v_b
    l(:,:,v)=l_0;
    l(:,v,v)=M;
end

p= zeros(v_b,v_b,v_b);
for v=1:v_b
    p(:,:,v)=p_0;
    p(:,v,v)=N;
end
%%
a=zeros(v_b,v_b);%a_ik
de=zeros(v_b,v_b);%the upper part of a_ik

for v=1:v_b
    for k=1:v_b
        de(v,k)=det(l(:,:,k)-e(v)*p(:,:,k));
        b=e-e(v);
        b(v)=[];

        a(v,k)=de(v,k);

        for mm=1:1:length(b)

            a(v,k)=a(v,k)/b(mm);

        end

    end
end
%% Step function
step=1000;
t=0:(5e-6/step):5e-6; %we only focus on the small time region of the rise time
ttt=size(t,2); % 2 represents for column and 1 represents for row
V_0=1;
V_source=V_0;
%%
w=sqrt(abs(e-(Delta/2)^2));
%% U
z_1=zeros(v_b,v_b,ttt);
z_0=zeros(v_b,1,ttt);
U=zeros(v_b,ttt);

for k=1:v_b
   for v=1:v_b
       if e(v)>(0.5*Delta)^2

           for j=1:ttt %related to time
               z_1(k,v,j)=(a(v,k)/e(v))*(1-cos(w(v)*t(j))*exp(-0.5*Delta*t(j))-(Delta
                   /(2*w(v)))*sin(w(v)*t(j))*exp(-0.5*Delta*t(j)));

               z_0(k,1,j)=det(p(:,:,k))*1;
           end

       elseif e(v)==(0.5*Delta)^2

           for j=1:ttt %related to time
               z_1(k,v,j)=a(v,k)*(4/Delta^2)*(1-exp(-0.5*Delta*t(j))-(0.5*Delta)*t(j)*
                   exp(-0.5*Delta*t(j)));

               z_0(k,1,j)=det(p(:,:,k))*1;
           end
```

```
310
311         elseif e(v)<(0.5*Delta)^2
312
313             for j=1:ttt %related to time
314                 z_1(k,v,j)=(a(v,k)/e(v))*(1-cos((1i)*w(v)*t(j))*exp(-0.5*Delta*t(j))-(
                        Delta/(2*w(v)*(1i)))*sin((1i)*w(v)*t(j))*exp(-0.5*Delta*t(j)));
315
316                 z_0(k,1,j)=det(p(:,:,k))*1;
317             end
318
319         end
320
321     end
322 end
323
324 ele_1=sum(z_1,2);
325 ele_0=z_0;
326 U=(ele_0+ele_1)/det(C_star);
327 %% Reshape of the voltage matrix
328 U =reshape(U, [v_b, ttt]);
329 U_1=U(1,:);
330 U_2=U(2,:);
331 U_3=U(3,:);
332 U_4=U(4,:);
333 U_5=U(5,:);
334 U_6=U(6,:);
335 U_7=U(7,:);
336 U_8=U(8,:);
337 U_9=U(9,:);
338 U_10=U(10,:);
339 U_11=U(11,:);
340 U_12=U(12,:);
341 U_13=U(13,:);
342 U_14=U(14,:);
343 U_15=U(15,:);
344 U_16=U(16,:);
345 U_17=U(17,:);
346 U_18=U(18,:);
347 U_19=U(19,:);
348 U_20=U(20,:);
349 U_21=U(21,:);
350 U_22=U(22,:);
351 U_23=U(23,:);
352 U_24=U(24,:);
353 U_25=U(25,:);
354 U_26=U(26,:);
355 U_27=U(27,:);
356 U_28=U(28,:);
357 U_29=U(29,:);
358 %% The graph made by Matlab code--Time stamps(ns)
359 num=41;
360 Time=5*(num-1);  %unit in ns
361 aaaa=zeros(1,29);
362 figure();
363 aaa=[U_1(num),U_2(num),U_3(num),U_4(num),U_5(num),U_6(num),U_7(num),U_8(num),U_9(num),
        U_10(num),U_11(num),U_12(num),U_13(num),U_14(num),U_15(num),U_16(num),U_17(num),
        U_18(num),U_19(num),U_20(num),U_21(num),U_22(num),U_23(num),U_24(num),U_25(num),
        U_26(num),U_27(num),U_28(num),U_29(num)];
364 plot(aaa)
365 legend('T=2000ns');
366 xlabel('Number of layers');
367 ylabel('Volts');
368 addToolbarExplorationButtons(gcf)
```

```
369 %% Voltage waveforms of each transformer turns
370 figure()
371 plot(t,U_1)
372 hold on
373 plot(t,U_2)
374 hold on
375 plot(t,U_3)
376 hold on
377 plot(t,U_4)
378 hold on
379 plot(t,U_5)
380 hold on
381 plot(t,U_6)
382 hold on
383 plot(t,U_7)
384 hold on
385 plot(t,U_8)
386 hold on
387 plot(t,U_9)
388 hold on
389 plot(t,U_10)
390 hold on
391 plot(t,U_11)
392 hold on
393 plot(t,U_12)
394 hold on
395 plot(t,U_13)
396 hold on
397 plot(t,U_14)
398 hold on
399 plot(t,U_15)
400 hold on
401 plot(t,U_16)
402 hold on
403 plot(t,U_17)
404 hold on
405 plot(t,U_18)
406 hold on
407 plot(t,U_19)
408 hold on
409 plot(t,U_20)
410 hold on
411 plot(t,U_21)
412 hold on
413 plot(t,U_22)
414 hold on
415 plot(t,U_23)
416 hold on
417 plot(t,U_24)
418 hold on
419 plot(t,U_25)
420 hold on
421 plot(t,U_26)
422 hold on
423 plot(t,U_27)
424 hold on
425 plot(t,U_28)
426 hold on
427 plot(t,U_29)
428 hold on
429 xlabel('Time(s)')
430 ylabel('Voltage(V)')
431 addToolbarExplorationButtons(gcf)
```

23.3 The Matlab code in the case of the lightning impulse wave

```
%% Voltage response for the kth transformer turn with respect to earth in time domain—
    Lightning impulse voltage source
clc
close all
clear
%%
load 'L_1.txt'
load 'R_1.txt'
R_1(1)=[];
L_1(1)=[];
R_1=transpose(R_1);
L_1=transpose(L_1);
%%
load 'L_2.txt'
load 'R_2.txt'
R_2(1)=[];
L_2(1)=[];
R_2=transpose(R_2);
L_2=transpose(L_2);
%%
load 'L_3.txt'
load 'R_3.txt'
R_3(1)=[];
L_3(1)=[];
R_3=transpose(R_3);
L_3=transpose(L_3);
%%
load 'L_4.txt'
load 'R_4.txt'
R_4(1)=[];
L_4(1)=[];
R_4=transpose(R_4);
L_4=transpose(L_4);
%%
load 'L_5.txt'
load 'R_5.txt'
R_5(1)=[];
L_5(1)=[];
R_5=transpose(R_5);
L_5=transpose(L_5);
%%
load 'L_6.txt'
load 'R_6.txt'
R_6(1)=[];
L_6(1)=[];
R_6=transpose(R_6);
L_6=transpose(L_6);
%%
load 'L_7.txt'
load 'R_7.txt'
R_7(1)=[];
L_7(1)=[];
R_7=transpose(R_7);
L_7=transpose(L_7);
%%
load 'L_8.txt'
load 'R_8.txt'
R_8(1)=[];
L_8(1)=[];
R_8=transpose(R_8);
L_8=transpose(L_8);
%%
```

```
load 'L_9.txt'
load 'R_9.txt'
R_9(1)=[];
L_9(1)=[];
R_9=transpose(R_9);
L_9=transpose(L_9);
%%
load 'L_10.txt'
load 'R_10.txt'
R_10(1)=[];
L_10(1)=[];
R_10=transpose(R_10);
L_10=transpose(L_10);
%%
load 'L_11.txt'
load 'R_11.txt'
R_11(1)=[];
L_11(1)=[];
R_11=transpose(R_11);
L_11=transpose(L_11);
%%
load 'L_12.txt'
load 'R_12.txt'
R_12(1)=[];
L_12(1)=[];
R_12=transpose(R_12);
L_12=transpose(L_12);
%%
load 'L_13.txt'
load 'R_13.txt'
R_13(1)=[];
L_13(1)=[];
R_13=transpose(R_13);
L_13=transpose(L_13);
%%
load 'L_14.txt'
load 'R_14.txt'
R_14(1)=[];
L_14(1)=[];
R_14=transpose(R_14);
L_14=transpose(L_14);
%%
load 'L_15.txt'
load 'R_15.txt'
R_15(1)=[];
L_15(1)=[];
R_15=transpose(R_15);
L_15=transpose(L_15);
%%
load 'L_16.txt'
load 'R_16.txt'
R_16(1)=[];
L_16(1)=[];
R_16=transpose(R_16);
L_16=transpose(L_16);
%%
load 'L_17.txt'
load 'R_17.txt'
R_17(1)=[];
L_17(1)=[];
R_17=transpose(R_17);
L_17=transpose(L_17);
%%
```

```
125 load 'L_18.txt'
126 load 'R_18.txt'
127 R_18(1)=[];
128 L_18(1)=[];
129 R_18=transpose(R_18);
130 L_18=transpose(L_18);
131 %%
132 load 'L_19.txt'
133 load 'R_19.txt'
134 R_19(1)=[];
135 L_19(1)=[];
136 R_19=transpose(R_19);
137 L_19=transpose(L_19);
138 %%
139 load 'L_20.txt'
140 load 'R_20.txt'
141 R_20(1)=[];
142 L_20(1)=[];
143 R_20=transpose(R_20);
144 L_20=transpose(L_20);
145 %%
146 load 'L_21.txt'
147 load 'R_21.txt'
148 R_21(1)=[];
149 L_21(1)=[];
150 R_21=transpose(R_21);
151 L_21=transpose(L_21);
152 %%
153 load 'L_22.txt'
154 load 'R_22.txt'
155 R_22(1)=[];
156 L_22(1)=[];
157 R_22=transpose(R_22);
158 L_22=transpose(L_22);
159 %%
160 load 'L_23.txt'
161 load 'R_23.txt'
162 R_23(1)=[];
163 L_23(1)=[];
164 R_23=transpose(R_23);
165 L_23=transpose(L_23);
166 %%
167 load 'L_24.txt'
168 load 'R_24.txt'
169 R_24(1)=[];
170 L_24(1)=[];
171 R_24=transpose(R_24);
172 L_24=transpose(L_24);
173 %%
174 load 'L_25.txt'
175 load 'R_25.txt'
176 R_25(1)=[];
177 L_25(1)=[];
178 R_25=transpose(R_25);
179 L_25=transpose(L_25);
180 %%
181 load 'L_26.txt'
182 load 'R_26.txt'
183 R_26(1)=[];
184 L_26(1)=[];
185 R_26=transpose(R_26);
186 L_26=transpose(L_26);
187 %%
```

```
188 load 'L_27.txt'
189 load 'R_27.txt'
190 R_27(1)=[];
191 L_27(1)=[];
192 R_27=transpose(R_27);
193 L_27=transpose(L_27);
194 %%
195 load 'L_28.txt'
196 load 'R_28.txt'
197 R_28(1)=[];
198 L_28(1)=[];
199 R_28=transpose(R_28);
200 L_28=transpose(L_28);
201 %%
202 load 'L_29.txt'
203 load 'R_29.txt'
204 R_29(1)=[];
205 L_29(1)=[];
206 R_29=transpose(R_29);
207 L_29=transpose(L_29);
208 %% Inductance matrix & Resistance matrix
209 L=[L_1 L_2 L_3 L_4 L_5 L_6 L_7 L_8 L_9 L_10 L_11 L_12 L_13 L_14 L_15 L_16 L_17 L_18
      L_19 L_20 L_21 L_22 L_23 L_24 L_25 L_26 L_27 L_28 L_29];
210 R=[R_1 R_2 R_3 R_4 R_5 R_6 R_7 R_8 R_9 R_10 R_11 R_12 R_13 R_14 R_15 R_16 R_17 R_18
      R_19 R_20 R_21 R_22 R_23 R_24 R_25 R_26 R_27 R_28 R_29];
211 %%
212 v_a=29; %the total number of the transformer layers(discs)
213 v_b=28;
214 %% Capacitance matrix & Adjacent matrix
215 load 'capacitance_matrix.txt'
216 C=capacitance_matrix*10^(-12);  %unit has been transformed into pF
217 A=[zeros(1,v_b) 0; eye(v_b) zeros(v_b,1)];
218 %% p_0 has been simplified as a (v_b*v_b) matrix---C_star
219 A1=transpose(A);
220 C_star=A1*C*A;
221 C_star(:,v_a)=[];
222 C_star(v_a,:)=[];
223 p_0=C_star;
224 %% l_0 is simplified as a (v_b*v_b) matrix---L_star^(-1)
225 E=eye(v_a);
226 L_star=(A-E)^(-1)*L*(A1-E)^(-1);
227 l_0=L_star^(-1);
228 l_0(:,v_a)=[];
229 l_0(v_a,:)=[];
230 %% The simplfied D is a (v_b*v_b) matrix
231 Delta=9.1e4;
232 D=Delta*E;
233 D(:,v_a)=[];
234 D(v_a,:)=[];
235 %%
236 DD=(A1-E)*(L^(-1))*R*((A1-E)^(-1)); %provide some hints to Delta
237 %% The calculation of the eigenvalues---natural network frequencies---v_b values
238 P=C_star^(-1)*l_0;
239 e=eig(P);
240 f0=(sqrt(e)/1e6)/(2*pi);  %the units are in MHz
241 %% The constant value part
242 F=[1;zeros(v_b,1)];
243 K_star=(-A1)*C;
244 N=K_star*F;
245 N(v_a,:)=[];%N is a v_b*1 matrix
246 M=(E-A1)*L^(-1)*F;
247 M(v_a,:)=[];%M is a v_b*1 matrix
248 %% Kramer's rule
```

```
l= zeros(v_b,v_b,v_b);
for v=1:v_b
    l(:,:,v)=l_0;
    l(:,v,v)=M;
end

p= zeros(v_b,v_b,v_b);
for v=1:v_b
    p(:,:,v)=p_0;
    p(:,v,v)=N;
end
%%
a=zeros(v_b,v_b);    %a_ik
de=zeros(v_b,v_b);   %the upper part of a_ik
for k=1:v_b
    for v=1:v_b
        de(v,k)=det(l(:,:,k)-e(v)*p(:,:,k));
        b=e-e(v);
        b(v)=[];
        a(v,k)=de(v,k);

          for mm=1:length(b)
              a(v,k)=a(v,k)/b(mm);
          end

    end
end
%% Lightning source---lightning impulse
Alpha=[1/(68.2e-6);1/(0.205e-6)];
step=2000;
t=0:(100e-6/step):100e-6;
ttt=length(t);
V_0=1; %the magnitude of the lightning impulse
V_source=V_0*(exp(-Alpha(1)*t)-exp(-Alpha(2)*t));
figure();
plot(t,V_source)
%%
w=sqrt(abs(e-(Delta/2)^2));
%%
x_1=zeros(v_b,2,ttt);
for k=1:2
    for v=1:v_b
        for j= 1:ttt

        x_1(v,k,j)=cos(w(v)*t(j))-((Alpha(k)-(Delta/2))/w(v))*sin(w(v)*t(j));

        end
    end
end

x_2=zeros(v_b,2,ttt);
for k=1:2
    for v=1:v_b
        for j= 1:ttt

        x_2(v,k,j)=1-(Alpha(k)-(Delta/2))*t(j);

        end
    end
end

x_3=zeros(v_b,2,ttt);
for k=1:2
```

```
312      for v=1:v_b
313          for j= 1:ttt
314
315          x_3(v,k,j)=cos((1i)*w(v)*t(j))-((Alpha(k)-(Delta/2))/((1i)*w(v)))*sin((1i)*w(v)*
                 t(j));
316
317          end
318      end
319 end
320 % x has 58 different cases and each case has ttt points
321 %%
322 %U
323 z_1=zeros(v_b,v_b,ttt);
324 z_2=zeros(v_b,v_b,ttt);
325 z_0=zeros(v_b,1,ttt);
326
327 U=zeros(v_b,ttt);
328
329 for k=1:v_b
330     for v=1:v_b
331         if e(v)>(0.5*Delta)^2
332
333             for j=1:ttt %related to time
334                 z_1(k,v,j)=(a(v,k)/((Alpha(1)*(Alpha(1)-Delta))+e(v)))*(exp(-Alpha(1)*t
                        (j))-x_1(v,1,j)*exp(-0.5*Delta*t(j)));
335
336                 z_2(k,v,j)=(a(v,k)/((Alpha(2)*(Alpha(2)-Delta))+e(v)))*(exp(-Alpha(2)*t
                        (j))-x_1(v,2,j)*exp(-0.5*Delta*t(j)));
337
338                 z_0(k,1,j)=det(p(:,:,k))*(exp(-Alpha(1)*t(j))-exp(-Alpha(2)*t(j)));
339             end
340
341         elseif e(v)==(0.5*Delta)^2
342
343             for j=1:ttt %related to time
344                 z_1(k,v,j)=(a(v,k)/((Alpha(1)*(Alpha(1)-Delta))+e(v)))*(exp(-Alpha(1)*t
                        (j))-x_2(v,1,j)*exp(-0.5*Delta*t(j)));
345
346                 z_2(k,v,j)=(a(v,k)/((Alpha(2)*(Alpha(2)-Delta))+e(v)))*(exp(-Alpha(2)*t
                        (j))-x_2(v,2,j)*exp(-0.5*Delta*t(j)));
347
348                 z_0(k,1,j)=det(p(:,:,k))*(exp(-Alpha(1)*t(j))-exp(-Alpha(2)*t(j)));
349             end
350
351         elseif e(v)<(0.5*Delta)^2
352
353             for j=1:ttt %related to time
354                 z_1(k,v,j)=(a(v,k)/((Alpha(1)*(Alpha(1)-Delta))+e(v)))*(exp(-Alpha(1)*t
                        (j))-x_3(v,1,j)*exp(-0.5*Delta*t(j)));
355
356                 z_2(k,v,j)=(a(v,k)/((Alpha(2)*(Alpha(2)-Delta))+e(v)))*(exp(-Alpha(2)*t
                        (j))-x_3(v,2,j)*exp(-0.5*Delta*t(j)));
357
358                 z_0(k,1,j)=det(p(:,:,k))*(exp(-Alpha(1)*t(j))-exp(-Alpha(2)*t(j)));
359             end
360
361         end
362
363     end
364 end
365
366 ele_1=sum(z_1,2);
367 ele_2=sum(z_2,2);
```

```
ele_0=z_0;
U=V_0*(ele_0+ele_1-ele_2)/det(C_star);
%%
U =reshape(U, [v_b, ttt]);
U_1=U(1,:);
U_2=U(2,:);
U_3=U(3,:);
U_4=U(4,:);
U_5=U(5,:);
U_6=U(6,:);
U_7=U(7,:);
U_8=U(8,:);
U_9=U(9,:);
U_10=U(10,:);
U_11=U(11,:);
U_12=U(12,:);
U_13=U(13,:);
U_14=U(14,:);
U_15=U(15,:);
U_16=U(16,:);
U_17=U(17,:);
U_18=U(18,:);
U_19=U(19,:);
U_20=U(20,:);
U_21=U(21,:);
U_22=U(22,:);
U_23=U(23,:);
U_24=U(24,:);
U_25=U(25,:);
U_26=U(26,:);
U_27=U(27,:);
U_28=U(28,:);
%% The voltage waveforms of each transformer turn
figure()
plot(t,U_1)
hold on
plot(t,U_2)
hold on
plot(t,U_3)
hold on
plot(t,U_4)
hold on
plot(t,U_5)
hold on
plot(t,U_6)
hold on
plot(t,U_7)
hold on
plot(t,U_8)
hold on
plot(t,U_9)
hold on
plot(t,U_10)
hold on
plot(t,U_11)
hold on
plot(t,U_12)
hold on
plot(t,U_13)
hold on
plot(t,U_14)
hold on
plot(t,U_15)
```

```
431 hold on
432 plot(t,U_16)
433 hold on
434 plot(t,U_17)
435 hold on
436 plot(t,U_18)
437 hold on
438 plot(t,U_19)
439 hold on
440 plot(t,U_20)
441 hold on
442 plot(t,U_21)
443 hold on
444 plot(t,U_22)
445 hold on
446 plot(t,U_23)
447 hold on
448 plot(t,U_24)
449 hold on
450 plot(t,U_25)
451 hold on
452 plot(t,U_26)
453 hold on
454 plot(t,U_27)
455 hold on
456 plot(t,U_28)
457 addToolbarExplorationButtons(gcf)
458 %% Select the maximum value from the voltage waveform
459 aa0=max(V_source);
460 aa1=max(U_1);
461 aa2=max(U_2);
462 aa3=max(U_3);
463 aa4=max(U_4);
464 aa5=max(U_5);
465 aa6=max(U_6);
466 aa7=max(U_7);
467 aa8=max(U_8);
468 aa9=max(U_9);
469 aa10=max(U_10);
470 aa11=max(U_11);
471 aa12=max(U_12);
472 aa13=max(U_13);
473 aa14=max(U_14);
474 aa15=max(U_15);
475 aa16=max(U_16);
476 aa17=max(U_17);
477 aa18=max(U_18);
478 aa19=max(U_19);
479 aa20=max(U_20);
480 aa21=max(U_21);
481 aa22=max(U_22);
482 aa23=max(U_23);
483 aa24=max(U_24);
484 aa25=max(U_25);
485 aa26=max(U_26);
486 aa27=max(U_27);
487 aa28=max(U_28);
488 aa29=0;
489 %%
490 figure();
491 qq=1:1:30;
492 aa=[aa0 aa1 aa2 aa3 aa4 aa5 aa6 aa7 aa8 aa9 aa10 aa11 aa12 aa13 aa14 aa15 aa16 aa17
      aa18 aa19 aa20 aa21 aa22 aa23 aa24 aa25 aa26 aa27 aa28 aa29];
```

```
493 plot(qq,aa)
494 addToolbarExplorationButtons(gcf)
```